ACOUSTIC EXCITATION OF CONTAINING STRUCTURES

by

FRANCIS JOHN FAHY

of the

Institute of Sound and Vibration Research,
Faculty of Engineering and Applied Science
University of Southampton

A thesis submitted for the degree
of
Doctor of Philosophy

December, 1969.

ACKNOWLEDGEMENTS

I should like to express my gratitude to the following:-

Professor B.L. Clarkson, for advice and encouragement.

The Central Electricity Generating Board, for the establishment and support of my lectureship and of the research.

Jill, my wife, whose love and patience have sustained me during difficult times.

Mrs. Barbara Pye, for the development of computer programmes.

Messrs. H. Eales, T. Kelly and H. Dawkins for construction and maintenance of experimental equipment.

Miss Maureen Andrews, whose superb typing has made a silk purse of a sow's ear.

ABSTRACT

FACULTY OF ENGINEERING AND APPLIED SCIENCE

INSTITUTE OF SOUND AND VIBRATION RESEARCH

Doctor of Philosophy

ACOUSTIC EXCITATION OF CONTAINING STRUCTURES

by Francis John Fahy

An analysis is made of the vibration of thin shell structures by time-random sound generated in a closed volume of fluid contained by the structures. Classical analysis, which uses the differential equations of motion of the structure, and integral equations for the sound field, is discarded in favour of an analysis which treats the time-average power flow between the vibration modes of the structure and the fluid.

Application to cases of (a) a rectangular panel which forms one wall of an otherwise rigid rectangular box and (b) a right circular cylindrical shell, indicates that, in cases of regular fluid volume geometry, existing two-oscillator power flow equations can be generalised to cover multimode coupling.

The response of containing structures to sound in the contained fluid is shown to be usually the same as that to a diffuse acoustic field in the external fluid above a frequency determined by the geometry and speed of sound of the fluid, and the material properties of the structure. Below this 'lower limiting frequency' the response falls below the diffuse field value and the transmission of sound through the cylindrical shell is also affected. It is shown that, with geometrically regular fluid volumes, the power flow is dominated by very few of the available mode pairs.

Coupled oscillator theory is extended to cover the case of the statistical dependence of oscillator inputs peculiar to point forces, and corresponding measurements of sound radiation are made.

Measurements of response of box-mounted panels and a cylindrical shell to valve noise in the contained air clearly demonstrate the lower limiting frequency phenomenon. Small perturbations of the fluid boundary geometry affect response only at frequencies below the lower limiting frequency. With low modal populations the response tends to follow the smoothly varying, statistically estimated curves, rather than the irregular curves computed from individual mode pair power flows.

LIST OF CONTENTS

LIST OF SYMBOLS

Special list for Chapter II

A_n	coefficient in series expression for velocity potential of fluid
B	viscous damping coefficient of shell
c_o	speed of sound in fluid
G_k	Greens function for simple harmonic time dependence of frequency ω $(= c_o k)$
grad_o	gradient normal to shell surface
f_m, f_n, f_p	normal mode shapes (eigenfunctions) of shell
k	wavenumber in fluid $(= \omega/c_o)$
k_n	wavenumber in fluid corresponding to natural frequency ω_n of acoustic mode n.
$[L]$	an operator giving local lateral elastic force per unit area from lateral shell displacement
m	mass per unit area of shell; structural mode subscript
n	a structural mode subscript
P	acoustic pressure in fluid
q	acoustic velocity potential source strength density
$\underline{r}$	position vector of point in fluid
$\underline{r}_o^s$	position vector of shell surface
S	surface of shell
t	time
V	fluid volume
V_o	fluid volume which contains acoustic sources
w	shell displacement normal to shell surface
β	viscous damping coefficient of shell
δ	Dirac delta function

∇	del operator
ρ_o	mean fluid density
ψ	velocity potential
ψ_m	eigenfunction of acoustic mode m
ω	radian frequency
ω_m	natural radian frequency of mode m
ξ_m, ξ_p	normal coordinates of shell displacement

General List

a	side length of rectangular panel; radius of cylinder
A	total area of shell surface
b	side length of rectangular panel
B_{rm}	coupling coefficient between mode m and mode r
c	depth of rectangular box
c_o	speed of sound in fluid
c_B	phase speed of flexural waves in structure
c_L	speed of longitudinal waves in structural material
D	bending stiffness per unit width of plate
$E[\ ]$	statistical expectation
f	frequency; centre frequency of band considered
Δf	frequency bandwidth
f_c	critical frequency
f_R	ring frequency

f_s	pressure distribution applied to surface of structure
F_m	generalised force per unit mass on structural mode m
F_m'	see equation (3.3a)
g	acoustic source strength distribution
g_{mr}	coupling factor between modes m and r
G_r	generalised acoustic source for acoustic mode r
G_r'	see equation (3.3b)
$h_m(\theta)$	response of structural mode m to unit impulse/unit mass $\delta(\theta)$
$h_r(\theta)$ $h_s(\theta)$	response of acoustic modes r and s to unit source impulses per unit structural mass
$H(i\omega)$	see equations (3.30) et seq.
I	acoustic intensity; integrals defined in Appendix III and equation (4.13) et seq.
I_x, I_y	integrals defined in Appendix II
J_{mr}	power flow per unit structural mass from mode m to mode r
k	wavenumber; acoustic mode subscript
k_1,k_2	clamped panel wavenumbers
k_p	panel wavenumber
k_{pqr}	wavenumber of acoustic mode of order (p, q; r)
k_r	wavenumber of acoustic mode r
Δk_r	thickness of shell segment in wavenumber space (= $(\beta_r + \beta_m)/(c_o)$
k_s	wavenumber of cylindrical shell
k_x	x-component of wavenumber
k_y	y-component of wavenumber
k_z	z-component of wavenumber
L	typical linear dimension of fluid volume
m	mass per unit area of structure; structural mode subscript; (with n) structural mode order

m'	structural mode subscript
M	total mass of structure
n	structural mode subscript; (with m) structural mode order
n'	structural mode subscript
$n_R(\omega)$	acoustic modal density
$n_s(\omega)$	structural modal density
N_s	total number of structural modes in frequency band considered
N_r	total number of acoustic modes in frequency band considered
N_{rm}	total number of well coupled mode pairs in frequency band considered
O	order of
p	acoustic pressure; with (q, r) acoustic mode order
q	(with p, r) acoustic mode order
q_r'	normal mode coordinate of acoustic velocity potential of fluid
q_r	$= (\rho V \varepsilon_r / M^2)^{\frac{1}{2}} q'r$
r	acoustic mode subscript; (with p,q) acoustic mode order; polar coordinate in cylinder analysis
$\underline{r}$	position vector of point in fluid
r'	acoustic mode subscript
R	autocorrelation function
R_{mech}	mechanical loss resistance ($= \beta_m M$)
R^f_{mech}	loss resistance of fluid
R_{rad}	Radiation resistance
R^{ext}_{rad}	radiation resistance for radiation into external fluid
R^{int}_{rad}	radiation resistance for radiation into internal fluid
R_{tot}	$= (R_{rad} + R_{mech})$
S	acoustic mode subscript
S_m'	normal coordinate of displacement of structure normal to its surface
S_m	$= (\varepsilon_m)^{\frac{1}{2}} S_m'$

$S(\omega)$	spectral density
U_m, U_r	time average vibration energy per unit mass of modes m and r
U_{m_o}, U_{r_o}	time average uncoupled vibration energy per unit mass of modes m and r
v	normal velocity of the surface of a structure
V	fluid volume
x	rectangular cartesian coordinate; curvilinear coordinate in cylinder analysis
x_a	see equation (4.11) et seq.
$\underline{x}$	position vector of point on surface of structure
y	rectangular cartesian coordinate
y_b	see equation (4.11) et seq.
z	axial coordinate in cylinder analysis
α	see equation (3.22) et seq.
β	phase angle between fluid and structural coordinates in cylinder analysis
β_m	viscous damping coefficient of structural mode m - equal to half power bandwidth of mode m
β_r	damping coefficient of acoustic mode r - equal to half power bandwidth of mode r
γ	a function defined in equation (3.49); angle defined in Figure 6.6
δ	Dirac delta function
ε	arbitrarily small constant; ratio of mode orders q/n
ε_m	$= M^{-1} \int_S \phi_m^2(\underline{x}) m(\underline{x}) d\underline{x}$ - normalising constant for structural modes
ε_r	$= V^{-1} \int_V \psi_r^2(\underline{r}) d\underline{r}$ - normalising constant for acoustic modes
ψ_r	velocity potential eigenfunction of acoustic mode r
ϕ	angle defined as $\cos^{-1}(f/f_R)^{\frac{1}{2}}$

ϕ_m	surface displacement eigenfunction of structural mode m
θ	time delay; polar coordinate in cylinder analysis
θ_m'	uncoupled energy per unit mass of structural mode (see also U_{m_o})
θ_r'	uncoupled energy per unit mass of acoustic mode (see also U_{r_o})
ρ	mean fluid mass density
ρ_s	density of structural material
π_m	instantaneous rate of energy input per unit mass to mode m
Π_m	time average of π_m
ω	radian frequency; centre frequency of band considered
ω_m	natural frequency of uncoupled mode m
ω_r	natural frequency of uncoupled mode r
$\Delta\omega$	radian frequency bandwidth
$\dot{}$	differentiation with respect to time
$'$	differentiation with respect to argument of function
$< >$	spatial average; modal average where stated
$\bar{}$	time average

LIST OF FIGURES

Chapter III

Chapter IV

Chapter V

Chapter VI

Chapter VI (cont.)

Chapter VII

Appendix II

CHAPTER I

INTRODUCTION

The research reported in this thesis forms part of a research programme which was initiated in 1966 after several cases of structural damage to the cooling-gas circuits of nuclear reactors had been ascribed to acoustically induced vibration and fatigue. A gas cooled reactor circuit can broadly be described as a closed duct circuit in which compressed gas is blown by a large compressor through a nuclear core, where it picks up heat, and then through a heat exchanger, where it heats water in tubes to produce steam. The compressor is typically of 15,000 shaft h.p. and normally generates high acoustic power of the order of 10^3 watts. This acoustic power is radiated into the gas circuit. The aims of the overall research programme are to increase understanding of the mechanisms of sound propagation in gas circuits, and to develop improved forms of analysis of acoustically induced structural response and strain distribution, for use at the design stage. The programme is supported by the Central Electricity Generating Board, the United Kingdom Atomic Energy Authority and members of the commercial nuclear industry.

The work reported here is supported by the C.E.G.B. and is concerned with the problem of acoustically induced vibration of plate and shell-like areas of the gas ductwork. The vibration problem in nuclear reactors differs in two main features from that of aero-space structures, on which much work has been done over the past decade. First, the duct structures are constructed typically of between two inch and

one-half inch unstiffened steel plate work, as opposed to the lightweight alloy stiffened structures of aircraft and missiles. Second, and more important, the sound fields are generated in the fluid contained by the responding structures, whereas the sound which excites aero-space structures is propagating largely in free space. Hence the fluid in the reactor ducts exhibits resonant, modal behaviour and its high frequency, multimodal pressure field characteristics are extremely complex. There is particular interest in the effect on response of limiting the volume of fluid in which the sound is contained, and in the dependence upon fluid sound speed.

1.1 Available Means of Analysis

Rational approaches to the estimation of the response of plate- and shell-like mechanical structures to acoustic fields may be broadly classified into (a) those which employ the equations of motion directly and, (b) those which consider energy flow between the fluid and mechanical systems. The former approach requires the definition of the fluctuating acoustic pressure distribution at the surface of the structure. Some studies assume that these pressures are given by the incident field characteristics, with either a simple pressure doubling correction for wave reflection (1), or a more careful correction for the rigid scattered pressure (2); other studies account for the additional pressures due to surface vibration by means of a matched boundary condition solution (3), or a radiation pressure approach (4, 5). In the last mentioned analysis use is made of the acoustic reciprocity principle to relate the surface

pressures causing modal response to the power radiated by vibration in that mode. However this analysis is restricted to cases of response to remote acoustic sources under free field conditions.

The energy flow from a fluid into a structure may formally be determined from a knowledge of the surface impedance of the structure, which can be obtained from the equations of motion of the structure. However, since it is necessary to determine the total surface acoustic pressure (incident + scattered), as previously mentioned, there is no advantage to be gained over a direct solution of the equation of motion. Indeed the impedance expressions of finite shell and plate structures are often so complex that usually only infinite systems have been considered (6).

It is in cases of random vibration of coupled fluid-mechanical systems that an energy flow approach may be shown to provide a powerful alternative to the force approach. Modal equations of motion, each describing the motion of one simple oscillator, are manipulated to produce expressions for the nett power flow from the fluid system into the mechanical system, without resort to impedance expressions. The relevance of this approach to the problem of acoustic excitation of containing structures by sound in the contained fluid will be appreciated from the following discussion.

It is necessary in all forms of analyses of acoustic excitation to assume a suitable form of idealised model of the incident acoustic field. The two most commonly assumed forms are the uni-directional plane wave field and the diffuse field. The latter is defined to consist of plane waves travelling in all directions with equal probability, a con-

dition approximately satisfied at high frequencies in rooms of many acoustic wavelengths in size. It is one of the concerns of the present work to consider those situations where structures that contain a sound field have typical dimensions of the order of a wavelength, in which case the diffuse field model is not necessarily applicable. Because a fluid in a structural container will often behave acoustically as a highly tuned, multimode system, the spatial and frequency variation of acoustic pressure on the container surface will be extremely complex, even for a well defined acoustic source strength distribution. In practice it is usually impossible to estimate the source strength distribution in detail, but an estimate of the acoustic power supplied to the fluid can often be made (e.g., steam valve noise in industrial pipes). Consequently, it will be appreciated that the use of the coupled oscillator, energy flow approach, which demands only a knowledge of the acoustic power supplied to the fluid, and works directly in terms of the eigenfunctions and frequencies of the separate mechanical and fluid systems, is a natural choice for the present problem.

A further reason for the use of coupled oscillator theory is that it may be 'forced into service' to provide guidelines to the important parameters in high frequency, multimode situations where the classical, normal mode and finite element analyses become unwieldy and where statistical approaches come into their own. The term in inverted commas is used because no rigorous analysis of multimode power flow has yet been produced (7) with which to compare the results of approximate theory.

As yet there has been no analytical treatment of the random

acoustic excitation of containing vessels by sound in a contained fluid. Some studies have been made (8-14) of the related problems of sound radiation by wall vibration into a closed space but, of these, only Kihlman's study (8) of a panel-box system at supercritical frequencies, and Crocker and Bhattacharyas' study (9) of sound transmission into a closed box,have any relevance to the present problem. Kihlman's analysis is restricted to frequencies above the critical (lowest coincidence) frequency of a panel. Crocker and Bhattacharyas' analysis does not display the controlling parameters in a simple fashion. Pretlove's study (10) of forced vibration of a panel on a box is restricted to the lower order modes of the panel and the analysis could not be practicably extended to higher frequencies. The analysis by Fahy and Pretlove (11) is more concerned with the effect of a duct on panel damping than with response to sound in the duct. In the papers of Eichler (12), Lyon (13) and White (14) various assumptions are made about the radiation efficiency of structures without specific analysis.

1.2 Content of the Thesis

The main concern of the thesis is the application of coupled oscillator, energy flow analysis to calculation of the response of two geometrically regular containing structures to broad band random sound in the contained air. These structures are (a) a closed right circular cylindrical shell and (b) a rectangular plate which forms one wall of an otherwise rigid rectangular box. Geometrically regular systems have been chosen because they are amenable to analytical and numerical studies of the coupling between the fluid and the structure, which allow the results

of statistical theory to be checked for accuracy. Considerable interest is however shown in the effects of irregularities of fluid boundary geometry on the coupling and on the resulting structural response. The cylinder response analysis is also used to investigate the transmission of sound from the inside to the outside air.

A formal solution for the response to acoustic sources having simple harmonic time dependence, which uses a classical modal approach, is presented in Chapter II. This solution is presented in order to demonstrate the impracticability of using a classical approach to the problem of high frequency, random acoustic excitation. It has also been used to derive scaling parameters for a dynamic model of a reactor gas circuit, which is being constructed as part of the general research programme. It is concluded that the coupled oscillator, energy flow approach provides a more promising means of analysis.

The development of coupled oscillator theory is reviewed in the first part of Chapter III. Newland's perturbation method (22) is then used to compare the results of approximate and exact two-oscillator power flow analysis for gyroscopic (acoustic) coupling. Perturbation analysis is also used to produce a new result for the particular case of statistically dependent modal input forces which is produced by the application of a point force to a structure. The implications for oscillator set-to-set power flow are discussed.

Coupled oscillator theory is then applied to the case of the rectangular panel-box system in Chapter IV. The implications of the observed high degree of spatial and frequency selectivity of panel-fluid mode pairs are discussed at length: they lead to approximate mode-set power flow and response equations which differ from those previously

presented by Lyon and Maidanik (16). Both simply supported and clamped panel boundary conditions are treated. The analysis for the latter case extends analyses previously presented in the literature (29, 23). Important mode coupling statistics are derived from a statistical analysis which is supported by a computational study. The concept of a 'lower limiting frequency', below which a diffuse acoustic field model is untenable, is derived from these statistics. The point excited panel is also studied. Experimental measurements of panel response and radiation follow in Chapter V where the results are compared with those of statistical and computational analyses. The effects of irregularity of fluid boundary geometry are investigated experimentally.

Similar theoretical and experimental studies of cylinder response and radiation are presented in Chapter VI and measurements of the transmission of sound through the cylinder are presented in Chapter VII. Conclusions and recommendations for further research form the concluding chapter.

CHAPTER II

GENERAL EQUATIONS OF MOTION: THE FORMAL SOLUTION

2.1 Introduction

This chapter presents a formal solution to the problem of vibration of a shell-like containing structure by acoustic sources which are situated in the contained fluid and have harmonic time dependence. This classical solution is presented so that its complexity may be appreciated, thereby affording some justification for the resort to a more recently developed form of analysis in the following chapters. The formal harmonic solution also displays some of the important physical characteristics of a closed shell-fluid system, and therefore forms a basis on which to build a physical understanding of the dynamic behaviour of such a system with any type of time-dependent acoustic source strength.

2.2 Equation of Motion of a Shell

The equation of motion governing the bending vibration of a thin shell structure of mass per unit area m, which is subjected on one side to a time dependent pressure $P(\underline{r}_s, t)$ at position vector $\underline{r}_s$, is

$$[L]\, w(\underline{r}_s) + m(\underline{r}_s) \frac{\partial^2 w(\underline{r}_s)}{\partial t^2} + B(\underline{r}_s) \frac{\partial w(\underline{r}_s)}{\partial t} = P(\underline{r}_s, t) \qquad (2.1)$$

$[L]$ is an operator which relates the local lateral elastic force per unit area to the local surface displacement $w(\underline{r}_s)$. B is an ad hoc viscous damping coefficient which accounts for energy dissipation by mechanical

means, excluding acoustic radiation losses.

The surface displacement may be expanded in terms of the in-vacuo normal modes of the undamped structure as $w(\underline{r}_s) = \sum_{m=1}^{\infty} f_m(\underline{r}_s)\zeta_m(t)$, where the mode shapes f_m satisfy the equations of undamped free vibration

$$\{[L] - \omega_m^2 m(\underline{r}_s)\} f_m(\underline{r}_s) = 0 \qquad (2.2)$$

Substituting for $f_m(\underline{r}_s)$ in equation (2.1) from equation (2.2), multiplying through by $f_n(\underline{r}_s)$, and applying the condition of orthogonality between normal modes, gives

$$\left[\omega_m^2 \zeta_m(t) + \ddot{\zeta}_m(t)\right] \int_S f_m^2(\underline{r}_s) m(\underline{r}_s) dS + \int_S \sum_{m=1}^{\infty} B(\underline{r}_s) f_m(\underline{r}_s) f_n(\underline{r}_s) \dot{\zeta}_m(t) dS$$

$$= \int_S P(\underline{r}_s, t)\, f_n(\underline{r}_s) dS \qquad (2.3)$$

If we further assume that there is no damping coupling between modes by virtue of mechanical, but not acoustic, forces, then we may assume that $B(\underline{r}_s) = \beta m(\underline{r}_s)$ where β is a constant. Then the orthogonality relationship holds for the damping terms, which leads to the harmonic form

$$\zeta_m \int f_m^2(\underline{r}_s) m(\underline{r}_s) dS \left[\omega_m^2 - \omega^2 + i\omega\beta\right] = \int_S P(\underline{r}_s) f_m(\underline{r}_s) dS. \qquad (2.4)$$

2.3 Acoustic Equations

The acoustic field in the enclosed fluid is assumed to have a velocity potential Ψ, i.e. we are dealing with an irrotational field. The acoustic pressure is related to the potential by

$$P(\underline{r}, t) = -\rho_o \frac{\partial \psi(\underline{r}, t)}{\partial t} \tag{2.5}$$

where ρ_o is the mean fluid mass density. For harmonic oscillations of frequency ω, $P(\underline{r}, t) = P(\underline{r})e^{i\omega t} = i\omega\rho_o\psi(\underline{r})e^{i\omega t}$; or $P(\underline{r}) = i\omega\rho_o\psi(\underline{r})$.

Reference (15) gives the relationship, for steady wave (harmonic) conditions, between the acoustic velocity potential within a closed volume V, any enclosed acoustic velocity potential source strength density $q(\underline{r}_o)$, and the boundary conditions on ψ at the walls as follows:-

$$\psi(\underline{r}) = \int_{V_o} q(\underline{r}_o)G_k(\underline{r}/\underline{r}_o)dV_o + (1/4\pi)\int_{S_o} [G_k(\underline{r}/\underline{r}_o{}^s)\text{grad}_o\psi(\underline{r}_o{}^s) - \ldots \psi(\underline{r}_o{}^s)\text{grad}_o\, G_k(\underline{r}/\underline{r}_o{}^s)]dS_o \tag{2.6}$$

for $\underline{r}$ within and on S_o and where the gradient and surface vectors point outward from the enclosing surface.

The Green function, G_k, satisfies, for a source at $\underline{r}_o$, the partial differential equation

$$(\nabla^2 + k^2)G_k = -4\pi\delta(\underline{r} - \underline{r}_o) \tag{2.7}$$

where δ is the Dirac delta function and $k = \omega/c_o$ where c_o is the speed of sound: k is known as the acoustic wavenumber. The Green function for a completely enclosed fluid can be expressed in terms of the eigenfunctions of the fluid in the presence of rigid walls. Let these eigenfunctions be ψ_n and the corresponding eigenvalues be k_n; that is

$$(\nabla^2 + k_n{}^2)\psi_n = 0. \tag{2.8}$$

It is assumed that the eigenfunctions form a complete set so that it is possible to expand $G_k(\underline{r}/\underline{r}_o)$ in a series of ψ_n:

$$G_k(\underline{r}/\underline{r}_o) = \sum_{n=1}^{\infty} A_n \psi_n(\underline{r}) \tag{2.9}$$

Introducing this series into equation (2.7) we find that

$$(\nabla^2 + k^2)\sum_n A_n \psi_n(\underline{r}) = -4\pi\delta(\underline{r} - \underline{r}_o) \tag{2.10}$$

Thus

$$\sum_n (-k_n^2 + k^2) A_n \psi_n(\underline{r}) = -4\pi\delta(\underline{r} - \underline{r}_o) \tag{2.11}$$

Multiplying through by ψ_p and using the orthogonality condition for rigid wall acoustic modes, $\int_V \psi_n \psi_p dV = 0; \quad n \neq p$, we obtain

$$A_n = 4\pi\psi_n(\underline{r}_o)\left[(k_n^2 - k^2)\int \psi_n^2(\underline{r})dV\right]^{-1} \tag{2.12}$$

After normalising by choosing ψ_n such that $\int_V \psi_n^2(\underline{r})dV = 1$ we obtain, from equations (2.9) and (2.12),

$$G_k(\underline{r}/\underline{r}_o) = \sum^{\infty} \frac{4\pi\psi_n(\underline{r})\psi_n(\underline{r}_o)}{(k_n^2 - k^2)} \tag{2.13}$$

Substitution of this expression into equation (2.6) gives

$$\psi(\underline{r}) = 4\pi\int_{V_o} q(\underline{r}_o) \sum_{n=1}^{\infty} \frac{\psi_n(\underline{r})\psi_n(\underline{r}_o)}{(k_n^2 - k^2)} dV_o + \int_{S_o} \left[\sum_{n=1}^{\infty} \frac{\psi_n(\underline{r})\psi_n(\underline{r}_o^s)}{(k_n^2 - k^2)}\right.$$

$$\left.\text{grad}_o\, \psi(\underline{r}_o^s) - \psi(\underline{r}_o^s)\text{grad}_o\left(\sum_{n=1}^{\infty} \frac{\psi_n(\underline{r})\psi_n(\underline{r}_o^s)}{(k_n^2 - k^2)}\right)\right].dS_o \tag{2.14}$$

Now $\text{grad}_o\, \psi_n(\underline{r}_o^{\,s})$ is zero for a rigid surface because it is proportional to the acoustic particle velocity normal to that surface. Hence the last term in equation (2.14) is zero. The convenience afforded by expressing the Green Function in terms of the rigid wall acoustic modes is therefore seen to be the elimination of the term involving the unknown surface pressure $\psi(\underline{r}_o^{\,s})$ at other points than the point, $\underline{r}$, considered.

The term $\text{grad}_o\psi(\underline{r}_o^{\,s})$ is given by the normal velocity of the vibrating wall since $\text{grad}_o\psi(\underline{r}_o^{\,s})e^{i\omega t} = \frac{\partial}{\partial t}\sum_{p=1}^{\infty} f_p(\underline{r}_o^{\,s})\zeta_p(t) = i\omega\sum_{p=1}^{\infty} f_p(\underline{r}_o^{\,s})\zeta_p(t)$ for harmonic oscillation. The surface pressure $P(\underline{r}_s)$, may therefore be expressed as follows

$$P(\underline{r}_s) = i\omega\rho_o\{4\pi\int_{V_o} q(\underline{r}_o)\sum_{n=1}^{\infty}\frac{\psi_n(\underline{r}_s)\psi_n(\underline{r}_o)}{(k^2 - k_n^{\,2})}\,dV_o + i\omega\int_{S_o}\sum f_p(\underline{r}_o^{\,s})\zeta_p \sum_{n=1}^{\infty}\frac{\psi_n(\underline{r}_s)\psi_n(\underline{r}_o^{\,s})}{(k^2 - k_n^{\,2})}\,dS_o\} \qquad (2.15)$$

Substituting this expression into equation (2.4) we obtain

$$\zeta_m\int_S f_m^{\,2}(\underline{r}_s)m(\underline{r}_s)dS[\omega_m^{\,2} - \omega^2 + i\omega\beta] =$$

$$i\omega\rho_o\Big[4\pi\int_S f_m(\underline{r}_s)dS\int_{V_o} q(\underline{r}_o)\sum_{n=1}^{\infty}\frac{\psi_n(\underline{r}_s)\psi_n(\underline{r}_o)}{(k^2 - k_n^{\,2})}\,dV_o$$

$$+ i\omega\int_S f_m(\underline{r}_s)dS\int_{S_o}\sum_{p=1}^{\infty} f_p(\underline{r}_o^{\,s})\zeta_p\sum_{n=1}\frac{\psi_n(\underline{r}_s)\psi_n(\underline{r}_o^{\,s})}{(k^2 - k_n^{\,2})}\,dS_o\Big] \qquad (2.16)$$

Collecting terms in ζ_m we finally obtain

$$\zeta_m\Big[\int_S f_m^2(\underline{r}_s)m(\underline{r}_s)dS(\omega_m^2 - \omega^2 + i\omega\beta) + \omega^2\rho_o\Big(\int_S f_m(\underline{r}_s)dS \int_{S_o} f_m(\underline{r}_o^s) \sum_{n=1}^{\infty} \frac{\psi_n(\underline{r}_s)\psi_n(\underline{r}_o^s)}{(k^2 - k_n^2)} dS_o\Big)\Big]$$

$$= i\omega\rho_o \Big[4\pi \int_S f_m(\underline{r}_s)dS \int_{V_o} q(\underline{r}_o) \sum_{n=1} \frac{\psi_n(\underline{r}_s)\psi_n(\underline{r}_o)}{(k^2 - k_n^2)} dV_o$$

$$+ i\omega \int_S f_m(\underline{r}_s)dS \int_{S_o} \sum_{p\neq m=1}^{\infty} f_p(\underline{r}_o^s)\zeta_p \sum_{n=1}^{\infty} \frac{\psi_n(\underline{r}_s)\psi_n(\underline{r}_o^s)}{(k^2 - k_n^2)} dS_o \Big] \qquad (2.17)$$

2.4 Discussion

This formal solution for the shell mode generalised coordinate ζ_m demonstrates the nature of the coupled structural-acoustic system problem. The second term in round brackets on the left hand side of the equation represents the effect of the fluid on the mode due to its own motion - a direct virtual mass or stiffness effect. Notice that the magnitude of the contribution of each term under the summation sign depends upon the proximity of the driving frequency ω to the natural frequency of the acoustic mode ψ_n, through the difference between k $(= \omega/c_o)$ and k_n $(= \omega_n/c_o)$. It is obvious that some form of ad hoc acoustic damping would have to be incorporated into the mathematical model for practical purposes.

The first term on the right hand side of the equation represents the generalised acoustic force on the mode ζ_m due to the distribution of

acoustic sources q_o. Again acoustic mode resonance effects are evident. The magnitude of the contribution of any acoustic mode is seen to depend also on the degree of spatial matching between the acoustic mode 'shape' ψ_n and the structural mode shape f_m. It also depends upon the degree of matching between the acoustic source distribution and the particular acoustic mode shape. The last term in equation (2.17) represents the coupling forces between the mode and the other structural modes p via the fluid pressures. Here there is a double dependence upon spatial matching between acoustic and structural modes, as well as the frequency difference dependence.

It will be realised that for any practical multi-mode system, an appreciation of even the simple harmonic behaviour would be difficult to achieve. It is unnecessary to demonstrate formally that the situation in which the acoustic sources are random functions of time, having possibly wide frequency spectra, represents a formidably complex situation. The formal random solution contains expressions which represent the statistically expected relationship between acoustic sources, and thereby between acoustic and structural modes, for which it would be very difficult to assume reasonable analytic forms. There are indeed very few practical acoustic sources for which such characteristics have been reliably measured. A further most important consideration is that even if such characteristics could be adequately described, the resultant behaviour of the structure would be derived in such a form that a reasonably simple parametric study, such as it is important for a designer to be able to assimilate and to use in making design decisions, would probably not be forthcoming.

It is well known that the acoustic source distribution of most real random noise sources, such as compressors, jets and valves, are not sufficiently well understood to enable adequate mathematical models to be formulated. However in many cases quite good estimates can be made of the total acoustic power output of such sources. Hence it is very reasonable to look to an approach to the calculation of structural response which utilises only the acoustic power output of the source. Such an approach is the coupled oscillator, energy flow approach which is used in the following chapters.

CHAPTER III

COUPLED OSCILLATOR THEORY

3.1 Survey of the Development of the Theory

The first application of coupled oscillator, energy flow theory to randomly vibrating mechanical systems of engineering interest was that of Lyon and Maidanik in 1962 (16). They demonstrated the proportionality of power flow between two linearly, conservatively, lightly coupled oscillators to the difference between the time average energies of the oscillators when subjected to the same applied forces, but when uncoupled from each other. Their proof depended upon an 'ad hoc' linearisation of the power flow equations, on the basis of the smallness of the coupling force coefficient compared with the modal damping force coefficients. They applied the analysis formally to the interaction between the acoustic modes of a room and one flexible wall, but did not properly explore the details of this problem. Consequently some of their assumptions were not of general validity, such as that concerning the much greater number of participating acoustic modes than structural modes. Some of their assumptions were in general unnecessary, such as that concerning the spectral properties of their pseudo input force produced by formal reduction of the problem to a two oscillator problem. These matters are discussed further in later chapters.

A number of papers and reports (12, 14, 17, 18, 19) followed the publication of Lyon and Maidanik's paper in which 'ad hoc' extensions

of two oscillator theory was made to the interaction between sets of modes. The powerflow expression was written in terms of the average coupled modal energy difference between the coupled systems, and a modal average coupling loss factor was defined (cf. reference 20). Ungar (21) was first to point out the dangers of such an arbitrary extension and he discussed the conditions under which the two oscillator power flow relationship could be validly extended to multimode systems. These conditions were (a) uncorrelated force inputs to the individual oscillators AND (b) equal modal energies in each set OR uniform mode to mode coupling.

Newland (22) was the first to present a power flow analysis which enabled estimates to be made of the errors involved in the use of approximations such as those made by Lyon and Maidanik in their ad hoc linearisation. This perturbation method also allowed certain statistics of the power flow process to be evaluated, such as the spectrum of the power flow.

Scharton and Lyon (7) first demonstrated that the power flow between randomly excited coupled oscillators is proportional to the difference between their actual time-average coupled energies, even when they are strongly coupled, provided that the oscillator energies are correctly defined (i.e., the coupling energy has to be correctly divided up among the oscillators). However they regretted that 'the calculations used to demonstrate the proportionality for the two-oscillator system become very tedious for an arbitrary system of even three oscillators'. Kakar's work (24) confirms this statement, but he is at least able to demonstrate that in the general three-oscillator case the power flow-

energy difference proportionality relationship is not valid. However his detailed consideration of errors arising from an assumption of this proportionality shows that, unless the oscillators have very close natural frequencies, they will normally only be of the order of 1%. Both Scharton and Kakar show that the relationship holds for N identical, and identically coupled, oscillators. This case is not of great interest to the engineer, except possibly in the case of multi-element structures such as turbine discs and blades, or periodically stiffened panels.

A considerable amount of effort has gone into the calculation and measurement of the constants of proportionality in the power flow equation for different mechanical systems (25, 19, 7, 26, 27). In many cases a direct calculation of the modal coupling forces and velocities is very difficult and resort is had to a wave transmission calculation (cf. 7, 27). It is generally found that the wave approach, with the assumption of an infinite 'receiving' system, gives identical results to a modal, or frequency-averaging calculation. This appears to be a very convenient property of multi-mode systems and should considerably ease the problem of high frequency vibration transmission in complex systems.

This thesis is not primarily concerned with the development of coupled oscillator theory. The theory is used as a tool to analyse the response of containing structures to sound in a contained fluid; but the results of the analyses and the associated experiments allow certain observations to be made regarding the application of coupled oscillator to lightly coupled fluid-mechanical systems, particularly with respect to deviations from average behaviour at frequencies where modal populations

are rather small. Also, important corrections to the widely used equations of Lyon and Maidanik (16) are derived to account for the wide variation in modal coupling factors associated with closed fluid systems of small volume.

3.2 Power Flow Between Gyroscopically Coupled Oscillators

3.2.1 The Equations of Motion

The symbols used in this and succeeding sections differ from those used in Chapter II. The reason is that the theory of Chapter II is largely based upon acoustic Green function theory presented by Morse and Feshbach (15), and deviation from their nomenclature would make reference to their work difficult. Much of the theory of the present Chapter is based upon Lyon and Maidanik's paper (16) and it is their nomenclature that has been used in the author's papers to which extensive reference will be made. Apart from an initial reference to Chapter II, the following theory is self contained, and therefore it is hoped that the minimum of confusion will ensue from the use of two sets of symbols.

The modal equations of motion of the structure are of the form of equation (2.3). The acoustic pressure is proportional to the time derivative of the acoustic velocity potential ψ, and the total pressure is written in the form of a summation over a series of coupling terms between the particular structural mode and all the acoustic modes. The acoustic equations are of similar form. Following (16) we write the modal equations as

$$\ddot{s}_m + \beta_m \dot{s}_m + \omega_m^2 s_m + \sum_r B_{rm} \dot{q}_r = F_m \qquad (3.1a)$$

$$\ddot{q}_r + \beta_r \dot{q}_r + \omega_r^2 q_r - \sum_m B_{mr} \dot{s}_m = G_r \qquad (3.1b)$$

It will be seen from equation (2.16) in Chapter II that the coupling coefficients B are such that $B_{rm} = B_{mr}$. Reference (16) shows that the form of equations (3.1) is such that no energy is dissipated in the coupling. The terms in equations (3.1) are defined as follows:-

$$q_r = (\rho V \varepsilon_r / M)^{\frac{1}{2}} q_r'$$

$$G_r = (c_o^2 \rho / MV\varepsilon_r)^{\frac{1}{2}} \int_V g(\underline{r}, t)\psi_r(\underline{r}).d(\underline{r})$$

$$s_m = (\varepsilon_m)^{\frac{1}{2}} s_m'$$

$$F_m = (\varepsilon_m M^2)^{-\frac{1}{2}} \int_S f_s(\underline{x}, t)\, \phi_m(\underline{x}).d(\underline{x})$$

$$B_{rm} = (c_o^2 \rho / V\varepsilon_r \varepsilon_m M)^{\frac{1}{2}} \int_S \psi_r(\underline{x})\phi_m(\underline{x}).d(\underline{x}) \qquad (3.2)$$

where velocity potential, $\psi(\underline{r}, t) = \sum_r q_r'(t)\psi_r(\underline{r})$

shell displacement, $\phi(\underline{x}, t) = \sum_m s_m'(t)\phi_m(\underline{x})$

acoustic source strength distribution = $g(\underline{r}, t)$

pressure distribution applied to shell = $f_s(\underline{x}, t)$

$$M\varepsilon_m = \int_S \phi_m^2(\underline{x})m(\underline{x})d\underline{x}$$

$$V\varepsilon_r = \int_V \psi_r^2(\underline{r})d(\underline{r})$$

Lyon and Maidanik reformulate each of the modal differential equations of forced motion (3.1) by incorporating the terms representing coupling to all except one of the modes of the other system into a new

forcing term; thus equations(3.1) become

$$\ddot{s}_m + \beta_m \dot{s}_m + \omega_m^2 s_m + B_{rm}\dot{q}_r = F_m - \sum_{k\neq r} B_{km}\dot{q}_k = F_m' \qquad (3.3a)$$

$$\ddot{q}_r + \beta_r \dot{q}_r + \omega_r^2 q_r - B_{mr}\dot{s}_m = G_r + \sum_{n\neq m} B_{nr}\dot{s}_n = G_r' \qquad (3.3b)$$

With the further assumption that these new forces F' and G' are independent and 'white', equations (3.3) represent the coupled motion of only two oscillators, to which Lyon and Maidanik apply their previously derived linearised power flow equation, in which they write the power flow per unit mass from the m^{th} to the r^{th} mode as

$$j_{mr} = g_{mr}(\theta_m' - \theta_r') \qquad (3.4)$$

θ' are the average uncoupled energies per unit mass when driven by forces F' and G'. The linearisation in this case is based upon the smallness of (B_{mr}/β_r) and (B_{mr}/β_m). Neglecting squares and products of these ratios, the coefficient g_{mr} is given as

$$g_{mr} = \frac{B_{mr}^2 (\beta_m \omega_r^2 + \beta_r \omega_m^2)}{(\omega_m^2 - \omega_r^2)^2 + (\beta_m + \beta_r)(\beta_m \omega_r^2 + \beta_r \omega_m^2)} \qquad (3.5)$$

The most interesting and important feature of this expression is the strong sensitivity of the denominator to the difference between the structural and acoustic mode natural frequencies, ω_m and ω_r, which enables the following first order approximation to be made

$$g_{mr} \simeq \begin{cases} B_{mr}^2(\beta_r + \beta_m)^{-1} & : \quad 2|\omega_m - \omega_r| < (\beta_m + \beta_r)^* \qquad (3.6a) \\ 0 & : \quad 2|\omega_m - \omega_r| > (\beta_m + \beta_r) \qquad (3.6b) \end{cases}$$

---

*An error appears to have been made here in reference (16). The original condition virtually excluded any power flow with practical damping values, whereas the present modification restricts significant power flow to modes of which the natural frequencies are less than the sum of half their half power bandwidths apart.

3.2.2 Perturbation Analysis

A perturbation method presented by Newland (22) is used to derive the power flow equation for gyroscopic coupling and a two mode analysis provides one estimate of the errors involved in the approximate results presented above.

3.2.2.1 Power flow

Following reference (22) we rewrite the equations of motion (3.1) as

$$\ddot{s}_m + \beta_m \dot{s}_m + \omega_m^2 s_m + \sum_r \varepsilon B_{rm} \dot{q}_r = F_m \tag{3.7a}$$

$$\ddot{q}_r + \beta_r \dot{q}_r + \omega_r^2 q_r - \sum_m \varepsilon B_{mr} \dot{s}_m = G_r \tag{3.7b}$$

where εB_{rm} replaces B_{rm} and ε is a constant which may be made arbitrarily small ($\epsilon \ll 1$)

The rate of energy input per unit mass to the m^{th} structural oscillator from the r acoustic oscillators, which we denote by π_m, is given by

$$\pi_m = - \sum_r \dot{s}_m \varepsilon B_{rm} \dot{q}_r \tag{3.8}$$

The time average power flow is given by

$$\Pi_m = E(\pi_m) = - \sum_r \varepsilon B_{rm} E[\dot{s}_m \dot{q}_r] \tag{3.9}$$

where $E[\ ]$ denotes the expectation or statistical average.

It is assumed that the solutions for $s_m(t)$ and $q_r(t)$ permit expansion in powers of the parameter ε:

$$s_m(t) = s_{m_o}(t) + \varepsilon s_{m_1}(t) + \varepsilon^2 s_{m_2}(t) + \ldots \tag{3.10a}$$

and

$$q_r(t) = q_{r_o}(t) + \varepsilon q_{r_1}(t) + \varepsilon^2 q_{r_2}(t) + \ldots \tag{3.10b}$$

Substitution of equations (3.10) into the equations(3.7) gives, if the resulting equations are to be satisfied identically in ε,

$$\ddot{s}_{m_o} + \beta_m \dot{s}_{m_o} + \omega_m^2 s_{m_o} = F_m \tag{3.11a}$$

$$\ddot{s}_{m_1} + \beta_m \dot{s}_{m_1} + \omega_m^2 s_{m_1} + \sum_r B_{rm} \dot{q}_{r_o} = 0 \tag{3.11b}$$

... ...

and

$$\ddot{q}_{r_o} + \beta_r \dot{q}_{r_o} + \omega_r^2 q_{r_o} = G_r \tag{3.12a}$$

$$\ddot{q}_{r_1} + \beta_r \dot{q}_{r_1} + \omega_r^2 q_{r_1} - \sum B_{mr} \dot{s}_{m_o} = 0 \tag{3.12b}$$

... ...

Now in the case of interest there are no direct mechanical input forces; $F_m = 0$. Thus

$$s_{m_o} = q_{r_1} = s_{m_2} = q_{r_3} = s_{m_4} = q_{r_5} = \ldots = 0 \tag{3.13}$$

Hence we have

$$q_r(t) = q_{r_o}(t) + \varepsilon^2 q_{r_2}(t) + \varepsilon^4 q_{r_4}(t) + \varepsilon^6 q_{r_6}(t) + \ldots \tag{3.14a}$$

and

$$s_m(t) = \varepsilon s_{m_1}(t) + \varepsilon^3 s_{m_3}(t) + \varepsilon^5 s_{m_5}(t) + \ldots \tag{3.14b}$$

The product in brackets in equation (3.9) becomes

$$E[\dot{s}_m \dot{q}_r] = \varepsilon E[\dot{s}_{m_1} \dot{q}_{r_o}] + O(\varepsilon^3) \qquad (3.15)$$

Now the solution of equation (3.11b) is given by the convolution integral

$$s_{m_1}(t) = -\sum_s B_{sm} \int_0^\infty h_m(\theta) \dot{q}_{s_o}(t - \theta) d\theta, \qquad (3.16)$$

where $h_m(\theta)$ is the response of the m^{th} mode to a unit impulse $q_{s_o}(t) = \delta(\theta)$.

Similarly the solution of equation (3.12a) is given by

$$q_{r_o}(t) = \int_0^\infty h_r(\theta) G_r(t - \theta) d\theta \qquad (3.17)$$

Hence equation (3.16) becomes

$$s_{m_1}(t) = -\sum_s B_{sm} \int_0^\infty h_m(\theta_1) \int_0^\infty \dot{h}_s(\theta_2) G_s(t - \theta_2 - \theta_1) d\theta_1 d\theta_2$$

The expectation of equation (3.15) therefore may be written, to second order in ε,

$$E[\dot{s}_m \dot{q}_r] = -\varepsilon \sum_s B_{sm} \int_0^\infty \dot{h}_m(\theta_1) \int_0^\infty \dot{h}_s(\theta_2) \int_0^\infty \dot{h}_r(\theta_3) E[G_s(t - \theta_2 - \theta_1) G_r(t - \theta_3)] \, d\theta_1 d\theta_2 d\theta_3 \qquad (3.18)$$

Now if the generalised acoustic sources G_s are assumed to be statistically independent of each other then $E[G_s(t - \theta_2 - \theta_1) G_r(t - \theta_3)] = 0$: $r \neq s$. Hence equation (3.18) becomes

$$E[\dot{s}_m \dot{q}_r] = -\varepsilon B_{rm} \int_0^\infty \dot{h}_m(\theta_1) \int_0^\infty \dot{h}_r(\theta_2) \int_0^\infty \dot{h}_r(\theta_3) E[G_r(t - \theta_2 - \theta_1) G_r(t - \theta_3)] \, d\theta_1 d\theta_2 d\theta_3 \qquad (3.19)$$

which may be further reduced to

$$E[\dot{s}_m \dot{q}_r] = -\varepsilon B_{rm} \int_0^\infty \dot{h}_m(\theta_1)\, E[\dot{q}_{r_o}(t-\theta_1)\dot{q}_{r_o}(t)]\, d\theta_1$$

$$= -\varepsilon B_{rm} \int_0^\infty \dot{h}_m(\theta_1) R''q_{r_o}(\theta_1) d\theta_1 \qquad (3.20)$$

for stationary random excitation (30). $R'(\theta)$ denotes the derivative of R with respect to θ. Hence the mean power flow per unit mass from the r acoustic modes into the m^{th} structural modes is given, to order ε^2, by

$$\Pi_m = \varepsilon^2 \sum_r B_{rm}^2 \int_0^\infty \dot{h}_m(\theta_1) R''q_{r_o}(\theta_1) d\theta_1 \qquad (3.21)$$

For the special case of acoustic white noise excitation of spectral density S_G the autocorrelation of the response of an acoustic mode is given, in the notation of equations (3.7), by (31)

$$Rq_{r_o}(\theta) = \frac{\pi S_G}{\beta_r \omega_r^2} e^{\frac{\beta_r \theta}{2}} \{\cos \sqrt{1-\alpha^2}\, \omega_r\theta + \frac{\beta_r/2\omega_r}{\sqrt{1-\alpha^2}} \sin \sqrt{1-\alpha^2}\, \omega_r\theta\} \qquad (3.22)$$
$$\theta>0$$

where $\alpha = (\beta_r/2\omega_r)$

and the impulse response function $h_r(\theta)$ is given by

$$h_r(\theta) = \frac{1}{\sqrt{1-\alpha^2}\, \omega_r} e^{-(\beta_r/2)} \{\sin \sqrt{1-\alpha^2}\, \omega_r\theta\} \qquad (3.23)$$

From (3.22), the first derivative of $Rq_{r_o}(\theta)$ is given by

$$R'q_{r_o}(\theta) = -\frac{\pi S_G}{\beta_r \omega_r \sqrt{1-\alpha^2}} e^{-(\beta_r/2)} \{\sin \sqrt{1-\alpha^2}\, \omega_r\theta\} \qquad (3.24)$$

so that

$$\frac{R'q_{r_o}(\theta)}{h_r(\theta)} = \frac{R''q_{r_o}(\theta)}{\dot{h}_r(\theta)} = -\frac{\pi S_G}{\beta_r} \qquad (3.25)$$

Hence the power flow equation (3.21) may be written

$$\Pi_m = -\varepsilon^2 \sum_r B_{rm}^2 \int_0^\infty \dot{h}_m(\theta)\dot{h}_r(\theta).\frac{\pi S_G}{\beta_r}d\theta \qquad (3.26)$$

Now $M\pi S_G/\beta_r$ is the mean energy of the uncoupled r^{th} acoustic mode when subject to a flat (white) acoustic source spectrum S_G. Evaluation of the integral in equation (3.26) leads to the following expression for power flow per unit mass

$$\Pi_m = \varepsilon^2 \sum_r B_{rm}^2 U_{r_o} \left[\frac{\beta_r\omega_m^2 + \beta_m\omega_r^2}{(\omega_r^2-\omega_m^2)^2 + (\beta_m+\beta_r)(\beta_r\omega_m^2+\beta_m\omega_r^2)}\right] \qquad (3.27)$$

where MUr_o is the mean energy of the r^{th} uncoupled acoustic oscillator. Note that this expression agrees to second order in ε with those of Lyon and Maidanik (equations (3.4) and (3.5) in this thesis). The total power flow per unit mass to the complete set of structural oscillators is of course given by the sum of the power flows to individual modes, i.e. $\sum_m \Pi_m$.

3.2.3 Exact power flow equations for two gyroscopically coupled oscillators

The approximate power flow equation (3.27) can be used to calculate the ratio of the mean energy of an indirectly driven oscillator m to that of a directly driven, but uncoupled, oscillator r. Newland (22) used the equations of motion of two stiffness coupled oscillators to

investigate the accuracy of the approximate result. He found that the accuracy depends upon the closeness of the 'blocked' natural frequencies of the oscillators, and the strength of the coupling. Strong coupling leads to a reduction in the energy of the directly driven oscillator, if its frequency is near that of the indirectly driven oscillator, which is not accounted for in the approximate theory.

The equations of motion of two gyroscopically coupled oscillators are used below to demonstrate that the power flow equation may be expressed in terms of the difference between the actual coupled oscillator energies, and that the factor of proportionality is the same as that in equation (3.27) for the uncoupled energy difference. A similar analysis to that of Newland's is used to calculate the actual oscillator energies.

Consider the coupled equations of motion of one structural mode m, subject only to a gyroscopic coupling force, and one acoustic mode r subject to a random acoustic source of spectral density S_G which is uniform in frequency,

$$\ddot{s}_m + \beta_m \dot{s}_m + \omega_m^2 s_m + \varepsilon B_{rm} \dot{q}_r = 0 \qquad (3.28a)$$

$$\ddot{q}_r + \beta_r \dot{q}_r + \omega_r^2 q_r - \varepsilon B_{rm} \dot{s}_m = G_r \qquad (3.28b)$$

The equations may be combined in the following forms, which are not independent,

$$\dddot{s}_m + \ddot{s}_m (\beta_r + \beta_m) + \ddot{s}_m(\omega_m^2 + \beta_m\beta_r + \omega_r^2 + \varepsilon^2 B_{rm}^2) + \dot{s}_m(\beta_r\omega_m^2 + \beta_m\omega_r^2)$$

$$+ s_m(\omega_r^2\omega_m^2) = - \varepsilon B_{rm} \dot{G}_r \qquad (3.29a)$$

and

$$\dddot{q}_r + \ddot{q}_r(\beta_r + \beta_m) + \dot{q}_r(\omega_r^2 + \beta_m\beta_r + \omega_m^2 + \varepsilon^2 B_{rm}^2) + q_r(\beta_m\omega_r^2 + \beta_r\omega_m^2)$$

$$+ q_r(\omega_m^2\omega_r^2) = \omega_m^2 G_r + \beta_m \dot{G}_r + G_r \qquad (3.29b)$$

By using the standard relationships for spectral densities (31) we obtain

$$E(\dot{s}_m)^2 = \varepsilon^2 B_{rm}^2 S_G \int_{-\infty}^{\infty} \omega^4 [H_1(i\omega)]^2 d\omega \qquad (3.30a)$$

and

$$E(\dot{q}_r)^2 = -S_G \int_{-\infty}^{\infty} \omega^2 [H_2(i\omega)]^2 d\omega \qquad (3.30b)$$

where $H_1(i\omega) = (\omega^4 - i\omega^3 P - \omega^2 Q - i\omega R + S)^{-1}$

and $H_2(i\omega) = (\omega_m^2 + i\omega\beta_m - \omega^2)(\omega^4 - i\omega^3 P - \omega^2 Q + i\omega R + S)^{-1}$

where $P = \beta_r + \beta_m$

$Q = \omega_r^2 + \beta_m\beta_r + \omega_m^2 + \varepsilon^2 B_{rm}^2$

$R = \beta_m\omega_r^2 + \beta_r\omega_m^2$

$S = \omega_m^2\omega_r^2$

Crandall and Mark (31) evaluate the integrals in equations (3.30) which lead to the following expressions for the average values of modal velocity and pressure.

$$E(\dot{s}_m^2) = \frac{\pi S_G \varepsilon^2 B_{rm}^2}{\beta_r\beta_m} \left[\frac{\beta_m\omega_r^2 + \beta_r\omega_m^2}{(\omega_m^2-\omega_r^2)^2 + (\beta_m + \beta_r)(\beta_m\omega_r^2+\beta_r\omega_m^2)(1+\varepsilon^2 B_{rm}^2/\beta_m\beta_r)} \right] \qquad (3.31a)$$

$$E(\dot{q}_r^2) = \frac{\pi S_G}{\beta_r}\left[\frac{(\omega_m^2 - \omega_r^2)^2 + ((\beta_m\omega_r^2 + \beta_r\omega_m^2)((\beta_m + \beta_r))(1+\varepsilon^2 B_{rm}^2/\beta_m(\beta_m+\beta_r))}{(\omega_m^2 - \omega_r^2)^2 + (\beta_r+\beta_m)(\beta_m\omega_r^2 + \beta_r\omega_m^2)(1 + \varepsilon^2 B_{rm}^2/\beta_m\beta_r)}\right]$$

(3.31b)

Note that the actual energy of the mode r, which is given by $ME(\dot{q}_r^2)$, differs little from the uncoupled energy, given by $M\pi S_G/\beta_r$, if $\varepsilon^2 B_{rm}^2/\beta_m\beta_r$, $\varepsilon^2 B_{rm}^2/\beta_m^2$ and $\varepsilon^2 B_{rm}^2/\beta_r^2 << 1$; in other words, the actual and uncoupled energies of the directly driven mode r differ little with light coupling, or with widely spaced natural frequencies ω_r and ω_m.

The net power flow from mode r to mode m is dissipated by mode m so that we may write

$$\Pi_m = \beta_m E(\dot{s}_m^2) = \frac{\pi S_G \varepsilon^2 B_{rm}^2}{\beta_r}\left[\frac{\beta_m\omega_r^2 + \beta_r\omega_m^2}{(\omega_m^2 - \omega_r^2)^2 + (\beta_m+\beta_r)(\beta_m\omega_r^2 + \beta_r\omega_m^2)(1+\varepsilon^2 B_{rm}^2/\beta_m\beta_r)}\right]$$

(3.32)

This expression may be compared with that of equation (3.27), where U_{r_o} is given by $\pi S_G/\beta_r$. Again the accuracy of the approximate expression is seen to depend upon the magnitude of the ratio $(\varepsilon^2 B_{rm}^2/\beta_m\beta_r)$ and the natural frequency separation. Figure 3.1 illustrates this comparison.

The power flow Π_m may also be expressed in terms of the difference between the actual mean energies of oscillators r and m. This energy difference is given by $E(\dot{q}_r^2) - E(\dot{s}_m^2) = E(\dot{q}_r)^2(1 - E(\dot{s}_m^2)/E(\dot{q}_r^2))$, which from equations (3.31) is given as

$$E(\dot{q}_r^2) - E(\dot{s}_m^2) = E(\dot{q}_r)^2\left[\frac{(\omega_m^2 - \omega_r^2) + (\beta_m\omega_r^2 + \beta_r\omega_m^2)(\beta_m + \beta_r)}{(\omega_m^2 - \omega_r^2)^2 + (\beta_m\omega_r^2 + \beta_r\omega_m^2)(\beta_m + \beta_r)(1+\varepsilon^2 B_m^2/\beta_m(\beta_r+\beta_m)}\right]$$

(3.33)

Substituting $E(\dot{q}_r^2)$ from equation (3.31b) we have

$$E(\dot{q}_r)^2 - E(\dot{s}_m^2) =$$

$$\frac{\pi S_G}{\beta_r}\left[\frac{(\omega_m^2 - \omega_r^2)^2 + (\beta_r\omega_m^2 + \beta_m\omega_r^2)(\beta_m + \beta_r)}{(\omega_m^2 - \omega_r^2)^2 + (\beta_r + \beta_m)(\beta_m\omega_r^2 + \beta_r\omega_m^2)(1 + \varepsilon^2 B_{rm}^2/\beta_m\beta_r)}\right] \quad (3.34)$$

Substituting into the denominator of equation (3.32) from equation (3.34) we obtain

$$\Pi_m = \varepsilon^2 B_{rm}^2 \left[E(\dot{q}_r^2) - E(\dot{s}_m^2)\right]\left[\frac{\beta_m\omega_r^2 + \beta_r\omega_m^2}{(\omega_m^2 - \omega_r^2)^2 + (\beta_r\omega_m^2 + \beta_m\omega_r^2)(\beta_m + \beta_r)}\right] \quad (3.35)$$

We thus see that the power flow is proportional to the difference between the actual coupled mean energies, and that the constant of proportionality is identical to that of the approximate expressions of equations (3.27) and (3.5). This result has previously been derived in a somewhat different manner by Scharton and Lyon (7). Figure 3.1 compares exact and approximate values of power flow between two modes as a function of $(\varepsilon B_{rm}/\beta)$. The interesting feature of acoustic coupling is that there is no energy associated with the coupling 'elements', as there is with inertial and elastic coupling. Hence blocked and uncoupled conditions are equivalent. This fact greatly eases acoustic power flow analysis.

It may easily be shown that the ratios of mean energy of the indirectly driven oscillator m to that of the oscillator r

as given by the approximate and the exact analyses, are respectively as follows:

$$\left(\frac{U_m}{U_{r_o}}\right)_{\text{approx.}} = \frac{\varepsilon^2 B_{rm}^2}{\beta_m} \left[\frac{\beta_m \omega_r^2 + \beta_r \omega_m^2}{(\omega_r^2 - \omega_m^2)^2 + (\beta_r + \beta_m)(\beta_m \omega_r^2 + \beta_r \omega_m^2)}\right] \tag{3.36}$$

$$\left(\frac{U_m}{U_r}\right)_{\text{exact}} = \frac{\varepsilon^2 B_{rm}^2}{\beta_m} \left[\frac{\beta_m \omega_r^2 + \beta_r \omega_m^2}{(\omega_r^2 - \omega_m^2)^2 + (\beta_r + \beta_m)(\beta_m \omega_r^2 + \beta_r \omega_m^2)(1+\varepsilon^2 B_{rm}^2/(\beta_m(\beta_m + \beta_r))}\right] \tag{3.37}$$

Again it is seen that the difference between the exact and approximate expressions depends upon the strength of the coupling coefficient as compared with the modal damping coefficient and also on the closeness of the natural frequencies. The asymptotic value of the exact ratio of energies as $\varepsilon B_{rm}/\beta$ becomes large is unity; this is a condition of equipartition of energy.

3.2.4 Multimode Power Flow

An exact multimode analysis would be exceedingly laborious (22, 7). Kakar (24) has treated the case of three coupled oscillators and has demonstrated that in most practical cases, where the oscillator frequencies are not expected to be very close together, use of the approximate power flow expressions leads to errors of the order of 1%. However even this extension to only three modes involved extremely tedious calculations and lengthy expressions. Fortunately in the following treatment of the acoustic excitation of containing vessels it is found that in many practical

situations the problem effectively reduces to one involving a set of effectively singly coupled oscillators by virtue of the spatial and frequency selectivity of the power flow proportionality constant. Hence in much of the rest of the work the total power flow between a set of acoustic oscillators and a set of structural oscillators is expressed as a summation over mode pairs of the power flow between individual pairs, each oscillator pair power flow equation being given by equation (3.35) in terms of the difference between actual coupled mean energies.

3.2.5 Power Flow Between a Point-Excited Panel and a Fluid

Measurements are often made of the sound power radiated into a fluid from a panel which is subjected to mechanical excitation at a single point. In this case the generalised forces on the plate modes cannot be considered to be statistically independent. For this reason it is not immediately obvious whether or not the Radiation Resistance measured in this manner corresponds to that calculated, through the previous response equations, from panel response to random acoustic excitation of the fluid. In the latter case the degree of independence of the acoustic mode generalised sources will depend upon the means of acoustic excitation (3.19); in other words, on the type of source. For instance, the jet noise excitation used in the present work is more likely to give independent modal excitations than, say, a loudspeaker, which is approximately a point source. The following perturbation analysis was made in order to try to discover those characteristics of a coupled system which could cause the results of measurements using statistically independent and dependent force inputs to differ significantly in a practical situation.

3.2.5.1 Perturbation analysis for a point excited panel

The analysis closely follows that of section 3.2.2 but in this case it is assumed that the acoustic sources G_r are zero and that the only inputs are the mechanical forces F_m.

The rate of energy input per unit panel mass to the r^{th} acoustic mode from all the structural modes is given by

$$\pi_r = \sum_m \varepsilon B_{mr} \dot{s}_m \dot{q}_r \tag{3.38}$$

Comparison with equation (3.8) shows that $B_{rm} = B_{mr}$ if the coupling is conservative. The time average power flow is given by

$$\Pi_r = E(\pi_r) = \sum_m \varepsilon B_{mr} E[\dot{s}_m \dot{q}_r] \tag{3.39}$$

From equations (3.11), with $G_r = 0$, we have

$$\ddot{s}_{m_o} + \beta_m \dot{s}_{m_o} + \omega_m^2 s_{m_o} = F_m \tag{3.40a}$$

$$\ddot{q}_{r_o} + \beta_r \dot{q}_{r_o} + \omega_r^2 q_{r_o} = 0, \tag{3.40b}$$

$$\ddot{s}_{m_1} + \beta_m \dot{s}_{m_1} + \omega_m^2 s_{m_1} = 0 \tag{3.40c}$$

$$\ddot{q}_{r_1} + \beta_r \dot{q}_{r_1} + \omega_r^2 q_{r_1} = B_{mr} \dot{s}_m \tag{3.40d}$$

$$\begin{aligned} s_{m_1}(t) = s_{m_3}(t) = s_{m_5}(t) = \ldots = 0 \\ q_{r_o}(t) = q_{r_2}(t) = q_{r_4}(t) = \ldots = 0 \end{aligned} \tag{3.41}$$

Hence $$s_m(t) = s_{m_o}(t) + \varepsilon^2 s_{m_2}(t) + \ldots \tag{3.42a}$$

and $$q_r(t) = q_{r_1}(t) + \varepsilon^3 q_{r_3}(t) + \ldots \tag{3.42b}$$

Solutions of equation (3.40d) and (3.40a) are

$$q_{r_1}(t) = \sum_n B_{nr} \int_0^\infty h_r(\theta)\dot{s}_{n_o}(t - \theta)d\theta \tag{3.43}$$

$$s_{m_o}(t) = \int_0^\infty h_m(\theta)F_m(t - \theta)d\theta \tag{3.44}$$

where the impulse response functions $h(\theta)$ are defined as before.

$$\text{Thus} \quad q_{r_1}(t) = \sum_n B_{nr} \int_0^\infty h_r(\theta_1) \int_0^\infty \dot{h}_n(\theta_2)F_n(t - \theta_1 - \theta_2)d\theta_1 d\theta_2 \tag{3.45}$$

$$\text{and} \quad E[\dot{s}_m\dot{q}_r] = \varepsilon\sum_n B_{nr} \int_0^\infty \dot{h}_r(\theta_1)\int_0^\infty \dot{h}_n(\theta_2)\int_0^\infty \dot{h}_m(\theta_3)d\theta_1 d\theta_2 d\theta_3\, E[F_n(t - \theta_2 - \theta_1)F_m(t - \theta_3)] + O(\varepsilon^3).. \tag{3.46}$$

When the force applied to the structure has a white noise nature the expectation in equation (3.46) is given by

$$E[F_n(t - \theta_2 - \theta_1)F_m(t - \theta_3)] = M^{-2}(\varepsilon_m\varepsilon_n)^{\frac{1}{2}}\, \delta((\theta_2 + \theta_1) - \theta_3) \times 2\pi S_{f_s}(\omega) \int_S \phi_m(\underline{x})\delta(\underline{x} - \underline{x}_o)d(\underline{x}) \int_S \phi_n(\underline{x})\delta(\underline{x} - \underline{x}_o)d(\underline{x}) \tag{3.47}$$

where $S_{f_s}(\omega)$ is the uniform power spectral density of the input force, $\underline{x}_o$ is the position vector of the applied force, and δ is the Dirac delta function. Equation (3.46) therefore becomes

$$E[\dot{s}_m\dot{q}_r] = \varepsilon \sum_n B_{nr} \int_0^\infty \dot{h}_r(\theta_1) \int_0^\infty \dot{h}_n(\theta_2)\dot{h}_m(\theta_1 + \theta_2)d\theta_1 d\theta_2 \times 2\pi S_{f_s}(\omega)M^{-2}(\varepsilon_m\varepsilon_n)^{-\frac{1}{2}} \phi_m(\underline{x}_o)\phi_n(\underline{x}_o) \tag{3.48}$$

It will be noted that, because of the nature of the input force, the

expectation consists of a sum over all the structural modes, whereas in the case of statistically independent excitation only functions of the modes m and r would appear. An important feature of equation (3.48) is the presence of the mode shape factors evaluated at $\underline{x}_o$, the point of application of the force. This feature will be further discussed later in this section.

The integrals in equation (3.48) appear innocuous enough but in fact they involve exceedingly lengthy algebraic operations which are better suited to an accountant than to an engineer. Some details of the calculation are given in Appendix IV which will give some appreciation of the immense book keeping task involved. The result of these calculations is as follows:

$$\int_0^\infty \dot{h}_r(\theta_1)\int_0^\infty \dot{h}_n(\theta_2)\,\dot{h}_m(\theta_1+\theta_2)\,d\theta_1 d\theta_2 = \gamma(m,n,r) =$$

$$\frac{(\beta_m\omega_n^2+\beta_n\omega_m^2)(\beta_m\omega_r^2+\beta_r\omega_m^2)-\omega_m^2(\omega_m^2-\omega_r^2)(\omega_m^2-\omega_n^2)}{\left[(\omega_m^2-\omega_n^2)^2+(\beta_m+\beta_n)(\beta_m\omega_n^2+\beta_n\omega_m^2)\right]\left[(\omega_m^2-\omega_r^2)^2+(\beta_m+\beta_r)(\beta_r\omega_m^2+\beta_m\omega_r^2)\right]} \tag{3.49}$$

This expression bears close resemblance to the expression in equation (3.27). Indeed the denominator and numerator contain products of two expressions which are identical in form to those of equation (3.27). The important difference lies in the second term of the numerator, the magnitude of which depends upon the difference of natural frequencies of the structural and acoustic modes m and r and that of the structural modes m and n.

Substitution of the evaluated integral of equation (3.49) into

equation (3.48), and use of equation (3.39), leads to the following expression for the power flow into acoustic mode r from the structural modes,

$$\Pi_r = \varepsilon^2 2\pi S_f(\omega) M^{-2} \sum_m B_{mr} \sum_n B_{nr} \gamma(m, n, r)(\varepsilon_m \varepsilon_n)^{-\frac{1}{2}} \phi_m(\underline{x}_o)\ \phi_n(\underline{x}_o) \qquad (3.50)$$

where $\gamma(m, n, r)$ represents the integral of equation (3.49), which is a function of the natural frequencies and dampings of modes m, n and r.

3.2.5.2 Statistically independent forces

With statistically independent modal forces only the terms with m = n would be non-zero. In that case $\gamma(m, n, r)$ is given by

$$\gamma(m, n, r) = \frac{(\beta_m \omega_r^2 + \beta_r \omega_m^2)}{2\beta_m[(\omega_m^2 - \omega_r^2)^2 + (\beta_m + \beta_r)(\beta_r \omega_m^2 + \beta_m \omega_r^2)]} \qquad (3.51)$$

Now the mean energy per unit mass of the m^{th} uncoupled mode subject to generalised random force F_m, with a flat spectrum of value $S_{F_m}(\omega)$, is given by

$$U_{m_o} = S_{F_m}(\omega)/\beta_m = \pi S_f(\omega)\phi_m(\underline{x}_o)/(M^2 \varepsilon_m)\beta_m \qquad (3.52)$$

Equations (3.46) et seq. give the power flow per unit mass in the case of statistically independent input forces as

$$\Pi_r = \varepsilon^2 \sum_m B_{mr}^2\, U_{m_o} \left[\frac{\beta_r \omega_m^2 + \beta_m \omega_r^2}{(\omega_r^2 - \omega_m^2)^2 + (\beta_m + \beta_r)(\beta_r \omega_m^2 + \beta_m \omega_r^2)} \right] \qquad (3.53)$$

This equation is of exactly the same form as equation (3.27), the only difference between them being that U_{m_o} replaces U_{r_o}.

3.5.2.3 Two structural modes subject to statistically dependent forces

In the case of statistically related generalised forces, F_m, the situation is not so simple. In the extreme case of the existence of only two structural modes m and n, which have identical frequencies and dampings ($\omega_m = \omega_n$; $\beta_m = \beta_n$), but which have different mode shapes, equation (3.49) gives

$$\gamma(m, n, r) = \frac{2\beta_m\omega_m^2(\beta_m\omega_r^2 + \beta_r\omega_m^2)}{4\beta_m^2\omega_m^2[(\omega_m^2 - \omega_r^2)^2 + (\beta_m + \beta_r)(\beta_r\omega_m^2 + \beta_m\omega_r^2)]} \tag{3.54}$$

This is the same expression as for statistically independent modal forces. The power flow per unit mass from these two modes into mode r is given by

$$\Pi_{r(m,n)} = \varepsilon^2 2\pi S_{f_s}(\omega) M^{-2} \gamma(m,m,r) \left[B'^2_{mr}\varepsilon_m^{-1}\phi_m^2(\underline{x}_o) + B_{nr}^2\varepsilon_n^{-1}\phi_n^2(\underline{x}_o) + 2B_{mr}B_{nr}(\varepsilon_n\varepsilon_m)^{-\frac{1}{2}}\phi_m(\underline{x}_o)\phi_n(\underline{x}_o)\right] \tag{3.55}$$

or

$$\Pi_{r(m,n)} = \varepsilon^2\{\left[B_{mr}^2 U_{m_o} + B_{nr}^2 U_{n_o} + B_{mr}B_{nr}\left(U_{m_o}\frac{\phi_n(\underline{x}_o)}{\phi_m(\underline{x}_o)}\left(\frac{\varepsilon_n}{\varepsilon_m}\right)^{\frac{1}{2}} + U_{n_o}\frac{\phi_m(\underline{x}_o)}{\phi_m(\underline{x}_o)}\left(\frac{\varepsilon_m}{\varepsilon_n}\right)^{\frac{1}{2}}\right]\right.$$

$$\left. \times \left[\frac{\beta_r\omega_m^2 + \beta_m\omega_r^2}{(\omega_r^2 - \omega_m^2)^2 + (\beta_m + \beta_r)(\beta_r\omega_m^2 + \beta_m\omega_r^2)}\right]\right. \tag{3.56}$$

The power flow from these two modes to acoustic modes r is therefore different from that in the case of statistically independent forces. It cannot immediately be determined whether or not the power flow is greater or less than that in the latter case because the signs of the 'cross terms' in equation (3.56) depend upon the relative signs of $\phi_m(\underline{x}_o)$ and $\phi_n(\underline{x}_o)$ and of B_{mr} and B_{nr}.

3.2.5.4 The general case

Consideration of one of the terms of the double summation of equation (3.50) in the general case shows that if any two structural modes, m and n, and an acoustic mode r, are sufficiently close in natural frequency to simultaneously satisfy the conditions,

$$2|\omega_m - \omega_n| < (\beta_m + \beta_n); \quad 2|\omega_m - \omega_r| < (\beta_m + \beta_r) \tag{3.57}$$

then that term reduces to the following approximate form

$$\Pi_{r(m,n)} \simeq \varepsilon^2 2\pi S_{f_s}(\omega) M^{-2} \frac{B_{mr}B_{nr}(\phi_m(\underline{x}_o)\phi_n(\underline{x}_o))}{(\beta_m + \beta_n)(\beta_m + \beta_r)(\varepsilon_n \varepsilon_m)^{\frac{1}{2}}} . \tag{3.58}$$

If it is assumed that the structural mode damping coefficients are similar, i.e. $\beta_m \simeq \beta_n = \beta_M$, then equation (3.58) becomes

$$\Pi_{r(m,n)} = \varepsilon^2 \frac{B_{mr}B_{nr}}{(\beta_M + \beta_r)} \left(\frac{\phi_n(\underline{x}_o)}{\phi_m(\underline{x}_o)} \left(\frac{\varepsilon_m}{\varepsilon_n}\right)^{\frac{1}{2}}\right) U_{m_o} \tag{3.59a}$$

or

$$\Pi_{r(m,n)} = \varepsilon^2 \frac{B_{mr}B_{nr}}{(\beta_M + \beta_r)} \left(\frac{\phi_m(\underline{x}_o)}{\phi_n(\underline{x}_o)} \left(\frac{\varepsilon_n}{\varepsilon_m}\right)^{\frac{1}{2}} U_{n_o}\right) \tag{3.59b}$$

Consequently it is possible to classify modal interactions in terms of

natural frequency proximity in a similar manner to that discussed in section 3.2.1.

If we restrict the consideration of power flow to those mode triplets which satisfy the conditions of expression (3.57), then the total power flow per unit mass to an acoustic mode may be written as

$$\Pi_{r'} = \frac{\varepsilon^2}{(\beta_M + \beta_r)} \left\{ \sum_{m'} B^2_{m'r'} U_{m'_o} + \sum_{\substack{m',n' \\ m' \neq n'}} B_{m'r'} B_{n'r'} \left(\frac{\phi_{n'}(\underline{x}_o)}{\phi_{m'}(\underline{x}_o)} \right) U_{m'_o} \right\} \tag{3.60}$$

where it is assumed that $\varepsilon_m = \varepsilon_n$ and the prime refers to modes which satisfy the frequency proximity condition stated above. The total power flow per unit panel mass to the fluid is given by $\sum_r \Pi_{r'}$. Of course, in the multimode case, the power flow can only be evaluated if the spatial coupling factors εB can be calculated for the modes of the coupled systems.

As with the two mode case previously discussed, the factor $(\phi_n(\underline{x}_o)/(\phi_m(\underline{x}_o))$, which is the ratio of the modal amplitudes at the point of application of the force, appears in the cross terms. The contribution of the cross terms can only be assessed by reference to specific coupled systems. As will be seen later, in section 4.7, the variation in magnitude of the spatial coupling factors εB from mode to mode, and the consequent dominance of the total power flow by certain types of mode triplets, determines the contribution of the cross terms to the total power flow. However it can be seen from the expression for γ in (3.49) that, for non-proximate mode coupling, the average difference between structural mode natural frequencies $(\omega_m - \omega_n)$, will affect the contribution of the cross terms through the second term of the numerator.

It would also appear from the presence of the summation over n in the expression (3.60) which distinguishes this expression from that for statistically independent forces, that structures of high modal density, and high damping, with many modes which satisfy the frequency proximity criterion $2|\omega_m - \omega_n| < (\beta_m + \beta_n)$, would be more sensitive to the degree of statistical dependence of the modal generalised forces. However, sophisticated statistical arguments may be advanced in some future work to refute these tentative suggestions. It might be noted here that the value of the cross term in equation (3.58), when averaged over the surface of the panel, is zero by virtue of the condition of orthogonality between normal modes.

CHAPTER IV

APPLICATION OF COUPLED OSCILLATOR THEORY TO A PANEL-BOX SYSTEM

In the following chapter application of the exact two-mode power flow equation to the case of coupling between two multimode systems is considered in terms of the range of magnitude of the individual mode pair coupling factors. The systems consist of a rectangular panel and an adjacent fluid in a rectangular box. Under circumstances where the coupling factor is large for only relatively few of the available mode pairs, the problem can be considered to reduce substantially to one of power flow between a number of independent mode pairs. The response of one system to direct excitation of the other can then be written in terms of a summation over the dominant mode pair coupling factors. This summation is expressed as a parameter known as the Radiation Resistance (R_{rad}), (cf. ref. 16). Panel response to broad band sound in the box is derived in terms of R_{rad}. The rest of the chapter is concerned with statistical and computed evaluations of the Radiation Resistance for a panel-box system and also with an assessment of the affect on power flow of statistical dependence of modal forces under point excitation of the panel.

4.1 The Response Equation

The relevant mode pair power flow equation for acoustic excitation of a containing structure is

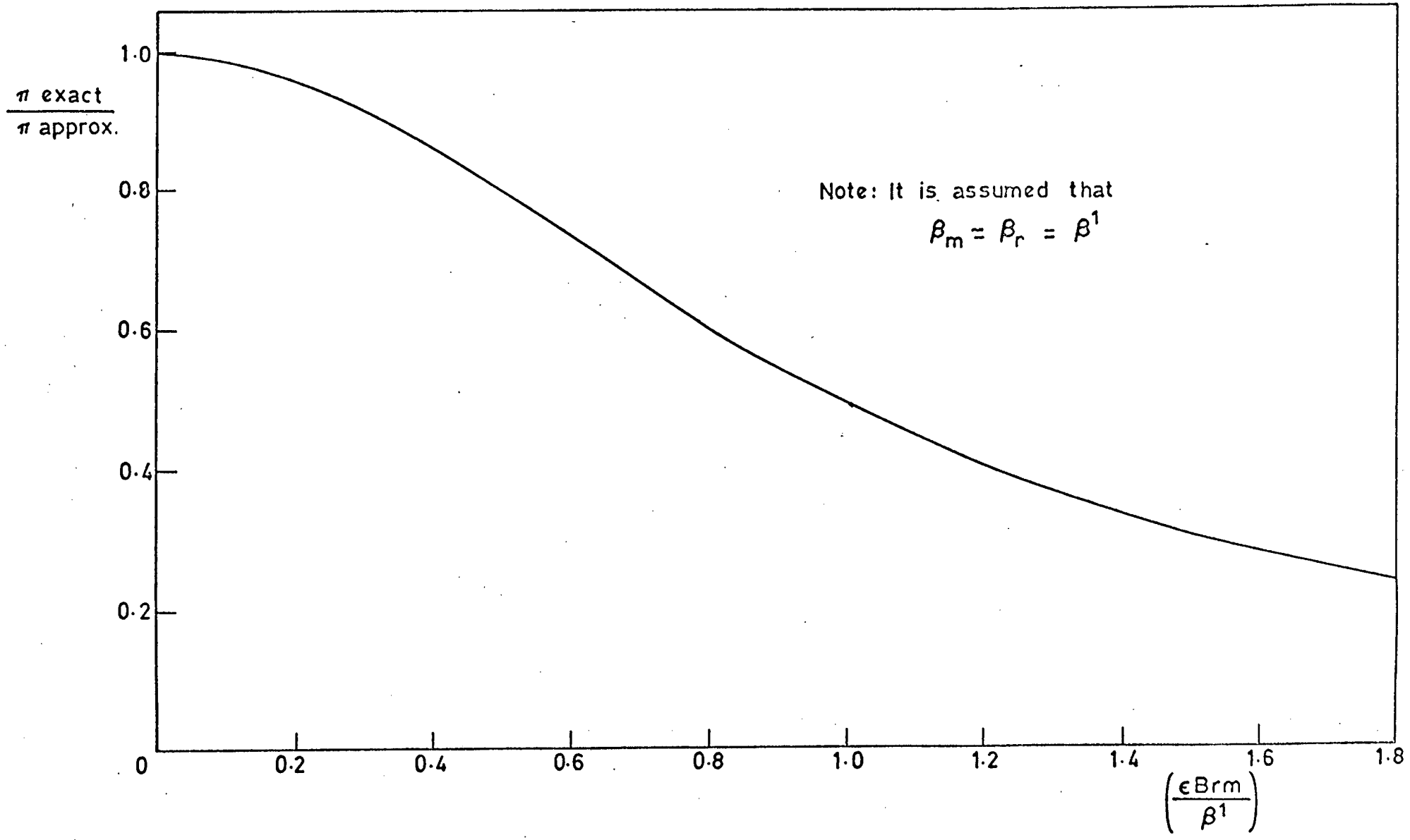

Fig. 3·1 Ratio of energy flow between two oscillators as calculated by exact and approximate theories.

$$\Pi_{mr} = g_{mr}(U_r - U_m) \qquad (4.1)$$

where g_{mr} is defined by equation (3.5) and U is the mean coupled modal energy. B_{mr}, rather than εB_{mr}, is used for the coupling coefficient in all future work; it is defined by equation (3.2).

Ungar (21) suggests that this form of power flow equation may be generalised for use with two sets of coupled oscillators, provided that the individual mode excitation forces are statistically independent, and that the coupling factors g_{mr} are all approximately equal. Although Ungar's analysis is not considered to be rigorous it is likely that some form of classification of mode pairs into groups according to the magnitude of the individual coupling factors could lead to a useful generalisation of equation (4.1) in certain practical circumstances.

For instance, the following analyses of geometrically regular panel-box and cylinder systems show that the coupling factors can be classified into four groups on the basis of their magnitudes.

One group, which is associated with acousto-structural mode pairs which are well coupled by virtue of both natural frequency proximity and good matching of wavelength components, contains coupling factors which are of an order greater than those of the other three groups. It is also found that, for small fluid volumes, these well coupled modes occur on average in single pairs; well coupled triplets, quadruplets, etc. are the exception rather than the rule, (see sections 4.5.1 and 4.5.2).

Under these circumstances it seems reasonable to (a) independ-

ently sum the power flow between well coupled mode pairs by virtue of their occurrence in independent pairs; (b) independently sum the power flow between the poorly coupled mode pairs by virtue of the smallness of the corresponding factors (B_{rm}/β) and application of the approximate power flow equation.

The mode set to mode set power flow equation is therefore written as

$$\Pi_{mr} = \sum_{m,r} g_{mr}(U_r - U_m)$$

It is of course realised that the use of a sum of independent terms does not take into account the fact that the power flow from a poorly coupled acoustic mode into a structural mode, which itself is well coupled to another acoustic mode, will be made even smaller by the fact that the energy of the structural mode is raised above its approximate uncoupled value. Similarly the reduction of energy level of a well coupled acoustic mode will affect the power flow to structural modes to which it is poorly coupled. These effects, however, will tend to further reduce the contribution of the poorly coupled mode pairs to the total power flow.

If it is further assumed that the acoustic modes are all directly excited to similar uncoupled energy levels, which can be shown to be reasonable for volume distributed random acoustic sources such as jet noise (32), then we may write

$$\Pi_{mr} = \sum_{n=1}^{4} \{ \langle U_r \rangle_n - \langle U_m \rangle_n \} \sum_{m,r(n)} g_{mr} \qquad (4.2)$$

where n refers to the mode classification which is based upon the magnitude of the coupling factors g_{mr}. The brackets < > denote modal average.

It is shown later that for the geometrically regular systems investigated, one class of g_{mr} is such that the summation over the coupled accustic and structural modes in that class greatly exceeds those of the other three classes. With primarily singly coupled mode pairs, and with corresponding values of (B_{mr}/β) of the order of unity or less, equation (3.31b) shows that the actual energy of the acoustic modes which are well coupled to structural modes will not be significantly less than that of modes which are poorly coupled. In addition, equation (3.37) shows that, for close natural frequencies, the actual energy ratio U_m/U_r is less than 0.5 for values of (B_{rm}/β) less than unity. A comparison between two-mode power flows based upon the approximate and exact theories, in terms of the magnitude of B_{mr}/β, is shown in Figure 3.1.

It may therefore be reasonably assumed that the term in equation (4.2) which represents that class of mode pair which has the largest coupling factor will dominate the total power flow when (B_{rm}/β) is less than unity, because the corresponding modal average energy difference will not be significantly smaller than that of the poorly coupled modes. In other words an assessment of the number and type of modes which dominate the total power flow can be based entirely upon a consideration of the magnitude of the coupling coefficients. Hence, we may write

$$\Pi_{mr} \simeq \{\langle U_r \rangle_1 - \langle U_m \rangle_1\} \sum_{m,r(1)} g_{mr} \qquad (4.3)$$

where the subscript 1 refers to the class of modes having maximum g_{mr}.

It has been shown in equation (3.6) that power flow is only significant between oscillators which have natural frequencies differing by no more than half the sum of their half power bandwidth. For all practical purposes this means that the power flow may be considered in independent frequency bands of width much greater than an individual modal bandwidth, provided that there are sufficient modes in the band to render modes near the band limits of little consequence (33). If we write the average number of well coupled mode pairs in a band of width $\Delta\omega$ as N_{rm}, the average number of acoustic modes in a band as N_r, and the average number of structural modes in a band as N_s, then equation (4.3) may be written as

$$\Pi_{mr} \simeq \{\langle\bar{p}^2\rangle V/N_r\rho c_o^2 - M\langle\bar{v}^2\rangle/N_{rm}\} \sum_{m,r(1)} g_{mr} \qquad (4.4)$$

where p is the acoustic pressure in the fluid, v is the normal panel velocity and the form $\langle\bar{}\rangle$ denotes a space and time average. $\bar{p}^2/\rho c_o^2$ is the energy density of the acoustic field. It has been assumed here that the number of well coupled structural modes is equal to the total number of well coupled mode pairs. It will be seen later, from a consideration of mode coupling structures, that this is the normal situation in small fluid volumes (Section 4.4). Equating this power flow to the power dissipated by the mechanical damping of the structural modes, and expressing N_r in terms of the acoustic modal density of a volume V we have,

$$\langle\beta_m\rangle_1\langle\bar{v}^2\rangle = \{[(\langle\bar{p}^2\rangle V)/(\omega^2 V/2\pi^2 c_o^3)\Delta\omega](\rho c_o^2)^{-1} - M\langle\bar{v}^2\rangle/N_{rm}\} \sum_{m,r(1)} g_{mr}$$

from which the ratio of space averaged mean square velocity to space averaged mean square pressure is given by

$$\frac{\langle\bar{v}^2\rangle}{\langle\bar{p}^2\rangle} = \frac{2\pi^2 c_o n_s(\omega)}{\omega^2 M\rho}\left[\frac{R_{rad}}{\langle R_{mech}\rangle_1 + (N_s/N_{rm})R_{rad}}\right] \qquad (4.5)$$

$R_{rad} = (M/N_s)\sum_{m,r(1)} g_{mr}$, $\langle R_{mech}\rangle_1 = \langle\beta_m\rangle_1 M$ and $n_s(\omega)$ is the modal density of the structure. On the basis of arguments set out above the sum $\sum_{m,r(1)} g_{mr}$ will be very nearly as great as the sum over all modes, $\sum_{m,r} g_{mr}$.

R_{rad} is known as the Radiation Resistance (16) and $\langle\beta_m\rangle_1$ is the modal average mechanical damping coefficient. Equation (4.5) is similar to equation (9.33) of reference (16) except for the ratio N_s/N_{rm} which appears in the denominator. This is the result of the difference between the assumption of uniform modal coupling implied in reference (16), and the present restriction of significant coupling to relatively few of the available mode pairs. Much of the following sections is devoted to an evaluation of R_{rad}.

4.2 The Model

The system analysed in this chapter consists of a thin elastic rectangular panel of uniform thickness and density, which forms one complete wall of an otherwise rigid rectangular box. A diagram is shown in Figure 4.1. The coupled multimode systems are the panel and the

fluid in the box. The object of the analysis is to estimate the response of the panel to broad band sound in the fluid, and to compare this response with that to a diffuse sound field, for which theoretical and experimental data exist (26).

If the panel is assumed to be simply supported the eigenfunctions of the fluid and the panel are given respectively as follows.

$$\psi_r(x,y,z) = \cos(\tfrac{p\pi x}{a})\cos(\tfrac{q\pi y}{b})\cos(\tfrac{r\pi z}{c}) \qquad (4.6a)$$

$$\phi_m(x,y) = \sin(\tfrac{m\pi x}{a})\sin(\tfrac{n\pi y}{b}) \qquad (4.6b)$$

Substitution of these eigenfunctions into equation (3.2) for B_{rm} gives

$$B_{rm} = (c_o^2\rho/V\varepsilon_r\varepsilon_m M)^{\frac{1}{2}}(-1)^r\left[\frac{ma}{p^2\pi}\{\frac{(-1)^{m+p}-1}{1-(m/p)^2}\}\right]\left[\frac{nb}{q^2\pi}\{\frac{(-1)^{n+q}-1}{1-(n/q)^2}\}\right] : \begin{matrix} m\neq p \\ n\neq q \end{matrix}$$

$$B_{rm} = 0 \qquad : (m+p) \text{ even} \quad \text{or } (n+q) \text{ even} \qquad (4.7)$$

Consideration of B_{rm} for a given panel mode order (m, n) shows that B_{rm} is an absolute maximum when $p = m \pm 1$ and $q = n \pm 1$ simultaneously. In these cases $B_{rm} \simeq (c_o^2\rho/V\varepsilon_r\varepsilon_m M)^{\frac{1}{2}}(ab/\pi^2)$ for $m, n \geq 3$. With $p = m \pm 1$ and $q = n \pm 3$, or $p = m \pm 3$ and $q = n \pm 1$, $B_{rm} \simeq (c_o^2\rho/V\varepsilon_r\varepsilon_m M)^{\frac{1}{2}}(ab/3\pi^2)$, and so on. Thus we see that g_{mr} will depend upon spatial matching of acoustic and structural modes, as well as on natural frequency proximity.

We can investigate the conditions under which the various degrees of coupling are possible by reference to Figures 4.2 and 4.3.

These are wavenumber, or frequency space, diagrams for sub-critical and supercritical panel frequencies. Because flexural waves are dispersive there is a unique frequency for every uniform elastic panel at which free waves travel with the same speed c_B as sound waves in the adjacent fluid. This frequency is called the critical frequency, f_c, and is given by $c_B^2 = c_o^2 = 1.8hf_cC_L$, where h is the panel thickness and C_L is the speed of longitudinal waves in the panel material. For example the critical frequency of a $\frac{1}{4}$ in. thick steel panel in air at N.T.P. is 2000 Hz; that for an $\frac{1}{8}$ in. thick panel is 4000 Hz, and so on.

The circular arc in the x,y plane of Figures 4.2-4.4 is the locus of the wavenumber vector k_p which corresponds to a constant panel frequency. At panel mode natural frequencies k_p is related to the simply supported panel mode order (m,n) by the relationship $k_p^2 = (m\pi/a)^2 + (n\pi/b)^2 = k_x^2 + k_y^2$. A typical mode point is shown in Figures 4.2 and 4.3. The relationship is not so simple for other boundary conditions as will be seen later.

For each panel mode it is necessary first to estimate the average number of acoustic modes having natural frequencies sufficiently close to the natural frequency of the panel mode to obey the frequency proximity condition of equation (3.6a). The acoustic wavenumber k_r corresponding to the acoustic mode order p, q, r is given by $k_r^2 = (p\pi/a)^2 + (q\pi/b)^2 + (r\pi/c)^2$. The lattice points of these acoustic modes are seen to lie within the segment of spherical shell of mean radius k_r, given by $\omega_r = k_rc_o = \omega_m = k_pc_B = k_pc_o(f_m/f_c)^{\frac{1}{2}}$. Hence $k_r = k_p(f_m/f_c)^{\frac{1}{2}}$. In the following sections the subscript m is dropped from f_m; the symbol f is used to denote the frequency of typical

panel modes in the frequency band of interest. The thickness of the shell segment is given by $\Delta k_r = (\beta_m + \beta_r)/c_o$, so that all acoustic modes lying within the shell are sufficiently close in natural frequency to the typical structural mode to obey equation (3.6a).

4.3 The Simply Supported Panel

4.3.1 Subcritical frequency range

A further selection of acoustic modes to which the typical panel mode is well coupled is made by reference to equation (4.7) et seq. Consideration of Figure 4.2 shows that the condition for absolute maximum B_{rm}, namely $p = m \pm 1$ and $q = n \pm 1$ simultaneously, cannot be achieved at sub-critical frequencies because $k_r < k_p$. The best subcritical coupling that can be achieved is with either $p = m \pm 1$ or $q = n \pm 1$. These conditions are necessarily associated respectively with the relationships $q \lesssim n$ and $p < m$. Figure 4.2 shows the acoustic modes given by $p = m + 1$, $q < n$.

Acoustic-structural mode pairs which both obey the frequency proximity condition (eq. 3.6a) and also have maximum possible coupling by virtue of wavelength component matching, (in one direction only at subcritical frequencies), are described as enjoying maximum proximate coupling; they may also be said to be well coupled. These mode pairs form the group referred to in section 4.1 as the dominant group.

With $p = m \pm 1$, $q = \varepsilon n$ and $p = \varepsilon m$, $q = n \pm 1$, where $\varepsilon < 1$, B_{rm} is given by

$$B_{rm} = (\rho c_o^2/V\varepsilon_r\varepsilon_m M)^{\frac{1}{2}} \left(\frac{a}{\pi}\right)\left(\frac{2b}{n\pi}\right)/(1 - \varepsilon^2) \quad : n(\varepsilon + 1) \text{ odd}$$

$$= 0 \qquad\qquad : n(\varepsilon + 1) \text{ even} \qquad (4.8a)$$

$$\text{and} \quad B_{rm} = (\rho c_o^2/V\varepsilon_r\varepsilon_m M)^{\frac{1}{2}}\left(\frac{b}{\pi}\right)\left(\frac{2a}{m\pi}\right)/(1 - \varepsilon^2) \quad : m(\varepsilon + 1) \text{ odd}$$

$$= 0 \qquad\qquad : m(\varepsilon + 1) \text{ even} \qquad (4.8b)$$

At frequencies below 25% of the critical frequency, $\varepsilon^2 << 1$ and equations(4.8) simplify. Subcritical coupling for $(m - 1 < p < m + 1: q = \varepsilon n)$ and $(n - 1 < q < n + 1: p = \varepsilon m)$ can be ignored because for any one structural mode they are no more in number than the set having maximum proximate coupling and their coupling constants g_{mr} $(\propto B_{mr}^2)$ are at most 10% of the values given in equations (4.8).

Since the parameter $(B_{rm}/\beta)^2$ is an important parameter by which the strength of the coupling may be gauged it is interesting to briefly consider its form. It is of course the largest values corresponding to maximum proximate coupling which are of interest. Except very near the critical frequency, the factor $(1 - \varepsilon^2)$ in equations (4.8) can be ignored in estimating the magnitude of maximum B_{rm} at subcritical frequencies. Also it may be assumed that $k_p \simeq (m\pi/a)$ for $p = m \pm 1$ and $k_p \simeq (n\pi/b)$ for $q = n \pm 1$. Hence from equation (4.8) we have

$$B_{rm} \simeq \left(\frac{\rho c_o^2}{V\varepsilon_r\varepsilon_m M}\right)^{\frac{1}{2}} \frac{2a}{\pi k_p} = \left(\frac{\rho c_o^2}{abc\varepsilon_r\varepsilon_m abh\rho_s}\right)^{\frac{1}{2}} \frac{a\sqrt{1.8hC_L}}{\pi^2\sqrt{f}} \quad : \quad p = m \pm 1$$

and

$$B_{rm} \simeq \left(\frac{\rho c_o^2}{V\varepsilon_r\varepsilon_m M}\right)^{\frac{1}{2}} \frac{2b}{\pi k_p} = \left(\frac{\rho c_o^2}{abc\varepsilon_r\varepsilon_m abh\rho_s}\right)^{\frac{1}{2}} \frac{b\sqrt{1.8hC_L}}{\pi^2\sqrt{f}} \quad : \quad q = n \pm 1$$

These expressions reduce respectively to

$$B_{rm} = \left(\frac{1.8\rho c_o^2 c_L}{c\varepsilon_r\varepsilon_m\rho_s}\right)^{\frac{1}{2}}\left(\frac{1}{b\pi^2 f^2}\right) \quad : \quad p = m \pm 1$$

and

$$B_{rm} = \left(\frac{1.8\rho c_o^2 c_L}{c\varepsilon_r\varepsilon_m\rho_s}\right)^{\frac{1}{2}}\left(\frac{1}{a\pi^2 f^2}\right) \quad : \quad q = n \pm 1.$$

It is thus seen that the magnitude of $(B_{rm}/\beta)^2$ depends, for given damping in a rectangular system, upon the ratio of the densities of the fluid and panel, upon the square of the speed of sound in the fluid and upon the first power of the speed of sound in the structure; it is inversely proportional to the frequency and varies with the typical length L of the fluid volume as L^{-3}. Coupling is therefore seen to be relatively stronger in systems of small volume. It is independent of panel thickness.

Returning to the problem of evaluating R_{rad} we find that the average number of well coupled acoustic modes per structural mode may be evaluated by consideration of the average number of acoustic mode lattice points in strips, one of which is shown in Figure 4.2. However if $f > 0.25f_c$, account must be taken of the variation of coupling with ε in evaluation of the sum $\sum_{m,r} g_{m,r}$ (see equations (4.8)). The details of this calculation are given in Appendix I. The result is as follows:

$$R_{rad} = \frac{64\rho h c_L (a + b)}{\pi^5}\left[\frac{\sin^{-1}(f/f_c)^{\frac{1}{2}}}{1 - (f/f_c)} + ((f_c/f) - 1)^{-\frac{1}{2}}\right] \quad : f/f_c < 0.9 \qquad (4.9)$$

An evaluation of R_{rad} cannot be made for $f \approx f_c$ without a detailed estimate of the number of acoustic modes per structural mode by graphical means.

For $f/f_c < 0.25$ equation (4.9) simplifies to $R_{rad} \approx (128\rho h c_L (a + b)/\pi^5)(f/f_c)^{\frac{1}{2}}$. This result agrees with that of Maidanik (26) for 'reverberant' field vibration of a panel radiating into free field conditions, to which it is compared in Figure 4.13. This result is yet another indication that frequency averaged coupling between finite vibrating systems approximates closely to coupling between semi-infinite systems. The radiation efficiency σ, defined by $\sigma = R_{rad}/\rho c_o ab$, is dependent upon the ratio of half the panel perimeter, $(a + b)$, to the panel area, (ab), and is also inversely proportional to the speed of sound for a given panel thickness and a given ratio of frequency to critical frequency. The radiation efficiency corresponding to equation (4.9) is plotted in Figures 4.5, 4.7 and 4.9 for 1/16 in., 1/8 in. and 1/4 in. x 2.67 ft. x 2.16 ft. panels.

4.3.2 Supercritical Frequency Range

At frequencies greater than the critical the simultaneous satisfaction of $p = m \pm 1$ and $q = n \pm 1$ is possible, as can be seen from Figure 4.3. Mode pairs having $p = m \pm 1$; $q = n \pm 3$, and vice versa, contribute about 25% of the total coupling, all other contributions being negligible. The details of the analysis are in Appendix I. The result is as follows:

$$R_{rad} = (156/\pi^5)(1 - f_c/f)^{\frac{1}{2}} \rho c_o ab \approx 0.5(1 - f_c/f)^{\frac{1}{2}} \rho c_o ab \qquad (4.10)$$

and $\sigma = 0.5(1 - f_c/f)^{\frac{1}{2}}$.

This result does not agree with any previous estimates of supercritical radiation resistance for baffled panels, which give a numerical constant of unity, or with Kihlman's analysis (8) of a panel-box system which gives a numerical constant near to unity. This is rather puzzling in view of the subcritical agreement with Maidanik's work. However no error has been found in the analysis by the author or by two other workers in the field (41). The corresponding radiation efficiency is plotted in Figures 4.5, 4.7 and 4.9.

Maximum B_{rm} at supercritical frequencies is given by

$$B_{rm} = \left(\frac{\rho c_o^2}{V\varepsilon_r\varepsilon_m M}\right)^{\frac{1}{2}} \left(\frac{ab}{\pi^2}\right) = \frac{1}{\pi^2}\left(\frac{\rho c_o^2}{c\varepsilon_r\varepsilon_m h\rho_s}\right)^{\frac{1}{2}}.$$

Hence the magnitude of $(B_{rm}/\beta)^2$ is independent of fluid volume and frequency, but depends upon panel thickness, unlike the subcritical case.

4.4 The Clamped Panel

No exact analytic expression has been found for the eigenfunctions of a clamped rectangular panel. Beam functions are often used in approximate frequency solutions. However for the present purpose of considering the coupling between a clamped panel and a sound field the asymptotic expressions developed by Bolotin (28) are rather easier to handle mathematically and also give a better physical understanding of the differences between the behaviour of simply supported and clamped

panels.

The displacement eigenfunctions are of the form

$$\phi(x,y) = \left[\sin k_1(x - x_a) + \sin k_1 x_a \exp(-(k_1^2 + 2k_2^2)^{\frac{1}{2}}x\right] \times$$

$$\left[\sin k_2(y - y_b) + \sin k_2 x_b \exp(-(k_2^2 + 2k_1^2)^{\frac{1}{2}}y\right] \qquad (4.11)$$

where $k_1 a = 2 \tan^{-1}(k_1/(k_1^2 + 2k_2^2)^{\frac{1}{2}}) + m\pi$

$$k_2 b = 2 \tan^{-1}(k_2/(k_2^2 + 2k_1^2)^{\frac{1}{2}}) + n\pi$$

$$k_1 x_a = \sin^{-1}(k_1/(2k_1^2 + 2k_2^2)^{\frac{1}{2}})$$

$$k_2 y_b = \sin^{-1}(k_2/(2k_1^2 + 2k_2^2)^{\frac{1}{2}})$$

Smith (29) has used similar functions to analyse the radiation resistance of panels with various edge conditions. The present analysis, detailed in Appendix II, shows that for panel modes having $k_1 << k_2$ or $k_2 << k_1$, ('edge modes' in the language of Lyon and Maidanik), the radiation resistance is twice that of a simply supported panel, in agreement with Smith. For $k_1 \simeq k_2$, a condition which Smith did not analyse, the radiation resistance is approximately the same as the simply supported plate. Consequently, the clamped plate radiation efficiency is approximately 3 dB greater than that of the simply supported panel at frequencies less than $0.5f_c$. The factor decreases as (f/f_c) approaches unity and is equal to unity (0 dB) at supercritical frequencies, (see Figures 4.6, 4.8 and 4.10). There is some uncertainty as to the rate at which this factor decreases between $0.5f_c$ and f_c because of analytical

difficulties discussed in Appendix II.

4.5 Statistics of Mode Coupling

4.5.1 Subcritical analysis

Three important conclusions may be drawn from the subcritical analysis of the simply supported panel presented in Appendix I. First, the average number of well coupled acoustic modes per individual structural mode is given closely by $[(\beta_r + \beta_m)(a + b)c/\pi hc_L](f/f_c)\sin^{-1}(f/f_c)^{\frac{1}{2}}$. If this number is less than unity, i.e. $(f/f_c)\sin^{-1}(f/f_c)^{\frac{1}{2}} < [\pi hc_L/(a + b)c(\beta_r + \beta_m)]$, it may be assumed that no mode of the acoustic oscillator set is significantly well coupled to more than one structural mode, and vice versa. A typical value of the right hand side of the inequality for, say, an $\frac{1}{8}$ in. thick steel panel and a small reverberation chamber ($20 \times 10 \times 25 ft^3$) might be given by $(\pi \times 10^{-2} \times 17 \times 10^3)/(20 \times 10 \times 25) = 0.1$. Thus $(f/f_c)^{3/2} < 0.1$ gives $f < 800$ Hz. Below this frequency the multimode interaction reduces effectively to a number of two mode interactions, so that any assumptions about F' and G', as in reference (16), are unnecessary. The multimode power flow equation will then be good to a degree determined by the magnitude of the ratios (B_{rm}'/β_r) and (B_{rm}'/β_m): B_{rm}' refers to the coupling coefficient of the proximate mode pairs which have the next best coupling to the maximum, for which $(B_{rm}')^2$ is approximately 10% of $(B_{rm_{max}})^2$ (eqn. (4.7) et seq.). For the experimental systems the corresponding frequencies are shown in Table 2.

Second, the average ratio of mode pairs having maximum proximate coupling, to the total number of mode pairs in a frequency band, is given

closely by $\frac{(a + b)c_o \sin^{-1}(f/f_c)^{\frac{1}{2}}}{ab\pi f}$. This ratio is inversely proportional to the typical dimensions of the box volume.

Third, the average total number of mode pairs in a finite frequency band of width $\Delta\omega$ which have maximum proximate coupling is given by $3[(\beta_r + \beta_m)(a + b)(abc)/(2\pi^2 h^2 c_L^2)](f/f_c)\sin^{-1}\Delta\omega$. When this number is less than unity, the probability of maximum proximate modal coupling in the band becomes small, and the statistical analysis of R_{rad} based upon such coupling becomes invalid. Table 1 compares statistical estimates of the total numbers of mode pairs having maximum proximate coupling in 1/3 octave bands with numbers obtained from a computer analysis described in section 4.6.

The presence of $(\beta_r + \beta_m)$ in the numerator of the expression above cancels its presence in the formula for g_{mr} $(= B_m^2/(\beta_m + \beta_r)$, when these two quantities are effectively multiplied together in the evaluation of $R_{rad} = (M/N_s) \sum_{m,r} g_{mr}$. Hence, as shown later by numerical analysis, the radiation resistance is more or less independent of the internal dampings of the coupled systems, except in that because $(\beta_r + \beta_m)$ appears in the equation for total number of maximum proximate mode interactions, an increase can make the difference between having one or no such coupled mode pairs in a frequency band.

4.5.2 Supercritical analysis

The corresponding expressions for the supercritical range are as follows:

(a) The number of well coupled acoustic modes per structural mode is given by $4c(\beta_m + \beta_r)/\pi c_o(1 - f_c/f)^{\frac{1}{2}}$. This is purely a function of volume dimension normal to the panel and not of panel dimensions.

Except for very large volumes, or near critical frequencies, this number is normally less than unity. For the experimental system, at $f_c/f = \frac{1}{2}$, the numbers are shown in Table 2.

(b) The average ratio of well coupled mode pairs to total number of proximate mode pairs is given by $8c_o^2/\pi f^2 ab(1 - f_c/f)^{\frac{1}{2}}$. This number will often be less than unity in practice.

(c) The average total number of mode pairs in a band of width $\Delta\omega$ which have maximum proximate modal coupling is given by $2\sqrt{3}abc(\beta_m + \beta_r)\Delta\omega/\pi^2 hc_o(1 - f/f_c)^{\frac{1}{2}}$.

4.6 Non-Proximate Mode Coupling

The statistical estimates of radiation resistance given in equations (4.9) and (4.10) are based upon consideration of only those modes for which the coupling factor g_{mr} is a maximum by virtue of both wavelength component matching and natural frequency proximity. The previous section has suggested that there is a lower frequency limit for such a restriction to be valid. A computer analysis described in section 4.7, together with the results of experiments made on a panel-box system and described in section 4.8, support this suggestion. For these reasons the statistical theory has been extended to cover those frequency bands in which the probability of maximum proximate coupling is very low.

It is assumed that in a frequency band of which the centre

frequency is below that estimated to be the lower limit for maximum proximate coupling, no acoustic modes have, on average, natural frequencies sufficiently close to that of a typical structural mode in the band to give such coupling. Hence, in the estimation of R_{rad} $(= (M/N_s)\sum g_{mr})$ the summation is taken only over acoustic modes having lattice points which lie outside the wave number shells of thickness Δk_r shown in Figures 4.2 and 4.3, but which lie within a shell of thickness $\Delta\omega/c_o$ ($\equiv$ analysis bandwidth), centred on $k_r = k_p c_o/c_B$, as shown in Figure 4.4.

The previous restriction to modes having only maximum B_{rm}, by virtue of wavelength component matching, has been retained, because the probability of coupling between a structural mode and an acoustic mode proximate in frequency, but having less than maximum B_{rm}, is not significantly greater than for maximum B_{rm}. This fact, together with the rapid decrease in B_{rm} with difference between p and m, and q and n, justifies the application of such a restriction. This set of mode pairs produce the second class of coupling factors g_{mr}, which dominate the power flow in the absence of the maximum proximate class.

The analysis follows that of Appendix I closely in the calculation of $\sum_{m,r} g_{mr}$ for those acoustic modes whose lattice points lie in a strip of width δk_r, and for which $p = m \pm 1$ or $q = n \pm 1$ (see Figure 4.4); there are however the following differences. In Appendix I the shell considered was of width Δk_r, which is equal to $(\beta_m + \beta_r)/c_o$. Also the approximate forms of g_{mr} arising from the frequency proximity restrictions of equation (3.6) were used in this analysis. When non-proximate mode coupling is considered the full expression for g_{mr}, given

in equation (3.5), must be used. The expression for $\sum_{m,r} g_{mr}$ which appears in equation (A.3.1) of Appendix I is

$$\sum_{m,r(\delta k_r)} g_{mr} = \frac{2c_o^2 \rho N_s (a+b) k_r \delta k_r}{\varepsilon_r \varepsilon_m M \pi^3} \left[\frac{\sin^{-1}(k_r/k_p)}{\pi(k_p^2 - k_r^2)} + \frac{1}{\pi k_p^2} \tan(\sin^{-1} k_r/k_p) \right]$$

$$\times \left[\frac{\beta_m \omega_r^2 + \beta_r \omega_m^2}{(\omega_m^2 - \omega_r^2) + (\beta_r + \beta_m)(\beta_m \omega_r^2 + \beta_r \omega_m^2)} \right] \qquad (4.12)$$

This expression is integrated over the two wave number integrals from $(c_B k_p/c_o - \Delta k/2)$ to $(c_B k_p/c_o - (\beta_r + \beta_m)/2c_o)$, and $(c_B k_p/c_o + (\beta_r + \beta_m)/2c_o)$ to $(c_o k_p/c_o + \Delta k/2)$; Δk is given by $\Delta\omega/c_o$, where $\Delta\omega$ is the bandwidth over which averages are taken. The simplifying approximation, $\tan(\sin^{-1} k_r/k_p) = \sin^{-1}(k_r/k_p) \simeq \omega_r c_B/\omega_m c_o$, may be made because the lower limiting frequency, below which non-proximate coupling becomes important, is normally below $f_c/4$.

The integration process is extremely lengthy and is described more fully in Appendix III. The result for simply supported panels is as follows:

$$\sigma = \frac{4(a+b)c_o}{ab\varepsilon_r \varepsilon_m \pi^4} \left[\frac{(f/f_c)^{\frac{1}{2}} \beta_m}{\omega_m} I_1 + \frac{(f/f_c)^{3/2} \beta_m}{\pi \omega_m^3} I_2 + (f/f_c)^{\frac{1}{2}} \beta_r \omega_m I_3 \right.$$

$$\left. + \frac{(f/f_c)^{3/2} \beta_r}{\pi \omega_m} I_4 \right] \qquad (4.13)$$

The integrals I_1, I_2, I_3 and I_4 are given to better than 90% accuracy

by the following approximate expressions:

$$I_1 \simeq \frac{3(f/f_c)(1 + f/f_c)}{8((\beta_r + \beta_m)\beta_m)^{\frac{1}{2}}} I \qquad I_2 \simeq \frac{\omega_m^2}{8((\beta_r + \beta_m)\beta_m)^{\frac{1}{2}}} I$$

$$I_3 \simeq \frac{(f/f_c)(1 + f/f_c)}{8_m^2((\beta_r + \beta_m)\beta_m)^{\frac{1}{2}}} I \qquad I_4 \simeq \frac{1}{8((\beta_r + \beta_m)\beta_m)^{\frac{1}{2}}} I$$

where I is given by $I = \{\tan^{-1}[\Delta\omega/((\beta_r + \beta_m)\beta_m)^{\frac{1}{2}}] - \tan^{-1}[(\beta_r + \beta_m)/((\beta_r + \beta_m)\beta_m)^{\frac{1}{2}}]\}$.

The radiation efficiency is effectively independent of the bandwidth of analysis because normally $\Delta\omega >> ((\beta_r + \beta_m)\beta_m)^{\frac{1}{2}}$; this is in fact a necessary condition for $\Delta\omega$ to be a suitable bandwidth over which to take statistical averages. Hence the first term of I is usually very close to $\pi/2$ and independent of ω or $\Delta\omega$. It is interesting to note that the half power bandwidths β_r and β_m do enter the expression for radiation efficiency whereas they do not feature in the proximate mode coupling expression of equation (4.9).

Calculations of σ using measured values of β_r and β_m are compared with experimental results in Figures 4.5-4.10. The agreement is remarkably good. It is always found that non-proximate coupling makes negligible contribution to the total power flow when modes having proximate coupling are available. The lower limit for non-proximate mode calculations is set by the frequency for which, on average, no mode pairs in the band have maximum B_{rm}. This frequency is usually so low that

extension to even lower frequencies, using non-maximum, non-proximate mode calculations is not justified by the inadequacy of modal density expressions at very low frequencies.

4.7 Computer Analysis for a Simply Supported Panel

The radiation resistance of a panel as defined by $R_{rad} = (M/N_s)\sum g_{mr}$ was computed for a number of panel and box configurations. A range of values of $(\beta_r + \beta_m)$ was considered in order to investigate the effect of this parameter on R_{rad} and on the lower limiting frequency for maximum proximate coupling. For each chosen value of $(\beta_m + \beta_r)$ only those mode pairs were considered which were sufficiently close in natural frequency to be within half the sum of the half power bandwidths of each other, i.e., they satisfied the frequency proximity condition of equation (3.6a): $2|\omega_m - \omega_r| < (\beta_m + \beta_r)$. No restriction was placed, however, on the magnitude of the spatial matching condition, or magnitude of B_{rm}. Thus all proximate mode pairs were considered. Checks on the errors in the computation of R_{rad} incurred by omitting all non-proximate mode pairs showed that they were never more than 5% provided that some mode pairs with maximum proximate coupling occurred within the band. Figures 4.5, 4.7 and 4.9 compare the computed values of radiation efficiency σ $(= R_{rad}/\rho c_o ab)$ with those calculated from the statistically derived expressions of equations (4.9) and (4.10). The upper limit on frequency for the computational calculations was set by computer running time which increased as $(\text{frequency})^5$. For instance the calculation for

the 1/16 in. panel at $f/f_c = 0.5$ (4000 Hz) took 1 hour; there were 91,000 mode pair coupling factors to calculate.

A limited study was made of the effect of slightly altering the dimensions of the panel-box system on the computed radiation efficiencies. The basic configuration was chosen to be the 2.16ft x 2.67 ft. x $\frac{1}{8}$ in. thick panel mounted on a 2.16ft. x 2.67 ft. x 2.0 ft. deep box. This corresponded to the experimental configuration. In one case the panel dimensions were altered by 10% to 2.94 ft. x 2.37 ft. The box then measured 2.94 ft. x 2.37 ft. x 2.0 ft. In the other case the basic panel dimensions were used but the box was made 2.20 ft. deep. The aim of this limited study was to investigate the sensitivity of the computed radiation efficiency to small changes in the dimensions of the (regular) geometry, since it was felt that the computer analysis would be useless for practical purposes if the results were over sensitive to such changes. Figure 4.11 shows that variations about the statistically estimated value of up to 5 dB are predicted for these small variations of geometry. This behaviour casts some doubt upon the usefulness of a computer analysis, a conclusion which is discussed further in later chapters.

4.8 Radiation Efficiency of a Point Excited Panel

Section 3.2.5 contains a perturbation analysis of the power flow between a point excited structure and a fluid, which is applicable to lightly coupled systems. The total power flow per unit structural mass to the fluid is given by

$$\sum_r \Pi_r = \varepsilon^2 2\pi S_f(\omega) M^{-2} \sum_r \sum_m B_{mr} \sum_n B_{nr}\, \gamma(m,n,r)(\varepsilon_m \varepsilon_n)^{-\frac{1}{2}} \phi_m(\underline{x}_o)\phi_n(\underline{x}_o) \qquad (4.14)$$

where $\gamma_{(m,n,r)}$ is a function of the modal frequencies ω_m, ω_n, ω_r and the modal damping coefficients β_m, β_n and β_r.

It has been demonstrated previously in this chapter that, in the case of statistically independent modal generalised acoustic sources, the power flow between a fluid in a rectangular box and a panel which forms one flexible wall is dominated by mode pairs which enjoy maximum proximate coupling by virtue of good spatial matching and close proximity of natural frequencies. Section 3.2.5 shows that the power flow between the panel and the fluid will be dominated by the same mode pairs when the panel modes are driven by statistically independent modal generalised forces.

It is further evident from section 3.2.5 that the differences between the power flow with statistically independent forces, and that for a single point force excitation, will be largely determined by those mode triplets which satisfy a natural frequency criterion of a similar nature to that used previously to define proximate modal coupling, (see equations (3.57)-(3.60)). Consideration of equation (3.60), which for convenience is presented again with εB replaced by B, thus

$$\Pi_{r'} = \frac{1}{(\beta_m + \beta_r)} \{ \sum_{m'} B^2_{m'r'} U_{m'o} + \sum_{\substack{m',n' \\ m' \neq n'}} B_{m'r'} B_{n'r'} \left(\frac{\phi_{n'}(\underline{x}_o)}{\phi_{m'}(\underline{x}_o)}\right) U_{m'o} \} \qquad \begin{matrix}(3.60)\\(4.15)\end{matrix}$$

shows that the dominant cross terms will involve those modes which have maximum spatial matching and which also satisfy the natural frequency proximity criterion. Reference to the wavenumber diagrams 4.2 and 4.3,

together with the evaluation of B_{mr} made in sections 4.1 and 4.2, shows that it is theoretically possible to have the condition $B_{m'r'} = \pm B_{n'r'} = B_{max}$, where B_{max} is defined for subcritical frequencies by equations (4.8a) and (4.8b), and in section 4.2.2 for supercritical frequencies.

Figure 4.12 shows such mode triplets. A typical acoustic mode is shown (*) together with a typical structural mode (+) to which it is well coupled. Figure 4.12 shows the situation at subcritical frequencies where the relationship between the integers which denote the acoustic mode order (p,q,r) and those which denote the structural mode order (m, n) is given by $m = p + 1$; $n > q$ in the particular case depicted. The other structural modes of order, say, (m', n'), which have $B_{nr'} = \pm B_{mr'}$, and also satisfy the frequency proximity condition, $2|\omega_m - \omega_n| < (\beta_m + \beta_n)$ are also shown (•). Their mode order integers must satisfy the conditions $m' = m$; $n > q$ OR $m' = p - 1 = m - 2$; $n' > q$ OR $m' > p$; $n' = q - 1$ OR $m' > p$; $n' = q - 1$. It will be seen from Figure 4.12 that the structural mode pairs of order (m, n) and (m', n') occur in four groups which correspond to these four alternative conditions. These groups contain approximately equal numbers of mode pairs, except for the first group, which contains the mode pair giving the direct term B_{mr}^2. Since two groups give a positive value of the product $B_{mr} \times B_{nr}$ ($= B_{mr}^2$), and two give a value equal in magnitude but negative in sign to the former, they would appear to make a nett contribution to the summation of cross terms in equation (4.15) which is equal in magnitude and of opposite sign to the direct term. Unfortunately each mode pair

product $B_{mr}B_{nr}$ has to be multiplied by the modal amplitude ratio at the driving point ($\underline{x}_o$). The statistics of this product cannot be reliably determined for the relatively small number of mode pairs involved in expression (4.15) when applied to a system of the size investigated experimentally. It is however considered reasonable to advance the hypothesis that, in summing expression (4.15) overall acoustic modes to obtain the total power flow, it is likely that the fluctuations about zero of the cross term contributions will be such as to give zero net contribution. In this case the average power flow from a panel driven by statistically independent modal forces and by a point force could be equal. Certainly, with large systems of high modal density this appears to be the case (cf. ref 55).

4.9 Summary

The main conclusion to be drawn from this chapter is that the power flow between geometrically regular rectangular panel and fluid systems is dominated by relatively few of the available mode pairs. Below a definable frequency the coupling can be considered to occur between independent mode pairs, so that the exact two oscillator power flow equation may reasonably be used to estimate panel response to, and radiation of, sound. Also there has been found to exist a lower limiting frequency below which the panel response to random sound in the contained fluid does not correspond to that produced by a diffuse field. Point force excitation of a panel is not thought likely to produce substantially different radiation from statistically independent modal forces.

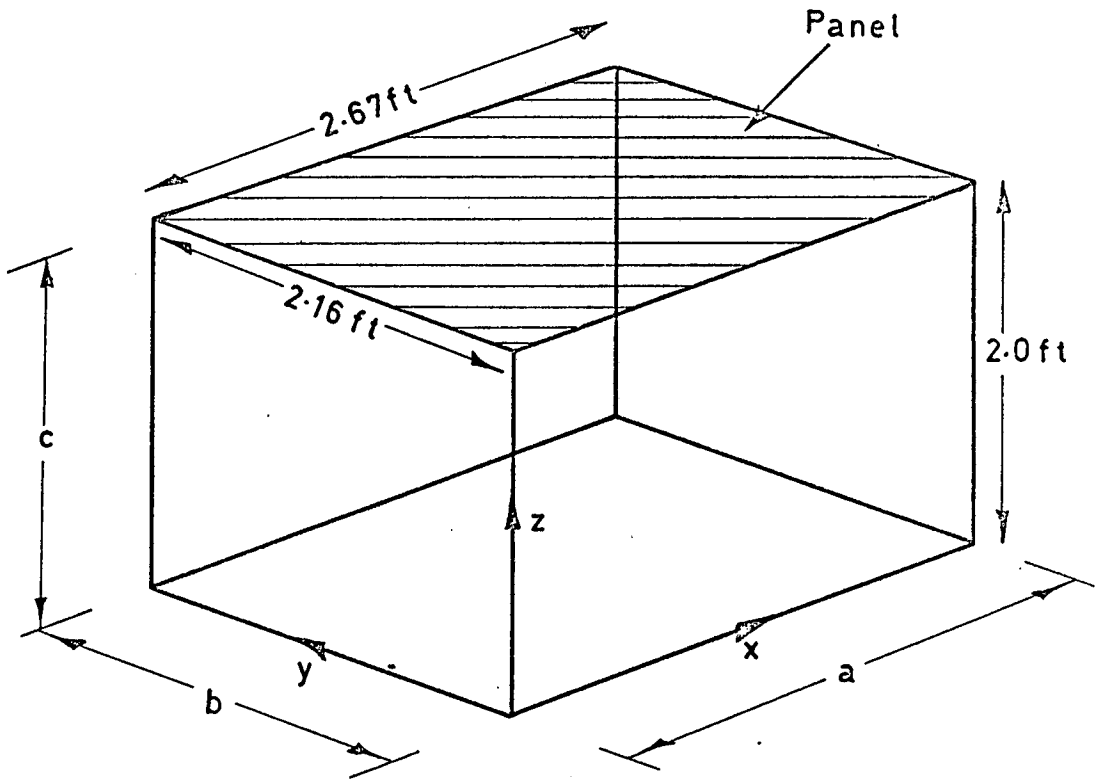

Fig 4.1 Panel-box model

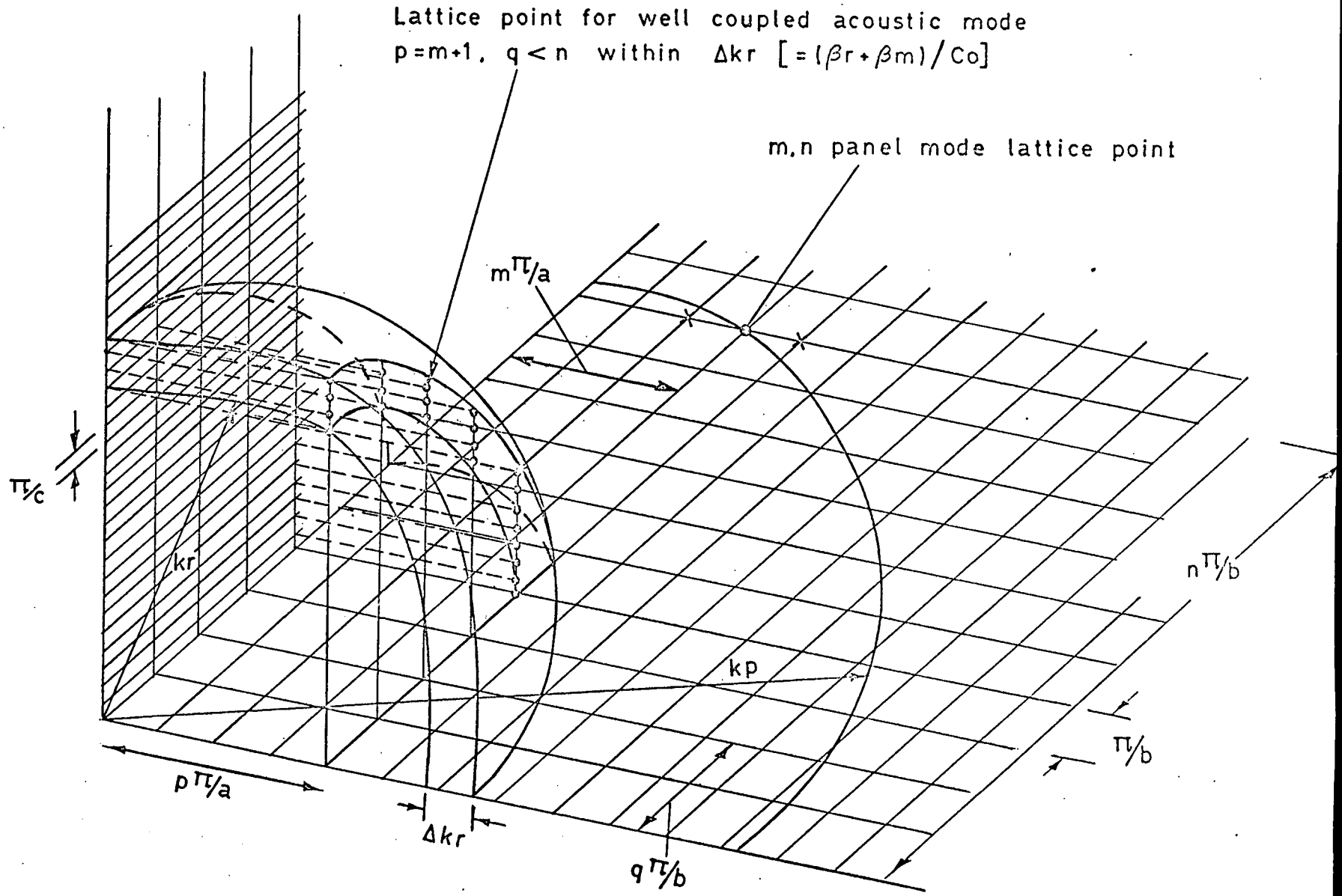

Fig 4.2 Subcritical wavenumber lattice diagram (kp > kr)

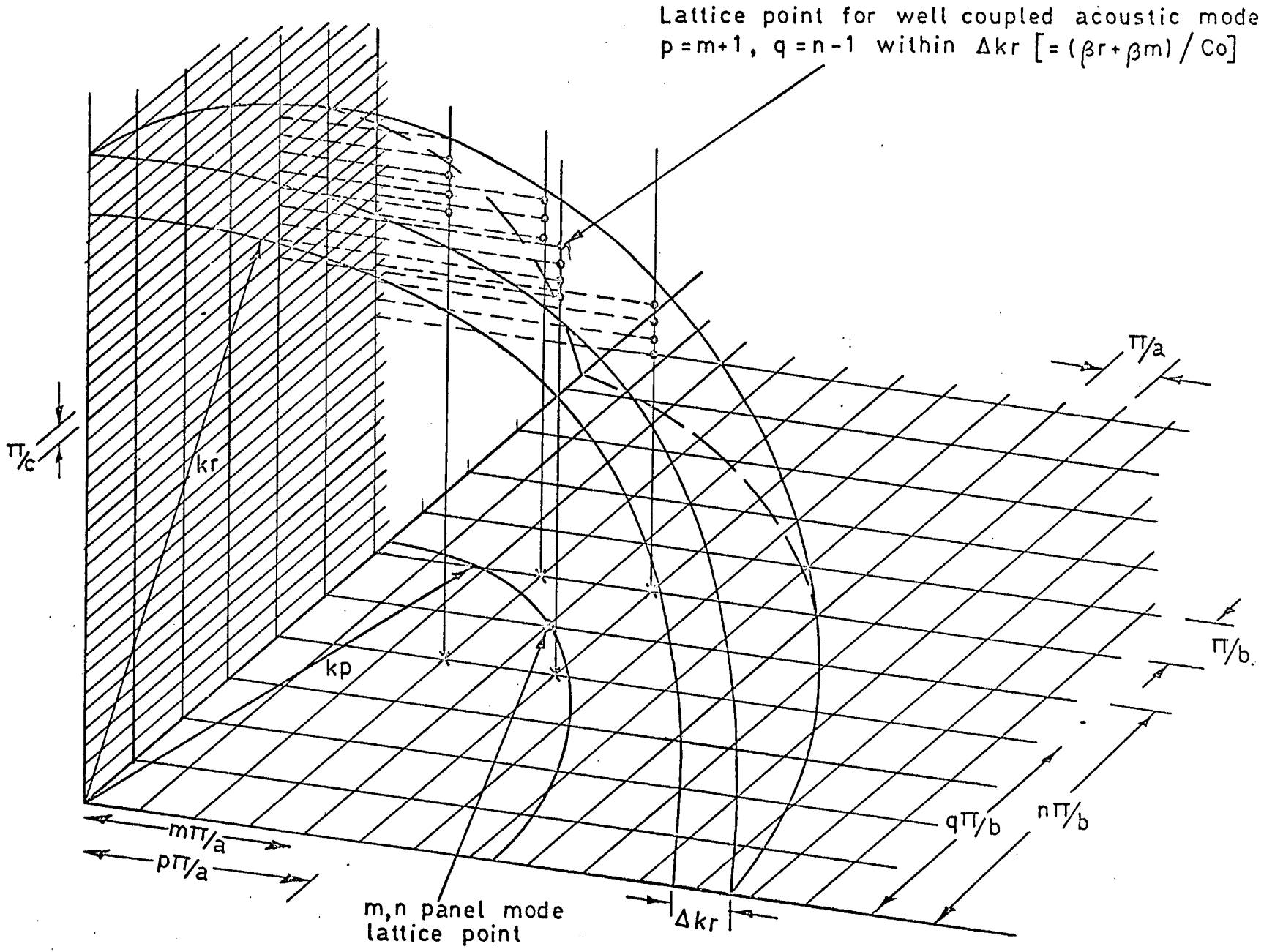

Fig 4.3 Supercritical wavenumber lattice diagram (kp < kr)

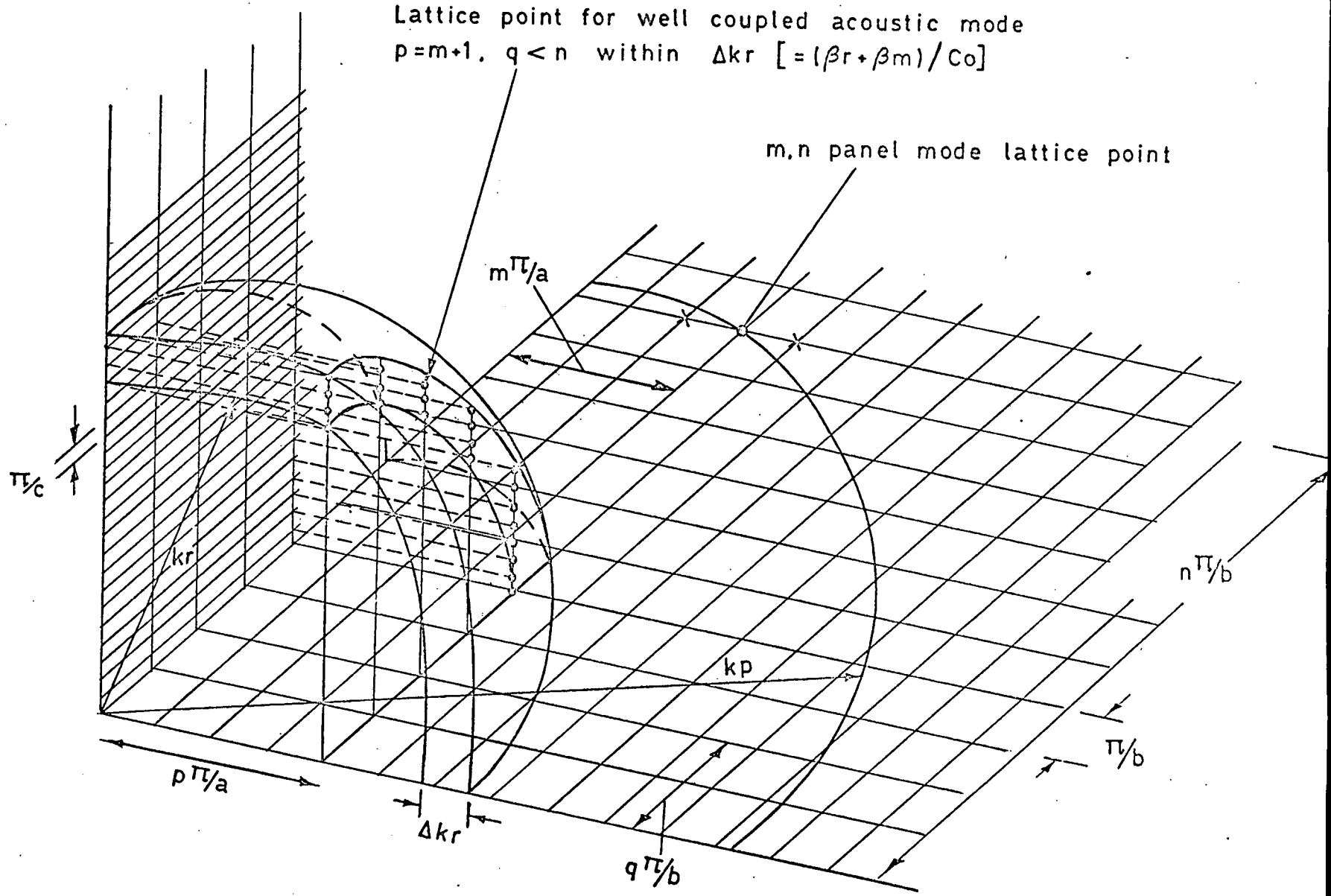

Fig 4.2 Subcritical wavenumber lattice diagram (kp > kr)

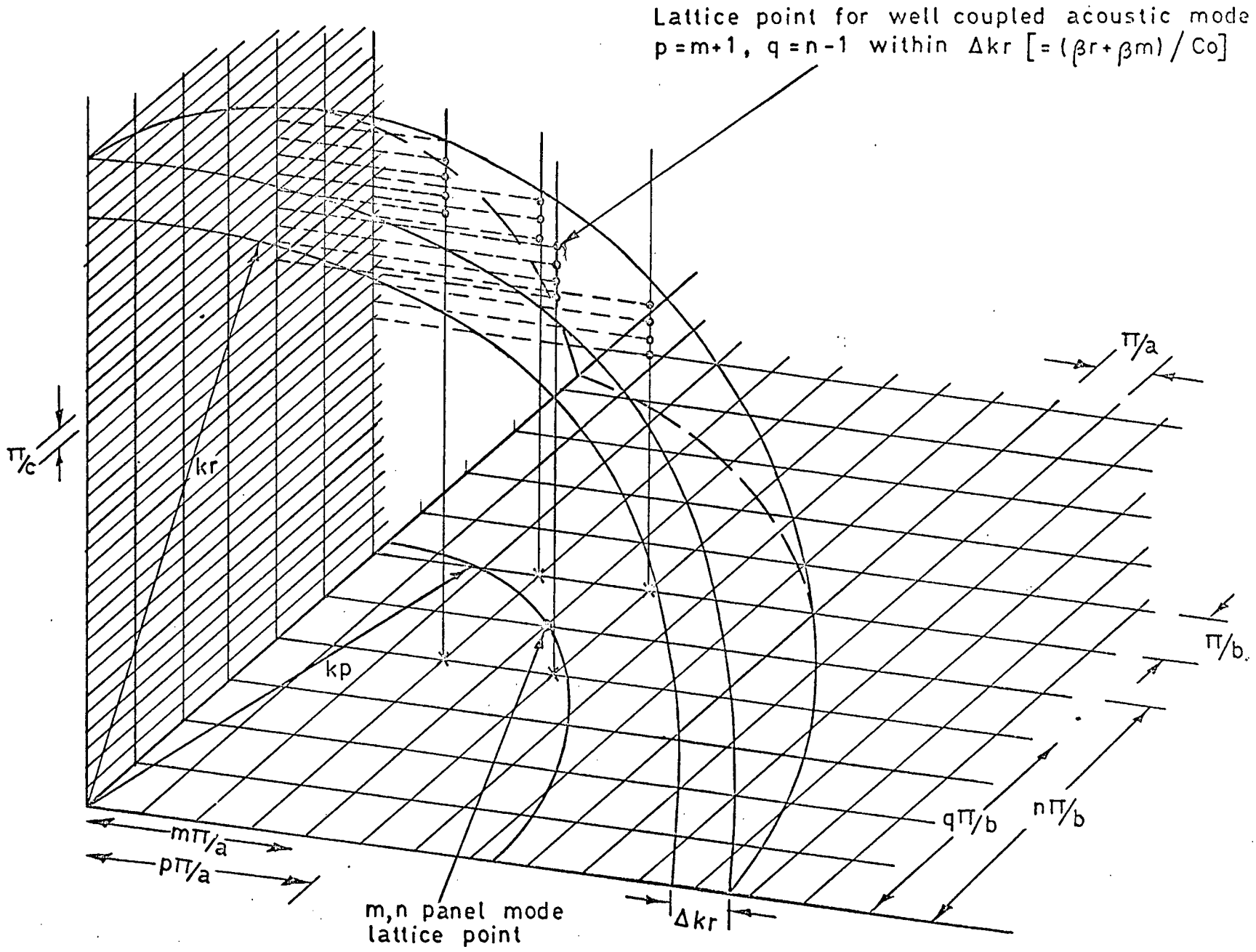

Fig 4.3 Supercritical wavenumber lattice diagram (kp < kr)

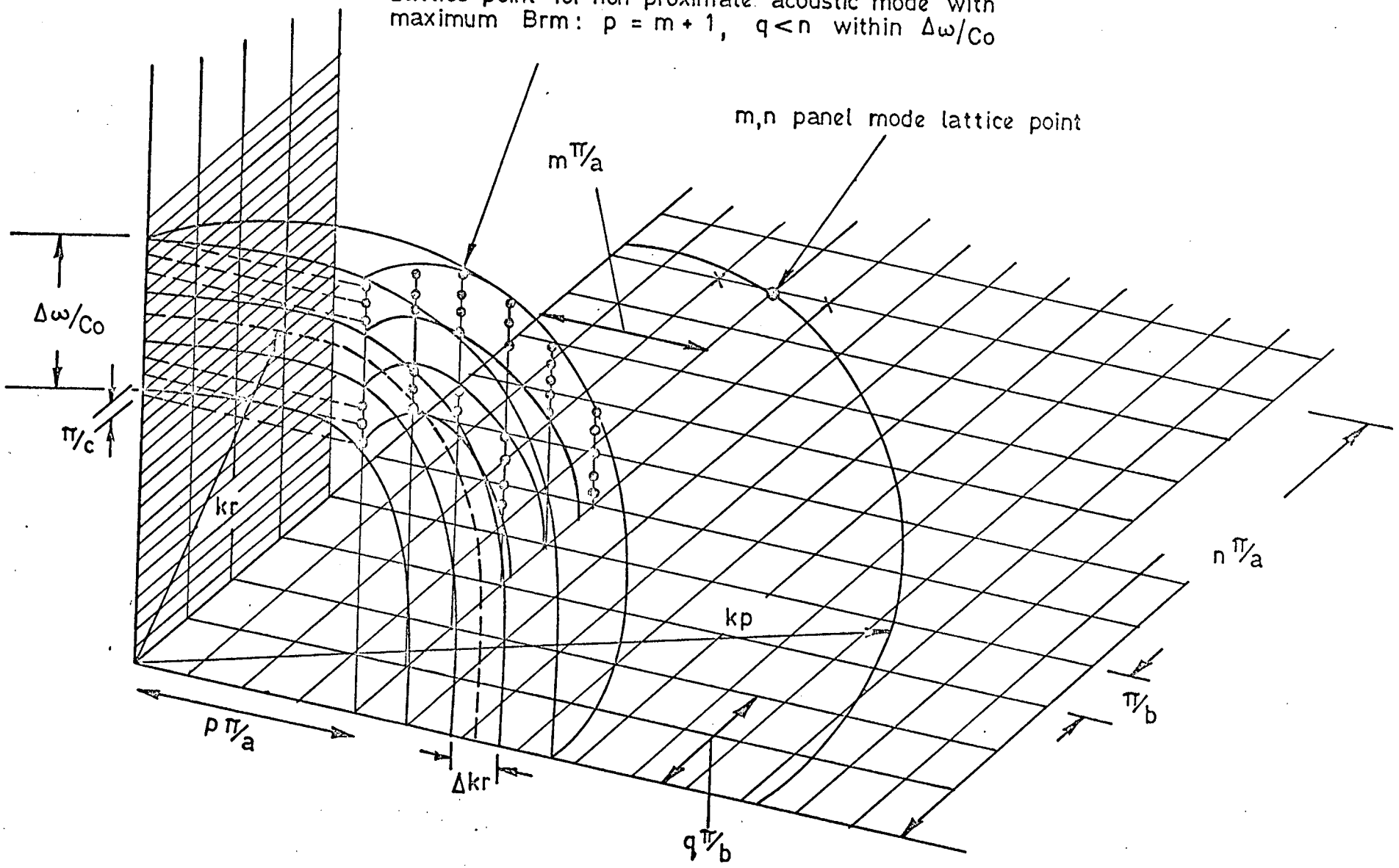

Fig 4.4. Subcritical wavenumber lattice diagram for non-proximate mode coupling. (kp > kr)

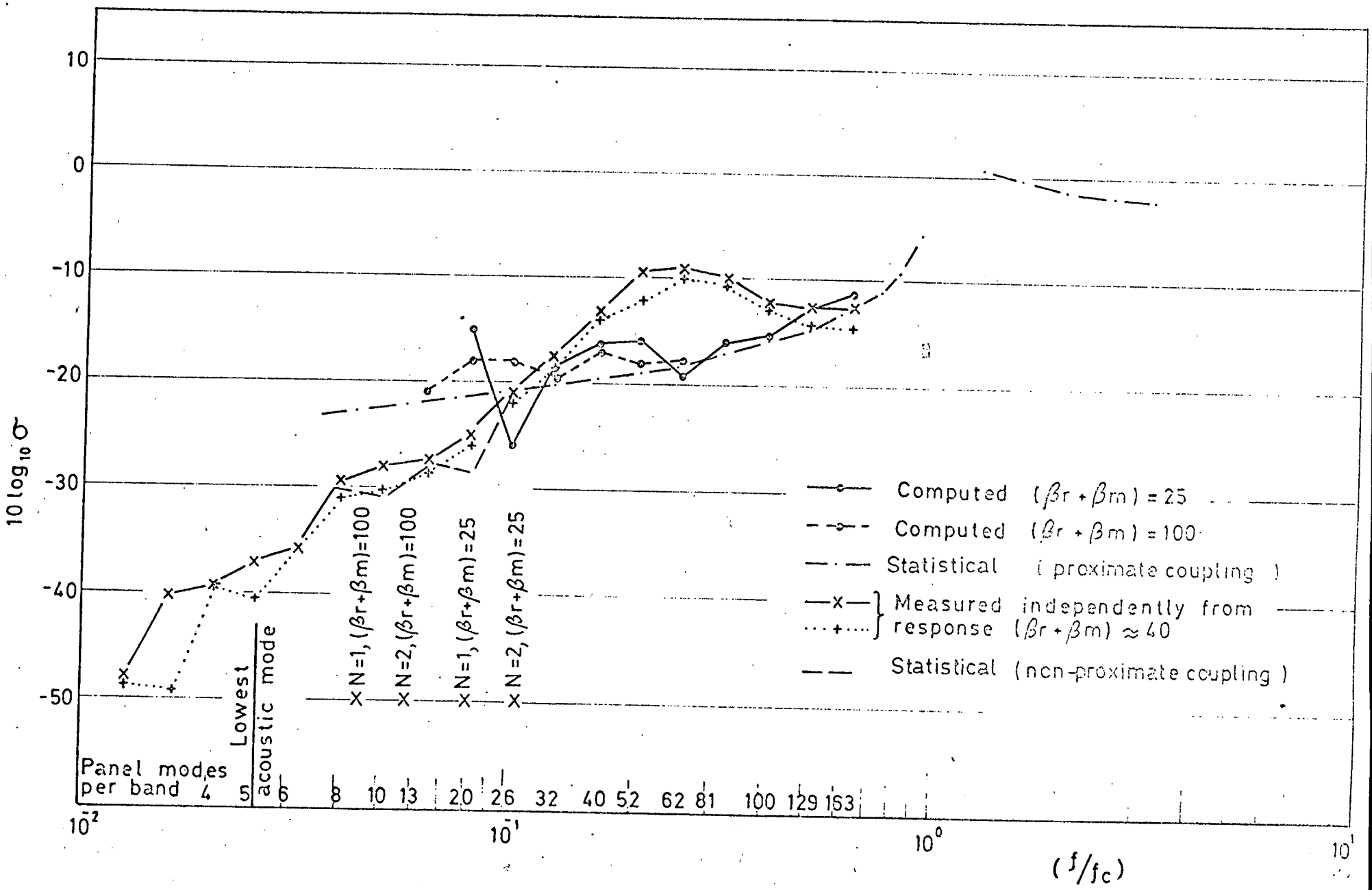

Fig.4.5 Radiation efficiency of simply supported 1/16 in panel
(1/3 octave band averages)

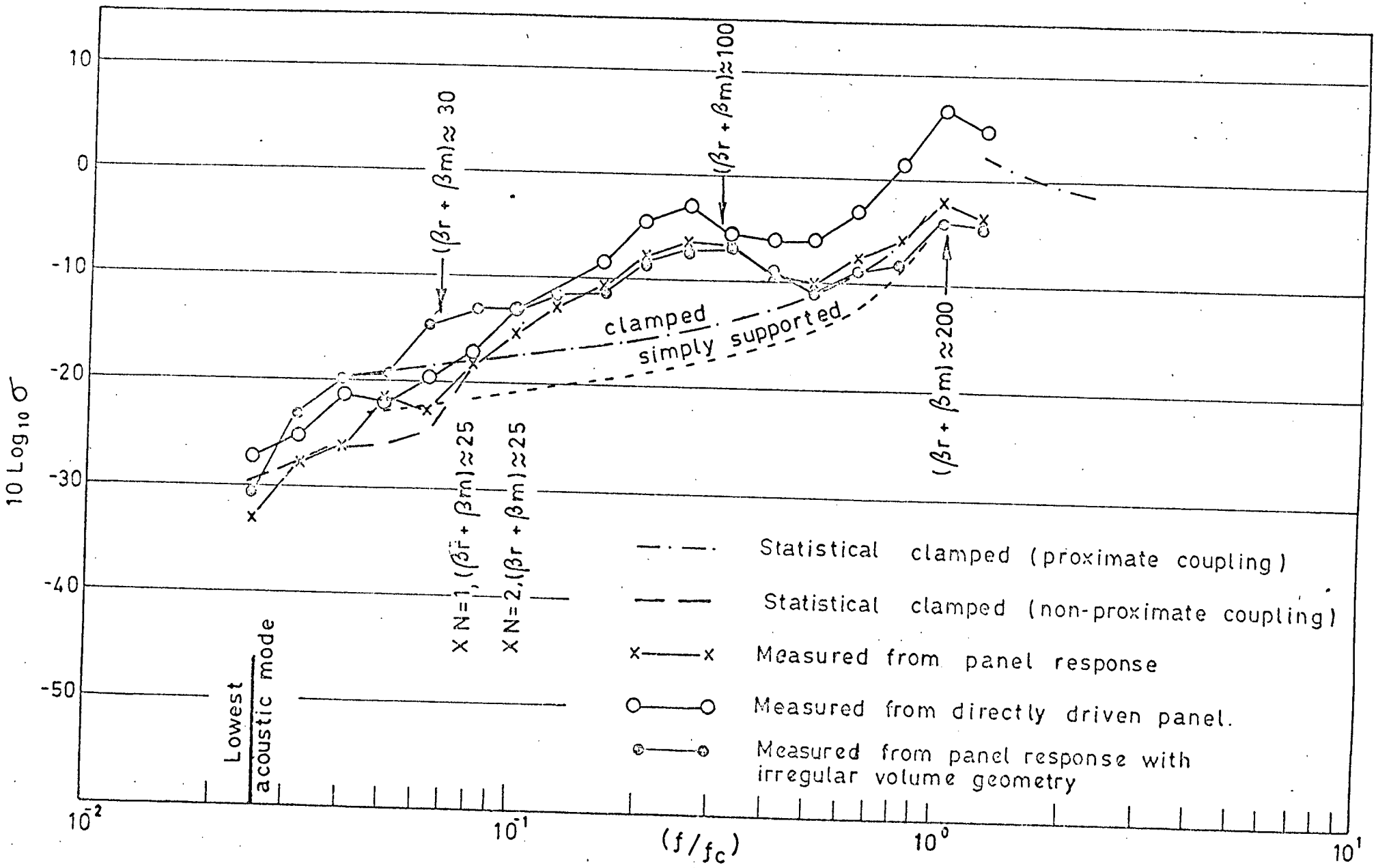

Fig. 4.6 Radiation efficiency of 1/16 in. clamped panel.
(1/3 octave band averages)

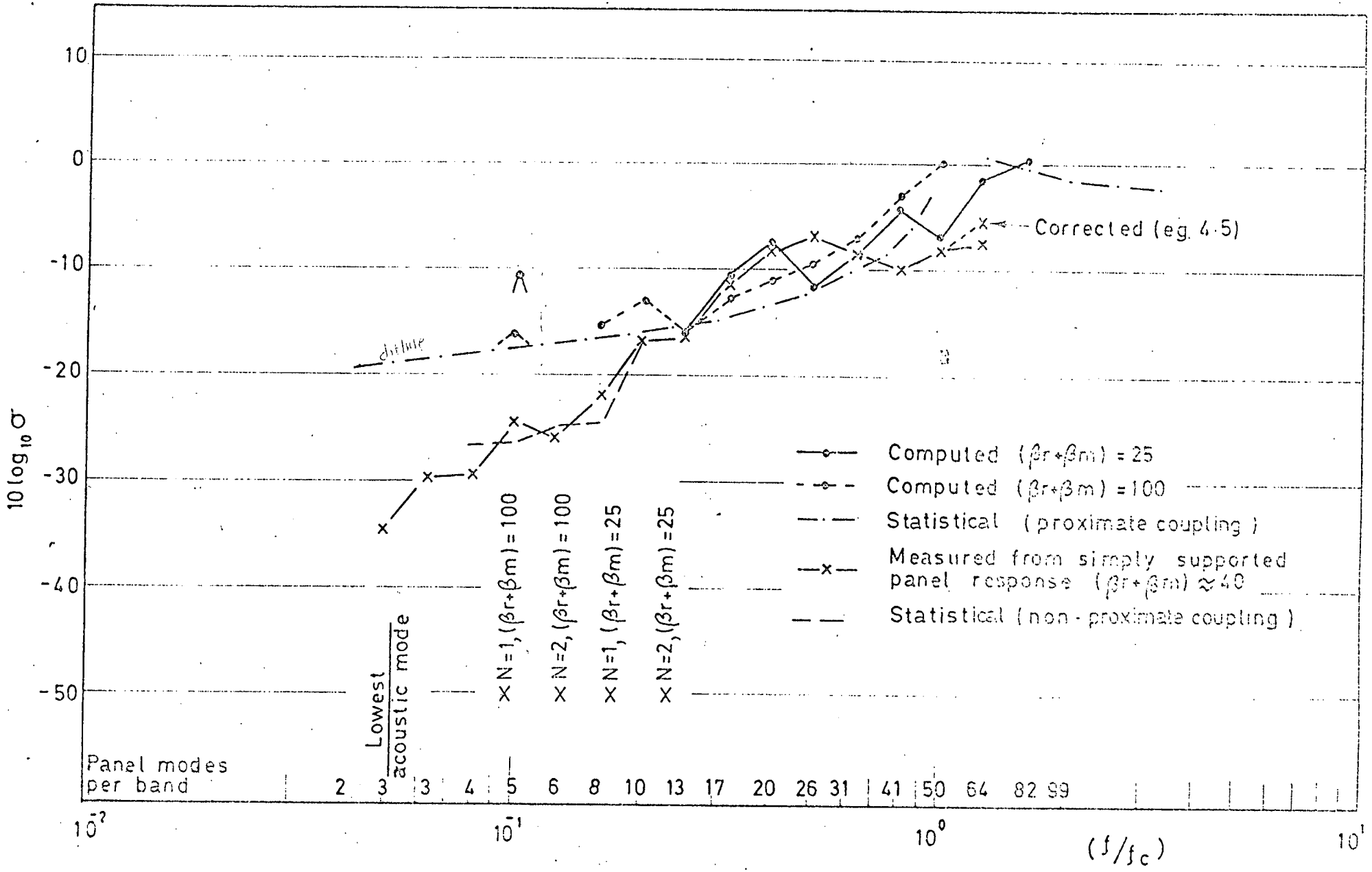

Fig. 4·7 Radiation efficiency of simply supported 1/8 in. panel
(1/3 octave band averages)

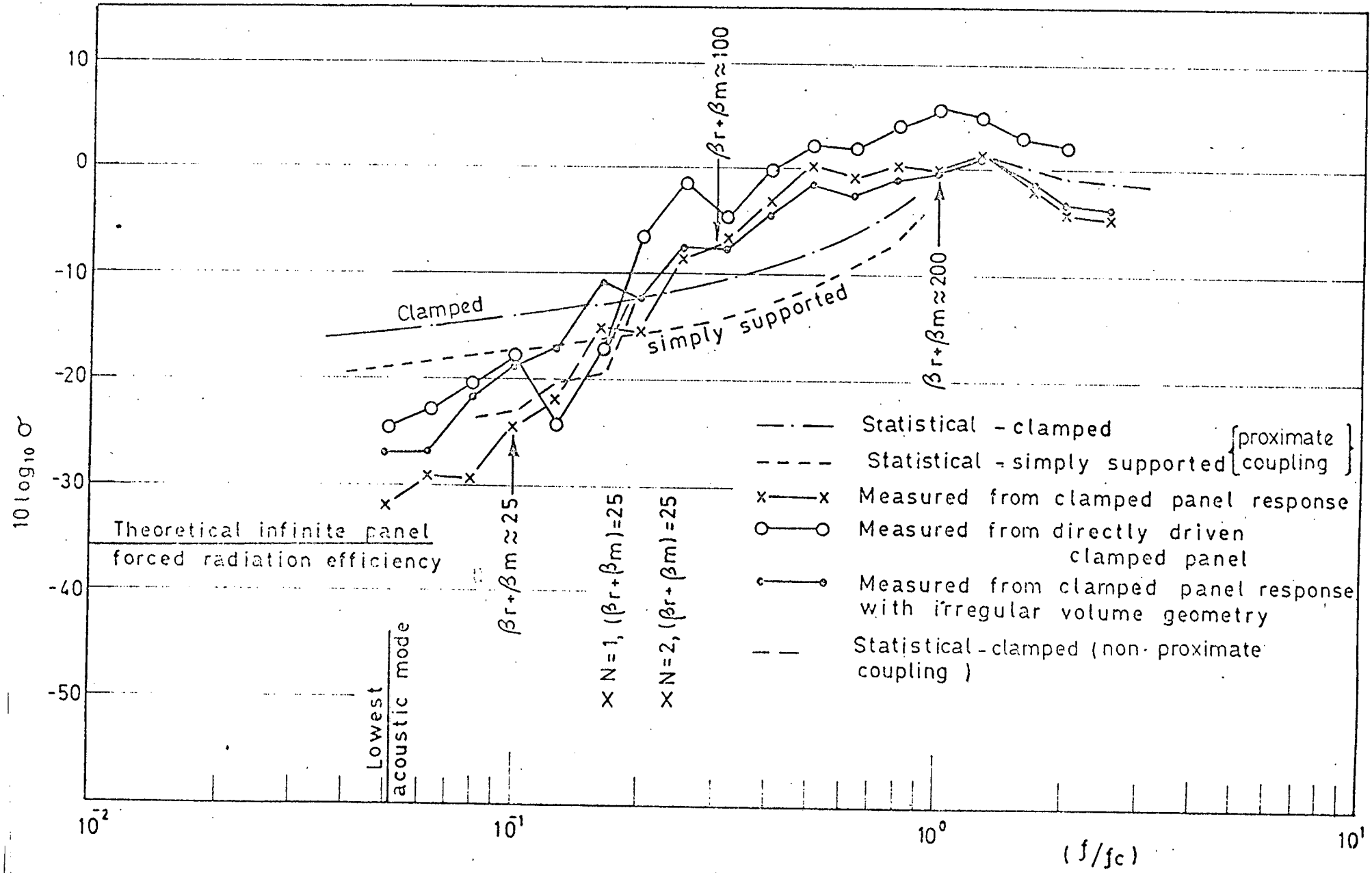

Fig. 4.8 Radiation efficiency of 1/8 in clamped panel.
(1/3 octave band averages)

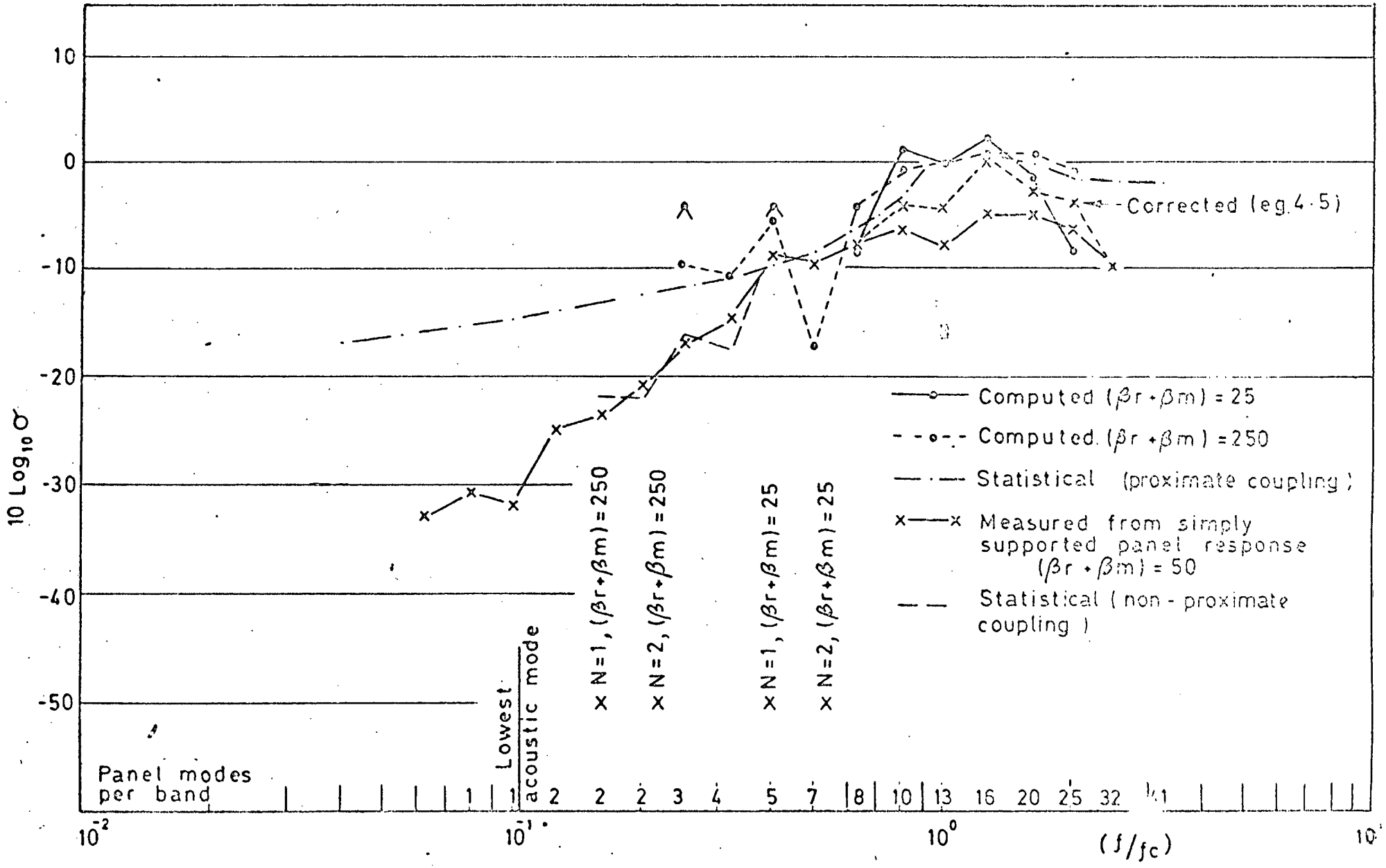

Fig 4.9 Radiation efficiency of simply supported 1/4 in. panel
(1/3 octave band averages)

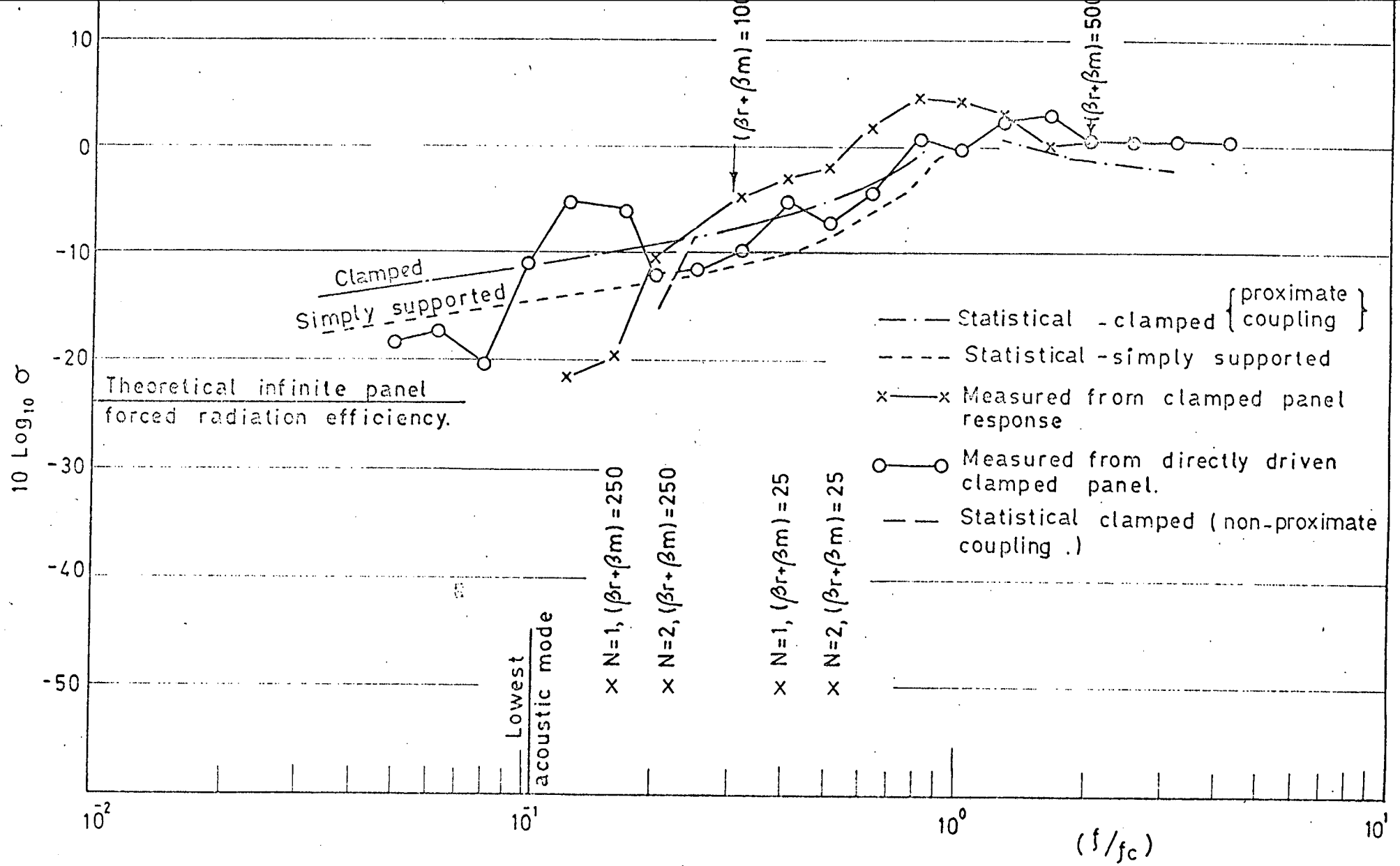

Fig. 4.10 Radiation efficiency of clamped 1/4 in panel.
(1/3 octave band averages)

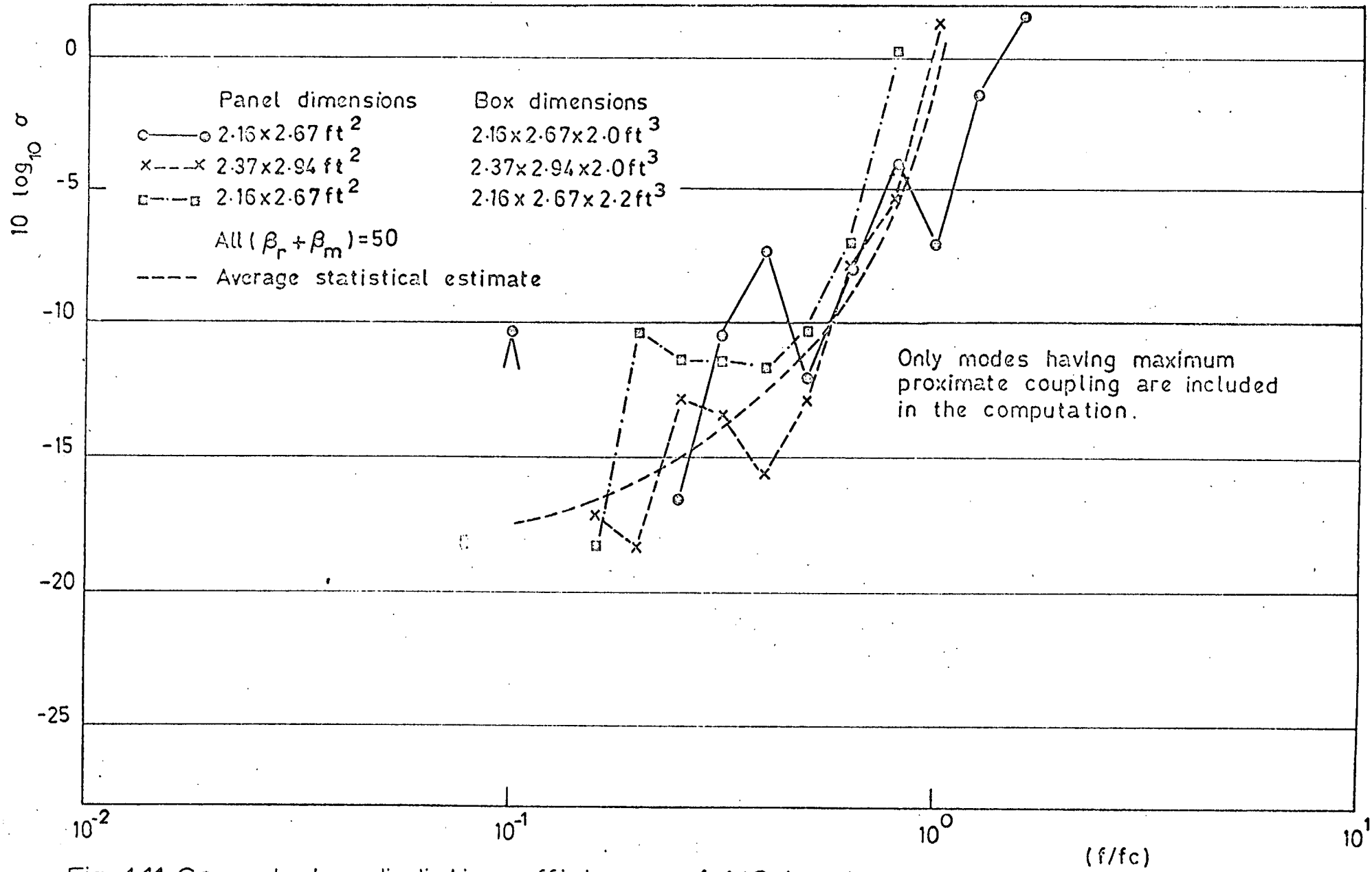

Fig. 4·11 Computed radiadiation efficiency of 1/8 in simply supported panel showing effect of small change in panel and box dimensions.

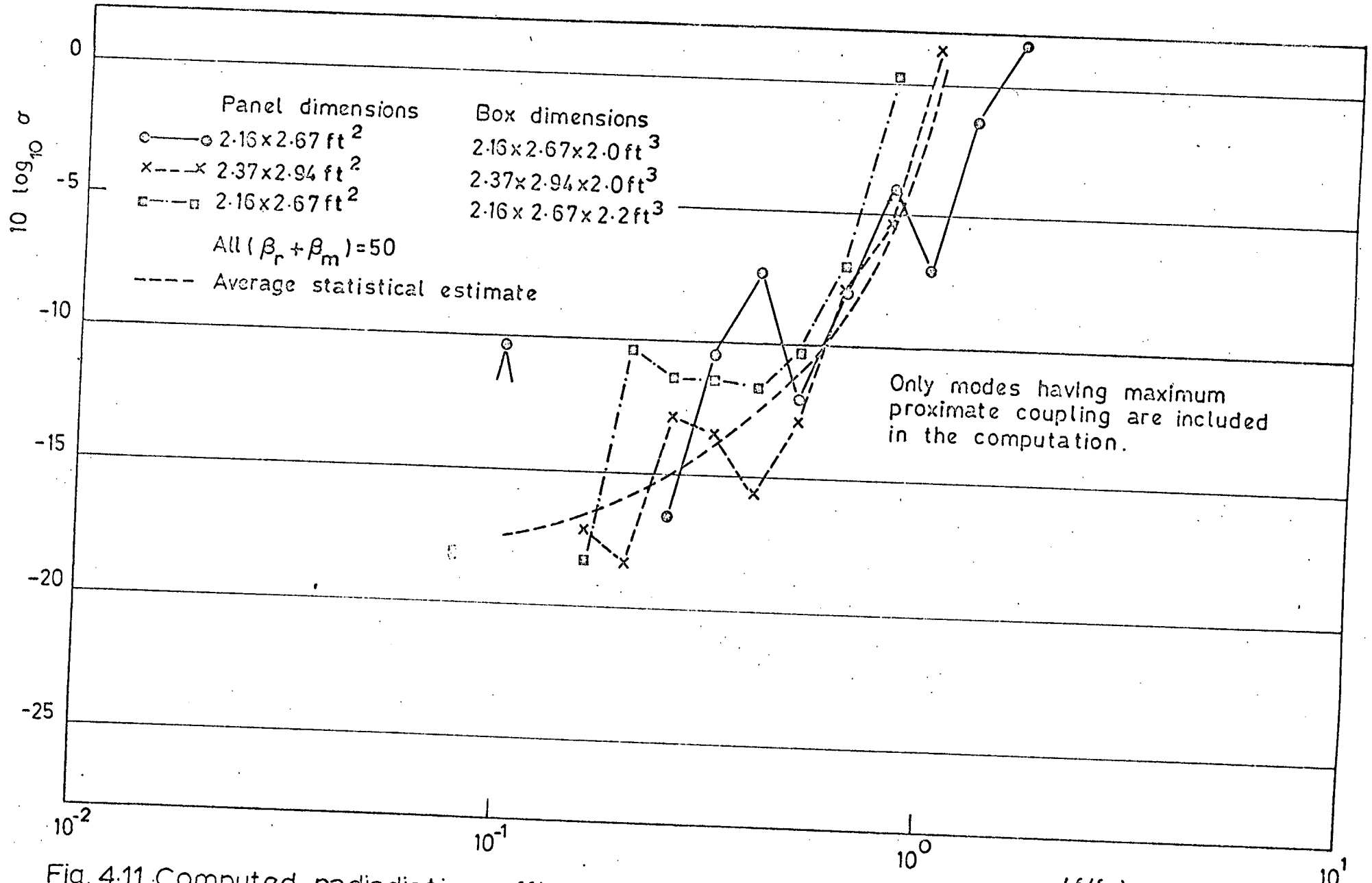

Fig. 4.11 Computed radiadiation efficiency of 1/8 in simply supported panel showing effect of small change in panel and box dimensions.

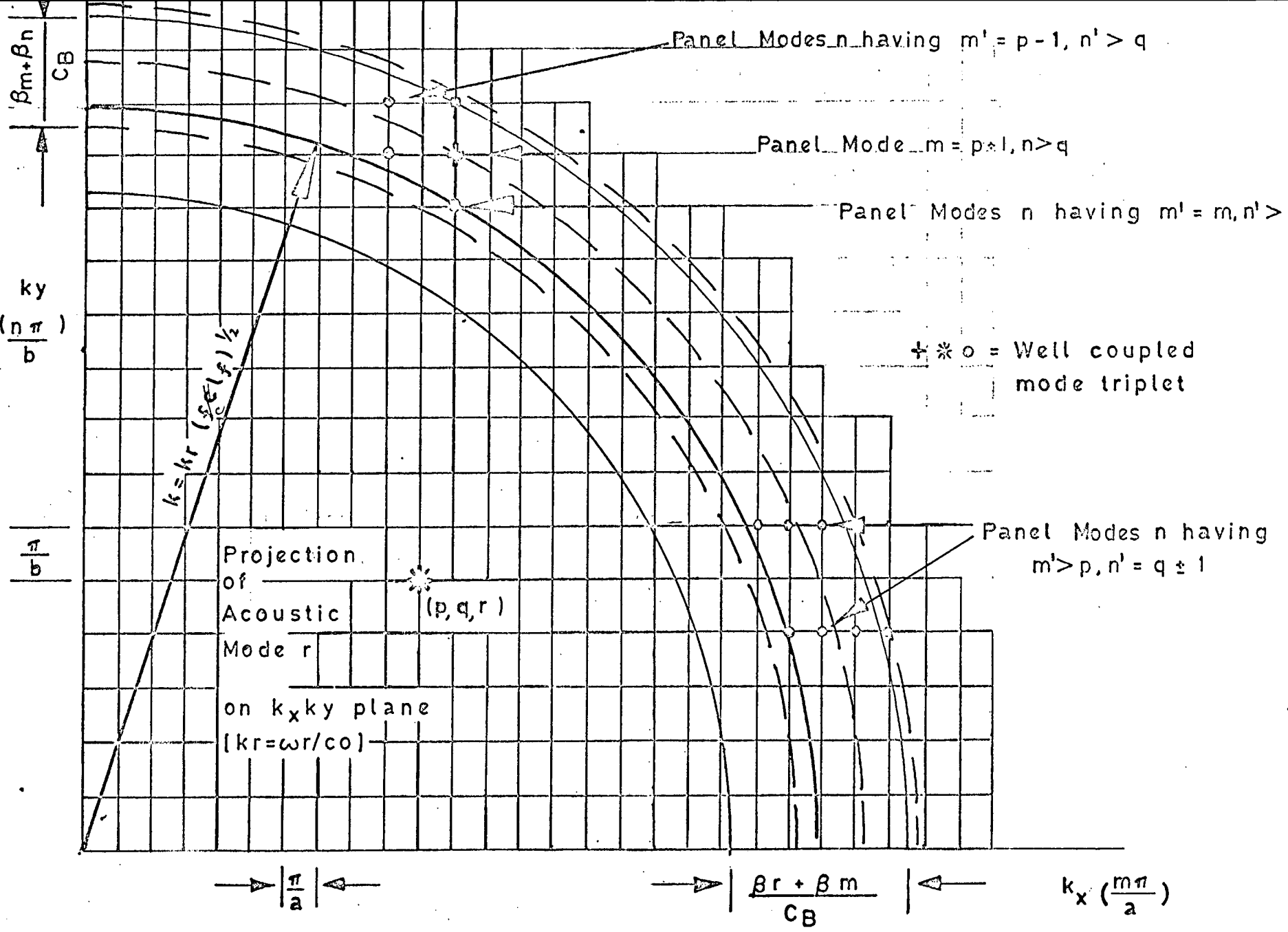

Fig 4.12. Well Coupled Mode Triplets for Single Point Excitation of Panel

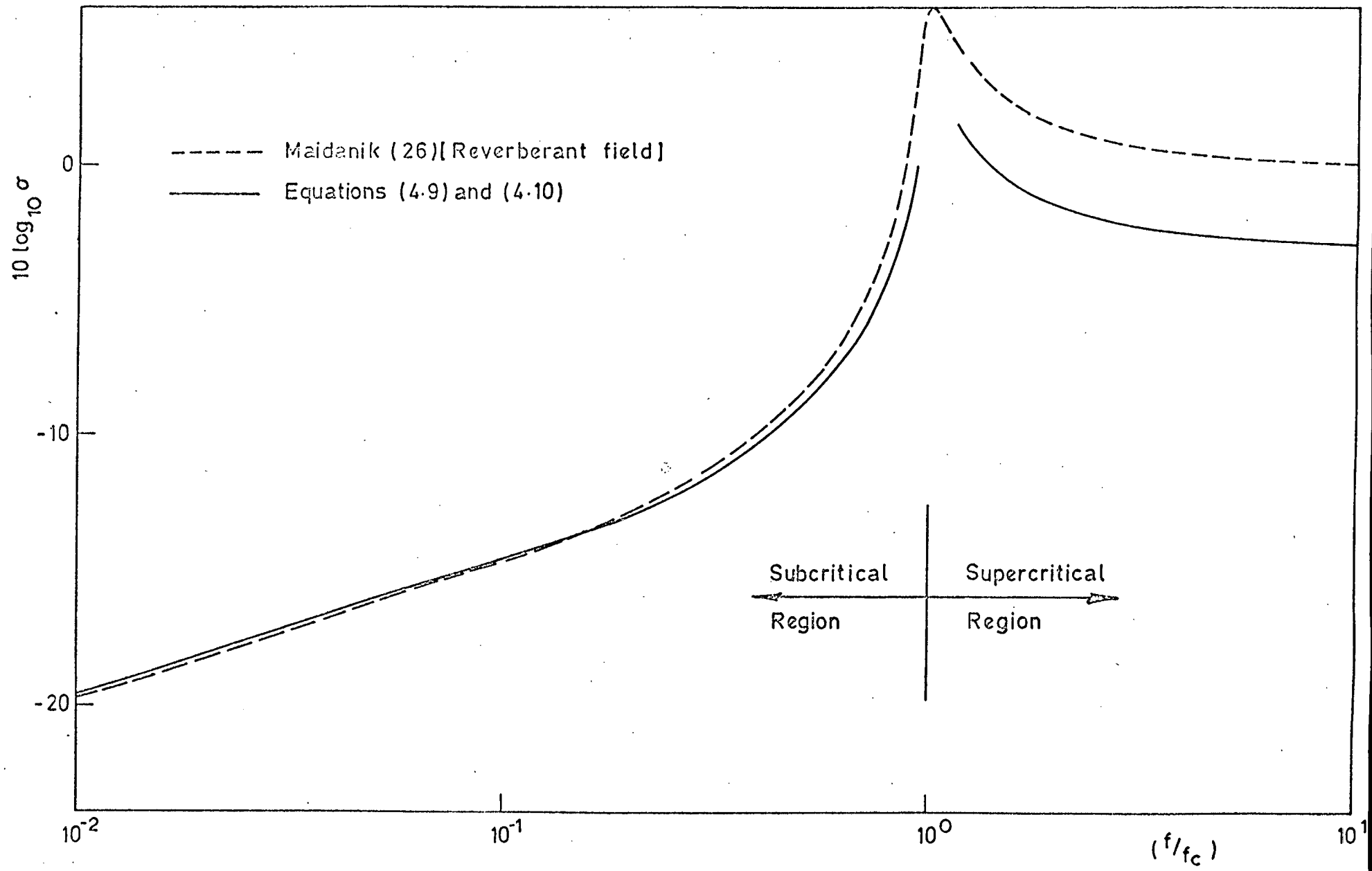

Fig. 4·13 Comparison between coupled oscillator and reverberant field results for the radiation efficiency of the 1/4 in. thick simply supported steel panel.

CHAPTER V

EXPERIMENTAL MEASUREMENTS OF RADIATION EFFICIENCY FOR A PANEL-BOX SYSTEM

This chapter presents the results of experimental measurements of panel response to broad band sound in an otherwise rigid rectangular box. The sound radiated into the box by point excited panels was also measured. Auxiliary measurements of panel and air volume damping are also described. The radiation efficiencies corresponding to the measured response and radiation are compared with theoretical estimates. The statistical, computed and measured results for radiation efficiency are discussed in detail.

5.1 Response Measurements

Rectangular, 2.67 ft x 2.16 ft steel panels, of uniform $\frac{1}{4}$ in, $\frac{1}{8}$ in and 1/16 in thicknesses, were supported so as to form one wall of a rectangular box. The edges of the panels were either bolted to a light channel section of low rotational and high shear stiffness (simply supported), or clamped by many bolts to a 1 in thick steel frame (clamped). The other walls were those of a 0.104 in thick steel rectangular water tank which was surrounded by a 4 in thick layer of sand in an outer wooden box (Figure 5.1). Intense broad band sound of 148 dB overall S.P.L. was produced in the tank by allowing high pressure air to enter

it at the base of one side through a gate valve. A typical sound spectrum is shown in Figure 5.2. The air left the tank through a pipe in the opposite wall. Aerodynamic buffeting of the panels was found to be negligible above 200 Hz, as shown by microphone measurements of fluctuating pressure near the surface of the panel with and without a microphone windshield. Microphone traverses of the fluid volume were made to determine space averaged, 1/3 octave band sound spectra. Windshielded microphone measurements were indistinguishable from unprotected microphone measurements at frequencies above 200 Hz. Twelve accelerometer positions were used to measure space averaged panel accelerations. The accelerometers were of the Bruel and Kjaer Type 4336 which weigh 2 gmf. In spite of this small mass, corrections had to be made to the 1/16 in plate response measurements to allow for accelerometer loading. These corrections were based upon the comparison of accelerometer and strain gauge measurements (34). It is considered that the conventional correction factor, based upon the point impedance of an infinite plate (35), is not relevant to finite panel measurements because of the wide range of point impedance variation about the infinite plate value.

Panel radiation efficiencies σ were calculated for 1/3 octave bands from the measured ratio of space averaged mean square vibration velocity to space averaged acoustic pressure, using the original uncorrected equation of Lyon and Maidanik (16)

$$\frac{\langle \bar{v}^2 \rangle}{\langle \bar{p}^2 \rangle} = \frac{2\pi^2 c_o n_s(\omega)}{\omega^2 M \rho} \left(\frac{R_{rad}}{\langle R_{mech} \rangle + R_{rad}} \right) , \qquad (5.1)$$

together with the relationship $R_{rad} = \rho c_o A \sigma$. Corrections to these calculated values, using the modified equation (4.5), were also calculated.

The results are presented in Figures 5.5 - 5.10.

5.2 Damping Measurements

In order to calculate radiation resistance, and hence radiation efficiency, from response measurements, it was necessary to know the modal average panel damping $\langle\beta_m\rangle$, or mechanical resistance, $\langle R_{mech}\rangle = M\langle\beta_m\rangle$. In the case of a panel-box system this damping included that due to radiation of acoustic energy to the fluid external to the box.

There are many ways of measuring the damping of a structure; these include harmonic frequency-amplitude plots, harmonic phase-amplitude plots, autocorrelation of response to random input, cross spectral density measurements between random input and response, vibration decay measurement following the cessation of harmonic or random force inputs, Fourier transformation of transient input and the resulting response (37), and the direct measurement of steady state mechanical power input (36). The quantity actually required for the present purpose was the modal average damping under acoustic excitation which, as is shown by reference (38) and Appendix V, depends upon the relative modal energy levels occurring under such excitation. After a considerable amount of experimentation it was found that the most reliable means of measuring the relevant modal average damping was the measurement of vibration decay in 1/3 octave bandwidths following the cessation of random acoustic excitation by a source external to the box ((38) and Appendix V).

Figure 5.3 shows the results of such measurements. At high frequencies (> 2500 Hz) it was necessary to use tape transport to show the decay rate so that the Bruel and Kjaer Level Recorder could correctly

time averages and plot the decays.

In the 'steady state' condition, before acoustic excitation is stopped, the panel transfers energy to the internal fluid, as well as dissipating it mechanically and re-radiating it to the external fluid. Hence it is necessary to consider exactly what is measured from the decay rate. For reasonably lightly damped systems it may be assumed that the steady state equations also describe the energy transfer process during decay (5). Hence the following equation may be written for the rate of change of panel energy

$$\frac{\partial}{\partial t}\left(M\langle\bar{v}^2\rangle\right) = \langle\beta_m\rangle M\langle\bar{v}^2\rangle + \left(\frac{M\langle\bar{v}^2\rangle}{N_s} - \frac{\bar{p}^2 V}{\rho c_o^2 N_{rm}}\right)\sum g_{mr} \qquad (5.2)$$

or

$$\frac{\partial}{\partial t}\left(M\langle\bar{v}^2\rangle\right) \simeq \langle\beta_m\rangle M\langle\bar{v}^2\rangle + M\langle\bar{v}^2\rangle\left(1 - \frac{VN_s}{M\rho c_o^2 N_{rm}} \frac{\langle\bar{p}^2\rangle}{\langle\bar{v}^2\rangle}\right)\left(\sum g_{mr}/N_s\right) \qquad (5.3)$$

From measurements of the ratio $\langle\bar{p}^2\rangle/\langle\bar{v}^2\rangle$ made during decay it was found that the term $\frac{VN_s}{M\rho c_o^2 N_{rm}} \cdot \frac{\langle\bar{p}^2\rangle}{\langle\bar{v}^2\rangle}$ was negligible compared to unity. Hence the exponential decay rate could be used to measure the sum $\left[\langle R_{mech}\rangle + R_{rad}\right]$.

Figures 5.4a and b show the value of the parameters $(B_{rm}/\beta_m)^2$ and $(B_{rm}/\beta_r)^2$ for the various panels.

It must be noted carefully that the values of $(B_{rm}/\beta_m)^2$ and $(B_{rm}/\beta_r)^2$ plotted in these graphs correspond to maximum proximate mode coupling, and hence are associated with relatively few of the total mode pairs. The next largest values of these ratios are approximately 10% of

the plotted values (eqn. 4.7 et seq.), while the great majority of mode pairs give values of the order of 1% of the plotted values. The ratio is not plotted for frequencies below the lower limiting frequency.

5.3 Direct Measurement of Radiation Efficiency

Measurements were also made of the radiation resistance and efficiency of the panels when driven mechanically at a single point by an electro magnetic vibration generator. Use of a multimode power flow equation similar to equation (4.4), with an assumption that no structural mode is well coupled to more than one acoustic mode, and vice versa, as discussed in Chapter IV, leads to the following relationship between average mean square pressure produced in the fluid and the average mean square velocity of the panel

$$\frac{\langle \bar{p}^2 \rangle}{\langle \bar{v}^2 \rangle} = \frac{\rho\omega^2 R_{rad} M}{2\pi^2 c_o n_r(\omega) \left[R_{rad} N_s / N_{rm} + R^f_{mech} \right]} \qquad (5.4)$$

where $n_r(\omega)$ is the modal density of the fluid volume, $R_{rad} = (M/N_s) \sum_{m,r} g_{mr}$, and R^f_{mech} is the loss resistance of the fluid due to internal and boundary effects. This must be compared with the corresponding equation derived by Lyon and Maidanik (16) without regard to variation in mode to mode coupling,

$$\frac{\langle \bar{p}^2 \rangle}{\langle \bar{v}^2 \rangle} = \frac{\rho\omega^2 R_{rad} M}{2\pi^2 c_o n_r(\omega) R^f_{mech}} \qquad (5.5)$$

It will be seen that use of equation (5.5) to derive R_{rad} will give a lower value than that in equation (5.4), the ratio being given by

$\left[1 + \frac{N_s R_{rad}}{N_{rm} R_{mech}}\right]^{-1}$. For the clamped panels, on which the direct measurements were made, the ratio $(N_s R_{rad}/N_{rm} R_{mech})$ was never significant compared with unity, because the mechanical damping was quite high at frequencies where R_{rad} was large (i.e., near the critical frequency). Of course these formulae do not take into account the statistical dependence of the generalised forces on the panel modes. In view of the uncertainty regarding the interpretation of the results of the theoretical analysis of section 4.7, it was of interest to compare the measurement with the results of the simple analysis.

Measurements were made of decay of the acoustic field in the box following the cessation of 1/3 octave band acoustic excitation from a loudspeaker. Averages were taken over microphone positions but, even so, the small volume of the box, and the resulting low modal density, caused a large scatter of results below about 500 Hz. From the measured decay rates it was possible to estimate the effective damping of the fluid cavity, and hence, R^f_{mech}. Steady state measurement of the sound pressures produced by 1/3 octave band mechanical excitation of the panel, together with accelerometer traverses of the panel, then yielded estimates of R_{rad}. The results are plotted in Figures 5.6, 5.8 and 5.10 for comparison with the results of the simple theoretical analysis.

5.4 Measurements of Panel Response with Irregular Fluid Volume Geometry

The theoretical analyses and corresponding experimental measurements were made with regular panel and fluid volume geometries. It was considered important to investigate whether the results of these studies were special to regular geometries or whether perturbation of the geometry

would cause significant changes in the behaviour of the system. It was much more convenient to alter the geometry of the fluid boundary, by the insertion of solid objects into the volume, than to change the shape of the boundaries of the panel. These objects took the form of five 30 in long, 4 in diameter closed steel pipes which were stacked in a pyramid in one of the bottom corners of the box. The total volume of the pipes was about 10% of the free fluid volume. Panel response measurements were made in the usual way and the resulting radiation efficiencies are plotted in Figures 5.6 and 5.8.

5.5 Discussion of Panel Results

5.5.1 Statistical and computed results

The most significant feature of the comparison between the statistical and computed estimates of R_{rad}, shown in Figures 5.5, 5.7 and 5.9, is the deviation of the latter estimate from the former in frequency bands where no mode pairs could be found which satisfied the frequency proximity condition for maximum proximate coupling. Examples occur with the $\frac{1}{4}$ in panel at $f/f_c = 0.5$; $(\beta_r + \beta_m) = 250$, and at $f/f_c = 2$; $(\beta_r + \beta_m) = 25$, and with the 1/16 in panel at $f/f_c = 0.1$; $(\beta_r + \beta_m) = 25$. An increase in $(\beta_r + \beta_m)$ is seen to bring some modes within the frequency proximity limits of equation (3.6a), which has the effect of lifting R_{rad} to near the statistically estimated value.

This condition can occur sporadically even at supercritical frequencies, with lightly damped systems and small box volumes. However it has been shown to be the general occurrence below a frequency which,

for regular rectangular geometries, can be predicted from a consideration of the combined acousto-structural wavenumber diagram. Most significantly this frequency represents a limit below which power flow calculations become more difficult because proximate modal coupling does not predominate, as it does above this frequency.

In order to support this conclusion, the statistical calculations were extended to include coupling between all non-proximate mode pairs which had maximum coupling by virtue of good wavelength component matching. The results of these calculations merge with those based upon maximum proximate coupling at frequencies close to those predicted from statistical considerations to be the lower limiting frequency. These are shown as crosses in the figures. The symbol N refers to the statistically estimated total number of well coupled mode pairs. This behaviour is more in accordance with the measured behaviour than that predicted to occur near this frequency from the computed results, where sporadic high values of radiation resistance are predicted. This is seen well in Figures 5.5, 5.7 and 5.9.

The largest discrepancy between computed and statistical values of radiation efficiency, in bands dominated by maximum proximate coupling, is seen at $f/f_c = 0.4$ (1,600 Hz) with the $\frac{1}{8}$ in panel, where the numerical value is about three times the statistical estimate, (Figure 5.7). Interestingly the experimental results also rise above the statistical curve in this region of frequency. Also the computed curve for the higher damping, $(\beta_m + \beta_r) = 100$), lies consistently about 3 dB above

the statistical curve between $f/f_c = 0.4$ and 0.8. Although there is no obvious reason for this discrepancy, it will be seen later to have relevance to the experimental results for the clamped $\frac{1}{8}$ in panel which has a similar value of damping in this frequency range. Figures 5.7 and 5.9 show computed points, at frequencies well below the estimated lower limiting frequencies for low damping, which lie well above even the statistically estimated curve for maximum proximate coupling. These are due to coupling between single computed mode pairs which have frequency separations far smaller than those estimated to be the average in these frequency bands. In this sense they are 'rogue' pairs. The relationship of such theoretical pairs to the practical behaviour of systems is discussed later in the thesis.

The mode pair statistics presented in sections 4.4.1 and 4.4.2 are of great interest because they clearly show that power flow between a geometrically regular structure and a geometrically regular fluid volume is associated with relatively few of the available mode pairs.

For instance, in one frequency band, ten of the 91,000 available mode pairs were computed to account for 82% of the power flow. The very important conclusion which may be drawn from this result is that mode set to mode set power flow may, in certain circumstances, be well represented by a set of independent two-oscillator equations. In addition, assumptions concerning the number of modes involved in power flow, which are based purely on considerations of modal density, such as those of Lyon and Maidanik (16), must be more carefully examined where geometrically regular coupled systems are concerned. An example is the modification to the response equation of reference (16), which is given by equation (4.5).

The lower limiting frequency estimated in section 4.4.1, from the equation $(f/f_c)\sin^{-1}(f/f_c) = (2\pi^2 h^2 c_L^2)/3(\beta_r + \beta_m)(a + b)(abc)$, indicates that this frequency is proportional to the square of the speed of sound in the fluid, c_o^2, for a given panel and volume. This follows from the relation $f_c = c_o^2/1.8hc_L$. One practical complication of this conclusion is that a given panel will be relatively less responsive to broad band noise, which spans the lower limiting frequency, generated in a fluid of high sound speed, such as helium, than, say, to noise of the same sound pressure level in air. This will be true provided that the value of structural mechanical damping, or R_{mech}, substantially exceeds R_{rad}; this is usually the case for practical structures. The reason for this restriction is that if $R_{rad} >> R_{mech}$, the structural response is independent of R_{rad} (see equation (4.5)).

5.5.2 Experimental results

5.5.2.1 Panel response

Values of radiation efficiency calculated from the response of the $\frac{1}{4}$ in, $\frac{1}{8}$ in and 1/16 in panels are presented in Figures 5.5 - 5.10. The upper limits of frequency for which results are presented were set by the highest frequencies for which reliable damping measurements could be made, and for which accelerometer loading effects could be satisfactorily determined. These were such that it was not possible to conclusively check the correctness, or otherwise, of the theoretical result for supercritical radiation efficiency presented in equation 4.10. The only available results are for the $\frac{1}{4}$ in clamped panel (Fig. 5.10) and for the

$\frac{1}{8}$ in clamped panel (Fig. 5.8), and these, unfortunately are conflicting.

A feature common to all the experimental results is that the measured radiation efficiency curves quite clearly fall away from the statistical curves based upon proximate coupling below frequencies close to those predicted as the lower limiting frequencies for the particular measured damping values. Also, the non-proximate statistical estimates of radiation efficiency below the lower limiting frequencies agree remarkably well with the measured results. This is considered to be a clear demonstration that, at low frequencies, the response of a structure to broad band random sound in an adjacent closed fluid volume can fall substantially below that estimated on the basis of the assumption of a diffuse sound field in the volume: this occurs at frequencies below a lower limiting frequency which can be simply estimated, at least for a rectangular geometry. This conclusion constitutes a major result of the research.

A further observation of great interest, and of some measure of surprise, is that the response curve below this frequency is rather smooth and does not exhibit the substantial irregularity that might be expected to be caused by the sporadic occurrence of well coupled modes of non-average frequency separation (39).

The experiments made with irregular volume geometry (Figures 5.6 and 5.8) indicate that the irregularity only significantly affects the response at frequencies below the lower limiting frequency, by as much as 7 dB at some frequencies. This result is consistent with the hypothesis that, where there are a sufficient number of mode pairs available for at

least some to satisfy the frequency proximity condition of equation (3.6a), then a random redistribution of the natural frequencies of one set of modes, such as the insertion of objects into the volume would be expected to cause (40), would not change the average radiation resistance. This is because the frequency difference term $(\omega_m^2 - \omega_r^2)^2$ is not significant in the expression for the coupling factor between proximate modes (see equation (3.6a)). However, where non-proximate coupling is dominant, then changes in this term may well affect the sum of the coupling factors, and hence the radiation resistance. To use Scharton and Lyons' terminology (7), the non-proximate coupling condition below the lower frequency limit constitutes, at least on average, a 'modal mismatch' situation. The presence of the damping coefficients in the expression for radiation efficiency (eqn. (4.13) is consistent with their calculations for this condition. That the introduction of irregularity raises the radiation efficiency would seem to indicate that a condition of statistical modal frequency separation is approached.

The general agreement between the radiation efficiency measured from response and the theoretical values at frequencies above the lower limiting frequencies is satisfactory except for the ranges of f/f_c from 10^{-1} to 5×10^{-1} (800-4,000 Hz) for the 1/16 in panels and from 3.2×10^{-1} to 8×10^{-1} (1,250-3,200 Hz) for the $\frac{1}{8}$ in clamped panel. It has already been noted that there is a constant discrepancy of about 3 dB between the computed and statistical curves for the $\frac{1}{8}$ in simply supported panel over the same frequency range. Although it cannot be explicitly shown to apply also the clamped panel, such a modification to the statistically estimated curve shown in Figure 5.8 would substantially reduce the

discrepancy between theory and experiment. It must also be remembered that the ratio of clamped panel to simply supported panel radiation efficiency has not been accurately estimated at frequencies between $0.5f_c$ and f_c.

The 'bumps' in the experimental 1/16 in panel curves in Figures 5.5 and 5.6 have been the subject of considerable concern since they were discovered. There seems to be little doubt that they truly represent the behaviour of 1/16 in panels because they have been observed with two different panels, attached to the box in quite different ways; with both regular and irregular fluid volume geometry; from measurements of both response and mechanically driven panel radiation; and, in the case of the simply supported panel response, by two different experimenters, one using strain gauges and one using accelerometers, in experiments separated in time by one year.

In spite of much thought and discussion as to the cause of these anomalous results no tenable explanation has been forthcoming. The fact that the discrepancy occurs over a frequency range similar to that mentioned above for the $\frac{1}{8}$ in clamped panel led to the suggestion that the box, rather than the panels, may be the culprit, because the acoustic modes are a function of the constant box dimensions, whereas the panel modes vary with the thickness of the panel. Examination of the sound field decays and pressure distributions has however shown no peculiarities associated with this frequency range. Regrettably, therefore, the matter has been left as a discomforting mystery.

The effect of the correction to the radiation efficiencies derived using Lyon and Maidanik's original equation, which is obtained

from equation (4.5), is clearly seen in Figure 5.9, where the corrected values lie far closer to the theoretical values than do the uncorrected results. This correction is only significant when the radiation resistance is of the same order, or greater than, the mechanical resistance. This circumstance only occurs with the simply supported panels near the critical frequency. The clamped panels have, in general, far higher mechanical damping near their critical frequencies and any correction is insignificant. It is interesting that the supercritical radiation efficiency of the $\frac{1}{4}$ in simply supported panel falls in accordance with the computed estimate which showed a lack of any well coupled modes in the frequency band corresponding to $f/f_c = 2$. The statistical estimate of the average number of well coupled mode pairs in this band is 1·8.

5.5.2.2 Panel radiation

The results of the measurement of panel radiation using single point mechanical excitation are shown in Figures 5.5-5.10. Three main features of the radiation efficiency curves are apparent. First, they follow the general shapes of the response curves, except for the $\frac{1}{4}$ in panel at low frequencies where very few modes exist. The $\frac{1}{4}$ in panel curve lies mostly below the response curve, whereas the $\frac{1}{8}$ in and 1/16 in panel curves lie mostly above the response curve. Second, the discrepancy between the two curves is greater at, or just below, the critical frequency. Third, the two curves tend to come closer together below the lower limiting frequency, again except for the $\frac{1}{4}$ in panel.

These results show that there is a close relationship between the radiation from a point excited panel and its response to broad band sound, particularly in respect of the lower limiting frequency. It has been

suggested that, with systems of very high modal density, the radiation resistance calculated from response and direct radiation measurements should be the same, and that the statistical dependence of modal generalised forces in single point excitation should be irrelevant. In the experimental systems, at frequencies above the lower limiting frequency, the power flow has been shown to be associated with relatively few of the available mode pairs. Under these conditions it is not reasonable to consider the results of averaging over many mode pairs. Therefore it cannot be determined whether or not the discrepancies mentioned above are caused by the statistical dependence of the modal forces. However it is interesting to note that the $\frac{1}{4}$ in panel, of low modal density, gave a lower radiation efficiency when driven, than in response, whereas the 1/16 in panel, of four times the modal density, gave the greatest positive discrepancy in the opposite sense near the critical frequency. It is also possible that the better agreement near and below the lower limiting frequency may be associated with the relatively greater proportion of available mode pairs which contribute significantly to the power flow below this frequency.

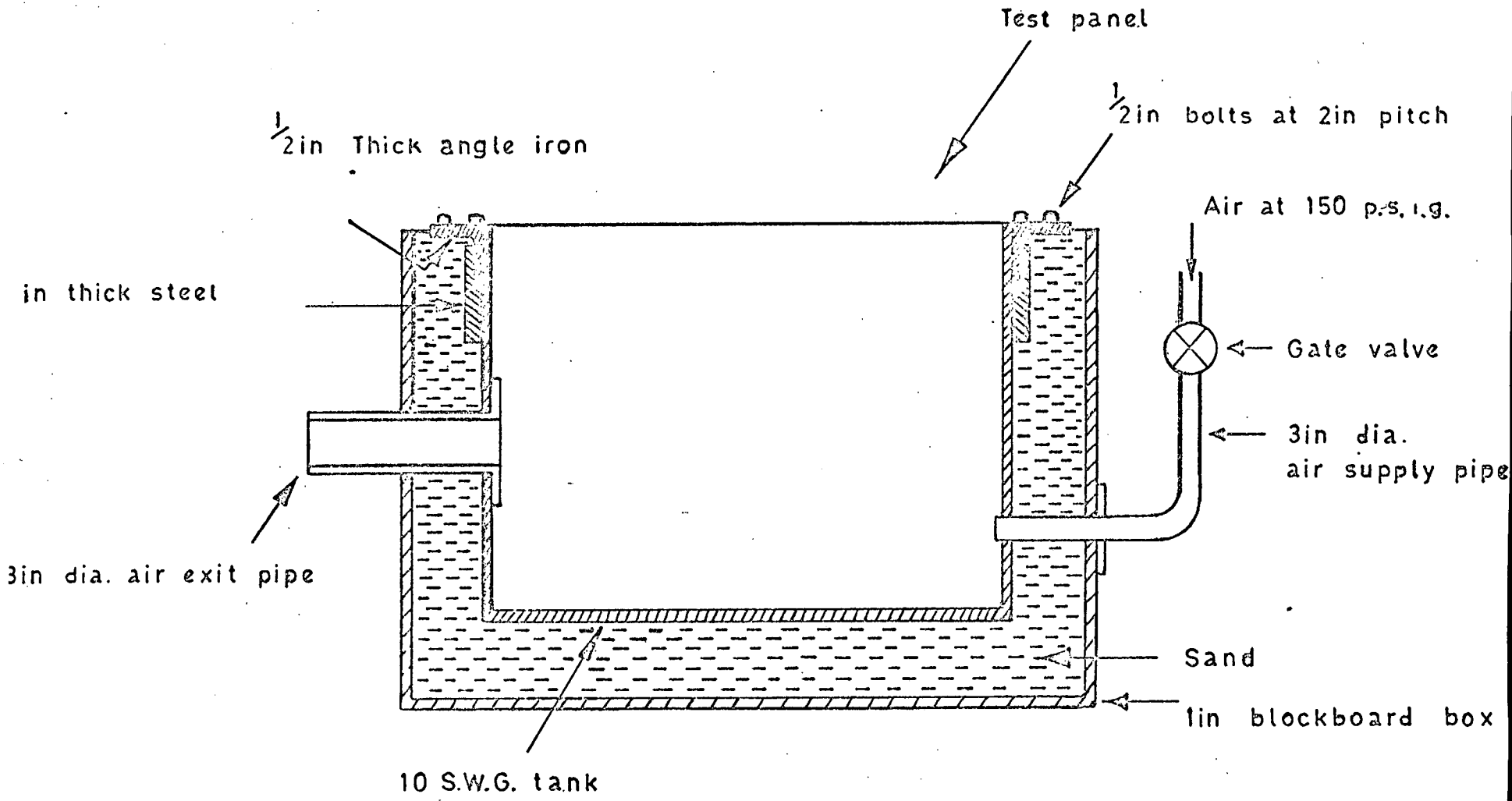

Fig 5.1. Experimental Panel - Box System (Clamped Configuration)

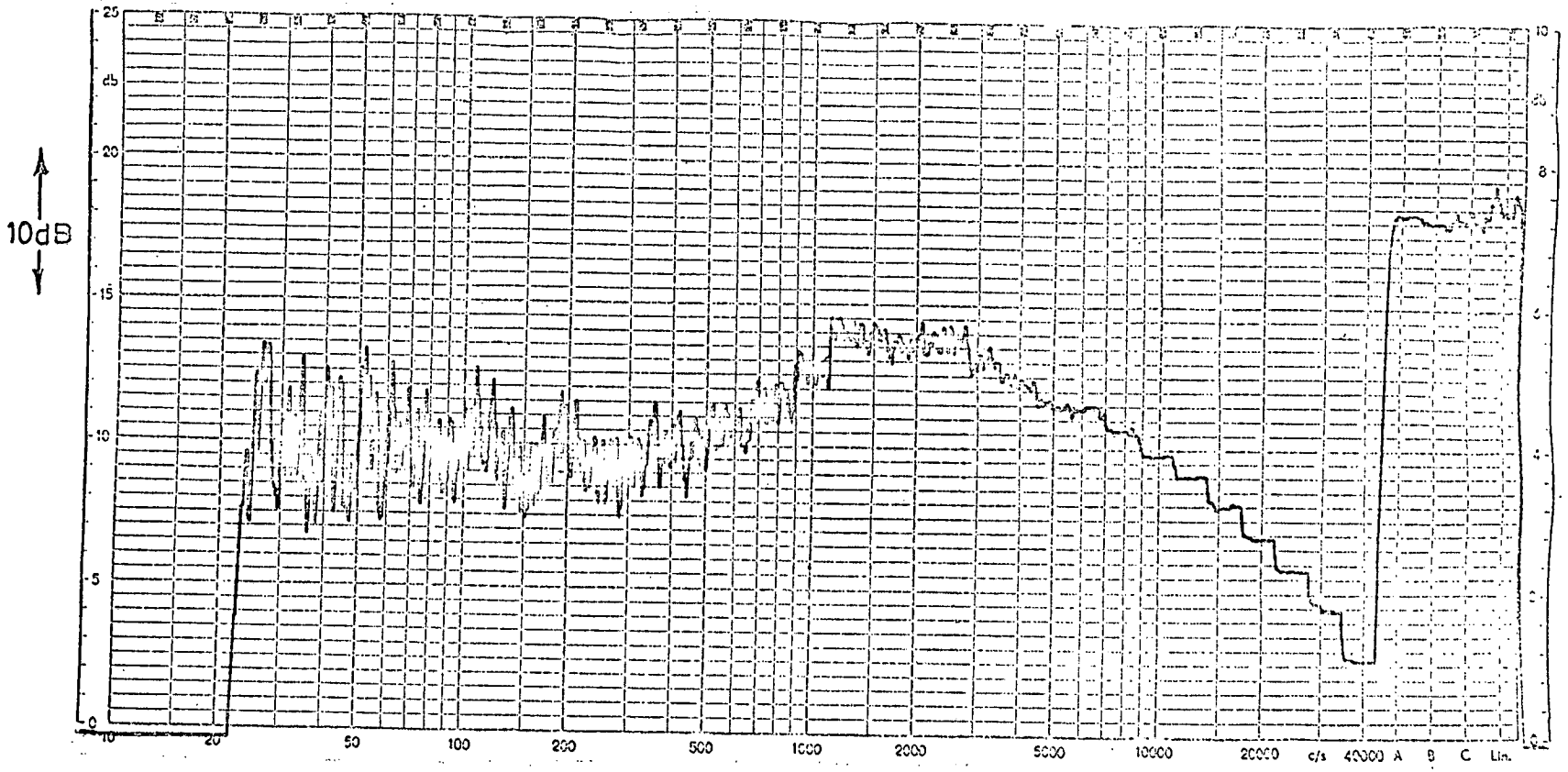

Fig. 5.2 Typical ⅓ octave acoustic pressure spectrum in box.

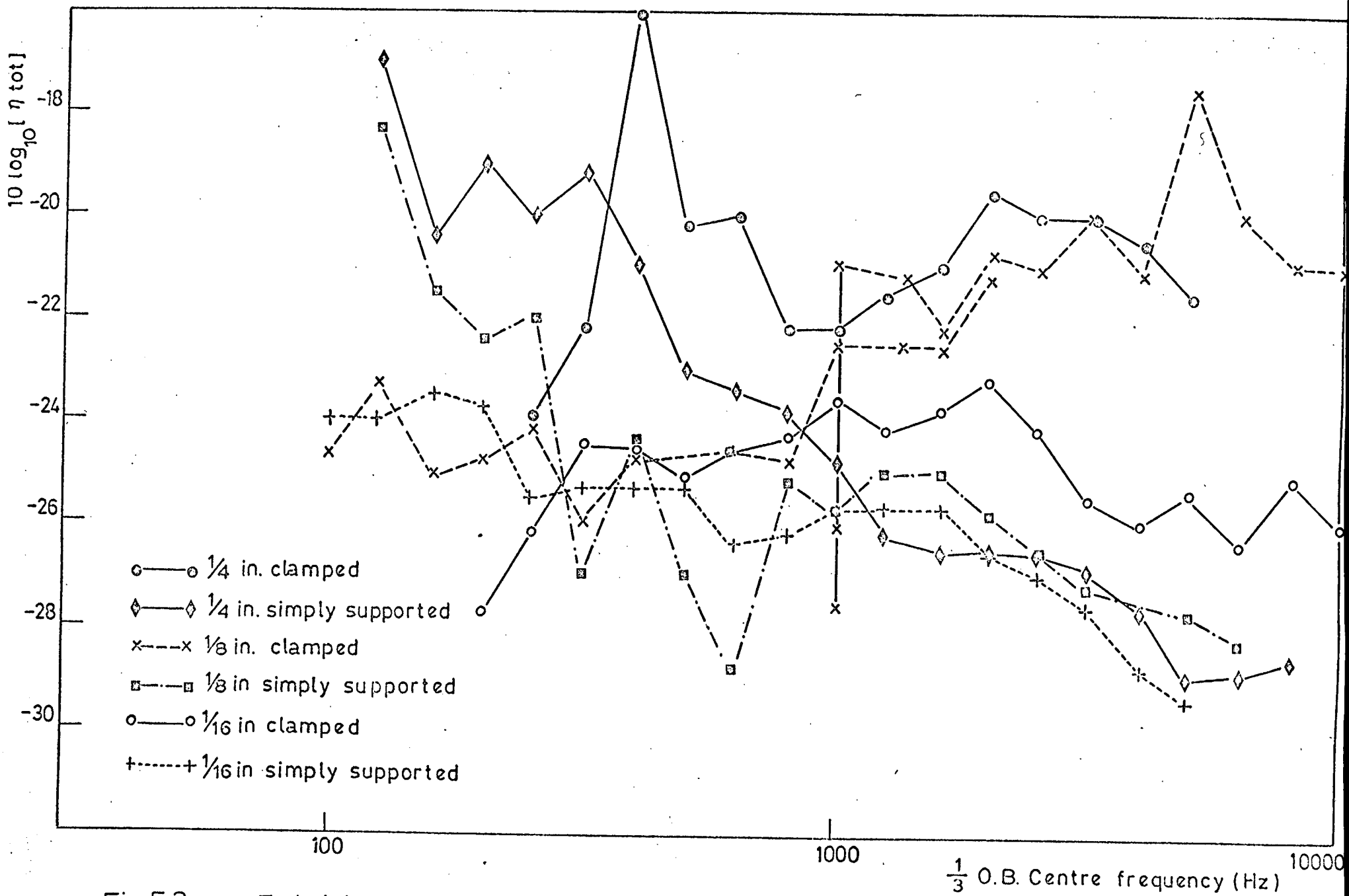

Fig.5.3 Total loss factors of panels.

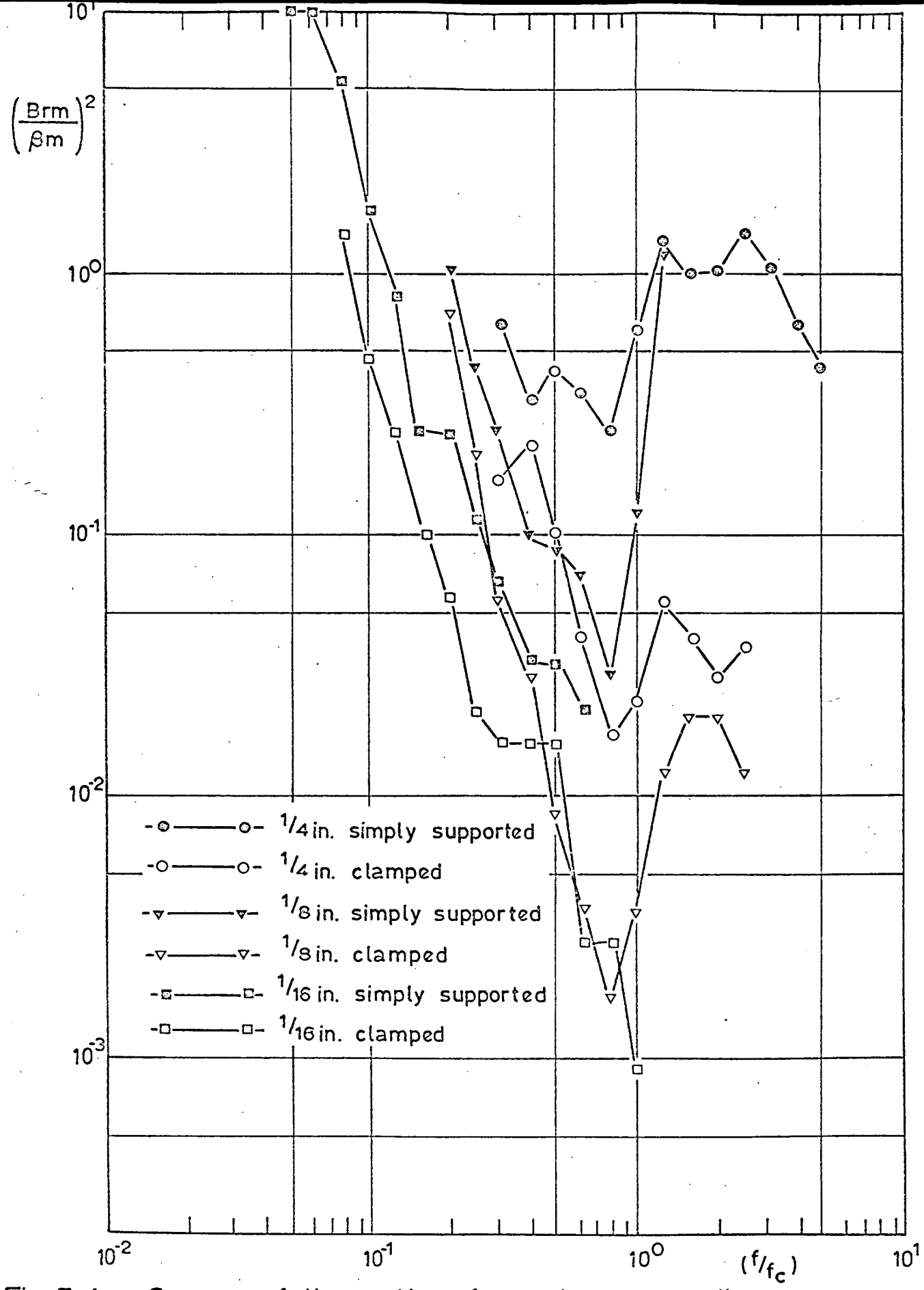

Fig. 5.4a Square of the ratio of maximum coupling coefficient to modal average mechanical damping coefficient.

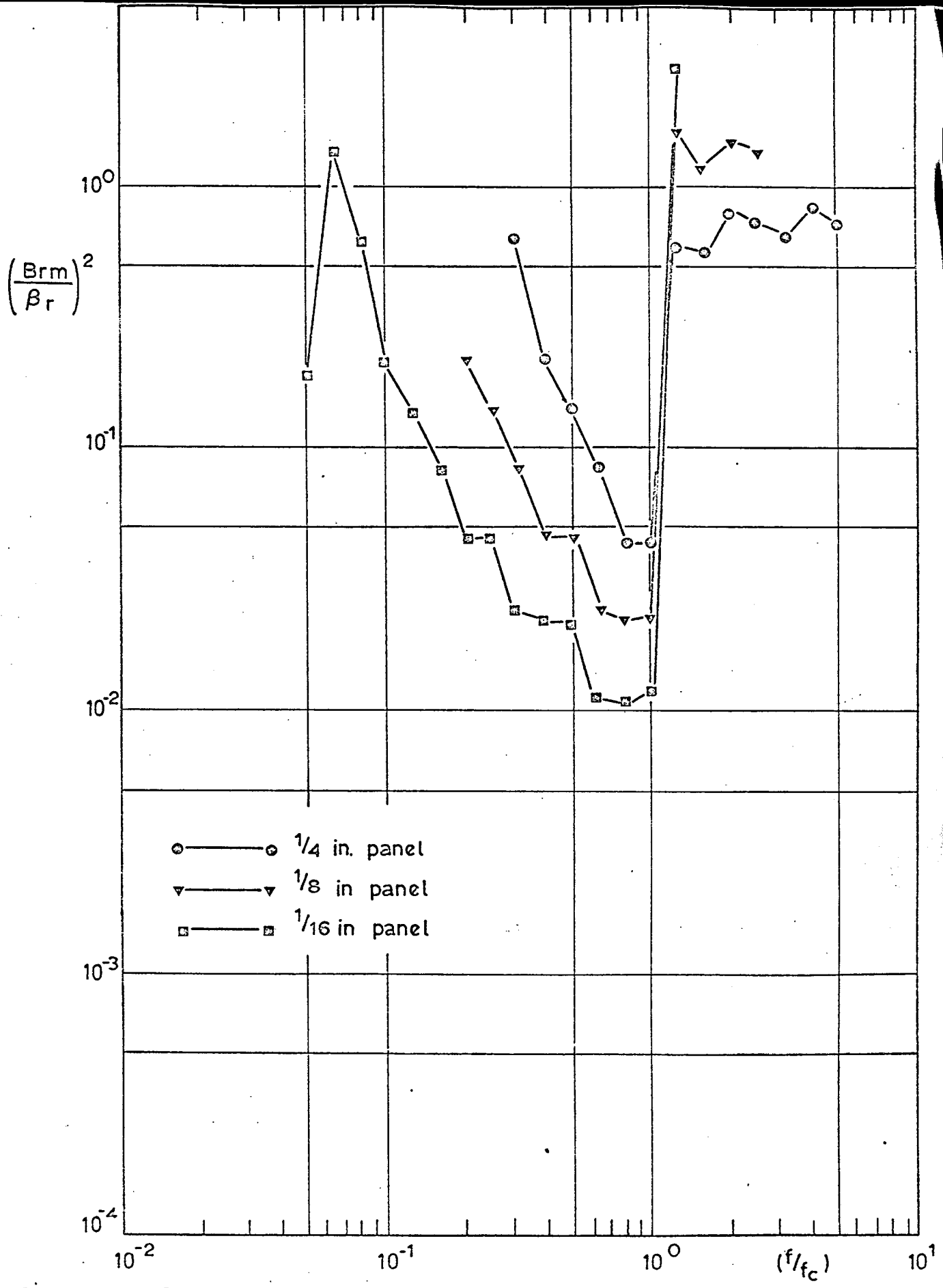

Fig.5.4b Square of ratio of maximum coupling coefficient to model average acoustic damping coefficient.

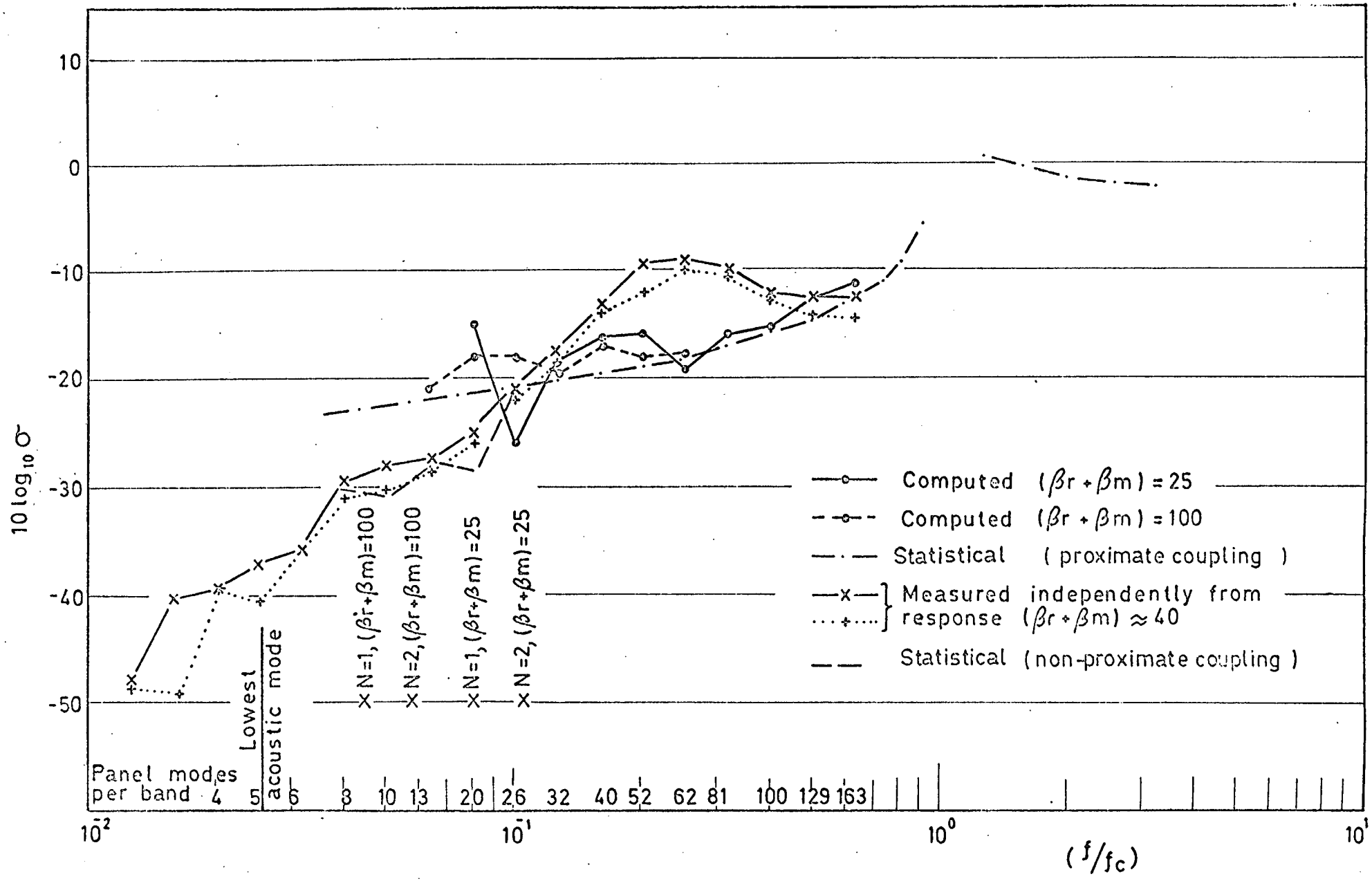

Fig.5.5 Radiation efficiency of simply supported 1/16 in panel
(1/3 octave band averages)

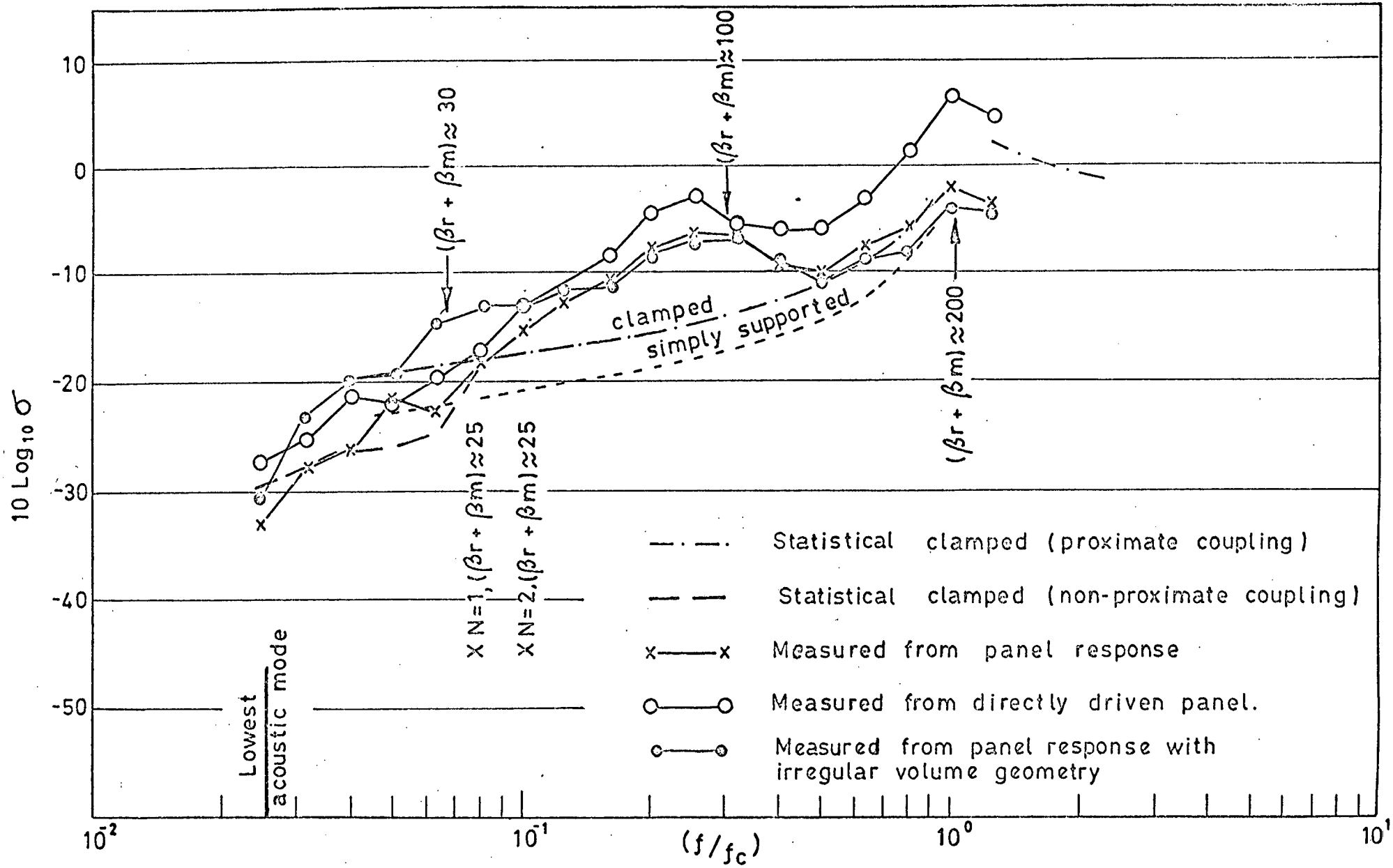

Fig. 5.6 Radiation efficiency of 1/16 in. clamped panel.
(1/3 octave band averages)

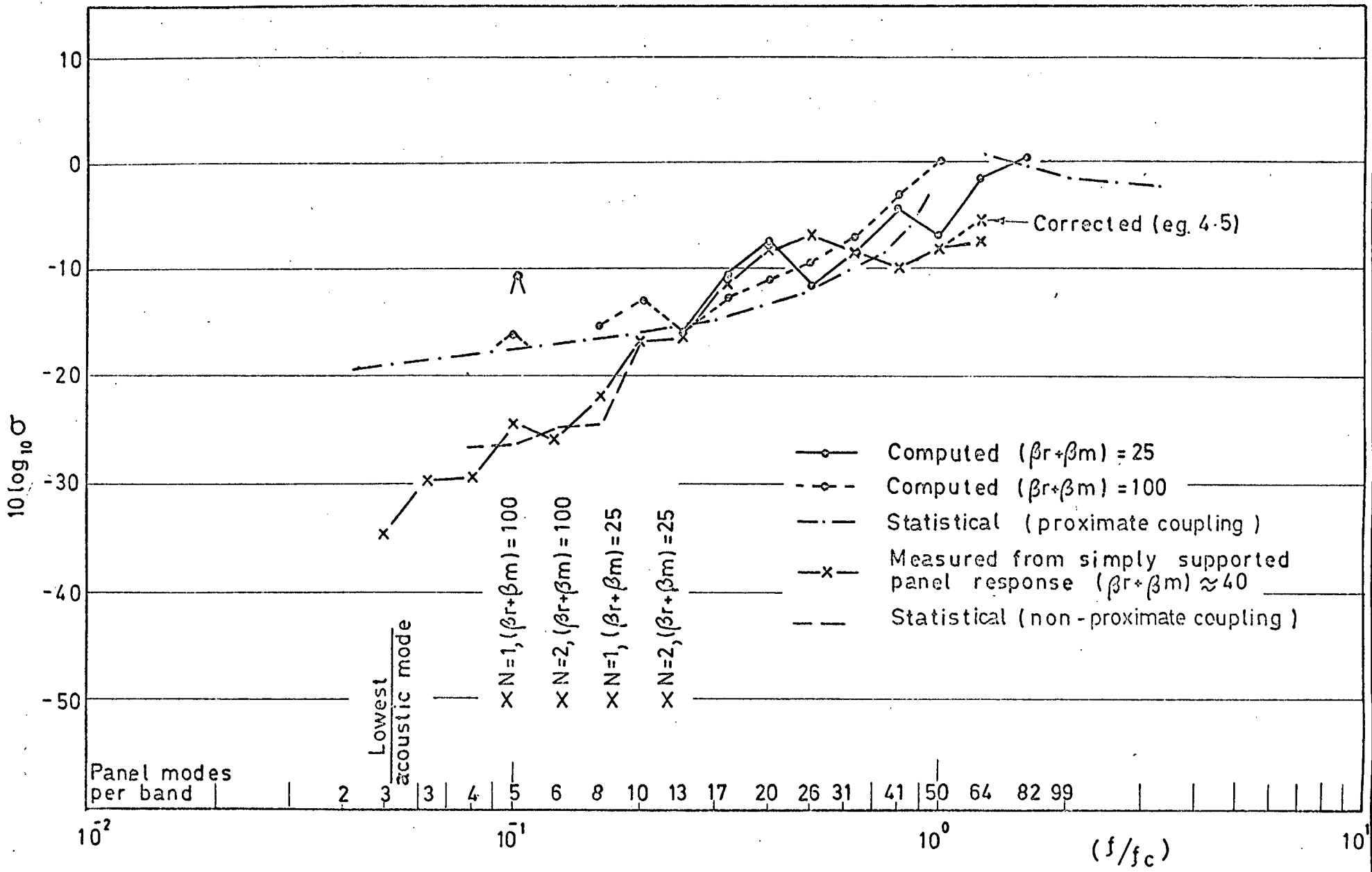

Fig.5.7 Radiation efficiency of simply supported 1/8 in. panel
(1/3 octave band averages)

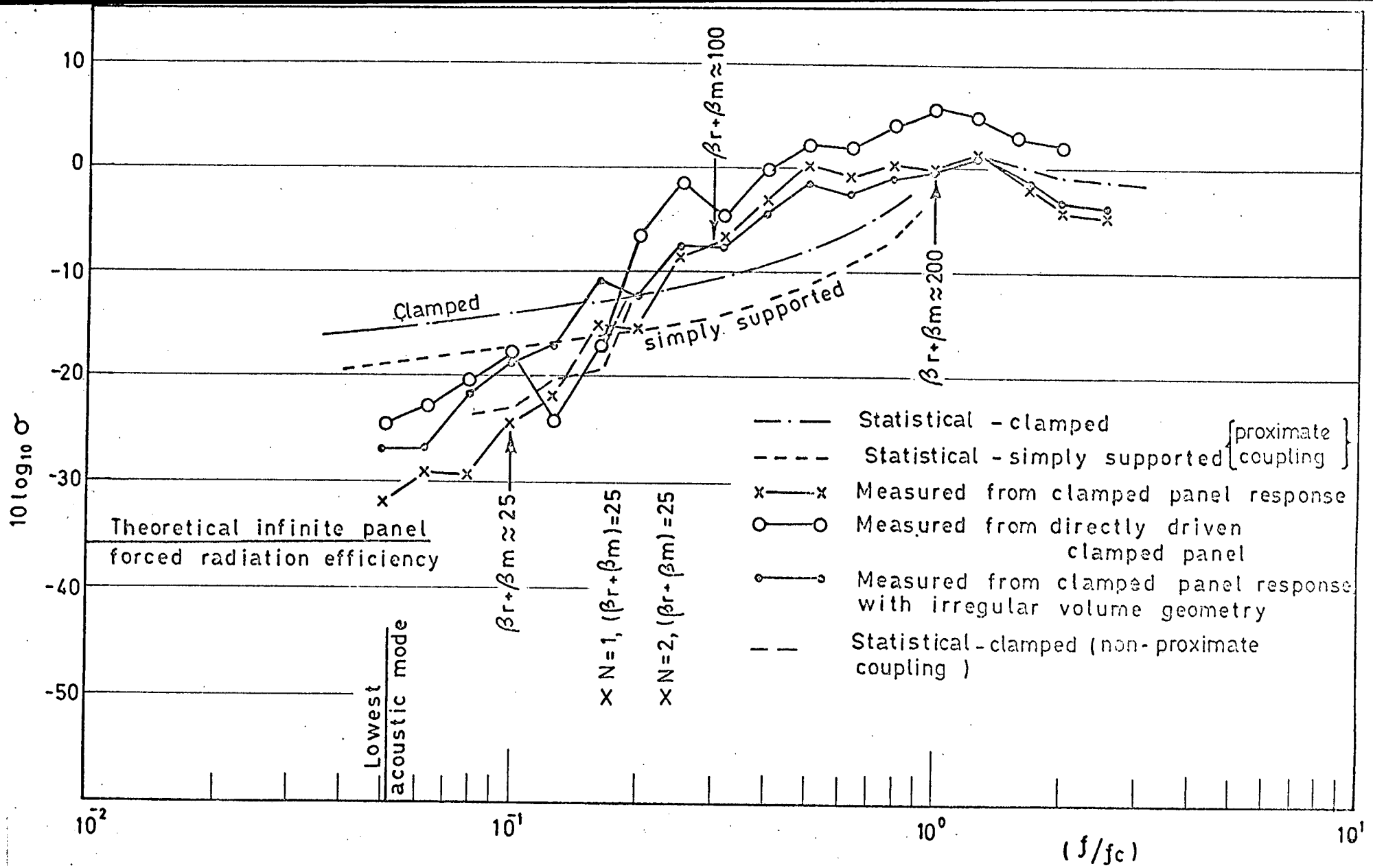

Fig. 5.8 Radiation efficiency of 1/8 in clamped panel.
(1/3 octave band averages)

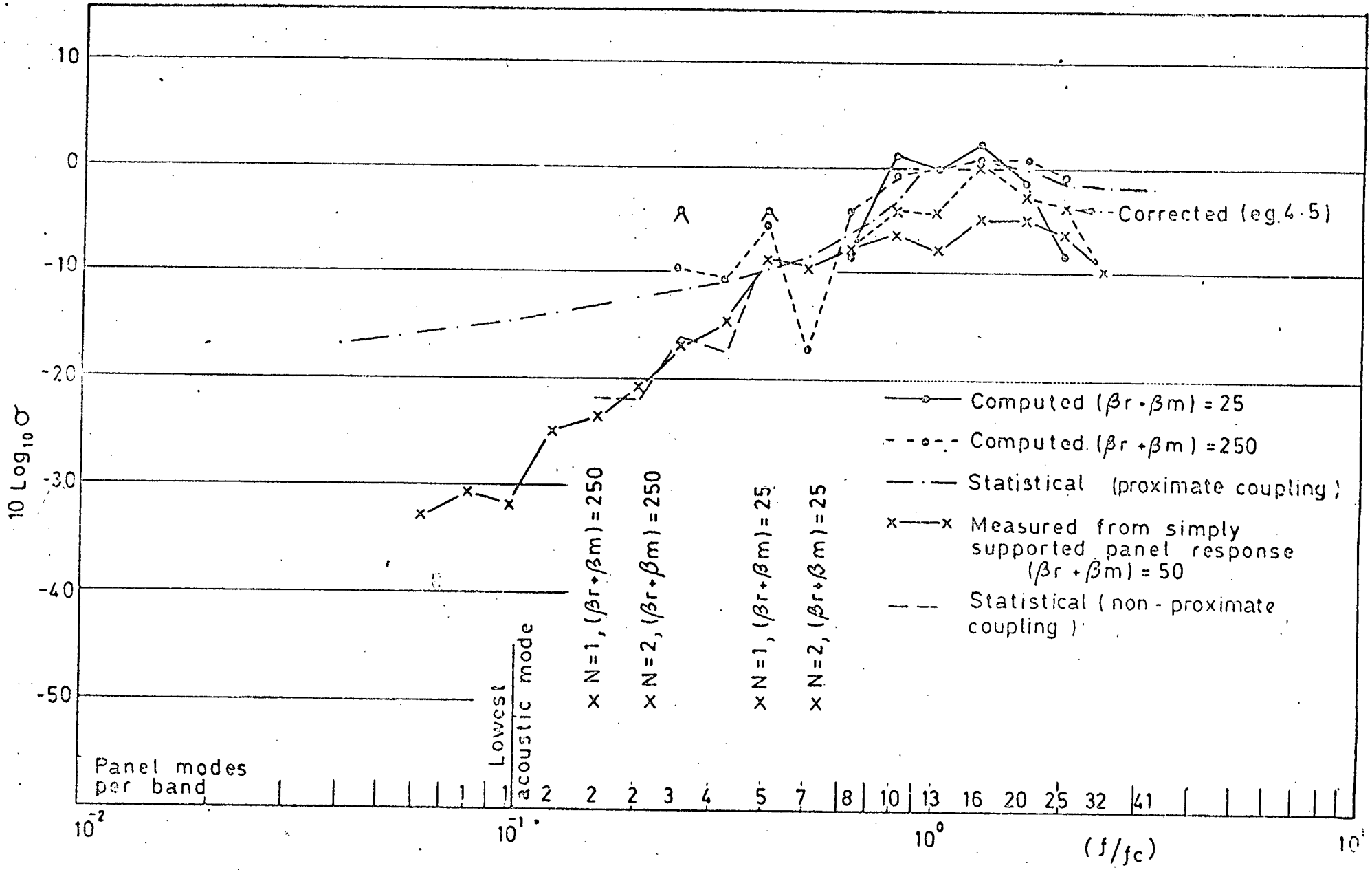

Fig 5.9 Radiation efficiency of simply supported 1/4 in. panel
(1/3 octave band averages)

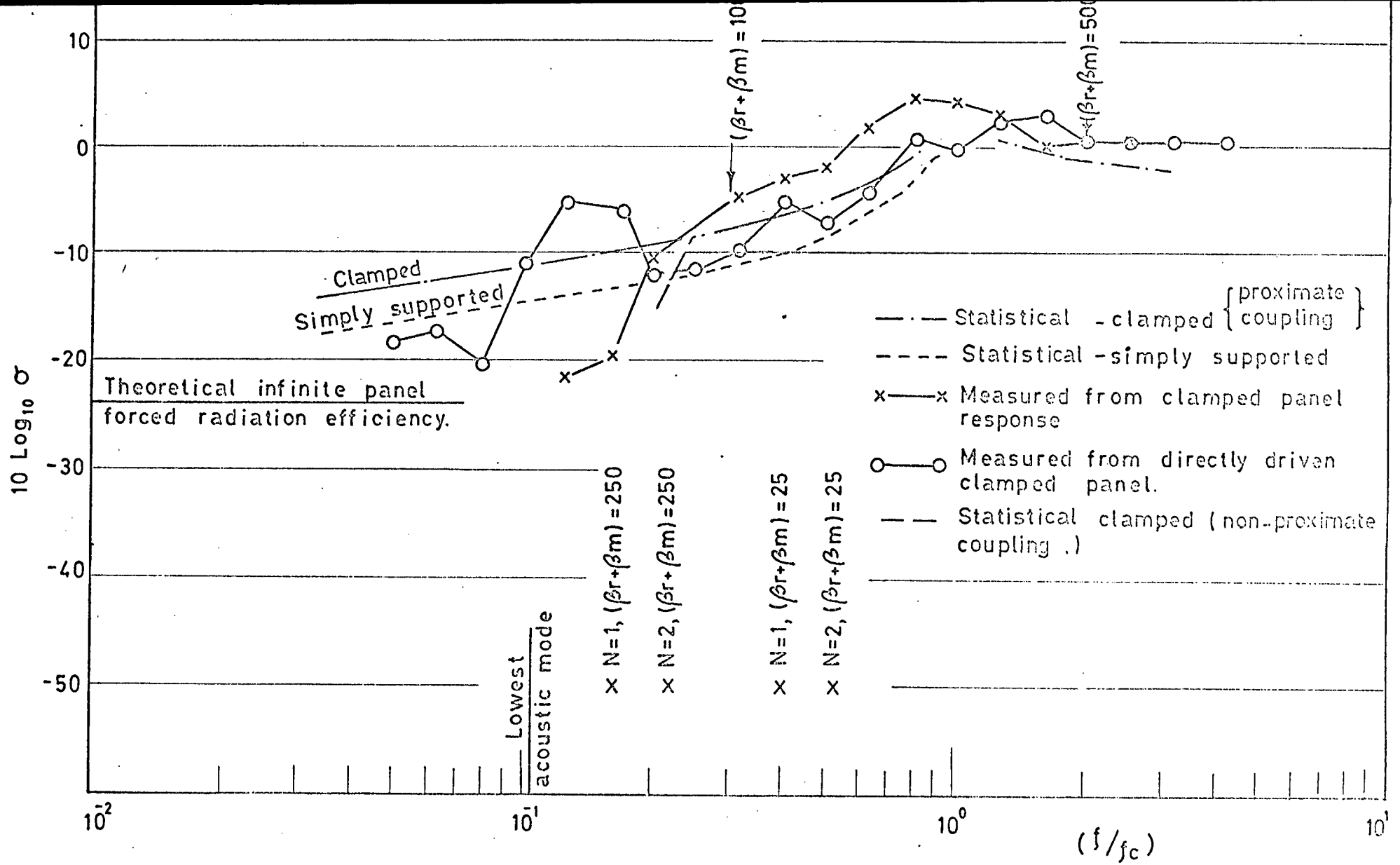

Fig. 5.10 Radiation efficiency of clamped 1/4 in panel.
(1/3 octave band averages)

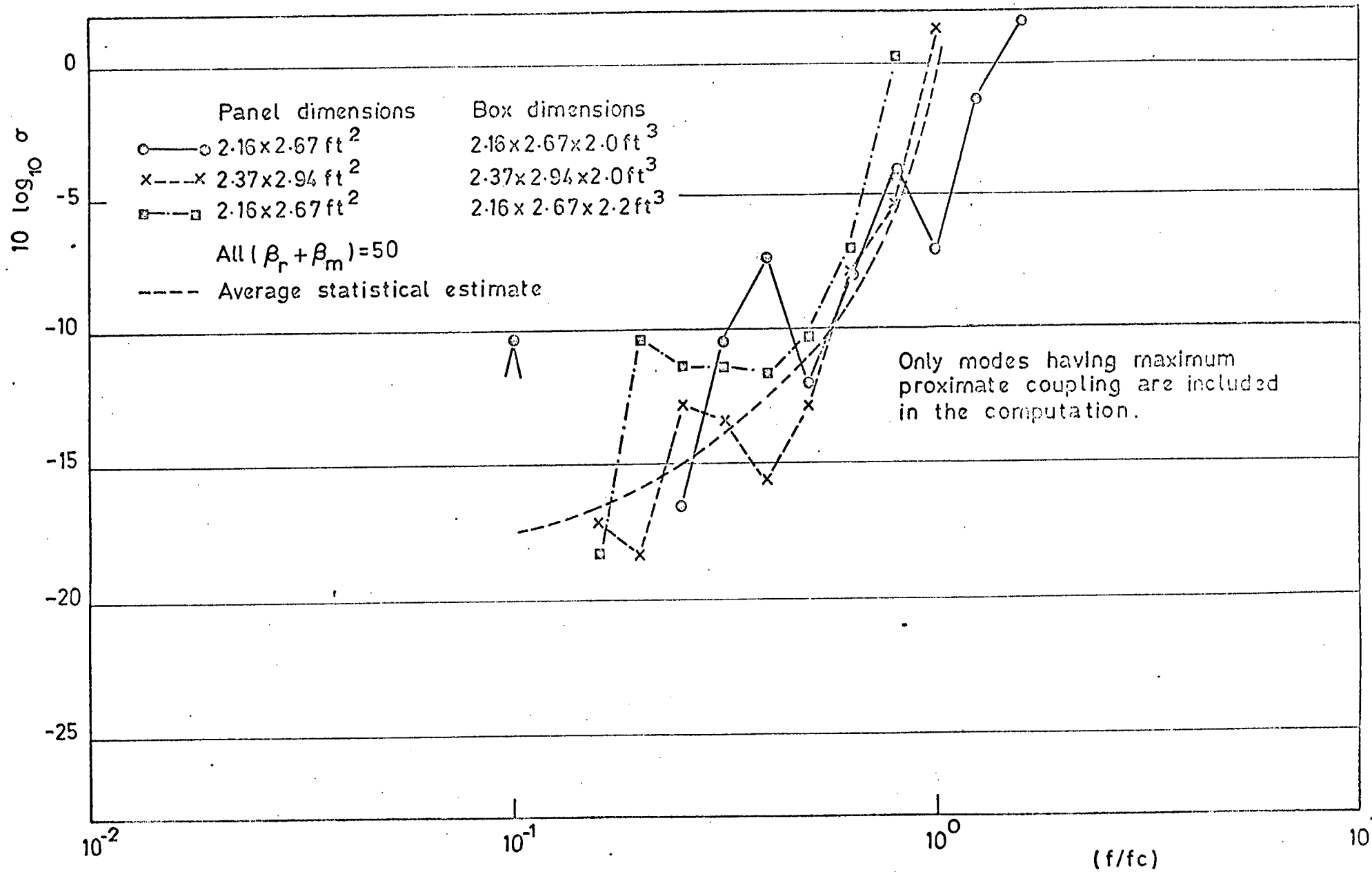

Fig 3-11 Computed radiadiation efficiency of 1/8 in simply supported panel showing effect of small change in panel and box dimensions.

CHAPTER VI

APPLICATION OF COUPLED OSCILLATOR THEORY TO A CYLINDRICAL SHELL

A problem of considerable interest in the design of nuclear reactor gas circuits, and industrial pipework in general, is that of the vibration of the walls of a cylindrical shell structure by sound in a contained fluid. A closely associated problem is that of the transmission of such noise to the surrounding air. This chapter deals with the response of a right cylindrical shell, with partially closed ends, to broad band sound in the contained air. Chapter 7 is concerned with the transmission of this sound through the cylinder walls.

6.1 Previous Analyses

The response of thin walled cylinders to externally incident discrete frequency sound has received considerable attention in the literature, notably in the work of Cremer (6), Smith (42), Heckl (43) and Franklin and Foxwell (44). A common feature of the approach of these workers has been the direct use of the fluid and infinite length shell equations of motion together with the interface boundary conditions of equality of radial velocity. Derived impedance expressions then lead to calculations of response and transmission characteristics. The assumption of incident field characteristics allows an assessment to be made, via the impedance, of the variation with angle of incidence of the waves of response and transmission characteristics. It would appear from these analyses that

sound transmission is very sensitive to angle of incidence to the cylinder axis and that for each frequency there is an angle for which transmission is virtually complete.

Excitation of a cylinder by randon sound was considered by Khabbaz (45) who took a semi-classical, semi-statistical approach. However his analysis was limited to axisymmetric vibration. Franken (46) took a purely empirical approach to the problem of sound induced vibration of a cylinder and his results have been used widely in missile response calculations (47). In a paper by White (14), which takes a completely statistical approach, it is pointed out that the classical approach used in references (6) and (42-44) has limitations when it is wished to consider the response and transmission of a finite length closed cylinder, particularly because of the diffraction of sound around the ends of the cylinder and the establishment of a reverberant field within the volume of the cylinder, which complicates the pressure field acting upon the inside of the shell. Experimental measurements presented in reference (14) of the variation of transmission with angle of incidence of the sound showed far less sensitivity to this angle than the infinite cylinder theories predict. This behaviour was attributed to the reverberant nature of the shell vibration field.

The analysis of reference (14) was based upon power flow equations between multimode systems, as presented by Lyon and Maidanik (16) and Eichler (12) for broad band random vibration. Essentially the equation for shell vibration energy states that the net power received from the external acoustic field must be partly dissipated by mechanical losses in the shell and partly radiated to the enclosed fluid volume.

The net power transmitted to the interior fluid must be dissipated therein. In reference (14) the author represented the coupling factor R_{rad}, which relates reponse of the shell to the energy of the external pressure field, and R_{int}^{rad}, which relates the acoustic power radiated to the interior fluid to the shell vibration energy, by flat plate free field radiation values; these were modified to account for the topology of the particular radiation spaces. He also assumed a ratio of mechanical (damping) resistance to radiation resistance on the basis of very little evidence. In spite of these gross assumptions, and errors in the estimates of R_{rad} and modal density (48), good agreement was obtained between the experimental results for transmission loss and the theory. It is felt, however, that a more rigorous analysis of R_{int}^{rad} should be undertaken since it is not at all obvious that plate radiation is relevant.

A paper by Manning and Maidanik (49) specifically considered the response of finite length cylindrical shells to an external diffuse sound field in terms of the free field modal radiation efficiencies, which have been shown by Smith (4), Lyon and Maidanik (16), Smith and Lyon (5) and others to govern the response of structural modes to diffuse sound. Multimode response to broad band sound can be approximately determined in terms of the modal average of the individual modal radiation efficiencies. However the efficiency with which structural modes exchange energy with the contained fluid was not considered in reference (14). Since the sound field inside a cylinder, of which the dimensions are of the same order as an acoustic wavelength, cannot approach the ideal diffuse condition, it is not necessarily correct to assume that the free field radiation efficiency

corresponds to the 'internal' radiation efficiency. A knowledge of this efficiency is necessary for calculations of the response of cylinders to sound in the contained fluid and of the transmission of this sound to the outside fluid. The present chapter presents a coupled oscillator, energy flow approach to this problem.

6.2 Cylinder Theory

6.2.1 Modal Coupling

Following reference (16) we may write the frequency band average radiation resistance, R_{rad}, as

$$R_{rad} = (M/N_s) \sum_{m,r} g_{mr} \tag{6.1}$$

where g_{mr} is given by

$$g_{mr} = \frac{B_{mr}^2 (\beta_m \omega_r^2 + \beta_r \omega_m^2)}{(\omega_m^2 - \omega_r^2)^2 + (\beta_m + \beta_r)(\beta_m \omega_r^2 + \beta_r \omega_m^2)} \tag{6.2}$$

and B_{mr} is proportional to the integral over the inside surface of the cylinder of the product of the structural displacement and acoustic velocity potential eigenfunctions of the m and r modes respectively.

$$B_{mr} = \left(\frac{c_o^2 \rho}{\sqrt{M} \varepsilon_r \varepsilon_m}\right)^{\frac{1}{2}} \int_S \psi_r(\underline{x}) \phi_m(\underline{x}) d\underline{x}. \tag{6.3}$$

In the case of a cylinder with rigid closed ends, and with

simple support conditions at these ends, as shown in Figure 6.1, the eigenfunctions may be written as

$$\psi_r(r, \theta, z) = \begin{matrix}\cos \\ \sin\end{matrix} (p\theta) \cos(\tfrac{r\pi z}{\ell}) J_p(\pi\alpha_{pq})$$

and

$$\phi_m(\theta, z) = \begin{matrix}\cos \\ \sin\end{matrix} (n(\theta + \beta)) \sin(\tfrac{m\pi z}{\ell})$$

Because the plane $\theta = 0$ is arbitrary, all structural and acoustic modes of an ideal system exist in pairs having the same natural frequencies. The argument $(\pi\alpha_{pq})$ of the p^{th} order Bessel function J_p is the solution of the equation $(dJ_p(\pi\alpha))/d\alpha = 0$, which satisfies the rigid wall acoustic boundary condition of zero radial velocity (cf. ref. 49). With the eigenfunctions used in equation (6.3), B_{mr} is given by

$$B_{mr} = \left(\frac{c_o^2 \rho}{VM\epsilon_r\epsilon_m}\right)^{\frac{1}{2}} m\ell a \cos(p\beta) \left[\frac{(-1)^{m+r} - 1}{(r^2 - m^2)}\right] J_p(\pi\alpha_{pq}) \quad : \quad \begin{matrix} p = n \\ \text{and } m \neq r \\ \text{and } \frac{m+r}{2} \neq \text{integer} \end{matrix} \qquad (6.4)$$

$$B_{mr} = 0 \quad : \quad \begin{matrix} p \neq n \\ \text{or } m = r \\ \text{or } \frac{m+r}{2} = \text{integer} \end{matrix}$$

Note that B_{mr} depends upon the phase angle β which determines the relative orientation of the acoustic mode nodal diameters and structural mode axial nodal lines around the cylinder axis. The coupling configurations are illustrated in Figure 6.2. It will already be seen that conditions on the mode orders given in equation (6.4) severely restrict

the number of acoustic modes capable of coupling with any one structural mode.

Equation (6.4) may be developed further to illustrate the paucity of mode pairs which are well coupled by virtue of their relative spatial amplitude distribution. The normalising constant for the acoustic modes ψ_r is given by

$$V\varepsilon_r = \pi a^2 \ell \varepsilon_r = \int_o^a J_p\left(\frac{\pi\alpha_{pqr}}{a}\right) J_{p'}\left(\frac{\pi\alpha_{p'q'r}}{a}\right) r dr$$

$$\times \int_o^\ell \cos\left(\frac{r\pi z}{\ell}\right)\cos\left(\frac{r'\pi z}{\ell}\right) dz \int_o^{2\pi} \cos p\theta \cos p'\theta d\theta$$

$$= \frac{\pi a^2 \ell}{2} \Lambda_{pq} \qquad (6.5)$$

where $\Lambda_{pq} = \frac{1}{2} J_p^2(\pi\alpha_{pq}) \left[1 - (p/\pi\alpha_{pq})^2\right]$: $p = p'$ and $r = r'$ and $q = q'$

$\Lambda_{pq} = 0$: $p \neq p'$ or $r \neq r'$ or $q \neq q'$

Hence when the expression for ε_r is substituted in equation (6.4) the Bessel function J_p disappears and the resulting expression for B_{rm} is

$$B_{mr} = \left[\frac{4c_o^2\rho}{M\varepsilon_m \pi \ell}\right]^{\frac{1}{2}} \left[\frac{1}{1 - (p/\pi\alpha_{pq})^2}\right]^{\frac{1}{2}} m\ell \cos(p\beta) \left[\frac{(-1)^{m+r} - 1}{(r^2 - m^2)}\right] : \begin{array}{l} p = n \text{ and} \\ m \neq r \text{ and} \\ \frac{m+r}{2} \neq \text{integer} \end{array}$$

$$B_{mr} = 0 : \begin{array}{l} p \neq n \text{ or} \\ m = r \text{ or} \\ \frac{m+r}{2} = \text{integer} \end{array} \qquad (6.6)$$

The following approximation may be written for non zero B_{rm}, with $r = m \pm s$; $m \geq 3$; s odd,

$$B_{mr} \simeq \frac{2}{((s^2/2m) + s)} \left[\left(\frac{c_o^2 \rho \ell}{M \epsilon_m \pi} \right) / (1 - (p/\pi\alpha_{pq}))^2 \right]^{\frac{1}{2}} \cos(p\beta) \qquad (6.7)$$

It will be seen that except for the $\cos(p\beta)$ factor, B_{rm} takes maximum values with $s = 1$ when $p = 0$, and with $s = 1$ and $p \simeq \pi\alpha_{pq}$ when $p \neq 0$.

In Chapter 4 and reference (50) it is shown that, because of the sensitivity of g_{mr} to $(\omega_m^2 - \omega_r^2)$, (eqn. (6.2)), acoustic structural mode pairs may be broadly classified into two groups. The first contains those which have modal natural frequencies separated by not more than half the sum of their half power bandwidths, which pairs are said to have proximate modal coupling. The second contains those whose natural frequencies are wider apart and for which the term $(\omega_m^2 - \omega_r^2)^2$ dominates the denominator of equation (6.2). These pairs are said to have non-proximate coupling. These conditions are represented by the following approximations:

$$g_{mr} \simeq B_{mr}^2/(\beta_r + \beta_m) \; : \; 2|\omega_m - \omega_r| < (\beta_m + \beta_r) \qquad (6.8a)$$

$$g_{mr} \simeq 0 \qquad : \; 2|\omega_m - \omega_r| > (\beta_m + \beta_r) \qquad (6.8b)$$

Mode pairs which satisfy both the conditions for maximum B_{mr} from equation (6.7) and also the frequency proximity condition of equation (6.8a) are said to have <u>maximum proximate modal coupling</u>, as

previously defined for the panel box system.

6.2.2 Evaluation of the Radiation Resistance

In the analysis of R_{rad} for a panel (50) it was found that it was possible to consider the summation in the equation $R_{rad} = (M/N_s) \sum_{m,r} g_{mr}$ in separate finite frequency bands provided that their bandwidths were substantially greater than the average modal bandwidth of the modes having natural frequencies in these finite bands. It was found by comparison of the results of a statistical analysis, which included only mode pairs in a band having maximum proximate modal coupling, and a numerical analysis, which included all mode pairs in the band having proximate coupling, that the former mode pairs dominated the total coupling. It was also found that mode pairs having natural frequencies more than half the sum of their half power bandwidths apart, (non-proximate mode pairs) did not contribute significantly to the total coupling in frequency bands in which, on average, at least one mode pair having maximum proximate coupling could be expected to exist. A lower limiting frequency was established above which non-proximate mode coupling could be neglected. The following sections describe analogous calculations on a cylindrical shell.

6.2.2.1 Numerical analysis

The sum $\sum_{m,r} g_{mr}$ was evaluated by computer for the cylindrical shell and volume shown in Figure 6.1, on which experimental measurements were made. As with the panel, all mode pairs sufficiently close in natural frequency to satisfy the proximate mode condition of equation (6.8a) were accounted for in the summation, whatever their wavelength

relationships, or B_{rm} values. Such a restriction was found to be satisfactory for the rectangular panel-box system above the lower limiting frequency and it is expected always to be reasonable for coupled acousto-mechanical systems with reasonably smooth modal density curves.

The structural mode frequency equation used was equation (8) of reference (51). The acoustic mode frequency equation was

$$f_r = (c_o/2)\{(r/\ell)^2 + (\alpha_{pq}/a)^2\}^{\frac{1}{2}} \qquad (6.9)$$

In evaluating $R_{rad} = (M/N_s)\sum g_{mr}$, the total number of structural modes in a frequency band, N_s, was obtained from the computer output. It agreed well with the 'modified Bolotin' curve of Miller (52).

R_{rad} does not depend upon whether the double degeneracy of the structural mode frequency distribution is taken into account or not because R_{rad} is inversely proportional to N_s. However the degeneracy of the acoustic mode frequency distribution produces a total number of mode frequencies in a given band which is half the total number of actual modes. This was taken into account by doubling the value of $\sum g_{mr}$ as computed. The term $\cos^2(p\beta)$ in each B_{rm} was considered to vary randomly over the set of mode pairs considered in each band and the average value of $\frac{1}{2}$ was applied as a factor to the sum. Hence the resulting value of R_{rad} corresponded to neglect of the acoustic mode frequency degeneracy and of the terms $\cos^2(p\beta)$.

The results of this numerical evaluation of radiation efficiency σ $(= R_{rad}/2\rho c_o \pi a \ell)$ are shown in Figure 6.10.

6.2.2.2 Statistical analysis

The Radiation Resistance may be evaluated by making a statistical estimate of the total number of mode pairs in any frequency band which enjoy maximum proximate coupling. This estimate can be combined with the relevant values of coupling coefficient, B_{rm} (equation (6.7)), together with use of the frequency proximity criterion of equation (6.8a), to calculate $(M/N_s)\sum_{m,r} g_{mr}$.

The mode pairs which satisfy the frequency proximity condition can be determined, as in Chapter IV, by consideration of a three-dimensional structural-acoustic wavenumber lattice diagram, or frequency space diagram, similar to those used in the statistical theory of room acoustics (cf. ref. 32). The structural modes of the shell are represented by points in a two dimensional lattice in the $k_y k_z$ plane. The distance from the origin of the coordinates to each lattice point is a measure of the wavenumber $(\omega_m/c_B = k_s)$ of that mode at its natural frequency (ω_m). c_B is the phase speed of flexural waves travelling in the shell in the direction of the wavenumber vector as defined by the angle of the line joining the lattice point to the origin. Figure 6.4 shows such a lattice for the experimental cylinder, where the modes are grouped in 1/3 octave bands.

The acoustic modes of the fluid space are represented in a three dimensional lattice, where the magnitude of the wavenumber of a mode at its natural frequency is represented by the distance from the lattice point to the origin. Those mode pairs which are proximate in frequency can be identified by drawing a typical line of constant frequency ω_m on the $k_x k_z$ plane, and then drawing two surfaces through the acoustic mode lattice

space which are separated by a distance corresponding to twice the allowable frequency difference between proximate structural and acoustic modes. The resulting shell has a middle surface given by $k_r = \omega_m/c_o = k_s c_B/c_o$, and a thickness given by $\Delta k_r = \Delta\omega/c_o = (\beta_r + \beta_m)/c_o$ (Figure 6.6). Acoustic modes of which the lattice points lie within this shell are proximate in frequency to structural modes having lattice points which lie on the constant frequency contour in the plane $k_x k_z$.

Application of the mode order restrictions given in equations (6.6) and (6.7) to the proximate mode pairs completes the identification of those mode pairs which enjoy maximum proximate coupling. A statistical estimate of the number of such acoustic modes for typical structural modes can be made from a knowledge of shell and volume eigenfrequency statistics, and the sum $(1/N_s) \sum_{m,r} g_{mr}$ can therefore be evaluated for well coupled mode pairs. It should be noted that in the analysis of R_{rad} for external radiation (49) in which there are no frequency or spatial matching criteria, all structural modes having $k_s < \omega/c_o$ $(= k_o)$ are called acoustically fast modes and are assumed to have a radiation efficiency of unity.

It was found in Chapter IV that there was a lower frequency limit below which, on average, no mode pairs having maximum proximate coupling existed in a frequency band. The following cylinder analysis also indicates the existence of such a lower 'limiting frequency', and a special estimate of R_{rad}, using an analysis of non proximate mode pair coupling, is presented in Appendix VI.

Manning and Maidanik (49), Heckl (51) and Chandiramini et al (53) have shown that lines of constant frequency for a finite cylindrical shell do not take a simple form and are a function of the ratio of the

frequency to the ring frequency of the cylinder, f_R, as shown in Figure 6.3. The latter depends only upon the diameter and material of the cylinder and is given by $f_R = (C_L/2\pi a)$, at which frequency the length of the cylinder circumference equals the wavelength of longitudinal waves in the cylinder material. It is associated with a peak in the modal density curve (52). An approximate form of constant frequency lines which may be used for frequencies given by $(f/f_R) < 0.8$ is also shown. It is interesting to compare it with the wavenumber lattice diagram which is shown in Figure 6.4 for the experimental cylinder.

There is no strict frequency space representation of the acoustic modes of a cylindrical volume because standing waves are made up of waves with components in all directions perpendicular to the axis of the cylinder. However Morse (49) suggests one formal representation of the allowed frequencies in a cylindrical room. Extensive computation of cylindrical space acoustic mode frequencies has produced the relatively simple wavenumber diagram shown in Figures 6.5a and 6.5b, for which Morse provided the inspiration. It has been found that the wavenumber corresponding to the natural frequency of a particular acoustic mode of mode order (p, q, r), may be remarkably well approximated by the simple expression $k^2_{pqr} \simeq 2.77(p/a)^2 + pq(\pi/a)^2 + (q\pi/a)^2 + (\pi r/\ell)^2$ for $q \neq 0$. For $q = 0$ the approximate expression of Morse (54), $k^2_{por} \simeq \{(\pi r/\ell)^2 + (p + 0.26\, p^{1/3})^2/a^2\}^{\frac{1}{2}}$, may be used. It was found that Morse's expression for $p > 1$, $p > q$, $q \neq 0$ did not compare well with computed values of k_{pqr}. The wavenumber diagram in Figures 6.5 and 6.6 include only one lattice point for each acoustic mode pair of equal frequency.

A combined approximate acoustic-structural lattice diagram is

shown in Figure 6.6, for a frequency which is both below the ring frequency, f_R, and the critical frequency, f_c, of a cylinder. The latter is calculated as for a flat plate of the same thickness and material of the cylinder material. For a detailed discussion of the importance of the ratio (f_R/f_c) the reader is referred to reference (49) and Figure 6.12. As before, the segment of spherical shell is of thickness $\Delta k_r = (\beta_r + \beta_m)/c_o$ and has a middle surface given by $k_r = 2\pi f_m/c_o$, where f_m is the frequency corresponding to the line of constant structural frequency being considered, as shown in the $k_x k_z$ plane of Figure 6.3. This shell segment contains the lattice points of acoustic modes which have frequencies sufficiently close to f_m to form proximate mode pairs with structural modes of frequency f_m, as defined by equation (6.8a).

If we restrict the terms in the summation $\sum g_{mr}$ to those given by mode pairs having maximum proximate coupling, as defined by equations (6.8c) and (6.7) with $s = 1$ and $p = n$, we are left only with the problem of deciding which acoustic modes have $p \simeq \pi a_{pq}$ and whether modes for which $p = 0$ or $p \neq \pi\alpha_{pq}$ can make significant contributions to the sum.

By reference to approximate expressions for α_{pq} given by Morse (54), and from a study of the computed values of the proximate mode terms for the particular case described in section 6.2.2.1, it is found that the largest values of the term $|1 - (p/\pi\alpha_{pq})^2|^{-1}$ occur for $q = 0$ when, for $p \gg 1$, $(p/\pi\alpha_{pq})^2 \simeq |1 + 0.8p^{-2/3}|^{-2}$. Figure 6.6 shows that the condition $p = n$, $q = 0$, always requires $p > 1$ so that the above expression may be used for all $q = 0$ modes.

The cases $p \neq 0$, $q \neq 0$ can be shown on average to give very

similar values of B_{rm} to the case $p = 0$, excepting the $\cos(p\beta)$ factor, because $p/\pi\alpha_{pq}$ varies between 0.3 and 0.1 for which $(1 - (p/\pi\alpha_p)^2 \simeq 1$ in equation (6.7).

The mode couplings for $s = 1$ (see eqn. (6.7) therefore fall into two groups as follows:

(a) $s = 1, \quad p = n > 1, \quad q = 0, \quad m > 3$

$$B^a_{mr} \simeq 2\left[\frac{c_o^2 \rho \ell}{M\epsilon_m \pi}\right]^{\frac{1}{2}} \left[1 - (1 + 0.8p^{-2/3})^{-2}\right]^{-1} \cos(p\beta) \qquad (6.10a)$$

with $p \simeq (2\pi f/c_o)(1 - f/f_r)^{\frac{1}{2}}$

(b) $s = 1, \quad p = n = 0, \quad m > 3$

or $s = 1, \quad p = n \neq 0, \quad q \neq 0, \quad m > 3$

$$B^b_{mr} \simeq 2\left[\frac{c_o^2 \rho \ell}{M\epsilon_m \pi}\right]^{\frac{1}{2}} \cos(p\beta) \qquad (6.10b)$$

We shall call these a- and b-type coupling respectively. Except for the factor $\cos(p\beta)$, B^a_{rm} is usually about three times B^b_{rm}. Structural modes which have the potential for such coupling correspond to the acoustically fast modes of reference (49). However, the frequency proximity restriction may not allow all these modes to couple well with an internal fluid.

The average number of mode pairs giving the above factors in any frequency band for which $(f/f_R) < 0.8$ and $(f/f_c) < 1$ can be determined approximately from Figure 6.7 which shows a section through

the combined wavenumber diagram (Figure 6.6) on a plane p = constant. The approximate form of the constant structural frequency line as shown in Figures 6.3 and 6.4 is used, for $(f/f_R) < 0.8$, to describe the average distribution of structural modes in a given frequency band over the $k_x k_z$ plane. For a given frequency band this means of determining the mode distribution in wavenumber space becomes more accurate as the shell thickness decreases, because the number of modes having natural frequencies less than the centre frequency of the given band increases, so that actual mode distribution deviates less from the average.

In a frequency band for which $f < 0.8f_R$, and for a cylinder having $f_R < f_c$, it can be shown from Figure 6.7 that the average total number of structural modes which are capable of having a-type coupling to the $q = 0$ acoustic modes is given by $(\Delta k_r \Delta\phi k_r a\ell/\pi)$. $\Delta\phi$ is given by (53),

$$\Delta\phi = \cos^{-1}\left[(f/f_R)(1 - \Delta f/2f)\right]^{\frac{1}{2}} - \cos^{-1}\left[(f/f_R)(1 + \Delta f/2f)\right]^{\frac{1}{2}} \tag{6.11}$$

If the thickness of the shaded strip of Figure 6.6, which is shown in plane in Figure 6.7, is substantially less than the separation (π/ℓ) between the structural mode lattice points in the k_z direction, then only a fraction of the total number of structural modes capable of a-type coupling will achieve it. This condition is given by $[\sqrt{2}\Delta k_r/(\cos\gamma + \sin\gamma)] < \pi/\ell$. γ is shown in Figure 6.6 from which $(\cos\gamma + \sin\gamma) = (1 + f/f_R)^{\frac{1}{2}}$. For practical purposes the condition approximates to $\ell < 2c_o/(\beta_r + \beta_m)$: a typical value of the right hand side of the inequality is 10 ft. The fraction of modes which will achieve a-type

coupling to acoustic modes is then given by $[\sqrt{2}\ \Delta k_r/(1 + f/f_R)^{\frac{1}{2}}]/(\pi/\ell)$ and the average total number of mode pairs having a-type coupling is given by

$$N_s^a = (2\sqrt{2}\ (\Delta k_r)^2 k_r \Delta\phi \ell^2 a)/(\pi^2(1 + f/f_R)^{\frac{1}{2}}) \qquad (6.12)$$

If $\sqrt{2}\ \Delta k_r/(\cos\gamma + \sin\gamma) > 2\pi/\ell$, then on average every structural mode capable of a-type coupling will achieve it, and N_s^a will be given by

$$N_s^a = 2\sqrt{2}\ (\Delta k_r)^2 k_r \Delta\phi \ell^2 a \qquad (6.13)$$

This will normally only occur for long, or heavily damped, cylinders and is not the case with the experimental cylinder.

The average total number of structural modes capable of having b-type coupling is given by $(\ell a k_r^2 \Delta\phi/2\pi)$. The average number of $q \neq 0$ acoustic modes having b-type coupling with each of these structural modes is given by $(2a\Delta k_r)$. Hence the average total number of mode pairs having b-type coupling is given by

$$N_s^b = \ell a^2 k_r^2 \Delta\phi \Delta k_r/\pi. \qquad (6.14)$$

The absence of acoustic mode lattice points in the arc between the $q = 0$ and $q = 1$ lines of Figures 6.5a and 6.5b can lead to some modification of equation (6.14) when n_{max}, given by $n_{max} = ak_r(1 - f/f_R)^{\frac{1}{2}}$, is greater than p_{max}, given by the expression for k_{pqr} with $q = 1$ and $r = 0$. However the alteration of the value of N_s^b is normally small for $f < f_R < f_c$. Now from equation (6.5) we have

$$g_{mr}^a = (B_{rm}^a)^2/(\beta_r + \beta_m) = 4\frac{(c_o^2 \rho \ell)}{(M\epsilon_m \pi)}\ [1 - (1 + 0.8p^{-2/3}]^{-1}\cos^2(p\beta)/(\beta_r + \beta_m) \qquad (6.15)$$

$$g^b_{mr} = (B^b_{rm})^2/(\beta_r + \beta_m) = 4\left(\frac{c_o^2 \rho \ell}{M \varepsilon_m \pi}\right) \cos^2(p\beta)/(\beta_r + \beta_m) \qquad (6.15)$$

Equations (6.15), (6.14), (6.11) and (6.1) give, for $(f/f_R) < 0.8$ and $f/f_c < 1$,

$$R_{rad} = (M/N_s) \sum_{m,r} g_{mr} \simeq (M/N_s)\left[N_s{}^a g_{mr}{}^a + N_s{}^b g_{mr}{}^b\right]$$

$$= \frac{4\rho a^2 \ell^2 \Delta\phi}{c_o \pi^2 N_s \varepsilon_m} \left\{ \frac{f\ell(\beta_r + \beta_m)}{a} \left[1 - (1 + 0.8p^{-2/3}]^{-1} + 2\pi^2 f^2\right\} \qquad (6.16)\right.$$

Note that p has been treated as a constant, and taken outside the summation sign. This is because, when $q = 0$, p is fixed by the coincidence of the constant frequency line of the structural modes and the intersection of the acoustic wavenumber shells with the $k_x k_z$ plane (Figure 6.6 and equation (6.10a)). The validity of this procedure has been confirmed by the computational study.

In equation (6.16) the factor $\cos^2(p\beta)$ has been treated as a random variable with an average value of $\frac{1}{2}$. Inclusion of the $s = 3$ modes will increase the numerical constant to 4.4. Mode pairs for which $s > 3$ do not contribute significantly to the sum.

At well supercritical frequencies, when $f >> f_c > f_R$, all structural modes have b-type coupling and there is no a-type coupling. Then the radiation resistance is given by $R_{rad} = (MN_s g^b_{rm}/N_s)(2a\Delta k_r)$ which gives, including the $s = 3$ modes,

$$R_{rad} = \frac{4.4 \rho c_o a \ell}{\pi \varepsilon_m} \qquad (6.17)$$

The supercritical radiation efficiency is thus given by

$$\sigma = 17.6/2\pi^2 \approx 0.9. \tag{6.18}$$

At frequencies just above the critical frequency some of the structural modes of large n cannot couple well with acoustic modes having $p = n$, $q \neq 0$. This is because of the previously mentioned absence of acoustic lattice points in the arc of the wavenumber shell between $q = 0$ and $q = 1$. This theoretically leads to a dip in the radiation efficiency curve between $f = f_c$, where a-type coupling with the $q = 0$ modes is dominant, and $f = 3f_c$ where all the structural modes enjoy b-type coupling and equations (6.19) and (6.18) become applicable.

It is interesting to compare the subcritical expression with that corresponding to the radiation efficiency of an externally radiating cylinder given by reference (49). If edge modes are neglected, and the idealised structural wavenumber diagram in Figure 6.3 is used to estimate the ratio of acoustically fast modes to total number of modes in a frequency band, the corresponding expression is

$$(R_{rad})_{ext} = (2\pi)^2 \rho f^2 \ell^2 a^2 \Delta\phi / c_o N_s \tag{6.19}$$

It is found that, except in cases where $\ell/a > 10$, the second term in the curly brackets of equation (6.16) is normally of one order greater than the first term. Using only the second term, $\epsilon_m = 1/4$, and the numerical constant 4.4, gives

$$\frac{R_{rad}}{(R_{rad})_{ext}} = \left(\frac{17.6}{2\pi^2}\right) = 0.89. \tag{6.20}$$

Inclusion of the first term in the curly brackets will normally bring this ratio to very near unity. Evaluation of R_{rad} for the experimental cylinder gives ratios insignificantly different from unity. The corresponding curve, in terms of radiation efficiency σ ($= R_{rad}/\rho c_o 2\pi a \ell$), is given in Figure 6.8, together with experimentally measured values obtained by applying the usual statistical equations from reference (16) to measurements of average acceleration and acoustic pressure of which details are given in section 6.4. Figure 6.9 compares an evaluation of $(R_{rad})_{ext}$ by the method of reference (49) using the computed modes and including edge modes, with the measured results. Figure 6.10 shows values of R_{rad} obtained from numerical analysis described in section 6.2.2.1. Examination of the terms of equation (6.16) show that the subcritical radiation efficiency, at frequencies below the ring frequency, will vary approximately as $(f)^1$. This is in disagreement with reference (14) which uses the subcritical flat plate variation of $(f)^{\frac{1}{2}}$. Figure 6.8 compares a line of this slope with the statistical and experimental results.

6.2.2.3 Statistical analysis for $f \simeq f_R < f_c$

It is not possible to obtain a statistical estimate for the frequency region near the ring frequency, when the ring frequency is less than the critical frequency, because the distribution of structural modes in the $k_x k_z$ wavenumber plane cannot be approximated by a simple expression, as can be seen from Figure 6.4. What in fact happens in this region is that the percentage of structural modes in a frequency band which can have a- and b-type couplings to acoustic modes increase significantly because of the preponderance of structural modes having small

k_x. Hence the radiation efficiency rises locally to a peak. If the critical frequency is more than twice the ring frequency, there will be a frequency region between the two in which no a- or b-type couplings will occur and the radiation efficiency will fall to values close to that of a plate of the same surface area and thickness as the cylinder at the same value of (f/f_c). As f approaches f_c a-type couplings will once again appear and will give a local peak at $f \simeq f_c$ as with a plate.

In view of the agreement between statistically estimated values of radiation resistance for external and internal radiation (equation (6.20)) it would seem reasonable to use the method of reference (49) to estimate R_{rad} in the region above about $0.8f_R$. However, corrections to the usual statistical response equations of the form described in equation (4.5) of Chapter 4, may have to be applied in the case of excitation by sound in the contained fluid.

6.2.2.4 Statistical analysis for $f_R > f_c$

The difference between the cases $f_R > f_c$ and $f_R < f_c$ is illustrated in Figure 6.12. Thick walled, small diameter pipes of the industrial plant type will usually have $f_R > f_c$. In this case the expression for R_{rad} given in equations (6.16) may be used for $(f/f_R) < 0.8$; $(f/f_c) < 1$ and that in equation (6.17) for $f >> f_c$. In the region of the critical frequency the number of a-type mode couplings will be far larger than that given by equation (6.12) because the radius of the acoustic wavenumber shell will correspond approximately with the radius of the circular part of the structural wavenumber line. The

resistance will rise locally to a maximum given approximately by

$$(R_{rad})_{f\simeq f_c} \simeq \frac{4\rho a^2 \ell^2}{c_o \pi N_s \varepsilon_m} \left\{ \frac{2\sqrt{2}\ell f \Delta f \sin^{-1}(f/f_R)^{\frac{1}{2}}}{a(1 + f/f_R)^{\frac{1}{2}}} \left[1 - (1 + 0.8p^{-2/3})^{-2}\right]^{-1} \right.$$

$$\left. + 2\pi f^2 \Delta\phi \right\} \qquad (6.21)$$

for $\left[(\beta_r + \beta_m)/c_o(1 + f/f_r)^{\frac{1}{2}}\right] < \pi/\ell$,

and

$$(R_{rad})_{f\simeq f_c} \simeq \frac{4\rho a^2 \ell^2}{c_o \pi N_s \varepsilon_m} \left\{ \frac{4\pi c_o f \Delta f \sin^{-1}(f/f_R)^{\frac{1}{2}}}{(\beta_r + \beta_m)a} \left[1 - (1 + 0.8p^{-2/3})^{-2}\right]^{-1} \right.$$

$$\left. + 2\pi f^2 \Delta\phi \right\} \qquad (6.22)$$

for $\left[(\beta_r + \beta_m)/c_o(1 + f/f_r)^{\frac{1}{2}}\right] > 2\pi/\ell$.

6.3 Lower Limiting Frequency

The sum of N_s^a and N_s^b from equations (6.12) and (6.13) and equation (6.14) gives the average total number of mode pairs in a frequency band which have 'maximum proximate coupling' as defined by equations (6.8a) and (6.7) with $s = 1$. Under conditions in which $[N_s^a + N_s^b]$ is less than unity, the expression for R_{rad} given in equation (6.16) will not be relevant, since it is based upon the coupling between mode pairs having maximum proximate coupling. In general $N_s^b >> N_s^a$ and an estimate of the lowest band centre frequency f for which on average at least one b-type coupled mode pair will exist may be obtained from the following equation

$$\frac{4\pi\ell a^2\Delta\phi(\beta_r + \beta_m)f^2}{c_o^3} = 1. \qquad (6.23)$$

The value of f given by equation (6.23) will depend upon the bandwidth of analysis through $\Delta\phi$, because for any centre band frequency it is always possible to envisage a bandwidth which is sufficiently large to encompass at least one well coupled mode pair. However, because analysis bandwidths are usually chosen so as not to obscure the trend of the results with variation of frequency, equation (6.23) will normally give a meaningful result for the lower limiting frequency. For a given cylinder and damping the lower limiting frequency is proportional to $(c_o)^{3/2}$ compared with c_o^2 for the panel-box system.

The value calculated for the experimental cylinder is shown in Figure 6.8.

6.4 Experimental Measurements and Reduction of Data

Measurements were made on a steel cylinder of dimensions given in Figure 6.1, with one fixed slightly domed end, and one removable $\frac{3}{8}$" thick end plate. The cylinder was mounted on a frame by six brackets giving local attachment. The cylinder had a fabrication weld of about $\frac{3}{8}$ in maximum thickness running parallel to the axis. A compressed air pipe entered the top of the cylinder near the fixed end through a heavy 12 in diameter, 2 in thick steel collar welded to the cylinder. The configuration in which the end plate is bolted to the end flange of the cylinder is referred to as 'partly closed'. Without this plate the cylinder is said to be 'open'. The ring frequency f_R for this cylinder is

1800 Hz and the critical frequency f_c is 2660 Hz in air at 15°C.

Compressed air was allowed to enter the cylinder through a gate valve and could exit through a 14 in. hole in the end plate, when this was attached. Acoustic pressure 1/3 octave spectra were measured with a ½ in. Bruel and Kjaer condenser microphone at 50 measuring points within the cylinder. This large number was necessary to obtain good space average values of pressure because, even at centre frequencies as high as 6300 Hz, interference patterns giving variations of up to ± 5 dB were observed near the walls of the cylinder. Accelerometers of 2 gm mass and semiconductor strain gauges at 22 positions were used to measure the spatial average response of the cylinder in 1/3 octave bands.

The cylinder was also excited mechanically by a vibration generator and the resulting average acceleration and sound pressure levels were measured as before. Total loss factors of the cylinder were measured by both impulsive and continuous mechanical excitations. The results obtained from these two methods agreed well (38). Average acoustic pressure decay times were measured in the partially closed cylinder following steady state 1/3 octave random loudspeaker excitation. No meaningful decays could be obtained for the open configuration.

The response measurements, together with the measured mechanical loss factors and the theoretical modal density of the cylinder (52), were used in the uncorrected statistical energy response equation, $S_a(\omega)/S_p(\omega) = 2\pi^2[n_s(\omega)/M|(c_o/\rho)|R_{rad}/R_{tot}]$, to calculate the radiation efficiency $\sigma = (R_{rad}/\rho c_o 2\pi a\ell)$. The acoustic pressures produced by mechanical point excitation, together with the acoustic decay measurements, were used in the statistical radiation equation, $S_p(\omega)/S_a(\omega) = (\rho/c_o)(R_{rad}/\beta_r)[2\pi^2 n_R(\omega)]^{-1}$, to estimate the radiation efficiency of the partially closed cylinder. The

results are shown in Figure 6.8.

6.5 Discussion of Results

6.5.1 Experimental and Statistical Results

The main feature of the experimental results shown in Figure 6.8 is the separation by up to 8 dB below 1250 Hz of the curves of radiation efficiency calculated from the response of the two cylinder configurations. Above 1250 Hz the curves are separated at most by 2 dB. The open cylinder curve deviates little from the statistically estimated curve for maximum proximate mode coupling above 400 Hz and below 1400 Hz ($0.8f_R$). This curve has also been theoretically shown to correspond to the statistically estimated response to excitation by an external diffuse field. The partially closed cylinder response values fall significantly below this curve below 1250 Hz.

This type of behaviour in which the response of a nearly closed structure falls below that calculated statistically for diffuse field excitation, and in which it is sensitive to a change in boundary condition, is very similar to that of the panel-box system below the lower limiting frequency. The separation of the cylinder curves occurs near the lower limiting frequency of 1100 Hz calculated from equation (6.23) using the measured values of $(\beta_r + \beta_m)$. The results at well supercritical frequencies agree with the statistical estimate of an asymptotic radiation efficiency of unity.

The statistical estimate of response for non-proximate modal coupling below the lower limiting frequency, shown in Figure 6.8, does not agree as closely with the measured values as the corresponding results for

the rectangular panel, but the general trend of the response is fairly well indicated. It is not surprising that the estimate of non-proximate mode coupling is rather less accurate than for the panel-box system because the cylinder response is far more dependent upon the particular mode pairs involved. This is because of the complicated variation of cylindrical shell natural frequency with variation of mode order, which makes estimates of the average difference between structural and acoustic mode frequencies, upon which non-proximate power flow depends, rather unreliable.

Figure 6.9 shows estimates of the external radiation efficiency determined by the method of Manning and Maidanik (49), using the actual wavenumber diagram of the experimental cylinder (Fig. 6.4). It is interesting to note that at frequencies below 1000 Hz these estimates oscillate considerably about the statistically estimated curve, because the radiation depends upon very few acoustically fast and edge modes. At frequencies below 400 Hz no fast or edge modes are found and mass law response is predicted. The tendency for low frequency response to correspond to statistically estimated, smoothly varying curves, which do not account for the deviations of modal distributions and couplings from the average, rather than to values calculated from a detailed theoretical consideration of the coupling of individual mode pairs, has been observed previously near the lower limiting frequencies of the panel-box system.

The correspondence above 400 Hz of the open cylinder response curve with the statistical estimate of externally excited response suggests that the lower limiting frequency is a function of the ratio of the opening dimension to an acoustic wavelength. In the 'open' configu-

ration the fluid in the cylinder is acoustically coupled to fluid in the surrounding room, which is very large compared with the cylinder. Consequently the fluid in the open cylinder is likely to have a much higher acoustic modal density than a completely closed cylinder. The degree of coupling between the fluid in the cylinder and the external fluid is a function of the ratio of opening diameter to an acoustic wavelength, and the type of acoustic mode considered. This explains why the partially closed cylinder acts as a closed cylinder and exhibits the lower limiting frequency phenomenon. At the lower limiting frequency the acoustic wavelength is equal to the end plate hole diameter and only modes for which $p = 0$ can be coupled to the external fluid. However, these modes cannot couple to the shell modes below 1600 Hz, and so the cylinder is effectively closed below 1600 Hz. The frequency at which the open cylinder response falls below the statistically estimated value also corresponds to equality of cylinder diameter and acoustic wavelength.

The radiation efficiency curve derived from the mechanically driven partially closed cylinder measurements, which is shown in Figure 6.8, follows the response curve closely except in the region of 400 Hz, and between 2000 and 3150 Hz bands. There is better agreement between these curves than for the panel-box system. There is no fully satisfactory explanation of the 400 Hz discrepancy, but it was found very difficult, because of strong resonances, to make decay measurements at this frequency, the results of which showed a wide spread and could not be considered reliable. The discrepancy in the region of the critical frequency is considered to be further evidence of the need for a correction to the usual statistical response equations in closed systems of high radiation efficiency and low mechanical damping as discussed in Chapters

4 and 5. It is discussed further in the next section.

6.5.2 Computed results

Radiation efficiency curves derived using computed mode frequencies as described in section 6.2.2.1 are presented in Figures 6.10 and 6.11. The partially closed response results are also shown for comparison.

As with the panel results, there are in general no proximate mode pairs indicated below the theoretical lower limiting frequencies corresponding to the particular values of $(\beta_r + \beta_m)$ chosen for the computation. An exception is in the 630 Hz band with $(\beta_r + \beta_m) = 50$. This isolated point, coming well above the measured results is contributed by one mode pair particularly close in calculated frequency and which is also the only contributing pair with $(\beta_r + \beta_m) = 150$. This point is typical of the effect produced by isolated mode pairs which have modal frequencies separation far smaller than statistically estimated average. As shown previously, computer analysis tends to predict such behaviour in sporadic frequency bands below the lower limiting frequency, but the experimental results do not usually correspond to this behaviour. Another peculiarity of the computed results for $(\beta_r + \beta_m) = 150$ is the absence of any mode pair having proximate coupling in the 800 Hz band, although the lower limiting frequency is calculated to be 630 Hz. for this damping value.

As before it is observed that variation of the damping of the system as expressed in $(\beta_r + \beta_m)$ does not substantially alter the computed radiation efficiency except where very few well coupled mode pairs exist in a band. This is the result of direct proportionality between the average number of well coupled mode pairs in a band and $(\beta_r + \beta_m)$,

coupled with the dependence of g_{mr} upon $(\beta_r + \beta_m)^{-1}$. Where significantly less than the average number of well coupled mode pairs are computed, as in the 1250 Hz band with $(\beta_r + \beta_m) = 50$, increase of $(\beta_r + \beta_m)$ significantly increases the radiation efficiency, and more important, non-proximate mode pairs can provide the major contribution to the total value, as they do below the lower limiting frequency. This effect is seen in Figure 6.10, where the values computed from non-proximate coupling compare favourably with the statistical estimate shown in Figure 6.8. Where a sufficiently large number of well coupled mode pairs exist in a band, the non-proximate pairs do not significantly contribute to the total power flow.

The discrepancy in the region of the critical frequency between the radiation efficiency curves calculated from cylinder response, that measured by mechanical excitation, and that computed may largely be explained by the statistical response equation correction given in equation (4.5). It is caused by the fact that relatively few of the available structural modes contribute to the total power flow. In the 3150 Hz band 10% of the structural modes contribute 82% of the total power flow. Similar figures for adjacent frequency bands lead to the corrected values of radiation efficiency, as estimated from response, shown in Figure 6.11. The discrepancy between radiation efficiency as measured from response and by point excitation cannot however be explained in this way for the frequency region immediately around the ring frequency. It is possible that this discrepancy, in a region of very high modal density, is related to that observed with the clamped 1/16 in panel on the box, but no direct evidence can be advanced to support this suggested

connection.

The dip in the radiation efficiency curves between f_c and $3f_c$ as predicted qualitatively in section 6.2.2.2 from a consideration of the coupled acoustic-structural wavenumber diagram, and as seen in the computed results of Figure 6.11, is not seen in the measured response, and is only weakly suggested by the mechanically driven radiation measurements in Figure 6.8. The vast number of mode pairs in frequency bands above 5000 Hz prevented complete investigation in this region. In the 5000 band, for instance, there were approximately 2.5×10^6 mode pairs to account for!

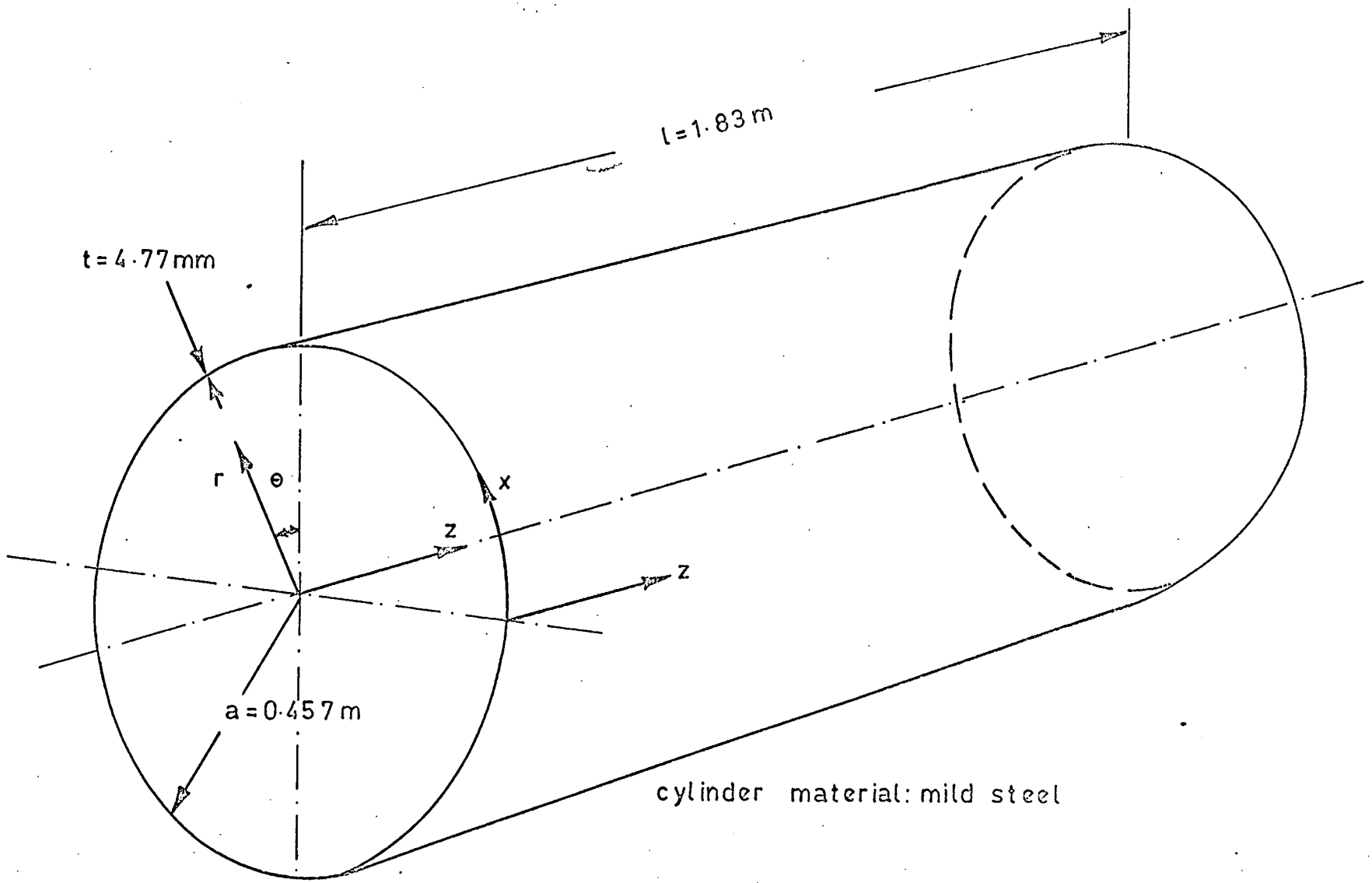

Fig. 6.1 Cylinder coordinates and dimensions.

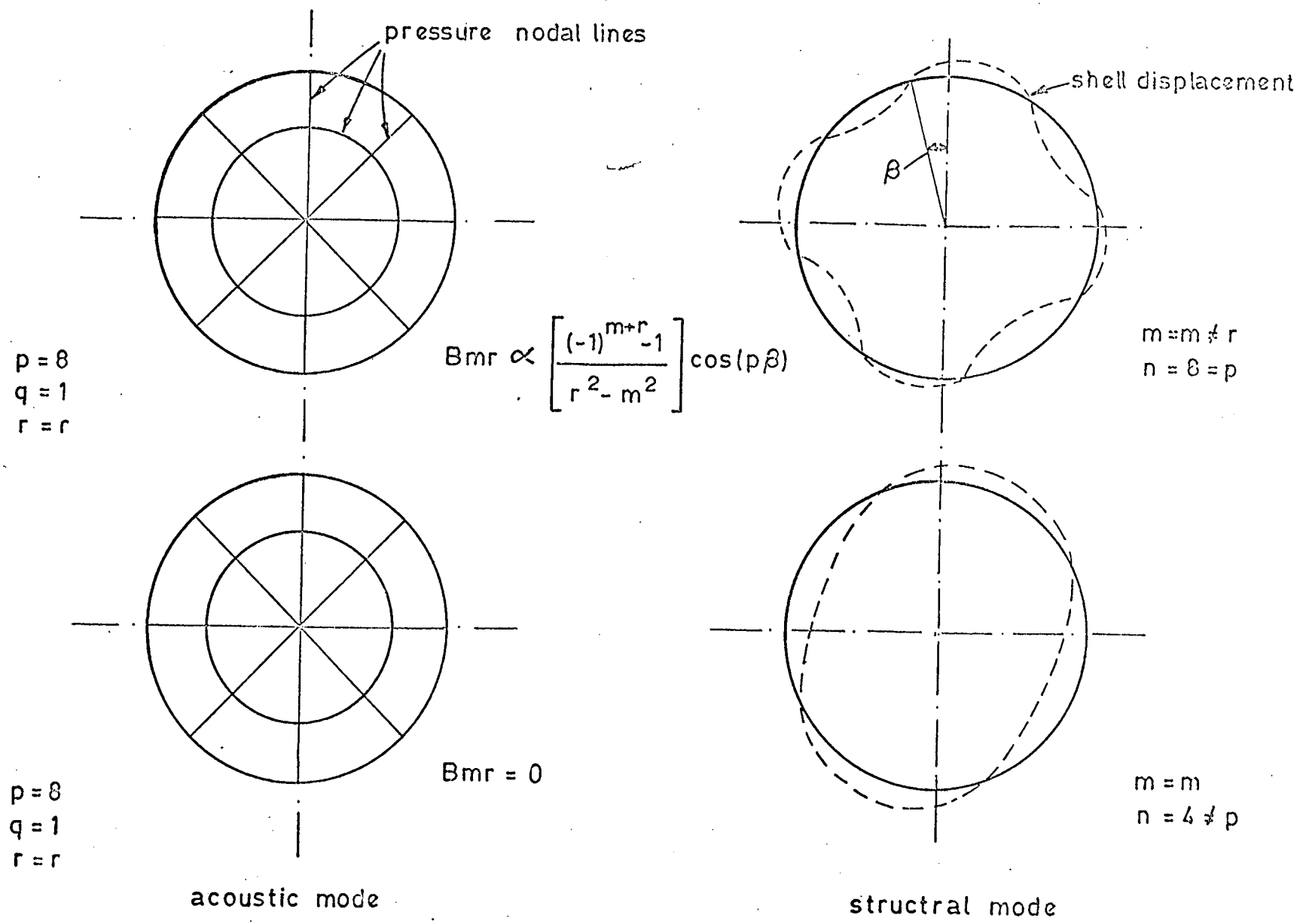

Fig. 6·2 Typical coupling configurations.

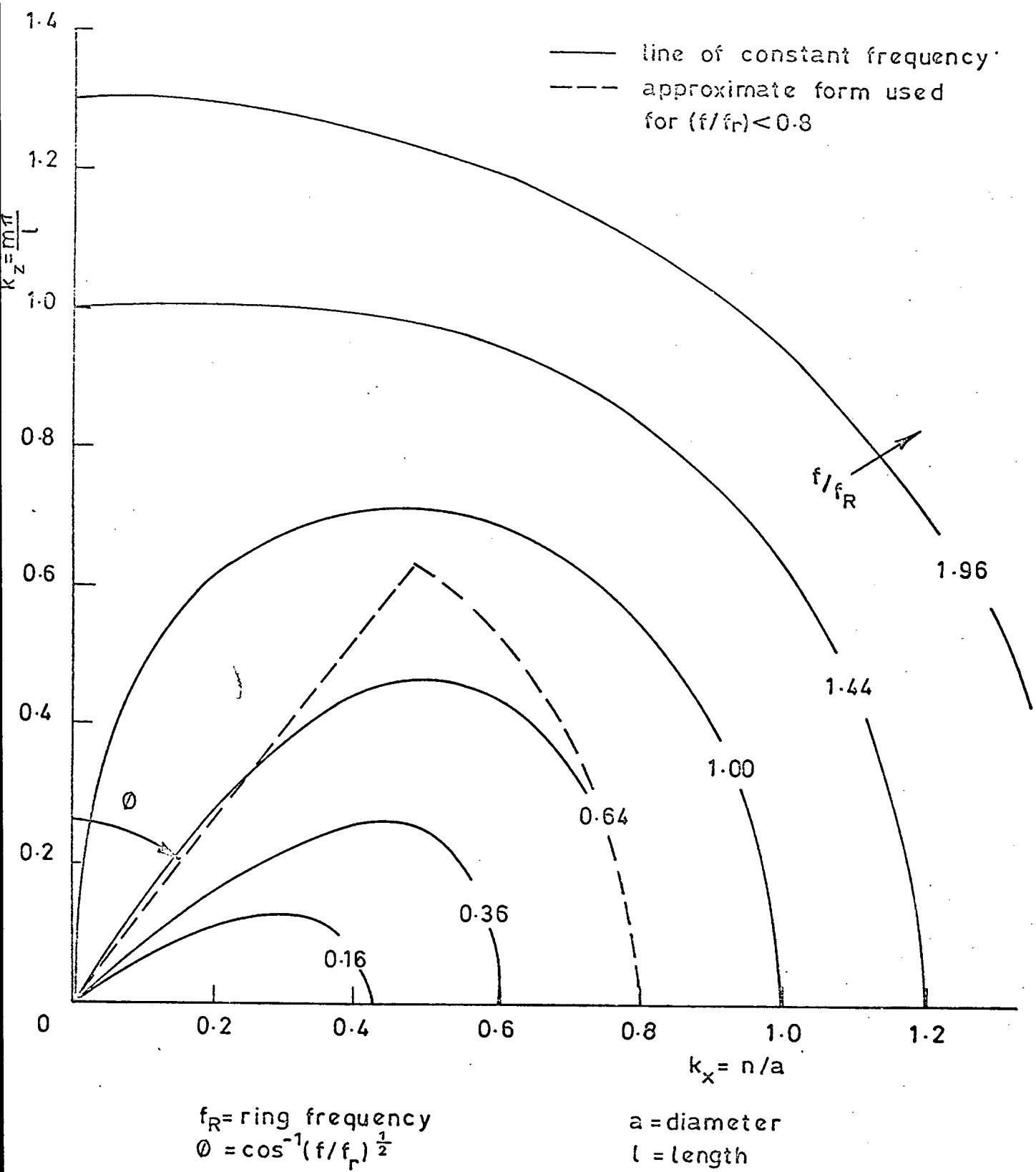

Fig 6·3 Wave number space for a cylinder.

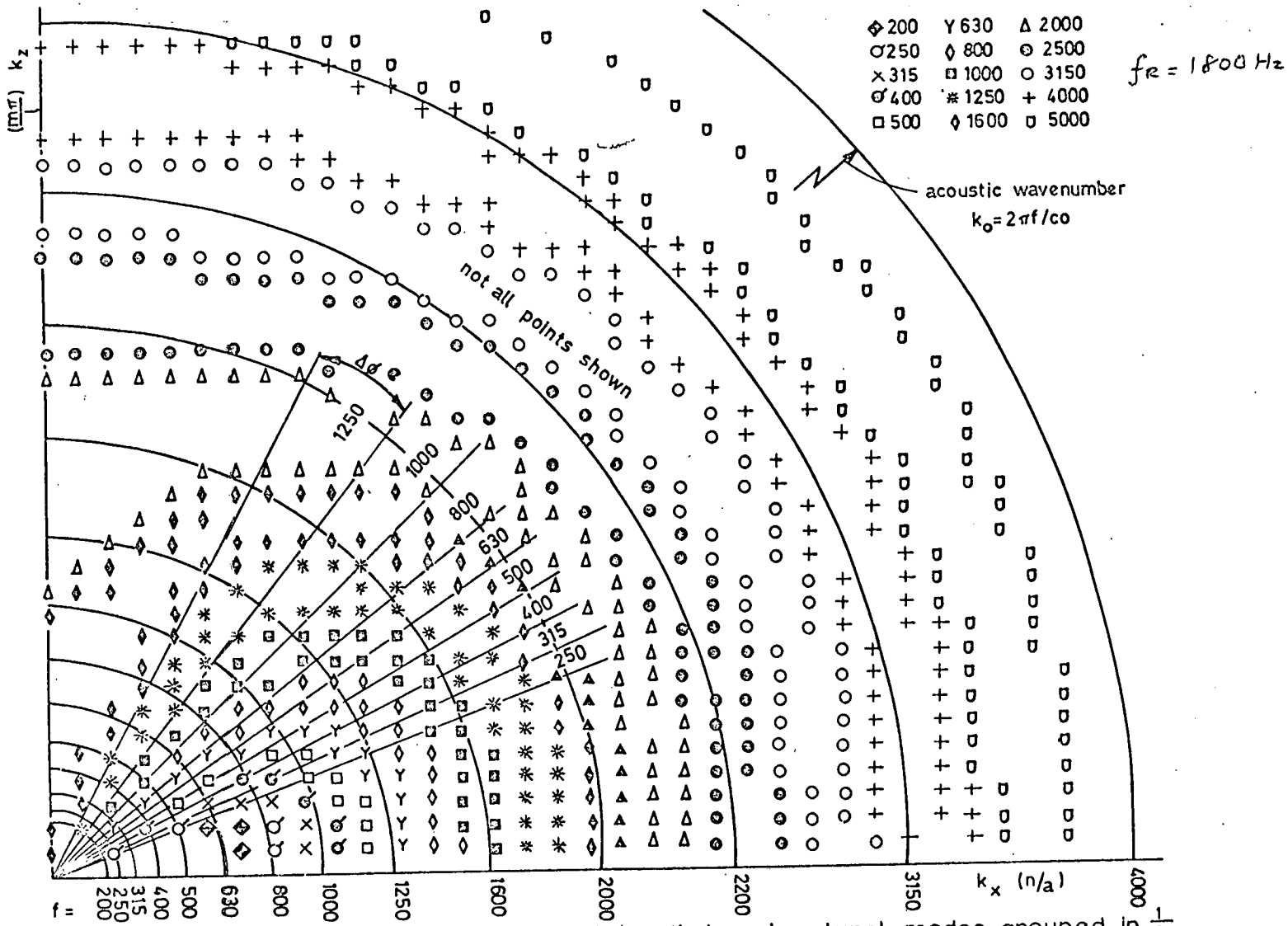

Fig 6.4 Wavenumber space for experimental cylinder: structural modes grouped in $\frac{1}{3}$ octave bands.

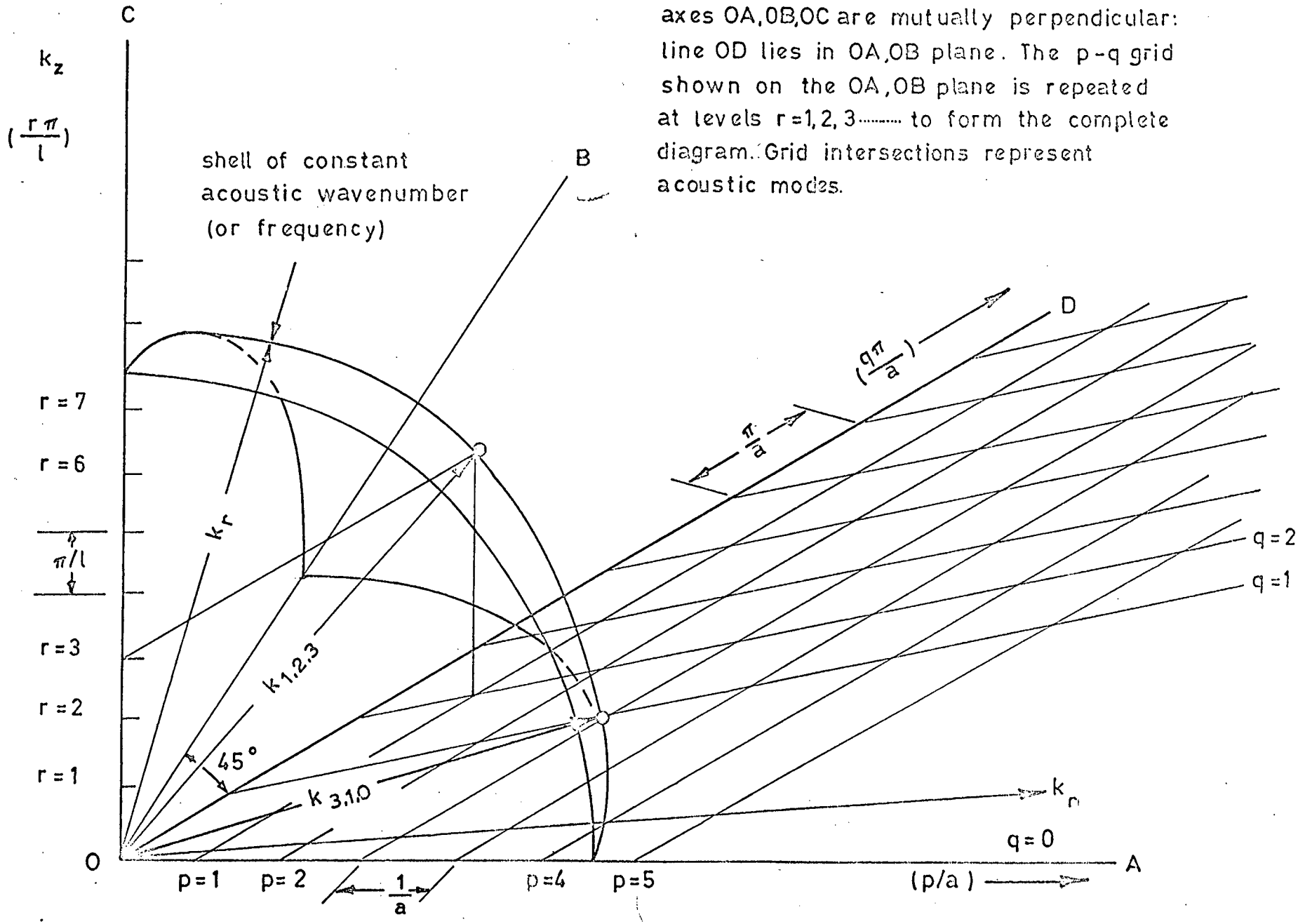

Fig. 6·5a Three dimensional acoustic wavenumber lattice diagram.

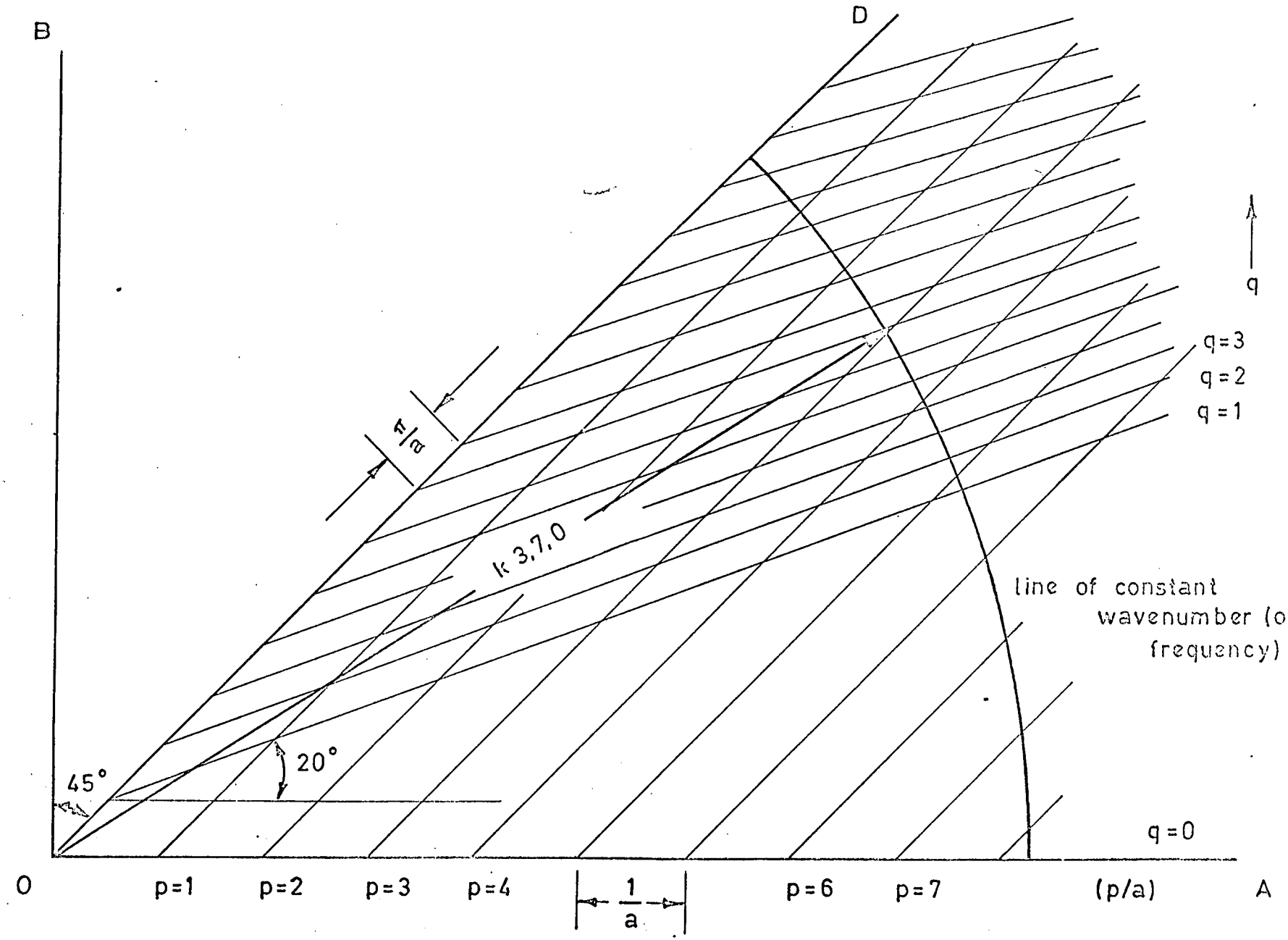

Fig. 6.5b Section of acoustic wavenumber lattice diagram on plane r = 0.

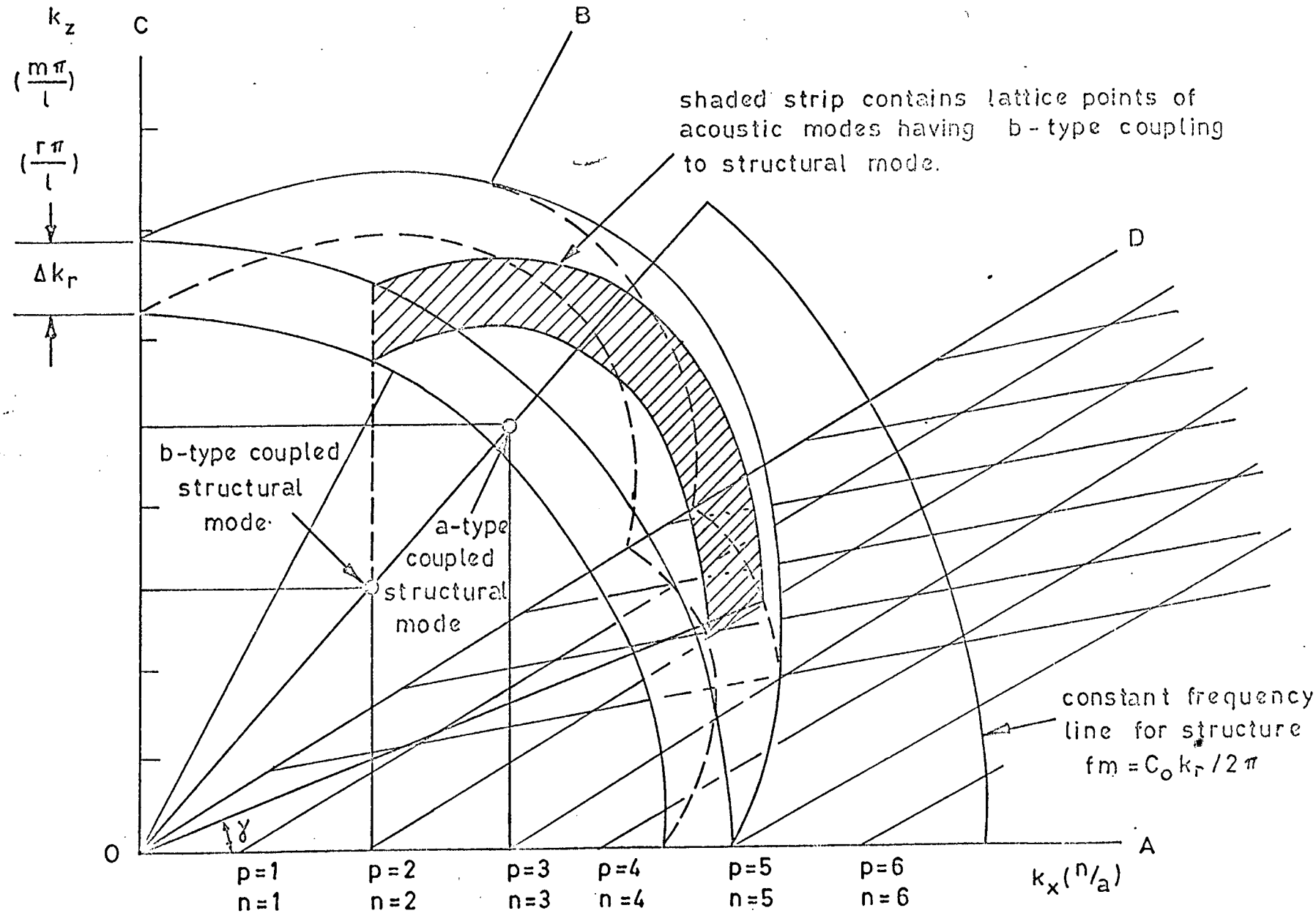

Fig. 6·6 Combined acoustic structural wavenumber diagram for $f < f_R < f_c$

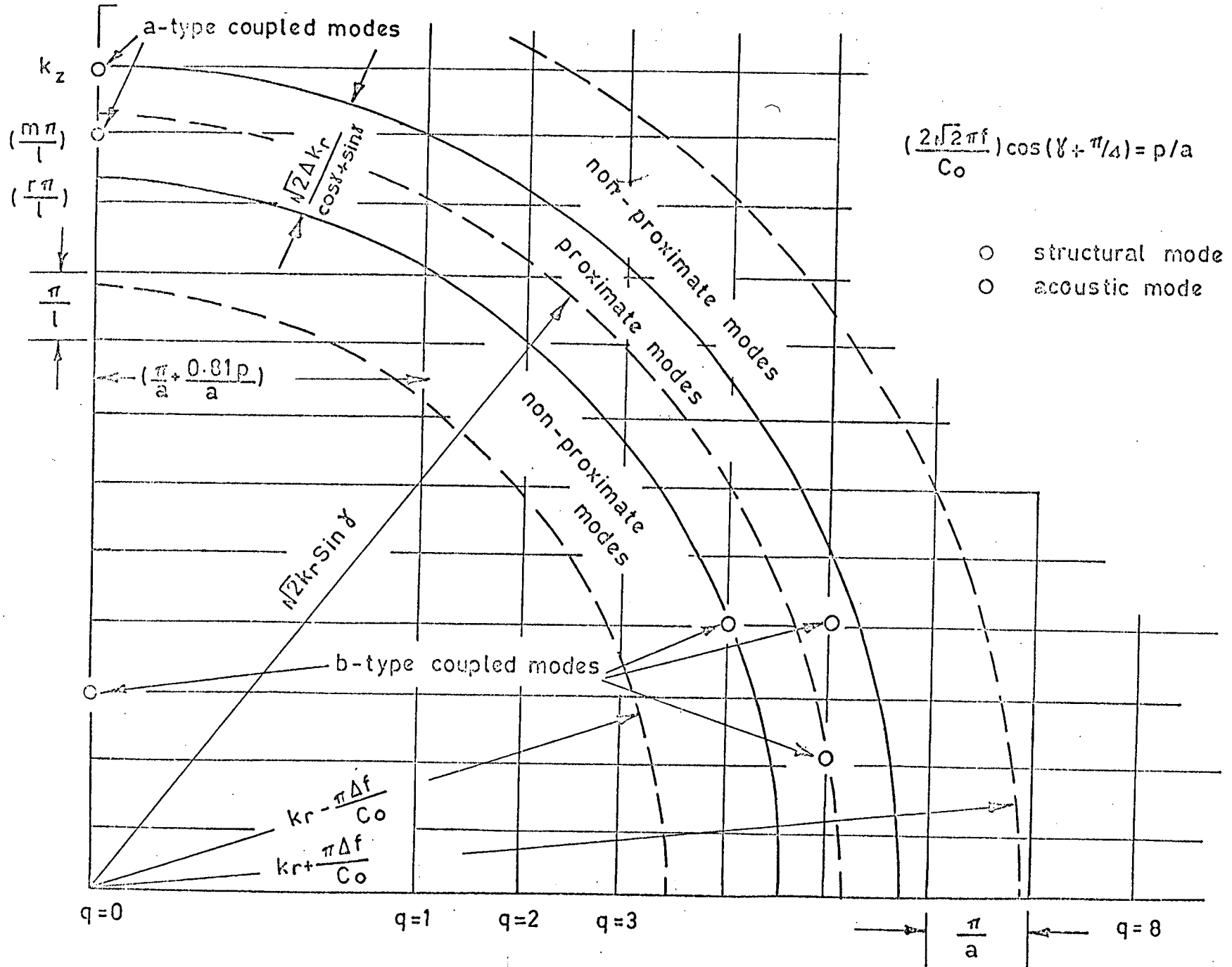

Fig.6.7 Section of combined wavenumber lattice diagram on plane p=constant

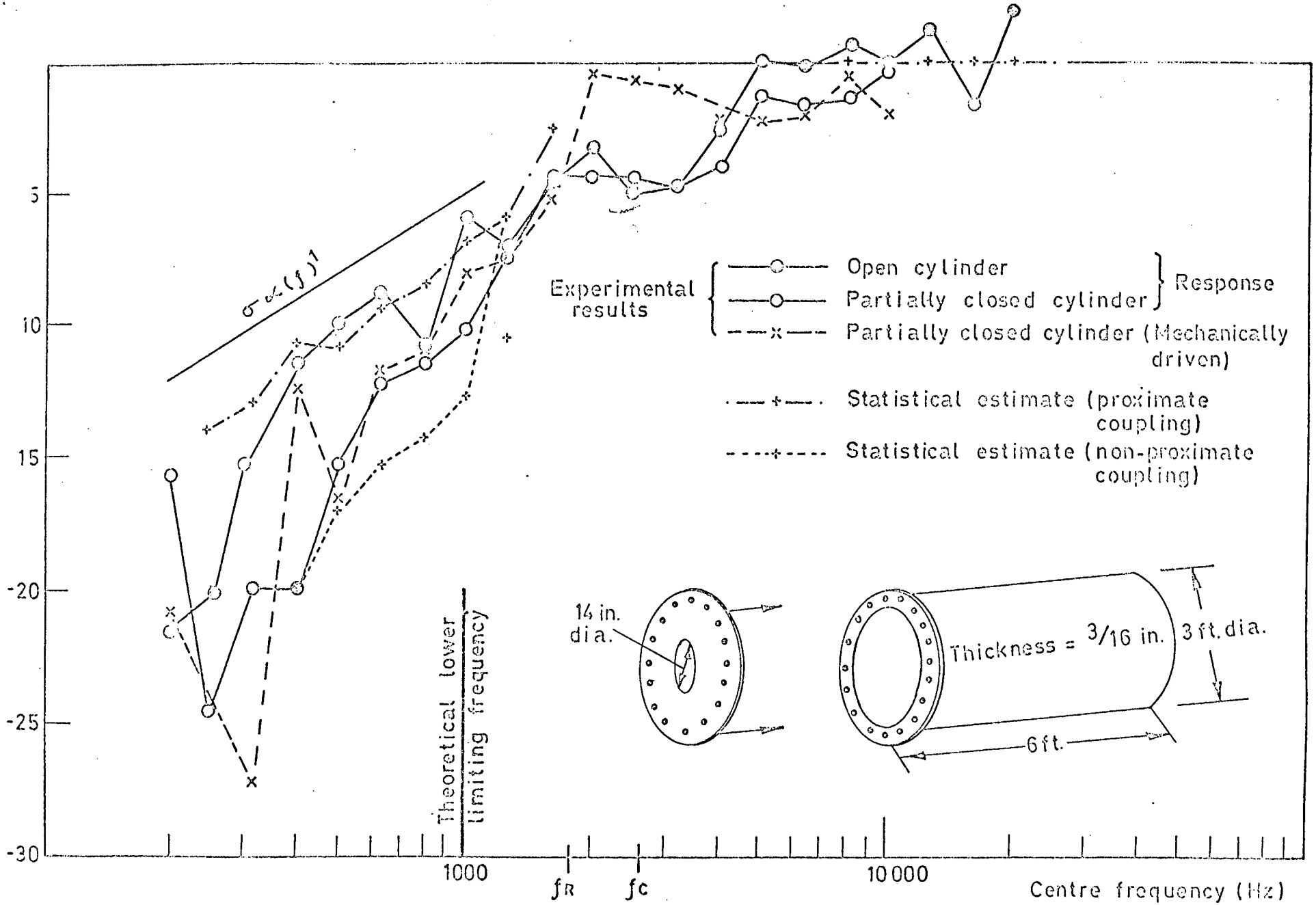

Fig. 6·8 1/3 Octave band average radiation efficiency of cylinder Statistical estimates and measured results.

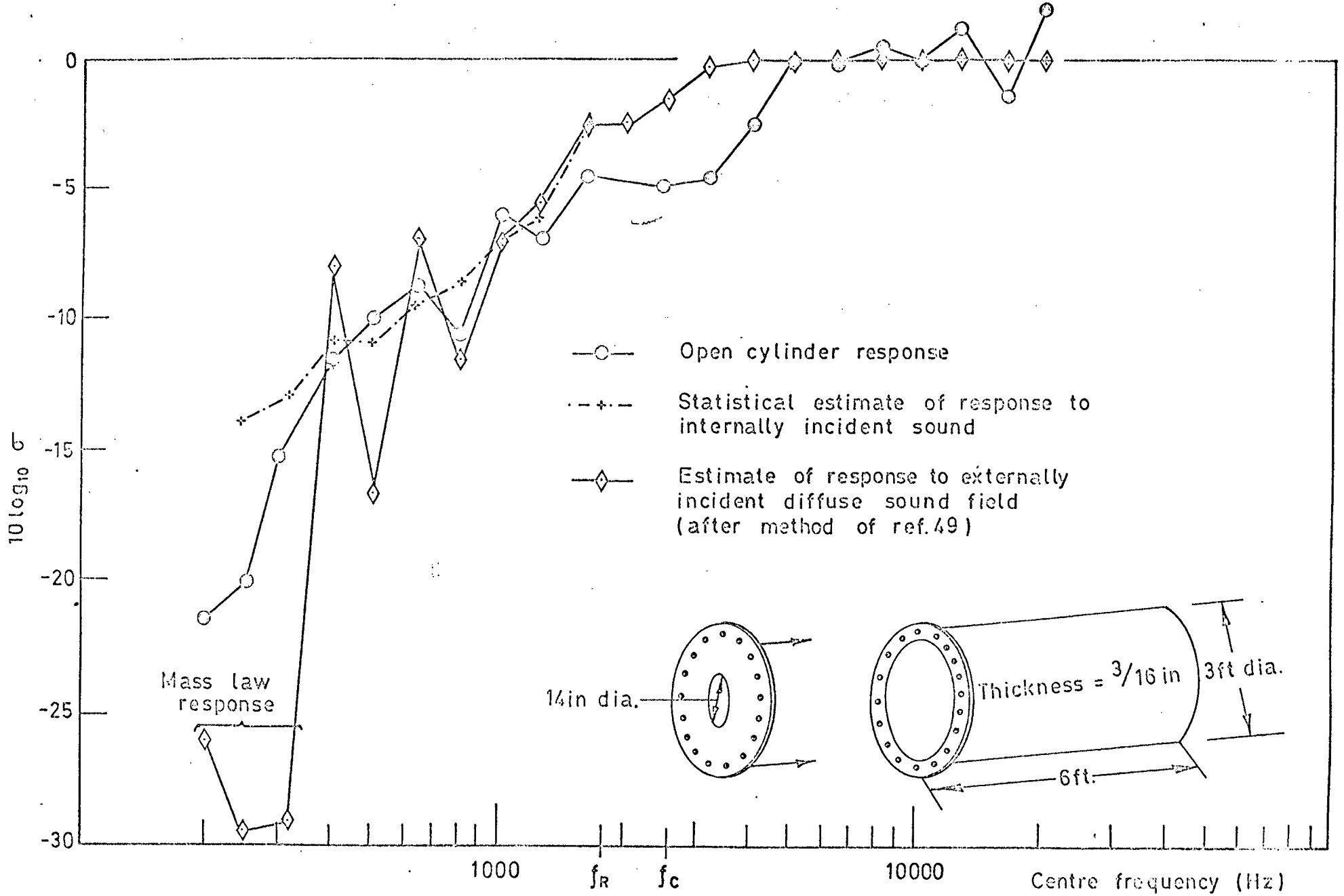

Fig. 6.9 1/3 Octave band average radiation efficiency of cylinder. Comparison between statistical estimates of response to internal and external acoustic fields.

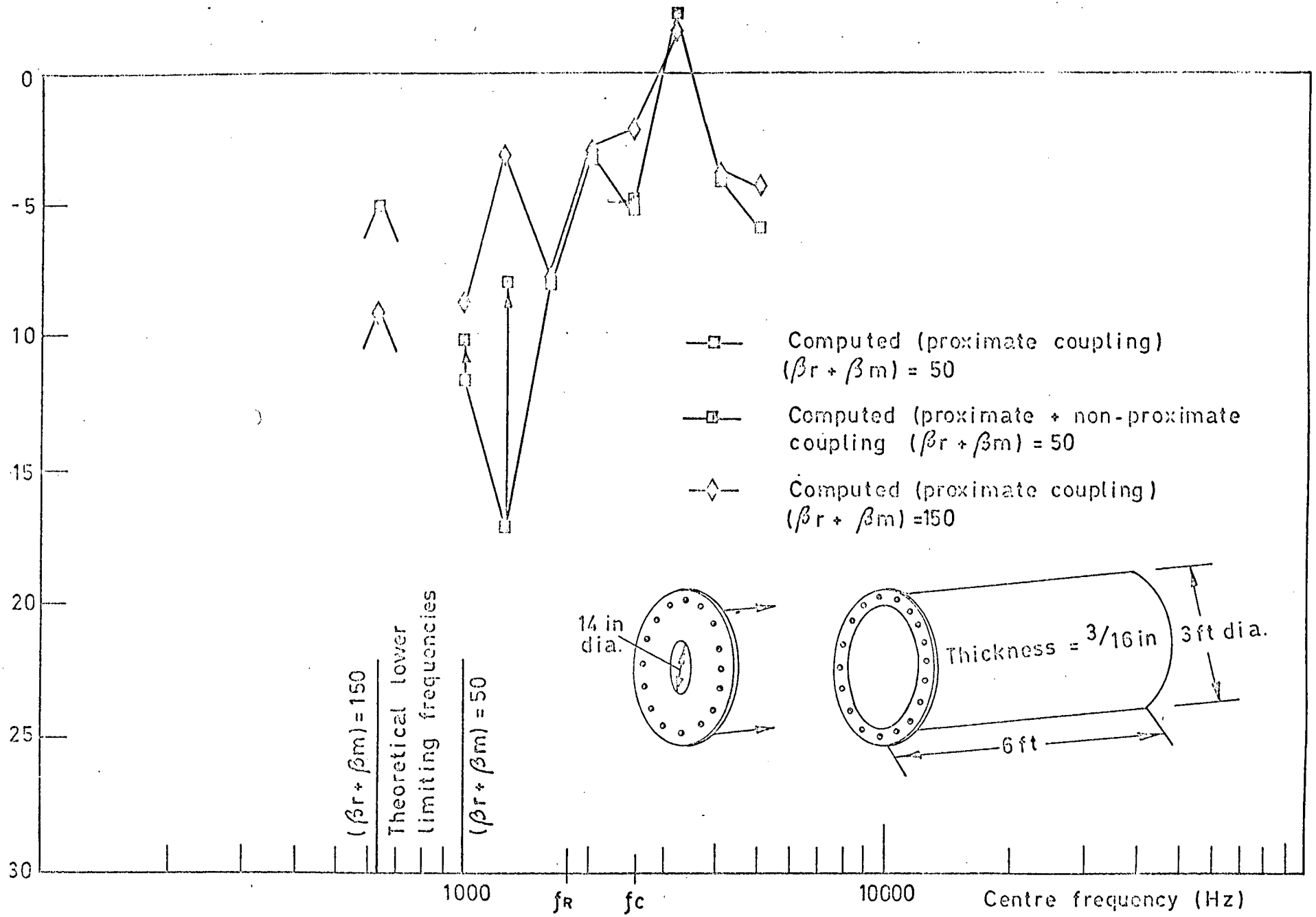

Fig. 6.10 1/3 Octave band average radiation efficiency of cylinder
Computed estimates for different values of $(\beta r + \beta m)$

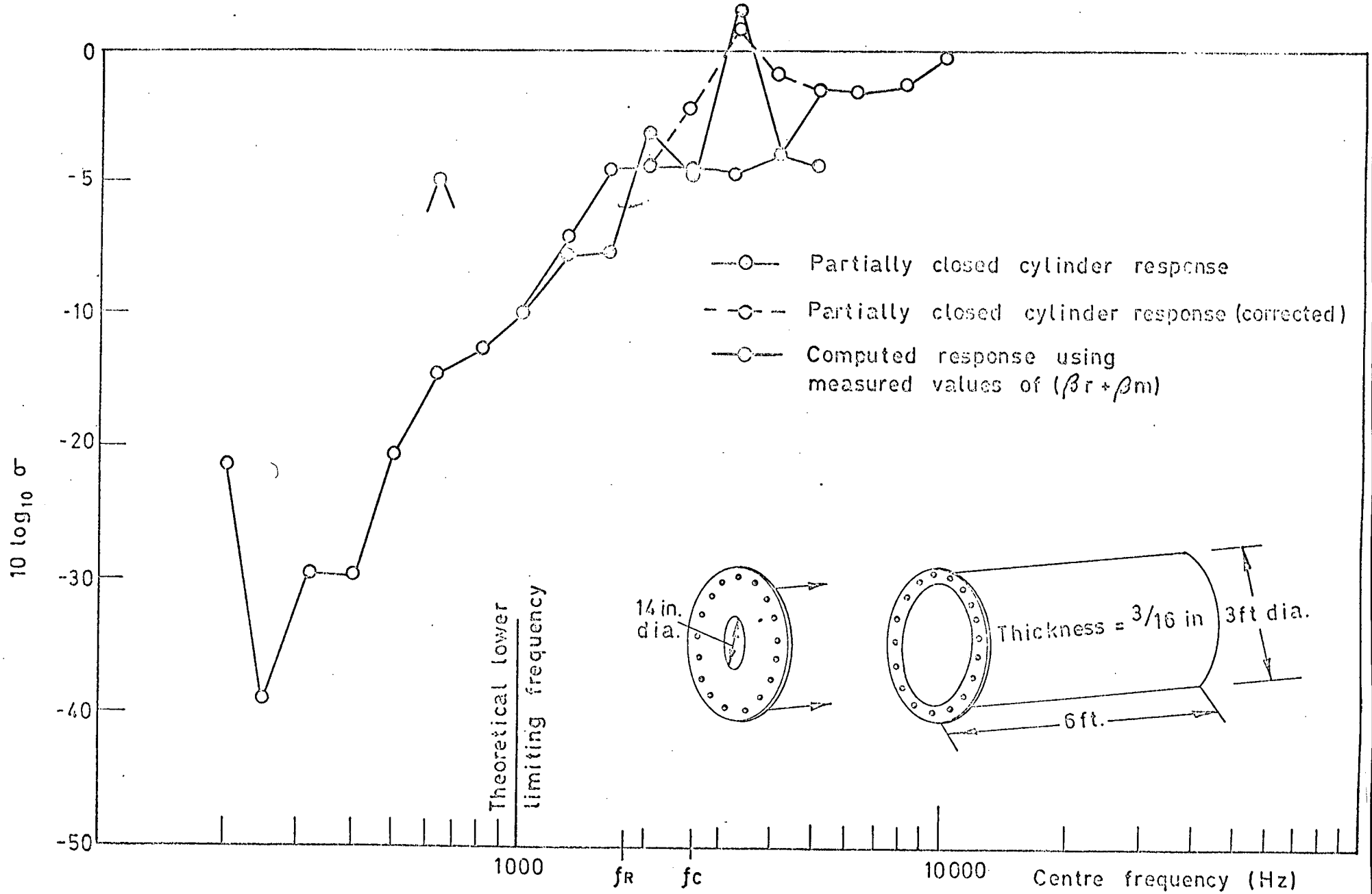

Fig. 6.11 1/3 Octave band average radiation efficiency of cylinder Comparison between computed estimate and measured results.

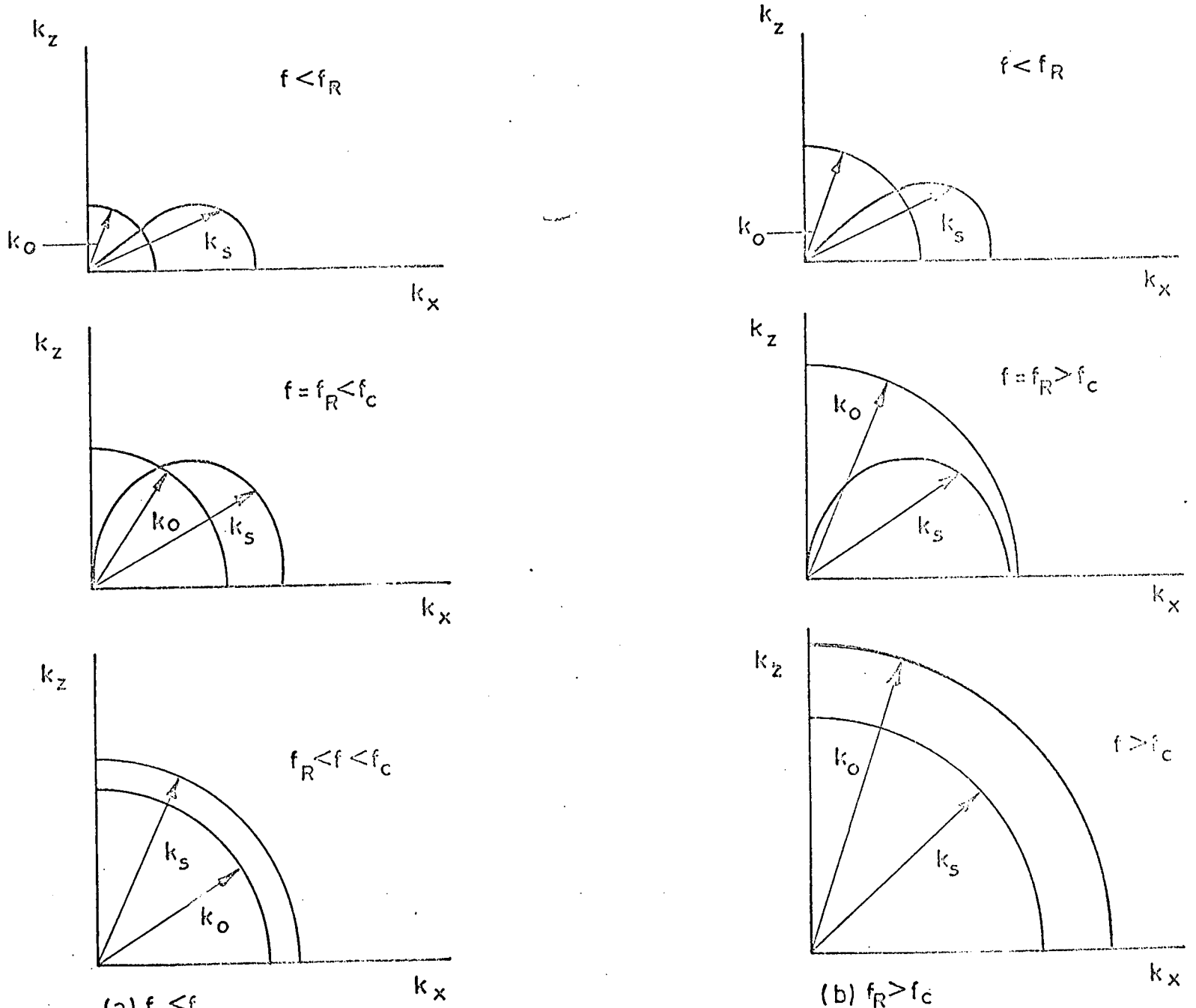

Fig 6.12 Constant frequency loci in wavenumber plane illustrating difference betwee
(a) $f_R < f_c$ and (b) $f_R > f_c$. (k_o = acoustic wavenumber: k_s = cylinder wavenumber

CHAPTER VII

TRANSMISSION OF SOUND THROUGH A CLOSED CYLINDRICAL SHELL

7.1 Introduction

The transmission of sound through a cylindrical shell is rather different in character from the more familiar transmission through a flat plate. The difference is associated with the particular forms of structural mode wavenumber diagrams which have been described in previous chapters. It is well known that, below the critical, or lowest coincidence frequency, sound is transmitted through a flat plate via vibration of low order modes forced at frequencies well above their natural frequencies (cf. ref. 9). This is because all subcritical modes are poor radiators at their natural frequencies. Consequently the transmission is mass controlled and energy flow analysis cannot easily be used to calculate the transmission (55). This phenomenon is closely related to the fact that maximum subcritical B_{rm} is always less than maximum supercritical B_{rm} (section 4.2.1.).

With a cylindrical shell however, some subcritical modes may be good radiators (or acoustically fast; cf. ref. 49), at their natural frequencies. These correspond to the a-type coupling described in section 6.2.2.2. Hence cylinder transmission may be resonance controlled at frequencies below the critical frequency, which is based upon only the shell thickness and type of material. However at low frequencies mass controlled, forced transmission can exceed resonant transmission.

It was of interest to study the transmission of sound out of the closed cylinder, previously described in chapter 6, to see if the lower limiting frequency phenomenon affected transmission, as well as resonant response.

7.2 Sound Transmission Calculation

Use of the straightforward response equations of Lyon and Maidanik, together with a definition of external Radiation Resistance in terms of power radiated to an external unbounded fluid,

$$\pi_{rad} = R_{rad}^{ext} \langle \bar{v}^2 \rangle , \tag{7.1}$$

leads to the following relationship between the intensity of sound in the contained fluid incident upon the walls of the cylinder and the intensity of sound transmitted through the cylinder:

$$\frac{I_{ext}}{I_{int}} = \frac{8\pi^2 c_o n_s(\omega)}{\omega^2 M A} \left[\frac{R_{rad}^{int} R_{rad}^{ext}}{R_{rad}^{int} + R_{mech}} \right] \tag{7.2}$$

The transmission loss is defined as $10 \log_{10} (I_{int}/I_{ext})$. R_{rad}^{int} is the internal radiation resistance which is affected by the lower limiting frequency phenomenon. R_{rad}^{ext} can be calculated by the method of reference (49).

7.3 Sound Transmission Measurements

The cylinder shown in Fig. 6.1 was completely closed by placing a heavy cover over the 14 in. diameter hole in the removeable end plate. A small loudspeaker was suspended in the enclosed volume. White noise

was generated by the loudspeaker and microphone traverses were made to determine the 1/3 octave sound pressure levels at 50 points in the volume. 1/3 octave sound pressure levels were also determined at 30 points at distances of 3 ft. from the outer surface of the cylinder in a semi-anechoic chamber. From these measurements estimates were made of the average sound intensities internal and external to the cylinder.

The cylinder was also driven mechanically at a single point and the same external microphone points were used to calculate the power radiated from the surface. 24 accelerometer measurements of cylinder vibration enabled the quantity R_{rad}^{ext} to be calculated from equation (7.1). The results are compared with theory (49) in Figure 7.1.

7.4 Discussion of Results

Figure 7.2 shows the results of the calculation of transmission loss using equation (7.2). Two features are of importance. First, it can clearly be seen that mass controlled transmission exceeds resonance (damping) controlled transmission at low frequencies. The mass law used is that for random incidence (cf. 56). Second, the measured results agree more closely with the calculation which uses the value of R_{rad}^{int} calculated from response measurements, and which exhibits the lower limiting frequency phenomenon, than with the calculation which uses the theoretical diffuse field value of R_{rad}^{int}, which does not fall off sharply below the lower limiting frequency.

The experiment shows that resonance controlled transmission can be affected by the lower limiting frequency phenomenon. The importance

of this effect will depend upon the specific pipe and fluid system of concern, but it may generally be concluded that it will be more important for fluids of high sound speed, such as steam and helium, than for air.

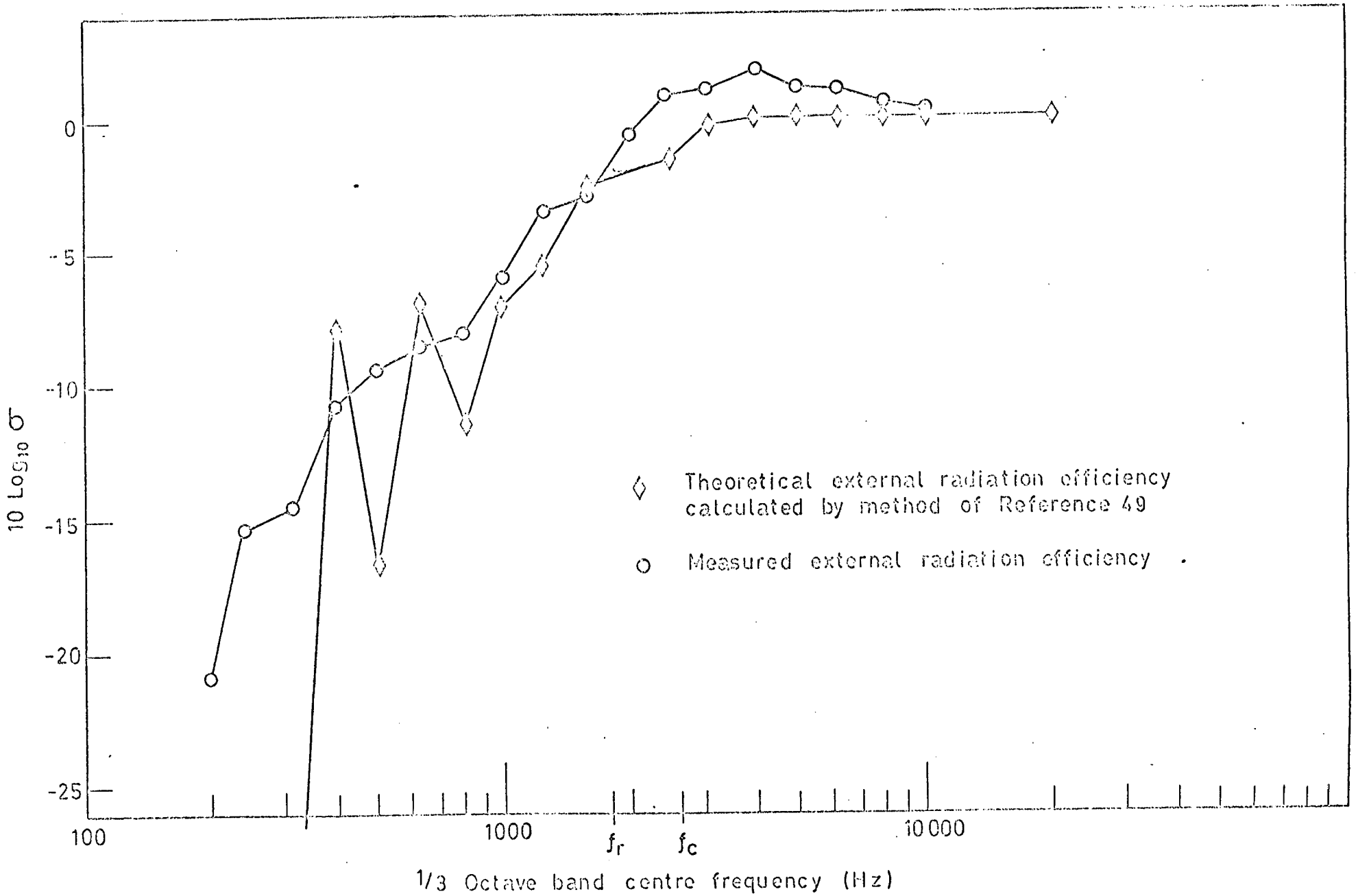

Fig. 7.1 External radiation efficiency of cylinder

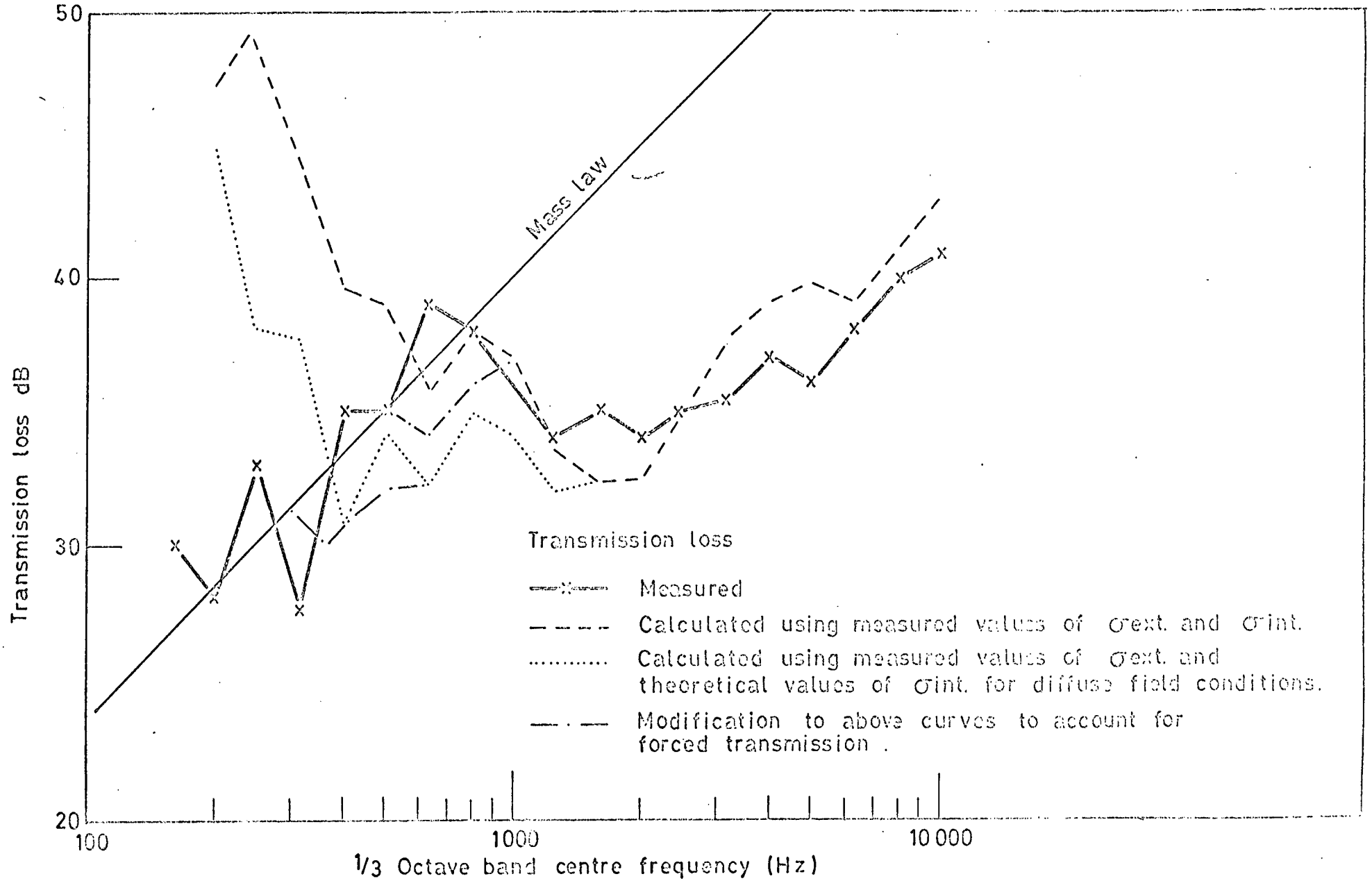

Fig. 7.2 Transmission loss of cylinder

CHAPTER VIII

CONCLUSIONS

The conclusions which have been drawn from the work reported in this thesis are presented below in order of importance as they appear to the author. There is, therefore, a mixture of conclusions concerning the general application of coupled oscillator, power flow analysis to problems of acoustic excitation of containing structures, and of conclusions specific to the particular rectangular and cylindrical systems analysed in detail.

It is apparent from the success with which coupled oscillator, power flow analysis has been applied to the systems studied, particularly in respect of mode coupling statistics, that this form of analysis is far superior to classical forms of analysis where broadband acoustic excitation of gas containing structures is concerned. It has yet to be shown that the advantage extends to the case of liquid filled structures, where even second order modal coupling is relatively strong. This form of analysis is particularly useful with gyroscopically coupled systems because the constant of proportionality between power flow and actual energy difference is expressed in terms of the uncoupled modal characteristics, which can usually be fairly easily estimated.

The study of mode coupling statistics for two geometrically regular systems has shown that, in many cases of practical interest, only a few of the available mode pairs transfer the major part of the energy from one system to another. (These mode pairs have been defined to enjoy

maximum proximate coupling.) This conclusion is very important because such a multimode interaction may be considered approximately as a set of independent two mode interactions, the degree of approximation being a function of the mode coupling forces of second order, and not of the major coupling forces. This constitutes a much less restrictive condition than had previously been considered.

Computation of mode pair coupling factors, together with mode pair coupling statistics, led to the idea of a frequency for a particular system, below which power flow would not be dominated by that between a few mode pairs which were well coupled by virtue of both good spatial and frequency matching: the response characteristics of both the rectangular panel-box system and the cylindrical shell, have clearly demonstrated the existence of such a 'lower limiting frequency' phenomenon. Statistical analysis has given extremely good agreement with experimental response results at frequencies below the lower limiting frequency. The lower limiting frequency has been found to be a function of c_o^2 for a panel-box system and $c_o^{3/2}$ for a cylinder. The important practical implication of these results is that a given mechanical system will be relatively less responsive to a given broadband sound pressure level in a fluid of high sound speed, such as water or helium.

It has also been demonstrated experimentally that the response of a geometrically regular system is sensitive to perturbation of volume geometry, and hence of acoustic mode characteristics, at frequencies below the lower limiting frequency, whereas it is relatively insensitive at higher frequencies. A reason is seen in the form of the coupling factor in which the term involving the difference of the modal natural frequencies

is insignificant of this difference is less than half the sum of the modal half power bandwidths (proximate modes). At frequencies below the lower limiting frequency, the dominant mode pairs are well matched spatially, but do not have close natural frequencies. Consequently, changes in the distribution of the frequency difference among the interacting modes can affect the coupling factors and the total power flow.

Calculation of modal average coupling factors for the rectangular and cylindrical systems from individual mode to mode coupling factors has in general shown good agreement with the statistically estimated values. However, although such calculations first indicated the existence of the lower limiting frequency phenomenon, by an absence of well coupled modes at low frequencies, they often indicate an irregularity of modal average response as a function of frequency, which is not observed in practice. Particular examples are found in the sporadic, high values of radiation efficiency below the statistically estimated lower limiting frequency, and the sporadic low values above this frequency. These irregularities are due to deviations of the modal distribution from the ideal system statistics. Other examples are seen in the very irregular curve of external radiation efficiency computed for the cylinder and the considerable sensitivity of computed modal average radiation efficiency of the rectangular panel to small variations in the panel-box dimensions. The limited number of measurements seen to indicate that real systems do not exhibit this type of irregularity and sensitivity, which is a point in favour of a statistical approach and against a deterministic approach via idealised models of complex systems. However it

must be said that the computation of individual mode coupling is a valuable guide in the development and use of statistical analysis.

A further consequence of the tendency for geometrically regular systems to exchange energy via a small percentage of the available modes is that the original widely used response and radiation equations of Lyon and Maidanik (16) have to be modified when the mechanical system is capable of radiating the same order of energy into the fluid as it is capable of dissipating mechanically. This usually occurs near the critical frequency of a lightly damped mechanical system; the modification increases in significance with increase of the fluid density.

Applications of power flow analysis to the closed rectangular box and cylinder systems has produced values of modal average coupling factor which correspond to the equivalent factor (e.g., R_{rad}) previously calculated for a semi-infinite or infinite fluid system. The exception has been the supercritical radiation efficiency of the plate, for which no explanation is forthcoming. Except for this case then, these results lend further weight to the hypothesis that modal average coupling factors may be calculated from the consideration of power flow between coupled, semi-infinitely extended (modeless) systems (7, 25). A general proof of such a hypothesis would be welcomed, but in its absence, relevant experimental and theoretical evidence is very valuable. Certainly the assumption of such a relationship greatly eases power flow calculations.

The analysis of power flow between a fluid and a point excited structure has produced a new coupling factor which is a function both of the natural frequency difference between an acoustic mode and a structural

mode and of the frequency difference between that structural mode and all the other structural modes. The power flow between acoustically coupled systems, of which one is point driven, would appear to approach that between systems of which one is driven by statistically independent modal forces, or sources, when the modal density of both systems becomes large. In the case of the experimental systems used in the present work, it could not be reliably determined theoretically whether or not the statistical dependence due to the single input force caused the discrepancy between the direct and indirect (response) measurements of the radiation efficiency. This aspect of the research needs further experimental and theoretical work.

As well as the agreement between values of panel radiation resistance calculated from power flow theory and previously reported 'free field' values, the coupled oscillator analysis, together with Bolotin's approach to boundary effects on shell vibration, has led to an estimate of modal average radiation resistance for a clamped panel. No such estimate has previously been reported, although some studies of clamped panel 'edge mode' radiation has been made. Experimental measurements have indicated that the calculated increase of 100% over the radiation resistance of the simply supported at low frequencies is unconservative, and that the factor does not decrease from two to unity, as the critical frequency is approached, as fast as theory would suggest.

Turning from the rectangular panel to the cylinder we find that, below the ring frequency, the 'internal' radiation efficiency is theoretically identical to the 'external' radiation efficiency, above the lower limiting frequency. It is also proportional to the first power of frequency in disagreement with assumptions previously made by other workers. For a

cylindrical shell with a hole in one end, the lower limiting frequency phenomenon has been found to be controlled by the degree of resonant coupling possible between modes of the internal and external fluid. Small central holes in an end plate do not constitute an opening from this point of view, whereas completely open ends tend to do so. This distinction can be important in an estimate of pipe and duct response to noise. The lower limiting frequency phenomenon has also been shown to affect the transmission of sound through a cylinder from an internal to an external fluid. Experiments have clearly shown the regions of mass controlled and resonance (damping) controlled transmission, and the effect of the limited fluid volume on the latter.

The results and conclusions of this work have already been applied to a number of practical problems by reactor designers. The cylinder theory has been used to estimate the r.m.s. strain in a model reactor diffuser subjected to broad band random excitation from flow through a sleeve valve. The difference between the theoretical and measured result was less than 10%. Cylinder theory has also helped to optimise the design of a boiler casing for minimum response to noise. A study of the implications for acoustically induced vibration of a change of heat transport fluid from carbon dioxide to helium has been aided by reference to the results of this research.

In conclusion it may be said that the value of coupled oscillator, power flow analysis in the present application to the problem of acoustic excitation of containing vessels, has been manifested largely in the establishment of a lower limiting frequency, below which the assumption of a diffuse field model of the acoustic field becomes untenable. The

main areas in which further work is needed are those relating to (a) the statistical dependence of input forces, (b) the acoustic power flow between a structure and a dense fluid (liquid) and (c) the effect of irregularity in the geometry of the structure and of the fluid volume.

REFERENCES

1. B.L. Clarkson and F.J. Fahy 1968. Chapter 16. Noise and Acoustic Fatigue in Aeronautics. Ed. E.J. Richards and D.J. Mead. J. Wiley and Son Ltd. Response of Practical Structures to Noise.

2. cf. Reference 32, pp. 352-354.

3. cf. References 6, 42, 43 and 44.

4. Smith, P.W., Jr. 1962. J. Acoust. Soc. Am. 34, (5), 640. Response and Radiation of Structural Modes Excited by Sound.

5. P.W. Smith and R.H. Lyon 1965. NASA CR-160. Sound and Structural Vibration.

6. L. Cremer 1955. Acustica 5, 245. Theorie der Luftschalldämmung zylindrischer Shalen.

7. T.D. Scharton and R.H. Lyon. 1968. J. Acoust. Soc. Am. 43 (6), 1332. Power Flow and Energy Sharing in Random Vibration.

8. T. Kihlman, 1967. Acustica 18, 11. Sound Radiation into a Rectangular Room. Applications to Airborne Sound Transmission.

9. M.C. Bhattaclararya and M.J. Crocker 1969. University of Liverpool, Department of Building Science, Report No. BS/A/69/1. Force Vibration of a Panel and Radiation of Sound in a Room.

10. A.J. Pretlove 1966. J. Sound Vib. 3, 252-261. Forced vibrations of a rectangular Panel Backed by a Closed Rectangular Cavity.

11. F.J. Fahy and A.J. Pretlove 1967. J. Sound Vib. 5(2), 28. Acoustic Forces on a Flexible Panel which is Part of a Duct Carrying Airflow.

12. E. Eichler, 1965. J. Acoust. Soc. Am. 37, (6), 995. Thermal Circuit Approach to Vibrations in Coupled Systems and the Noise Reduction of a Rectangular Box.

13. R.H. Lyon 1963. J. Acoust. Soc. Am. 35 (11), 1791. Noise Reduction of Rectangular Enclosures with One Flexible Wall.

14. P.H. White 1966. J.Acoust.Soc.Am. 40, 1124. Sound transmission through a finite, closed cylindrical shell.

15. Morse, P.M. and Feshbach, H. 1953. Methods of Theoretical Physics. Part I. McGraw Hill Book Co. Inc. New York.

16. R.H. Lyon and G. Maidanik 1962. J. Acoust. Soc. Am. 34 (5), 623. Power flow between Linearly Coupled Oscillators.

17. P.H. White and A. Powell 1965. J. Acoust. Soc. Am. 40 (4), 821. Transmission of Random Sound and Vibration through a Rectangular Double Walls.

18. E.E. Ungar and T.D. Scharton 1966. Shock and Vibration Bulletin 36, 41-53. Analysis of Vibration Distribution in Complex Systems.

19. R.H. Lyon and T.D. Scharton 1965. J. Acoust. Soc. Am. 38 (2), 253. Vibrational Energy Transmission in a Three Element Structure.

20. D.E. Newland 1966. Letter to the Editor, J.Acoust. Soc. Am. 39(4), 755. Comment on 'Vibrational-Energy Transmission in a Three Element Structure'.

21. E.E. Ungar 1966. AFFDL-TR-66-52, April 1966, AD637504. Fundamentals of Statistical Energy Analysis of Vibration Systems.

22. D.E. Newland 1966. J. Sound Vib. 3, 262. Calculation of Power Flow between Coupled Oscillators.

23. A.S. Nikiforov 1964. J. Sov. Phys. Acoust. 10, 178. Radiation from a Plate of Finite Dimensions with Arbitrary Boundary Conditions.

24. M.P. Kakar 1969. Proceedings of the British Acoustical Society Meeting, Liverpool. Power Flow Between Linearly Coupled Oscillators.

25. R.H. Lyon and E. Eichler 1964. J. Acoust. Soc. Am. 36 (7), 1344. Random Vibration of Connected Structures.

26. G. Maidanik 1962. J. Acoust. Soc. Am. 34(6), 809. Response of Ribbed Panels to Reverberant Acoustic Fields.

27. T. Kihlman 1967. National Swedish Institute for Building Research Report 9:1967. Transmission of Structure-Borne Sound in Buildings.

28. V.V. Bolotin 1966. Int. J. of Solids and Structures 2, 105. Broad Band Random Vibrations of Elastic Systems.

29. P.W. Smith, Jr. 1964. J. Acoust. Soc. Am. 36(8), 1516. Coupling of Sound and Panel Vibration below the Critical Frequency.

30. Y.K. Lin. 1967. Probabalistic Theory of Structural Dynamics. McGraw Hill Book Co.

31. S.H. Crandall and W.D. Mark 1963. Random Vibration in Mechanical Systems. Academic Press, New York and London.

32. P. M. Morse 1948. Vibration and Sound. Second Edition. McGraw Hill Book Co., Inc. New York.

33. D.E. Newland 1968. J. Acoust. Soc. Am. 43 (3) 553. Power Flow Between a Class of Coupled Oscillators.

34. S.M. Stearn 1969. Ph.D. Thesis, University of Southampton. Stress Distribution in Randomly Excited Complex Structures.

35. I.I. Klyukin 1959. Journal of Acoustics of the USSR 5 (1); also Jour. Sov. Phys. Acoust (5), 1. The Effect of a Vibrometer on the Motion of a Vibrating Surface.

36. F.J. Fahy 1969. J. Sound Vib. 10(3). Measurement of Mechanical Input Power to a Structure.

37. R.G. White 1969. University of Southampton. ISVR Technical Report 12. Measurement of Structural Frequency Response by Transient Excitation.

38. F.J. Fahy 1969. Letter to the Editor, J. Sound Vib. 9, 506. Reply to the Letter to the Editor "Damping in Plates" by M.J. Crocker and A.J. Price.

39. Suggestion of J. Manning of Bolt, Beranek and Newman, Inc., Cambridge, Mass., U.S.A.

40. M.R. Schroeder 1954. Acustica 4, No. 1, 456-468. Eigenfrequency and Excitation Statistics in Rooms.

41. Referees of Paper 'Vibration of Containing Structures by Sound in the Contained Fluid' 1969. F.J. Fahy. J. Sound Vib, 10,(3).

42. P.W. Smith, Jr. 1957. J. Acoust. Soc. Am. 29, 721. Sound transmission through thin cylindrical shells.

43. M. Heckl 1958. Acustica 5, 259 (Heft 1). Experimentelle Untersuchungen zur Schalldämmung von Zylindern.

44. J.H. Foxwell and R.E. Franklin 1959. Aero. Qtly. 10. The vibration of a thin-walled stiffened cylinder in an acoustic field.

45. G.R. Khabbaz 1965. Lockheed Missiles and Space Co. Report LMSC 6-65-65-23. Sound transmission due to a plane random grazing wave.

46. P.A. Franken 1962. J. Acoust. Soc. Am. 34, 453. Sound-induced vibrations of cylindrical vehicles.

47. R.H. Lyon 1967. The Shock and Vibration Information Centre Monograph SVM1. U.S. Department of Defense, Washington. Random Noise and Vibration in Space Vehicles.

48. J.E. Manning 1968. J. Acoust. Soc. Am. 43, 886. Comment on 'Sound Transmission through a Finite, Closed Cylindrical Shell'.

49. J.E. Manning and G. Maidanik 1964. J. Acoust. Soc. Am. 36, 1691. Radiation properties of Cylindrical Shells.

50. F.J. Fahy 1969. University of Southampton ISVR T.R. 11. Vibration of Containing Structures by Sound in the Contained Fluid. (See also ref. 41.)

51. M. Heckl 1962. J. Acoust. Soc. Am. 34 (1553). Vibrations of point driven cylindrical shells.

52. D.K. Miller 1967. M.S. Thesis. N. Carolina State Univ. at Raleigh. The Modal Density of Thin Cylindrical Shells.

53. K.L. Chandiramini et al. 1966. Bolt Beranek and Newman Report No. 1417. Structural Response to Inflight Acoustic and Aerodynamic Environments.

54. P.M. Morse 1944. Rev. Mod. Phys. 16, 70. Sound Waves in Rooms.

55. M.J. Crocker and A.J. Price 1969. J. Sound Vib. 9 (3). Sound Transmission Using Statistical Energy Analysis.

56. L.L. Beranek 1960. Noise Reduction. McGraw Hill Book Co., Inc. New York.

APPENDIX 1

Radiation Resistance of a Simply Supported Panel

A.1.1 Determination of Maximum Mode Coupling Conditions

The radiation resistance is determined by considering the magnitudes of the terms of the sum $\sum_{m,r} g_{mr}$ which appears in the equation $R_{rad} = M \sum_{m,r} g_{mr}/N_s$. For modes satisfying the frequency proximity condition of equation (3.6a), g_{mr} is given by $g_{mr} = B_{mr}^2/(\beta_r + \beta_m)$ where B_{mr} is given by $B_{mr} = (c_o^2\rho/V\varepsilon_r\varepsilon_m M)^{\frac{1}{2}} \int_o^a \int_o^b \phi_m(x, y)\psi_r(x, y, c)dxdy$. The eigenfunctions ψ and ϕ are for a simply supported panel given by $\phi_m = \sin(m\pi x/a) \sin(n\pi y/b)$ and $\psi_r = (-1)^r \cos(p\pi x/a) \cos(q\pi y/b)$. The integral becomes

$$(-1)^r \left[\frac{(-1)^{m+p} - 1}{1 - (m/p)^2}\right] \frac{ma}{p^2\pi} \left[\frac{(-1)^{n+q} - 1}{1 - (n/q)^2}\right] \frac{nb}{q^2\pi} \quad \text{for } p \neq m, \quad q \neq n.$$

The terms in the brackets are zero for $(m + p)$ or $(n + q)$ even. The maximum values of the terms in the curly brackets occur for $p = m \pm 1$ and $q = n \pm 1$, and are given respectively by a/π and b/π for $m, n \geq 3$.

For a given structural mode m, n having a subcritical natural frequency, the acoustic modes of order $(m \pm 1, n \pm 1, r)$ have frequencies far from the structural natural frequency, (see Fig. 4.2). But it is possible for acoustic modes $m \pm 1$, q $(< n)$, r, and p $(< m)$, $n \pm 1$, r to have natural frequencies close enough to satisfy the frequency proximity condition when $m\pi/a < k_r$ and $n\pi/b < k_r$ respectively. The modulus of the integral then has the value $(\frac{a}{\pi}) \left|\frac{(-1)^{n+q} - 1}{1 - (n/q)^2}\right|$ and

$(\frac{b}{\pi})\left[\frac{(-1)^{m+p}-1}{1-(m/p)^2}\right]$ respectively. The next largest values of the integral are given by $p = m \pm 3$, $q < n$ and $q = n \pm 3$, $p < m$, when the integrals have values one third of those given above and hence the corresponding g_{mr} have values of one ninth of those corresponding to $p = m \pm 1$ or $q = n \pm 1$. For $p = m \pm 5$, $q < n$ and $q = n \pm 3$, $p < m$ the factor is one twenty-fifth, and so on. The total number of non zero g_{mr} for each value of p or q greater or less than $m \pm 1$ or $n \pm 1$ is the same as for $p = m \pm 1$, or $q = n \pm 1$, so that only the $p = m \pm 1$, $n < q$ and $q = n \pm 1$, $p < m$ mode couplings need by considered in the sum $\sum_{m,r} g_{mr}$, the error being of the order of 10%.

A1.2 Evaluation of $\sum_{m,r} g_{mr}$ and R_{rad} at Subcritical Frequencies

Consider the sum $\sum_r g_{mr}$ for a given mode m, n, when $m\pi/a < k_r$, and only the acoustic modes having $p = m + 1$ are considered. Let $q = \epsilon n$. Then $B^2_{rm}(\epsilon) = K^2(a/\pi)^2(b/n\pi)^2[(-1)^{n(1+\epsilon)} - 1)/(1 - \epsilon^2)]^2$, where $K^2 = (c_o{}^2\rho/V\epsilon_r\epsilon_m M)$, for $n(1 + \epsilon)$ is odd, and zero for $n(1 + \epsilon)$ even. The average number of well coupled acoustic modes having a given ϵ is given by $N(\epsilon) = \left[\frac{k_r \Delta k_r c}{\pi(k_r{}^2 - (\frac{(m+1)\pi}{a})^2 - (\frac{\epsilon n\pi}{b})^2)^{\frac{1}{2}}}\right]$ from the geometry of Figure 4.2. This term is a much weaker function of ϵ than the term in the expression for $B^2_{rm}(\epsilon)$. Hence we may write

$$\sum_r g_{mr} \simeq K^2(\frac{a}{\pi})^2(\frac{b}{n\pi})^2 \quad \frac{k_r \Delta k_r c}{2(k_r{}^2 - (m\pi/a)^2)^{\frac{1}{2}}} \quad \sum_{\epsilon n=0}^{\epsilon' n} \left[\frac{(-1)^{n(1+\epsilon)} - 1}{(\epsilon n/n)^2 - 1}\right]^2 (\beta_r + \beta_m)^{-1} \tag{A1.1}$$

where $\frac{k_r \Delta k_r c}{2(k_r{}^2 - (m\pi/a)^2)^{\frac{1}{2}}}$ is the average number of well coupled acoustic

modes with a particular value of ε, and εn is given by $(b/\pi)(k_r^2 - (m\pi/a)^2)^{\frac{1}{2}}$. Now every second term in this series is zero, when $n(1 + \varepsilon)$ is even, but if we include the $p = m - 1$ mode set in the sum $\sum_r g_{mr}$ then the expression above holds.

Now since $\sum_{n=0}^{N} f(N) > \int_0^N f(x)dx > \sum_{n=0}^{N-1} f(N)$, a good approximation to this sum may be obtained from the integral $4 \int_{\varepsilon' n}^{0} (1 - (Fx)^2)^{-2} dx$, where $F = n^{-1}$ and $x = n$, because the N^{th} term of the series is small compared with the sum. The integral is given by

$$I = I_1 + I_2 = \frac{b(k_r^2 - (m/a)^2)^{\frac{1}{2}}}{\pi\left[1 - (\frac{b}{n\pi})^2(k_r^2 - (m\pi/a)^2)\right]} + \frac{n}{2} \log \tan\left[\frac{\pi}{4} + \frac{\sin^{-1}\frac{b}{n\pi}(k_r^2 - (\frac{m\pi}{a})^2)^{\frac{1}{2}}}{2}\right] \qquad (A1.2)$$

Thus

$$\sum_r g_{mr} = 4(K^2/c_o)(ab/n\pi^2)^2 \left[ck_r/2(k_r^2 - (m\pi/a)^2)^{\frac{1}{2}}\right](I_1 + I_2) \qquad (A1.3)$$

Here Δk_r has been written as $(\beta_r + \beta_m)/c_o$. By expressing K in its original form equation (A1.3) becomes

$$\sum_r g_{mr} = \frac{4c_o\rho abk_r}{2\varepsilon_r\varepsilon_m Mn^2\pi^4}\left[\frac{n^2\pi/2b}{k_p^2 - k_r^2} + \frac{n}{2(k_r^2 - (m\pi/a)^2)^{\frac{1}{2}}}\left\{\log\tan\left(\frac{\pi}{4} + \frac{\sin^{-1}\frac{b}{n\pi}(k_r^2 - (\frac{m\pi}{a})^2)^{\frac{1}{2}}}{2}\right)\right\}\right]$$

The second term in the square brackets may be shown to be very closely equal to $b/2\pi$ over the whole range of $\frac{m\pi}{a}$ $(< k_r)$. Hence

$$\sum_r g_{mr} = \frac{2c_o\rho abk_r}{\varepsilon_r\varepsilon_m Mn^2\pi^4}\left[\frac{n^2\pi/2b}{k_p^2 - k_r^2} + \frac{b}{2\pi}\right] = \frac{2c_o\rho ak_r}{\varepsilon_r\varepsilon_m M^3}\left[\frac{1}{2k_p^2(1 - f/f_c)} + \frac{b^2}{2n^2\pi^2}\right] \qquad (A1.4)$$

This expression has to be summed over all $m\pi/a < k_r$ for a given k_p to obtain $\sum_{r,m} g_{mr}$. The first term is independent of m and n for a given value of f/f_c. The average number of structural modes having a given m in a band containing a total of N_s modes is given by $2N_s b/an\pi$. Thus the sum, over m, of the second term in the square brackets becomes $\sum_{m\pi/a=0}^{k_r} (2N_s b/an\pi)(b^2/2n^2\pi^2) = (N_s/a) \sum_{m\pi/a=0}^{k_r} (b/n\pi)^3$. Now $(b/n\pi)^3 = (k_p^2 - (m\pi/a)^2)^{-3/2}$. Utilising the integral approximation $(N_s/ak_p^3) \int_{x=0}^{ak_r/\pi} (1 - (\pi x/ak_p)^2)^{-3/2} dx$ we obtain

$$\sum_{m,r} g_{mr} = \frac{2c_o \rho a N_s k_r}{\varepsilon_r \varepsilon_m M \pi^3} \left[\frac{\sin^{-1}(f/f_c)^{\frac{1}{2}}}{\pi k_p^2 (1-f/f_c)} + \frac{\tan(\sin^{-1}(f/f_c)^{\frac{1}{2}}}{\pi k_p^2} \right] \qquad \text{(A1.5)}$$

The sum $\sum_{m,r} g_{mr}$ for $n\pi/b < k_r$ takes the same form as equation (A1.5) with a replaced by b. The total sum $\sum_{m,r} g_{mr}$ therefore becomes

$$\sum_{m,r} g_{mr} = \frac{2c_o \rho N_s k_r (a + b)}{\varepsilon_r \varepsilon_m M \pi^4 k_p^2} \left[\frac{\sin^{-1}(f/f_c)^{\frac{1}{2}}}{1 - (f/f_c)} + \tan(\sin^{-1}(f/f_c)^{\frac{1}{2}}) \right]$$

from which $R_{rad} = M/N_s \sum_{m,r} g_{mr}$ is given by

$$R_{rad} = \frac{57.6 \rho h c_L (a + b)}{\pi^5} \left[\frac{\sin^{-1}(f/f_c)^{\frac{1}{2}}}{1 - (f/f_c)} + \tan(\sin^{-1}(f/f_c)^{\frac{1}{2}}) \right] \qquad \text{(A1.6)}$$

where ε_r is taken as 1/8 for most acoustic modes and $\varepsilon_r = 1/4$ for a panel. The numerical constant increases to 64 when the 1/9 contribution from the $p = m \pm 3$, $q < n$ and the $q = n \pm 3$, $p < m$ modes are included. The radiation efficiency is obtained from (A1.6) by dividing by $\rho c_o ab$, and is hence a function of c_o as well as of h and c_L.

A1.3 Evaluation of $\sum_{m,r} g_{mr}$ and R_{rad} at Supercritical Frequencies

The relevant wave number lattice diagram is shown in Fig. 4.3. At supercritical frequencies it is possible to have $p = m \pm 1$ and $q = m \pm 1$ simultaneously so that B_{rm}^2 takes the maximum value of $K^2(ab/\pi^2)^2$. The $p = m \pm 3$, $q = n \pm 1$, and $p = m \pm 1$, $q = n \pm 3$ modes give $B_{rm}^2 = K^2(ab/3\pi^2)^2$. All other contributions may be neglected. The average number of acoustic modes having $p = m \pm 1$, $q = n \pm 1$ per structural mode of order (m, n) is given by $N_a = 4c(\beta_r + \beta_m)/\pi c_o(1 - f_c/f)^{\frac{1}{2}}$, which is a function of box depth c, but not panel size. Hence $\sum_{m,r} g_{mr}$ is given by $\sum_{m,r} g_{mr} = N_s N_a K(ab/\pi^2)^2/(\beta_r + \beta_m)$ and the radiation resistance is given by $R_{rad} = (M/N_s) \sum_{m,r} g_{mr} = 128\rho c_o ab/\pi^5(1 - f_c/f)^{\frac{1}{2}}$. The well coupled $p = m \pm 3$, $q = n \pm 1$ and $p = m \pm 1$, $q = n \pm 3$ modes are twice as many as those $m \pm 1$, $n \pm 1$ modes. Hence the numerical constant becomes $128(1 + 2/9) = 156$. The radiation efficiency is therefore given by

$$\sigma = (156/\pi^5)(1 - f_c/f)^{\frac{1}{2}} \simeq 0.5(1 - f_c/f)^{\frac{1}{2}} \qquad \text{(A1.7)}$$

APPENDIX II

Radiation Resistance of a Clamped Panel

A.2.1 The Mode Shapes

In the calculation of natural frequencies of shells with clamped edges a common choice for the modal displacement distribution normal to the clamped edge is that of a beam having corresponding boundary conditions. A form which is more useful in the analysis of modal characteristics at high frequencies (asymptotic behaviour) was proposed by Bolotin (28). The displacement of a flat rectangular panel near the boundary $x = 0$ is written as follows

$$\phi(x,y) = \left[\sin k_1(x - x_a) + \sin k_1 x_a \exp(-(k_1^2 + k_2^2)^{\frac{1}{2}}x)\right] \times \left[\sin k_2(y - y_b) + \sin k_2 y_b \exp(-(k_2^2 + 2k_1^2)^{\frac{1}{2}}y\right] \qquad (A.2.1)$$

where

$$\sin k_1 x_a = \frac{k_1}{\sqrt{2}\,(k_1^2 + k_2^2)^{\frac{1}{2}}}$$

$$\sin k_2 y_b = \frac{k_2}{\sqrt{2}\,(k_2^2 + k_1^2)^{\frac{1}{2}}} \qquad (A2.2)$$

and the modal frequency equation is of the same form as that for the simply supported plate,

$$\omega^2 = (k_1^2 + k_2^2)(D/\rho_s h)^{\frac{1}{2}} \qquad (A.2.3)$$

The wavenumbers k_1 and k_2 are related to the mode orders m and n in the following way

$$k_1 a = 2 \text{ arc tg } \left[\frac{k_1}{(k_1^2 + 2k_2^2)^{\frac{1}{2}}} \right] + m\pi$$

$$k_2 b = 2 \text{ arc tg } \left[\frac{k_2}{(k_2^2 + 2k_1^2)^{\frac{1}{2}}} \right] + n\pi \qquad \text{(A.2.4)}$$

The form of displacement function in equation (A.2.1) gives a simple physical picture of the difference between the simply supported and clamped panel mode shapes. For large x and y, the second terms in the square brackets become insignificant, and the remaining functions are sinusoidal with phase shifts given by $k_1 a$ and $k_1 b$. Equations (A.2.4) show that for $k_1 >> k_2$ the phase shift in the x-direction approaches $\pi/4$ while that in the y-direction becomes small and approximately equal to $(k_2/\sqrt{2}\, k_1)$, and vice versa for $k_1 << k_2$. This displacement function is not general in the sense that there is no exponential term to account for the boundary opposite and parallel to the boundary $x = 0$. However the first term does represent pure symmetric or anti-symmetric motion over the region $0 < x < a$. The other exponential term can easily be accounted for in the evaluation of coupling coefficients, as will be seen in the next section.

A.2.2 The Surface Integral

As with the simply supported panel, the integral over the panel surface of the acoustic and panel eigenfunctions is required for the evaluation of the coupling coefficients B_{mr}. Use of the cosine functions for velocity potential, and of the clamped panel displacement function of equation (A.2.1), involves evaluation of the following integrals:

$$\cos k_1 x_a \int_0^a \cos\left(\frac{p\pi x}{a}\right) \sin k_1 x \, dx = I_{x_1}$$

$$- \sin k_1 x_a \int_0^a \cos\left(\frac{p\pi x}{a}\right) \cos k_1 x \, dx = I_{x_2} \qquad \text{(A.2.4)}$$

$$2 \sin k_1 x_a \int_0^a \cos\left(\frac{p\pi x}{a}\right) \exp(-k_1^2 + 2k_2^2)^{\frac{1}{2}} x \, dx = I_{x_3} \; : \; (m + p) \text{ even}$$

The integral I_{x_3} contains the factor two to account for the exponential factor near both boundaries, $x = 0$ and $x = a$. It is zero for $(m + p)$ even. The results of the integrations are as follows

$$I_{x_1} = \frac{((-1)^{p+1} \cos k_1 a + 1)}{k_1(1 - (p\pi/ak_1)^2)} \cos k_1 x_a \; : \; k_1 \neq \frac{p\pi}{a}$$

$$= 0 \; : \; k_1 = \frac{p\pi}{a} \qquad \text{(A.2.5)}$$

$$I_{x_2} = \frac{(-1)^{p+1} \sin k_1 a \sin k_1 x_a}{k_1(1 - (p\pi/ak_1)^2)} \; : \; k_1 \neq \frac{p\pi}{a}, \frac{k_1 a}{\pi} \text{ is non integer}$$

$$= 0 \; : \; k_1 \neq \frac{p\pi}{a}, \frac{k_1 a}{\pi} \text{ is integer} \qquad \text{(A.2.6)}$$

$$= -(a/2) \sin k_1 x_a \; : \; k_1 = \frac{p\pi}{a}$$

$$I_{x_3} = \frac{2(a/p\pi)^2(k_1^2 + 2k_2^2)^{\frac{1}{2}}}{(a/p\pi)^2(k_1^2 + 2k_2^2) + 1} \sin k_1 x_a \; : \; (m + p) \text{ odd}$$

$$= 0 \; : \; (m + p) \text{ even} \qquad \text{(A.2.7)}$$

The condition on I_{x_2} concerning the value of $(k_1 a/\pi)$ is necessary because in general this number is not an integer for a clamped panel, as

it is for simply supported boundary conditions. There are three corresponding integrals I_{y_1}, I_{y_2} and I_{y_3} for the y-direction.

A.2.3 Approximations

Because the values of $(k_1 a/\pi)$ and $(k_2 b/\pi)$ which correspond to the normal modes of a clamped panel are not normally integer values, it is very much more difficult to classify the various coupling coefficients by magnitude in terms of the mode orders (m, n) and (p, q, r), than it is in the case of the simply supported plate. Therefore it has been found necessary to consider the above integrals in terms of the relative orders of magnitude of the wavenumbers k_1 and k_2 in the x and y direction.

Reference to the expressions for k_1 and k_2 in equations (A.2.4) shows that the greatest differences between the wavenumbers of clamped and simply supported panel modes of the same order (m, n) occur when $k_1 \simeq (m + \frac{1}{2})\pi/a$ and $k_2 \simeq (n + \frac{1}{2})\pi/b$. These correspond to the conditions $k_1 >> k_2$ and $k_1 << k_2$ respectively. Consequently as may be seen from equation (A.2.3), the natural frequencies of corresponding high order modes of clamped and simply supported panels do not differ greatly. Also, the direction of the rectangular grid structural wavenumber diagram which is caused by clamping the edges of a panel is evident mainly near the axes of the diagram (Figure A.2.1). Hence it is reasonable, and indeed the only practicable course, to estimate modal coupling statistics from a consideration of a basically rectangular grid diagram, but with due account of the coupling coefficients proper to the clamped panel mode shapes.

It is evident from the expressions for integrals I_{x_1} and I_{x_2} in equations (A.2.5) and (A.2.6), that the best spatial matching, and hence the largest coupling coefficients B_{mr}, will be given by mode pairs for which $k_1 \simeq (p\pi/a)$ and $k_2 \simeq (q\pi/b)$. Hence, at well-subcritical frequencies, only those modes for which $k_1 << k_2$ or $k_1 >> k_2$ will simultaneously satisfy the frequency proximity condition and also the spatial matching condition. These are the clamped panel 'edge modes'. At higher, but still subcritical, frequencies, modes for which $k_1 \simeq k_2$ have to be considered.

A.2.3.1 Panel modes with $k_1 << k_2$ or $k_1 >> k_2$

For the condition $k_1 << k_2$ the following approximations may be made:

$$\sin k_1 x_a = \frac{k_1}{\sqrt{2}(k_1^2 + k_2^2)^{\frac{1}{2}}} \simeq k_1/\sqrt{2}k_2$$

$$\cos k_1 x_a \simeq 1$$

$$\sin k_2 y_b = \frac{k_2}{\sqrt{2}\,(k_2^2 + k_1^2)^{\frac{1}{2}}} \simeq \frac{1}{\sqrt{2}}$$

$$\cos k_2 y_b \simeq (1 - \tfrac{1}{2})^{\frac{1}{2}} = \frac{1}{\sqrt{2}}$$

$$k_1 a = 2 \operatorname{arctg} \left[\frac{k_1}{(k_1^2 + 2k_2^2)^{\frac{1}{2}}} \right] + m\pi \simeq m\pi + \sqrt{2}k_1/k_2$$

$$\sin k_1 a \simeq (-1)^m \sqrt{2}\, k_1/k_2$$

$$\cos k_1 a \simeq (-1)^m \cos (\sqrt{2}\, k_1/k_2) \simeq (-1)^m$$

$$k_2 b \simeq \pi/2 + n\pi$$

$$\sin k_2 b \simeq (-1)^n$$

$$\cos k_2 b \simeq 0$$

$$k_2 >> q\pi/b$$

Consideration of the integrals I_{x_1}, I_{x_2} and I_{x_3} with these approximations gives,

$$I_{x_1} \simeq \frac{((-1)^{m+p+1} + 1)}{k_1(1 - (p\pi/ak_1)^2)} \quad \begin{cases} = 0 & : \ p = m \\ \simeq a/\pi & : \ p = m \pm 1 \\ \simeq a/3\pi & : \ p = m \pm 3 \end{cases} \qquad \text{(A.2.8)}$$

$$I_{x_2} \simeq \begin{cases} -\frac{k_1 a}{2\sqrt{2}\, k_2} & : \ p = m \\ \frac{(-1)^{2m+1}\,(k_1/k_2)^2 a}{2\pi} & : \ p = m \pm 1 \end{cases} \qquad \text{(A.2.9)}$$

$$I_{x_3} \simeq k_1/k_2^{\,2} \quad : \text{ all p and m} \qquad \text{(A.2.10)}$$

$$I_{y_1} = \frac{((-1)^{q+1} \cos k_2 b + 1)}{k_2(1 - (q\pi/bk_2)^2)} \cos k_2 y_b$$

$$\simeq b/\sqrt{2}\, n\pi \quad : \ n > 1, \text{ all q, n} \qquad \text{(A.2.11)}$$

$$I_{y_2} = \frac{(-1)^{q+1} \sin k_2 b \sin k_2 y_b}{k_2(1 - (q\pi/bk_2)^2)} \quad : \ k_2 \neq \frac{n\pi}{b}$$

$$\simeq (b/\sqrt{2}\, n\pi)(-1)^{q+n+1} \quad : \ n > 1,\ k_2 \neq \frac{n\pi}{b} \qquad \text{(A.2.12)}$$

$$I_{y_3} = \left[\frac{2(b/q\pi)^2(k_1^2 + 2k_2^2)^{\frac{1}{2}}}{(b/q\pi)^2(k_1^2 + 2k_2^2) + 1}\right] \sin k_2 y_b \quad : (n+q) \text{ odd}$$

$$\simeq \sqrt{2}b/n\pi \quad : (n+q) \text{ odd} \qquad \text{(A.2.13)}$$

$$= 0 \quad : (n+q) \text{ even}$$

Summarising these results we have, where $I_x = I_{x_1} + I_{x_2} + I_{x_3}$ and $I_y = I_{y_1} + I_{y_2} + I_{y_3}$,

(a) $p = m \pm 1$, $(n + q)$ odd.

$$I_x \simeq (a/\pi) + (-1)^{2m+1}(k_1/k_2)^2 \times (a/2\pi) + k_1/k_2^2 \simeq (a/\pi)$$

$$I_y \simeq b/\sqrt{2}n\pi + b/\sqrt{2}n\pi + \sqrt{2}b/n\pi \simeq 2\sqrt{2}b/n\pi$$

(b) $p = m \pm 1$, $(n + q)$ even.

$$I_x \simeq (a/\pi) + (-1)^{2m+1}(k_1/k_2)^2 \times (a/2\pi) + (k_1/k_2^2) \simeq (a/\pi)$$

$$I_y \simeq b/\sqrt{2}n\pi - b/\sqrt{2}n\pi + 0 \simeq 0$$

(c) $p = m$.

$$I_x \simeq 0 - (k_1/k_2) \times (a/2\sqrt{2}) + (k_1/k_2^2)$$

$$I_y \simeq 2\sqrt{2}b/n\pi \quad : \quad (n + q) \text{ odd}$$

$$\simeq 0 \quad : \quad (n + q) \text{ even.}$$

(d) $p = m \pm 3$.

$$I_x \simeq (a/3\pi)$$

$$I_y \simeq 2\sqrt{2}b/n\pi \quad : \quad (n + q) \text{ odd}$$

$$\simeq 0 \quad : \quad (n + q) \text{ even}$$

The coupling coefficient B_{mr} is proportional to the product

$I_x I_y$. As with the simply supported panel the mode pairs having $p = m \pm 1$ (group (a)), produce the largest coefficient, followed by group (d). The condition $(n + q)$ odd also applies in the simply supported case. A corresponding result is obtained for panel modes with $k_1 >> k_2$.

The total number of well coupled mode pairs will be very similar in clamped and simply supported cases because of the previously mentioned form of distortion of the wavenumber diagram. Hence the relative radiation resistances of these panels may be estimated simply by considering the ratio of the squares of the values of the surface integrals for the well coupled mode pairs. Equation (4.8a) gives the value for the simply supported panel having $k_1 << k_2$ as $(2ab/n\pi)$. Thus the ratio of radiation resistances, at well subcritical frequencies, is given by

$$\frac{(R_{rad})_{clamped}}{(R_{rad})_{s.s}} = \frac{(2\sqrt{2}\ ab/n\pi)^2}{(2ab/n\pi)^2} = 2 \quad : \quad \begin{matrix} k_1 >> k_2 \\ \text{or} \\ k_2 << k_1 \end{matrix} \qquad \text{(A.2.14)}$$

This result agrees with those of Smith (29) and Nikiforov (23). It can be seen from the contribution of I_{x_3} to group (a) that the boundary near field causes the doubling effect.

A.2.3.2 Panel modes with $k_1 \simeq k_2$

This case presents more difficulties than the 'edge mode' calculation and has apparently not previously been tackled in the literature. The main problem is that the spatial phase shifts in the x and y directions, $k_1 x_a$ and $k_2 y_b$, are comparable. There are in the surface integral product many more contributing terms of the same order of magnitude.

The following approximations are made:

$$\sin k_1 x_a = \frac{k_1}{\sqrt{2}(k_1^2 + k_2^2)^{\frac{1}{2}}} \simeq \tfrac{1}{2} = \sin k_2 y_b$$

$$\cos k_1 x_a \simeq (1 - \tfrac{1}{4})^{\frac{1}{2}} = \sqrt{3}/2 \simeq \cos k_2 y_b$$

$$k_1 a = 2 \operatorname{arctg} \frac{k_1}{(k_1^2 + 2k_2^2)^{\frac{1}{2}}} + m\pi$$

$$\simeq [1 + m\pi]$$

$$k_2 b \simeq [1 + n\pi]$$

$$\sin k_1 a \simeq (-1)^m(\sqrt{3}/2)$$

$$\sin k_2 b \simeq (-1)^n(\sqrt{3}/2)$$

$$\cos k_1 a \simeq (-1)^m(1/2)$$

$$\cos k_2 b \simeq (-1)^n(1/2)$$

The various integrals then take the following principal values:

$$I_{x_1} \simeq 0.2a \quad : p = m$$
$$\simeq -0.3a \quad : p = m + 1$$
$$\simeq 0.16a \quad : p = m - 1$$
$$\simeq -(\sqrt{3}/40)a \quad : p = m + 2$$
$$\simeq (\sqrt{3}/40)a \quad : p = m - 2$$

(A.2.15)

$$I_{x_2} \simeq -0.1a \quad : p = m$$
$$\simeq -\sqrt{3}a/16 \quad : p = m + 1$$
$$\simeq \sqrt{3}a/32 \quad : p = m - 1$$
$$\simeq -\sqrt{3}a/40 \quad : p = m + 2$$
$$\simeq \sqrt{3}a/40 \quad : p = m - 2$$

(A.2.16)

$$I_{x_3} = 0 \qquad : p = m,\ (m + p) \text{ even}$$
$$\simeq \sqrt{3}a/4p\pi \qquad : p \neq m,\ m + p \text{ odd} \qquad (A2.17)$$
$$(p \simeq k_1 a/\pi)$$

$$I_{y_1} \simeq \sqrt{3}b/4n\pi \qquad : (n + q) \text{ even}$$
$$(q\pi/a < k_2) \qquad (A.2.18)$$
$$\simeq b/n\pi \qquad : (n + q) \text{ odd}$$

$$I_{y_2} \simeq \sqrt{3}b/4n\pi \qquad : (n + q) \text{ odd} \qquad (A.2.19)$$
$$\simeq -\sqrt{3}b/4n\pi \qquad : (n + q) \text{ even}$$

$$I_{y_3} = b/\sqrt{3}n\pi \qquad : (n + q) \text{ odd} \qquad (A.2.20)$$
$$= 0 \qquad : (n + q) \text{ even}$$

Summarising the results we have:

(a) $p = m$, $(n + q)$ even

$$I_x = 0.2a - 0.1a + 0 \quad = 0.1a \qquad (A.2.21)$$
$$I_y = \sqrt{3}b/4n\pi - \sqrt{3}b/4n\pi + 0 \quad = 0$$

(b) $p = m$, $(n + q)$ odd

$$I_x = 0.2a - 0.1a + 0 \quad = 0.1a \qquad (A.2.22)$$
$$I_y = b/n\pi + \sqrt{3}b/4n\pi + b/\sqrt{3}n\pi \quad = 2b/n\pi$$

(c) $p = m + 1$, $(n + q)$ odd.

$$I_x = -0.3a - \sqrt{3}a/16 + \sqrt{3}a/4p\pi \simeq -0.4a + \sqrt{3}a/4p\pi \qquad (A2.23)$$
$$I_y = 2b/n\pi$$

(d) $p = m-1$, $(n + q)$ odd

$$I_x = 0.16a + \sqrt{3}a/32 + \sqrt{3}a/4p\pi \simeq 0.2a + \sqrt{3}a/4p\pi \qquad (A2.24)$$

$$I_y = 2b/n\pi \qquad \text{(A.2.24)}$$

(e) $p = m + 2$, $(n + q)$ odd

$$I_x = -\sqrt{3}a/40 - \sqrt{3}a/40 + 0 \simeq -0.1a$$
$$I_y = 2b/n\pi \qquad \text{(A.2.25)}$$

(f) $p = m - 2$, $(n + q)$ odd

$$I_x = \sqrt{3}a/40 + \sqrt{3}a/40 + 0 = 0.1a$$
$$I_y = 2b/n\pi \qquad \text{(A.2.26)}$$

Considering the product $I_x I_y$ for each of the cases (a) - (f) we have

(a) $I_x I_y = 0$

(b) $I_x I_y \simeq 0.2ab/n\pi$

(c) $I_x I_y \simeq -0.8ab/n\pi + 2\sqrt{3}ab/4pn\pi^2$

(d) $I_x I_y \simeq 0.4ab/n\pi + 2\sqrt{3}ab/4pn\pi^2$

(e) $I_x I_y \simeq -0.2ab/n\pi$

(f) $I_x I_y \simeq 0.2ab/n\pi$.

The corresponding value of $I_x I_y$ for the simply supported panel is $2ab/n\pi^2$ for $p = m \pm 1$, $(n + q)$ even. Hence the ratio of the radiation resistance of the simply supported and clamped panels for $k_1 \simeq k_2$ is given by

$$\frac{(R_{rad})_{clamped}}{(R_{rad})_{s.s}} \simeq \frac{\frac{1}{2}[(0.2)^2 + (0.8)^2 + (0.4)^2 + (0.2)^2 + (0.2)^2]}{(2/\pi)^2} \simeq 1 \qquad \text{(A.2.27)}$$

A.2.4 Modal Average Radiation Resistance

At well subcritical frequencies the panel modes having $k_1 << k_2$ or $k_1 >> k_2$ are the only modes well coupled to the acoustic modes of the fluid. Hence the radiation resistance of a clamped panel at such frequencies is twice that of the simply supported panel. At higher frequencies, above about $0.5f_c$, some panel modes having $k_1 \approx k_2$ become well coupled and consequently the modal average radiation resistance starts to approach the simply supported value, until at frequencies near the critical frequency modes having $k_1 \quad k_2$ tend to dominate the total power flow, and hence the clamped and simply supported panels have approximately the same radiation resistances.

An accurate calculation of the radiation resistance curve at frequencies between $0.5f_c$ and f_c would be extremely difficult because of the need to use the full expressions for the coefficients B_{mr}, and not just their approximate forms, at frequencies above $0.5f_c$ (see equations (4.8) and (A.1.1). There is thus some uncertainty as to the rate at which the clamped and simply supported curves converge and this may well explain some of the discrepancies between the experimental and theoretical results for the clamped panel radiation efficiencies at frequencies between $0.5f_c$ and f_c.

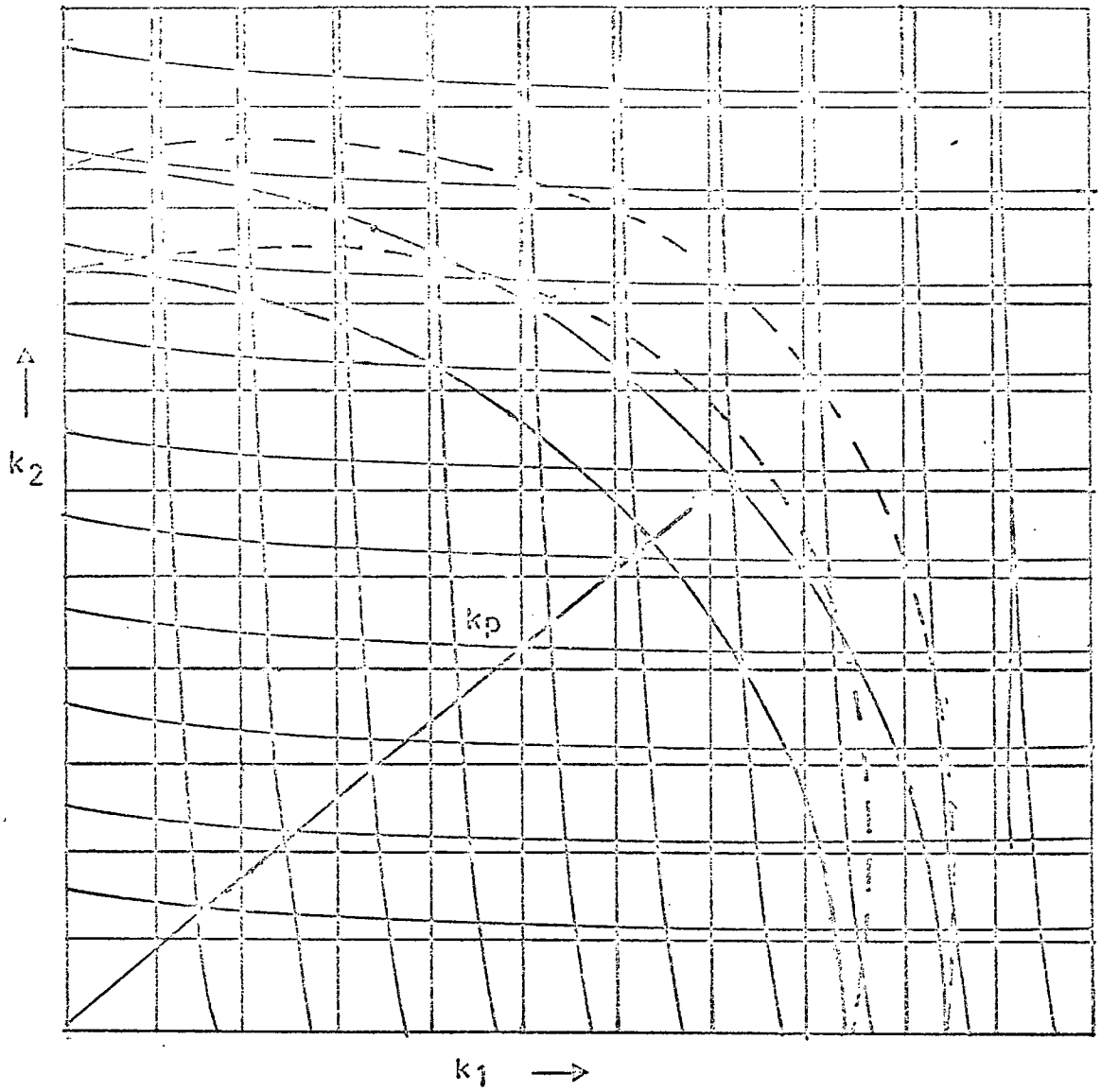

The circle and rectangular grid correspond to the simple supports; the dashed line and offset grid to the clamped plate.

Figure A.2.1. Wavenumber Diagram for a Simply-Supported and a Clamped Rectangular Panel.
(Diagramatic)

APPENDIX 3

Non-Proximate Modal Coupling at Subcritical Frequencies

For those frequency bands of analysis for which the average number of acoustic modes having maximum proximate coupling to the structural modes in the frequency band of analysis is less than unity, it is necessary to consider coupling between acoustic and structural modes of which the natural frequencies are further apart than half the sum of the half power bandwidths. Figure 4.4 shows the lattice points of acoustic modes which have natural frequencies within an analysis bandwidth centred on the natural frequency of a typical structural mode, but not within the bandwidth for proximate coupling.

The analysis of Appendix 1, Section A1.2 may be used to evaluate $\sum_{m,r} g_{mr}$ for those acoustic modes lying in a bandwidth $\delta\omega_r$ $(= c_o \delta k_r)$ which lies between the analysis band limits and the proximate coupling band. This sum is denoted by $\sum_{m,r(\delta k_r)} g_{mr}$ and is given by

$$\sum_{m,r(\delta k_r)} g_{mr} = \frac{2c_o^2 \rho N_s (a+b) k_r \delta k_r}{\varepsilon_r \varepsilon_m M^3} \left[\frac{\sin^{-1}(k_r/k_p)}{\pi(k_p^2 - k_r^2)} + \frac{1}{\pi k_p^2} \tan(\sin^{-1} k_r/k_p) \right]$$

$$\left[\frac{\beta_m \omega_r^2 + \beta_r \omega_m^2}{(\omega_m^2 - \omega_r^2)^2 + (\beta_r + \beta_m)(\beta_m \omega_r^2 + \beta_r \omega_m^2)} \right] \qquad \text{(A3.1)}$$

This expression is integrated over the frequency band previously defined and involves evaluation of the following integrals;

$$I_1 = \int_{\omega_L}^{\omega_u} \frac{\omega_r^4 \, d\omega_r}{A\omega_r^6 + B\omega_r^4 + C\omega_r^2 + D}$$

$$I_2 = \int_{\omega_L}^{\omega_u} \frac{\omega_r^4 \, d\omega_r}{B\omega_r^4 + C\omega_r^2 + D}$$

$$I_3 = \int_{\omega_L}^{\omega_u} \frac{\omega_r^2 \, d\omega_r}{A\omega_r^6 + B\omega_r^4 + C\omega_r^2 + D}$$

$$I_4 = \int_{\omega_L}^{\omega_u} \frac{\omega_r^2 \, d\omega_r}{B\omega_r^4 + C\omega_r^2 + D}$$

where $\omega_u = \omega_m - (\beta_r + \beta_m)/2$; $\omega_L = \omega_m - \Delta\omega/2$; $A = \omega_m^2(f_c/f)$; $B = 1$; $C = ((\beta_r + \beta_m)\beta_m) - 2\omega_m^2 \simeq -2\omega_m^2$; $D = (\beta_r + \beta_m)\beta_r\omega_m^2 + \omega_m^4 \simeq \omega_m^4$ and $G = ABC + BD \simeq \omega_m^4(1 - 2f_c/f)$.

I_1 is given by the following expression which is typical of all the integrals,

$$I_1 = (f_c/f - 1)^{-2} \{I_\alpha((f_c/f)^{3/2}/2\omega_m) + I_\beta((1 - f_c/f)8\omega_m) + (I_\gamma + I_\delta) \left|(3f_c/f - 1)/8((\beta_r + \beta_m)\beta_m)^{\frac{1}{2}}\right| \qquad \text{(A3.2)}$$

where

$$I_\alpha = \ell n\left\{\left[\frac{\omega_m((f_c/f)^{\frac{1}{2}} + 1) - (\beta_r + \beta_m)/2}{\omega_m((f_c/f)^{\frac{1}{2}} - 1) + (\beta_r + \beta_m)/2}\right]\left[\frac{\omega_m((f_c/f)^{\frac{1}{2}} - 1) + \Delta\omega/2}{\omega_m((f_c/f)^{\frac{1}{2}} + 1) - \Delta\omega/2}\right]\right\}$$

$$I_\beta = 2\ell n\left\{\left[\frac{2\omega_m - (\beta_r + \beta_m)/2}{(\beta_r + \beta_m)/2}\right]\left[\frac{\Delta\omega/2}{2\omega_m - \Delta\omega/2}\right]\right\}$$

$$I_\gamma = \{\tan^{-1}\left[\frac{2\omega_m - (\beta_r + \beta_m) + 2\omega_m}{((\beta_r + \beta_m)\beta_m)^{\frac{1}{2}}}\right] - \tan^{-1}\left[\frac{2\omega_m - \Delta\omega + 2\omega_m}{((\beta_r + \beta_m)\beta_m)^{\frac{1}{2}}}\right]\}$$

$$I_\delta = \{\tan^{-1}\left[\frac{\Delta\omega}{((\beta_r + \beta_m)\beta_m)^{\frac{1}{2}}}\right] - \tan^{-1}\left[\frac{(\beta_r + \beta_m)}{((\beta_r + \beta_m)\beta_m)^{\frac{1}{2}}}\right]\}$$

I_α is very small for $f_c/f > 4$ and third octave analysis, $(\Delta\omega/\omega \simeq 0.23)$. I_β is typically $2\ell n\ 10 \simeq 4.5$. I_γ is also very small and I_δ is typically 0.5.

Each of the integrals I_{1-4} is dominated by the term containing I_δ because it contains in its denominator the term $((\beta_r + \beta_m)\beta_m)^{\frac{1}{2}}$ whereas other terms, which are otherwise of similar order, have denominators which contain ω_m. The ratio of the former to the latter is of the order η which is of the order $10^{-2} - 10^{-3}$. The integrals I_1, I_2, I_3 and I_4 and the radiation efficiency may therefore be well approximated by the expressions presented in section 4.5.

APPENDIX 4

Calculation of the Coupling Factor for Point Driven Panels

Equation (3.48) gives the expected value of the product of the time rate of change of acoustic mode and structural mode generalised coordinates as

$$E[\dot{s}_m \dot{q}_r] = \varepsilon \sum_n B_{nr} \int_0^\infty \dot{h}_r(\theta_1)d\theta_1 \int_0^\infty \dot{h}_n(\theta_2)\dot{h}_m(\theta_1+\theta_2)d\theta_2 \times$$
$$2\pi S_f(\omega)M^{-2}(\varepsilon_m\varepsilon_n)^{-\frac{1}{2}}\phi_m(\underline{x}_o)\phi_n(\underline{x}_o) \qquad (A4.1)$$

where

$$\dot{h}_n(\theta_2) = \frac{e^{-(\beta_n/2)\theta_2}}{A}\left[A\cos A\theta_2 - (\beta_n/2)\sin A\theta_2\right]$$

$$\dot{h}_m(\theta_1+\theta_2) = \frac{e^{-(\beta_m/2)(\theta_1+\theta_2)}}{B}\left[B\cos B(\theta_1+\theta_2) - (\beta_m/2)\sin B(\theta_1+\theta_2)\right]$$

$$\dot{h}_r(\theta_1) = \frac{e^{-(\beta_r/2)\theta_1}}{D}\left[D\cos D\theta_1 - (\beta_r/2)\sin D\theta_1\right]$$

and $A^2 = \omega_n^2 - (\beta_n/2)^2$ $\qquad C = (\beta_n+\beta_m)/2$

$B^2 = \omega_m^2 - (\beta_m/2)^2$ $\qquad K = (\beta_r+\beta_m)/2$

$D^2 = \omega_r^2 - (\beta_r/2)^2$

The integrations give approximately 1,000 terms which are tabulated in a condensed form overleaf. Ultimately all but 7 of these terms are found to cancel out.

$$\int_0^\infty \dot{h}_r(\theta_1)d\theta_1 \int_0^\infty \dot{h}_n(\theta_2)\dot{h}_m(\theta_1+\theta_2)d\theta_2 =$$

$$D^2[C^3K - C^3\beta_r/2 + C^3\beta_m/2 - C^2K\beta_m/2 + C^2\beta_m\beta_r/4 - C^2K\beta_n/2 + C^2\beta_n\beta_r/2$$
$$- C^2\beta_n\beta_m/4 + CK\beta_n\beta_m/2 - C\beta_r\beta_m\beta_n/4]$$

$$+ A^2[-K^2\beta_m\beta_r/4 - K^3\beta_n/2 + K^2\beta_n\beta_r/4 + K^2\beta_n\beta_m/4 + CK^3 - CK^2\beta_r/2 - CK^2\beta_m/2$$
$$+ K^3\beta_m/2 - K\beta_r\beta_m\beta_n/4 + CK\beta_m\beta_r/2]$$

$$+ B^2[-C^2\beta_m\beta_r/4 - C^2K\beta_n/2 + CK^2\beta_n - C^2\beta_n\beta_r/4 - K^2\beta_n\beta_r/4 - CK\beta_n\beta_r$$
$$+ C^2\beta_n\beta_m/4 - K^2\beta_n\beta_m/4 + C^3K + CK^3 - C^2K^2 + C^3\beta_r/2 + KC^2\beta_r - C^3\beta_m/2$$
$$- CK^2\beta_m/2 - C^2K\beta_m/2 - K^3\beta_m/2 + CK\beta_n\beta_m/2 + K\beta_r\beta_m\beta_n/4 + C\beta_r\beta_m\beta_n/4$$
$$+ CK\beta_m\beta_r/2 - CK^2\beta_r/2 + K^3\beta_n/2 + K^2\beta_m\beta_r/4]$$

$$+ D^2A^2[CK - C\beta_r/2 + C\beta_m/2 + K\beta_m/2 - \beta_m\beta_r/4 - K\beta_n/2 + \beta_n\beta_r/4 - \beta_n\beta_m/4]$$

$$+ D^2B^2[CK + C^2 - C\beta_r/2 + C\beta_m/2 - K\beta_m/2 + \beta_m\beta_r/4 + K\beta_n/2 - C\beta_n/2 - \beta_n\beta_r/4$$
$$+ \beta_n\beta_m/4]$$

$$+ B^2A^2[CK + K^2 + C\beta_r/2 - K\beta_r - C\beta_m/2 + K\beta_m/2 + \beta_m\beta_r/4 - K\beta_n/2$$
$$- \beta_n\beta_r/4 + \beta_n\beta_m/4]$$

$$+ D^2A^2B^2[-1]$$

$$+ B^4[CK - K^2 - C^2 + C\beta_r/2 - C\beta_m/2 - K\beta_m/2 - \beta_m\beta_r/4 + K\beta_n/2 + C\beta_n + \beta_n\beta_r/4$$
$$- \beta_n\beta_m/4 + K\beta_r]$$

$$+ B^4D^2[+1] + B^4A^2[+1] + B^6[-1]$$

$$+ [C^2K^2\beta_m\beta_r/4 - C^2K^3\beta_n/2 + C^2K^2\beta_n\beta_r/4 + C^2K^2\beta_n\beta_m/4 + CK^3\beta_n\beta_m/2$$

$$-c^2K\beta_r\beta_m\beta_n/4 - CK^2\beta_r\beta_m\beta_n/4 + c^3K^3 - c^3K^2\beta_r/2 - c^3K^2\beta_m/2 - c^2K^3\beta_m/2$$

$$+ c^3K\beta_m\beta_r/2\Big]$$

The final result is as follows

$$\int_0^\infty \dot{h}_r(\theta_1)d\theta_1 \int_0^\infty \dot{h}_n(\theta_2)\dot{h}_m(\theta_1 + \theta_2)d\theta_2 =$$

$$\frac{(\beta_m\omega_n^2 + \beta_n\omega_m^2)(\beta_m\omega_r^2 + \beta_r\omega_m^2) - \omega_m^2(\omega_m^2 - \omega_r^2)(\omega_m^2 - \omega_n^2)}{\left[(\omega_m^2 - \omega_n^2)^2 + (\beta_m + \beta_n)(\beta_m\omega_n^2 + \beta_n\omega_m^2)\right]\left[(\omega_m^2 - \omega_r^2)^2 + (\beta_m+\beta_r)(\beta_r\omega_m^2 + \beta_m\omega_r^2)\right]}$$

(A4.2)

REPLY TO THE LETTER TO THE EDITOR "DAMPING IN PLATES" BY M. J. CROCKER AND A. J. PRICE

I welcome this letter [1] and a chance to reply to it because it brings into the open a matter which is often passed over lightly in the literature concerning experimental studies of the random vibrations of complex structures, and yet which is of vital importance in the comparison of experimental results and theory. Before discussing experimental techniques and interpretation of results it is necessary to point out that the object of the exercise is normally to measure the "average loss factor" of a structure in a frequency band which usually contains a number of mode natural frequencies, the concept of loss factor being generalized from the single mode application to a number of modes resonant in the band [2]. Thus the rate of loss of energy from the structure when excited by forces having spectra flat compared with the individual mode admittances is written as $\pi = \eta_{AV}\omega_c\bar{E}$ where ω_c is the centre frequency of a reasonably narrow frequency band, usually $\frac{1}{3}$-octave, and $\bar{E}$ is the time-average total energy of the structure. This equation may also be used for decay following the removal of such forces, provided that the damping is small. The rate of loss of energy is also given by $\pi = \eta_1\omega_1\bar{E}_1 + \eta_2\omega_2\bar{E}_2 + \cdots + \eta_n\omega_n\bar{E}_n$ for n modes resonant within the band. Hence, for $\omega_1 \simeq \omega_2 \simeq \omega_n \simeq \omega_c$, η_{AV} is given by

$$\eta_{AV} = \frac{\eta_1\bar{E}_1 + \eta_2\bar{E}_2 + \cdots + \eta_n\bar{E}_n}{\bar{E}_1 + \bar{E}_2 + \cdots + \bar{E}_n}.$$

The average loss factor is seen to depend upon the modal energy distribution and the variation of modal loss factor from mode to mode within the frequency band. The best guarantee that the measured average loss factor is meaningful for a particular experiment is a direct measurement of power input from the experimental steady-state excitation forces. However, only with single point mechanical excitation is this feasible. For more complex excitation forces the initial slope of the energy decay curve following removal of the particular type of excitation being studied will usually provide satisfactory results. Since the initial modal response to impulsive loading is largely independent of damping it would be expected that such measurements would indicate excessively high average loss factors. Figure 3 of reference 1 illustrates the effect well, but very often the inability of the recorder to follow the initial decay leads to an underestimate, rather than overestimate, of the loss factor from impulse-decay records.

I am therefore in agreement with Crocker and Price [1] that the use of impulse-decay records to measure modal average loss factors is not to be recommended. Unfortunately, I was not aware of the dangers of such a procedure at the time of publication of reference 3. However, I have established that by careful choice of hammer material (hide, copper or steel), together with the use of tape transport to overcome recorder response problems, reasonably good agreement may be obtained between measurements of loss factor from decay following steady-state acoustic excitation and impulsive excitation. Figure 1 shows such measurements together with individual modal loss factors measured from harmonic response vector plots. Figures 2 and 3 compare decay records following continuous and impulsive loading. It has generally been found that the decay records have a far better appearance than those presented in Figure 2 of reference 1.

The decay records from which Figure 4 of reference 3 were obtained have been re-analysed in the light of subsequent experience. The only significant errors that have been detected are

10 log$_{10}$ η tot

Figure 1. acoustic exc mode.

10 dB

Figure 2. 1000 Hz ⅓-

in the loss with the m

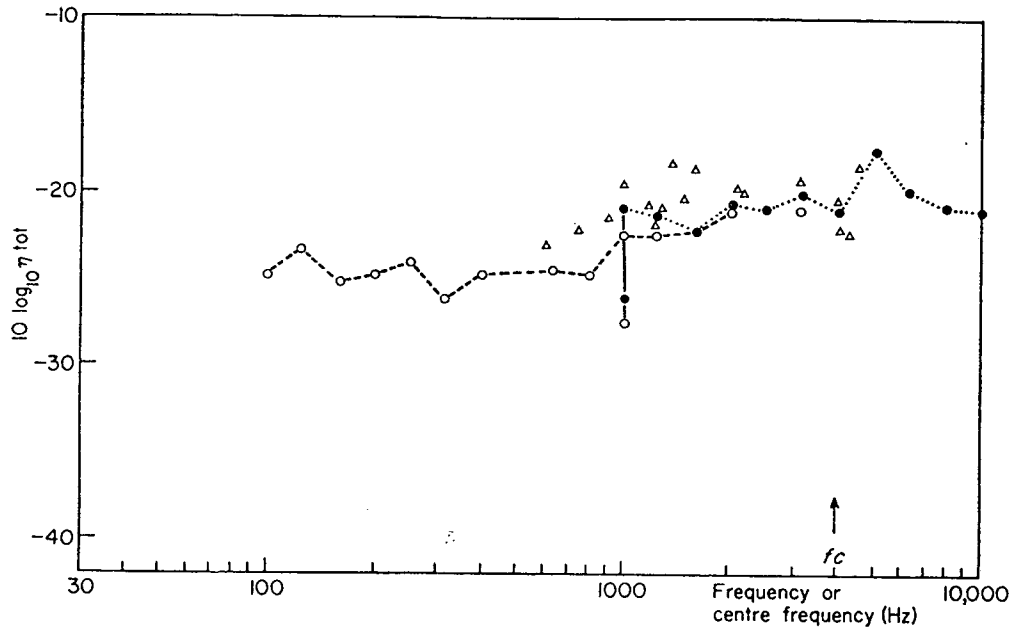

Figure 1. Total loss factors for $\frac{1}{8}$-in. clamped plate. ●, Decay after steady-state $\frac{1}{3}$-octave band acoustic excitation; ○, decay after impulsive mechanical excitation; △, vector plot on individual mode.

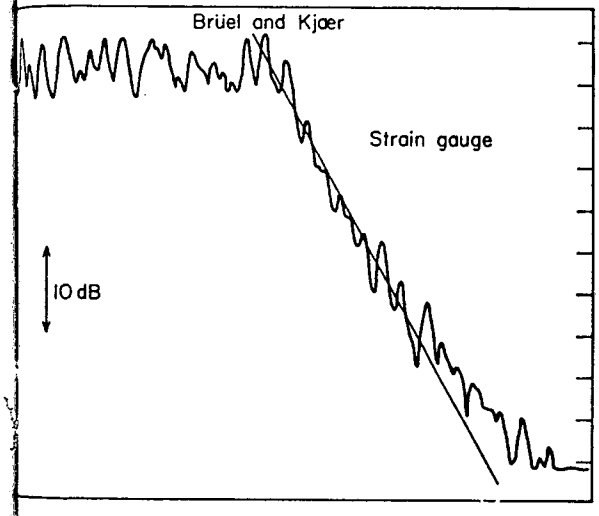

Figure 2. Decay of cylinder after continuous 1000 Hz $\frac{1}{3}$-octave band excitation.

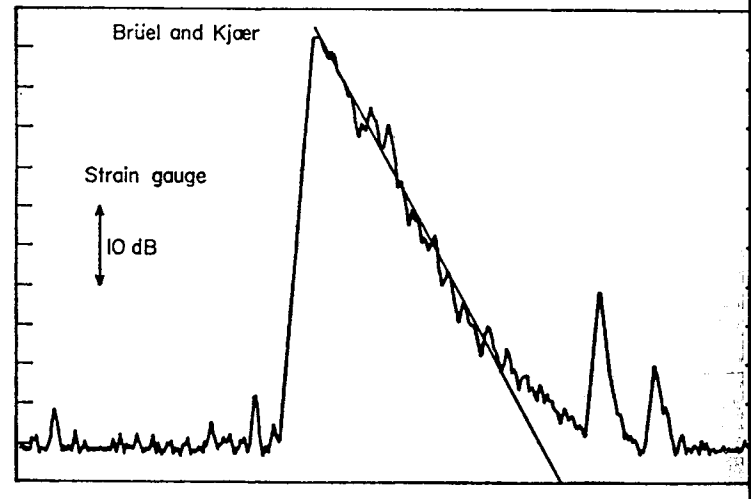

Figure 3. Decay of cylinder after impulsive excitation (filtered in 1000 Hz $\frac{1}{3}$-octave band).

in the loss factors for the riveted stiffener-plate combination. The corrected values, together with the modified radiation loss factors, are shown in Table 1.

TABLE 1

Riveted stiffener

Third-octave band centre frequency (Hz)	Loss factor η_t	Modified $10\log_{10}\eta_{rad}$
1000	$4{\cdot}6 \times 10^{-3}$	−60·5
2000	10×10^{-3}	−47
4000	9×10^{-3}	−66
5000	9×10^{-3}	−57

The modified results still show the riveted and point-bolted stiffeners to be far superior to the line-attached stiffener configuration by over 10 dB at most frequencies above 400 Hz. An apology is extended to the authors of reference 7 in reference 3 for a misguided rejection of their hypothesis.

In answer to the comments of reference 1 concerning the general behaviour of η_{tot} for plain panels it must be pointed out that the results presented in Figure 4 of reference 3 for the plain panel do indeed show η_{tot} to be approximately independent of frequency over most of the range. The actual value depends largely on the boundary conditions of the panel because the energy losses are dominated by frictional losses at the support and by the transmission of energy to connected structures. The $\frac{1}{8}$-in. angle section support described in reference 3 has been consistently found to behave more like a simple support than like a clamped support and has always given much lower mechanical loss factors than a 1-in. thick steel frame support which gave the results presented in Figure 1 of the present letter. "Clamping" of fairly large areas of the edges of panels generally leads to high mechanical loss factors through wave motion in the "clamped" areas. Hence it is not considered useful to generalize about the loss factors of plain panels. Careful measurements of η_{tot} on thick welded nuclear reactor structures have consistently given values which reduce with increase of frequency. The presentation of results in Figure 3 of reference 3 in the form of η_{rad} has been discussed in that paper.

With regard to the hypothesis of reference 1 concerning the transfer of energy from decaying low-order modes to high-order modes it must be concluded that the proposed coupling elements are the acoustic modes of the adjacent fluid. Since a structural mode decays at its individual natural frequency it will transfer energy substantially only to those acoustic modes with frequencies within a half-power bandwidth of this frequency. Except in the case of highly damped acoustic modes and high structural modal density such a process is thought extremely unlikely to operate with sufficient efficiency to cause the phenomenon, but the build-up of acoustic energy in these modes may well slow up energy transfer after a certain period of structural energy decay.

F. J. FAHY

Institute of Sound and Vibration Research,
University of Southampton,
Southampton,
SO9 5NH,
England

Received 23 *January* 1969

REFERENCES

1. M. J. CROCKER and A. J. PRICE 1969 *J. Sound Vib.* **9**, 501. Letter to the Editor: Damping in plates.
2. P. W. SMITH and R. H. LYON 1965 *NASA CR* 160. Sound and structural vibration.
3. F. J. FAHY and R. B. S. WEE 1968 *J. Sound Vib.* **7**, 431. Some experiments with stiffened plates under acoustic excitation.

APPENDIX VI

Non-Proximate Mode Coupling

A.6.1 b-type Coupling

Following the approach of reference (50) and Appendix III the coupling is considered between structural modes and acoustic modes which have maximum B_{rm}, by virtue of spatial distribution of velocity potential and displacement (equation (6.10a)), but which do not satisfy the condition of proximity of natural frequency (equation (6.8a)). The sum $\sum_{m,r} g_{mr}$ is formally expressed as follows

$$\sum_{m,r} g_{mr} = 2 \int_{k_{r_L}}^{k_{r_U}} \sum_{m,r} g_{mr_{(\delta k_r)}} dk_r \qquad (A.6.1)$$

where k_{r_U} and k_{r_L} are the acoustic wavenumbers which correspond respectively to the frequencies $(f_o - \Delta f/2)$ and $(f_o - c_o \Delta k_r/4\pi)$ where f_o is an analysis centre band frequency and Δf is the bandwidth. The integration is thus over that wavenumber space in which non-proximate acoustic modes exist, and excludes the shell of thickness Δk_r in which proximate modes exist.

The average number of acoustic modes in a shell of thickness δk_r which have b-type coupling to each structural mode is given by $2a\delta k_r$ (see equation (6.14) and Figure 6.7. The average number of structural modes capable of b-type coupling is given by $\ell a \Delta\phi k_r^2/2\pi$. Hence

$$\sum_{m,r} g^b_{mr} = \int_{k_{r_L}}^{k_{r_U}} \left(\frac{2\ell a^2 \Delta\phi k_r^2}{2\pi}\right) \left[\frac{(B^b_{mr})^2 (\beta_m \omega_r^2 + \beta_r \omega_m^2)}{(\omega_m^2 - \omega_r^2)^2 + (\beta_r + \beta_m)(\beta_m \omega_r + \beta_r \omega_m^2)}\right] dk_r$$

$$= 4\left(\frac{\ell a^2 \Delta\phi}{2\pi c_o^3}\right)\left(\frac{c_o^2 \rho \ell}{M \varepsilon_m \pi}\right) \int_{\omega_m + \frac{(\beta_r+\beta_m)}{2}}^{\omega_m+\Delta\omega/2} \left[\frac{\omega_r^2(\beta_m \omega_r^2 + \beta_r \omega_m^2)}{(\omega_m^2-\omega_r^2)^2 + (\beta_m+\beta_r)(\beta_m \omega_r^2 + \beta_r \omega_m^2)}\right] d\omega_r \qquad (A.6.2)$$

Using the integrations of Appendix III, equation (A.6.2) becomes

$$\sum_{m,r} g^b_{mr} = \left[\frac{\ell^2 a^2 \Delta\phi c_o^2 \omega_m^2}{2\pi^2 M \varepsilon_m}\right]\left(\frac{\beta_r + \beta_m}{\beta_m}\right)^{\frac{1}{2}} I \qquad (A.6.3)$$

$$\text{and} \quad \sigma^b \simeq R^b_{rad}/2\rho c_o \pi a \ell = M \sum_{m,r} g^b_{mr}/2\rho c_o \pi a \ell N_s = \frac{\ell a \Delta\phi \omega_m^2}{4\pi^3 \varepsilon_m N_s c_o^2}\left(\frac{\beta_r + \beta_m}{\beta_m}\right)^{\frac{1}{2}} \qquad (A.6.4)$$

where $I = \tan^{-1}\left[\Delta\omega/((\beta_r + \beta_m)\beta_m\right]^{\frac{1}{2}} - \tan^{-1}\left[\beta_r + \beta_m)/((\beta_r + \beta_m)\beta_m\right]^{\frac{1}{2}}$.

A.6.2 a-type Coupling

The problem with evaluating the power flow due to coupling of structural modes with the $q = 0$ acoustic modes is in the estimation of the average frequency difference $|\omega_m^2 - \omega_r^2|$ between non-proximate a-type coupled modes. An approximate average value may be found by considering the difference between k_{po_r} and $k_{po_{(r+1)}}$, because maximum B^a_{rm} is given by $r = m \pm 1$. Using equation (6.9) we have

$$(k_{po_{(r+1)}})^2 - (k_{po_r})^2 = (\pi/\ell)^2(2r + 1) \simeq (\pi/\ell)^2(2m + 1) \qquad (A6.5)$$

Now, from Figure 6.3, $\frac{r\pi}{\ell} = \frac{m\pi}{\ell} = k_r \sin\phi$

$$= k_r(1 - f_m/f_R)^{\frac{1}{2}} \qquad (A.6.6)$$

Hence $|\omega_m^2 - \omega_r^2| \simeq (c_o\pi/\ell)^2(2r + 1)$ and thus

$$(\omega_m^2 - \omega_r^2)/\omega_m \simeq (2\pi c_o/\ell)(1 - f/f_R)^{\frac{1}{2}} \qquad (A.6.7)$$

Use of this approximate formula for the average frequency difference between the structural and acoustic modes leads to the following form for g^a_{mr},

$$g^a_{mr} = \frac{(B^a_{mr})^2(\beta_m\omega_r^2 + \beta_r\omega_m^2)}{(\omega_m^2 - \omega_r^2)^2 + (\beta_m + \beta_r)(\beta_m\omega_r^2 + \beta_r\omega_m^2)}$$

$$\simeq \frac{(B^a_{mr})^2(\beta_r + \beta_m)}{(\omega_m^2 - \omega_r^2)^2/\omega_m^2 + (\beta_r + \beta_m)^2}$$

$$= 2(B^a_{mr})^2(\beta_r + \beta_m)/|(2\pi c_o/\ell)(1 - f/f_R) + (\beta_r + \beta_m)^2| \qquad (A.6.8)$$

The average number of mode pairs having a-type coupling is given closely by $(\ell a k_r \Delta\omega\Delta\phi/c_o\pi)$. The second term in the denominator of equation (A.6.8) can often be neglected in comparison with the first term. If this is done, the expression for radiation efficiency due to a-type coupling is given by

$$\sigma^a = \frac{5.5\ell^3\Delta\phi(\beta_r + \beta_m)f^2}{N_s c_o^3\pi^3(1 - f/f_c)} \qquad (A.6.9)$$

The total efficiency is given by $\sigma = \sigma^a + \sigma^b$. In general σ^b is larger than σ^a. Equations (A.6.4) and (A.6.5) have been used to calculate the non-proximate coupling curve in Figure 6.8.

TABLE 1

Comparison between numbers of well coupled mode pairs calculated by computation and by statistical analysis.

Band Centre Frequency (Hz)	1/16 in. Plate				$\frac{1}{8}$ in. Plate				$\frac{1}{4}$ in. Plate			
	$(\beta_r+\beta_m) = 25$		$(\beta_r+\beta_m) = 100$		$(\beta_r+\beta_m) = 25$		$(\beta_r+\beta_m) = 100$		$(\beta_r+\beta_m) = 25$		$(\beta_r+\beta_m) = 250$	
	N_c	N_s	N_c	N_s	N_c	N_s	N_c	N_s	N_c	N_s	N_c	N_s
400	-	0.10	-	0.40	-	0.08	-	0.32	-	0.05	-	0.51
500	-	0.19	1	0.76	-	0.17	-	0.68	1	0.09	1	0.92
630	1	0.33	2	1.32	-	0.25	-	1.00	-	0.17	3	1.72
800	-	0.70	5	2.80	-	0.44	3	1.76	1	0.31	7	3.10
1000	1	1.10	3	4.40	-	0.81	2	3.24	-	0.56	1	5.60
1250	4	1.92	11	7.68	3	1.47	7	5.88	1	0.98	9	9.80
1600	4	3.35	11	13.40	5	2.45	11	9.80	3	1.73	15	17.30
2000	3	6.11	21	24.44	6	4.66	25	17.64	5*	3.21*	33*	32.1*
2500	12	10.18	49	40.72	10	7.65	31	30.60	2	1.73	13	17.3
3150	19	18.85	76	75.40	14	10.60	59	42.40	1	1.57	18	15.7
4000	40	33.30					87*	98.4*	-	1.77	15	17.7
5000	56	62.80										
6300					10	7.13						

Number of well coupled mode pairs in a frequency band: N_s from statistical analysis

N_c as computed

*Band centred on critical frequency.

TABLE 2

2(a). Frequency ratios below which there is less than one acoustic mode well coupled to each structural mode (from subcritical mode statistics).

Plate type	$\frac{1}{4}$ in. simply supported	$\frac{1}{4}$ in. clamped	$\frac{1}{8}$ in. simply supported	$\frac{1}{8}$ in. clamped	1/16 in. simply supported	1/16 in. clamped
(f/f_c)	2.1	1.0	1.5	1.3	1.0	1.0

2(b). Average number of acoustic modes well coupled to each structural mode (from supercritical mode statistics).

$(f/f_c) = 2$

Plate type	$\frac{1}{4}$ in. simply supported	$\frac{1}{4}$ in. clamped	$\frac{1}{8}$ in. simply supported	$\frac{1}{8}$ in. clamped	1/16 in. simply supported	1/16 in. clamped
No. of modes	0.28	0.74	0.28	1.43	0.28	0.42